Influence of Slag Composition and Temperature on the Hydration and Performance of Slag Blends in Chloride Environments

Okiemute Roland Ogirigbo

Submitted in accordance with the requirements for the degree of

Doctor of Philosophy (PhD)

The University of Leeds

School of Civil Engineering

June, 2016

The candidate confirms that the work submitted is his own, except where work which has formed part of jointly-authored publications has been included. The contribution of the candidate and the other authors to this work has been explicitly indicated below. The candidate confirms that appropriate credit has been given where reference has been made to the work of others.

Parts of the work in chapters 4, 5, 6 and 7 have appeared in the following publications:

Proceedings of International Conference on Sustainable Structural Concrete, 15-18 September 2015, La Plata, Argentina, 2015, pp. 110-119. Ogirigbo O. R. and Black L. (Parts of Chapters 4, 5 and 7)

Proceedings of Concrete Repair, Rehabilitation and Retrofitting IV, Leipzig, Germany, 2015, pp. 501-506. Ogirigbo O. R. and Black L. (Parts of Chapters 4, 5, 6 and 7)

Proceedings of International Building Materials Conference, IBAUSIL, 15-17 September 2015, Weimar, Germany, 29-09. Ogirigbo O. R. and Black L. (Parts of Chapter 6)

For all the above, I wrote the introduction, methods, results, discussion and conclusion. Dr Black edited the work and rewrote parts of the introduction, methods and discussion. However, the analysis and interpretation were performed by me.

Acknowledgements

First, I wish to acknowledge God, the source and giver of all knowledge and wisdom.

My sincere thanks go to Dr Leon Black for the ideas, suggestions, guidance and timely contributions towards the progress of this work.

I thank my sponsor, the Petroleum Technology Development Fund (PTDF) of Nigeria, for providing the funds to enable me carry out this research. I also thank Heidelberg Cement Company for providing the materials used for this research.

I thank all my friends and well-wishers, especially the members of Power Connections. You guys made my stay in Leeds an interesting one. You are indeed a family. My special thanks to Pastor Ralph, Pastor Foluke, leaders of Power Connections (CLC and GLC), members of the bible study and technical unit of Power Connections, and most especially to the Inspirators.

I thank all my mothers and fathers, Mr and Mrs Ogirigbo, Mr and Mrs Ighama, Pastor Alonge and family, my siblings and in-laws, for all the prayers, guidance and support you offered me through the whole period of my study.

Lastly, my thanks goes to my precious family, Perfect and Praise, for your lovely smiles and cheerfulness, and to my darling wife, for being beside me all through the entire journey, offering unflinching love and support.

Abstract

The use of GGBS as supplement for cements has been shown to improve the long-term strength and durability properties of concrete. In practice, while the chemical composition of GGBS from a single plant may be constant, due to the varying sources from which GGBS is obtained the chemical composition from plant to plant may vary. The wide variability in the use of GGBS as a SCM in different climates, coupled with differences in chemical composition, is bound to have impact on the performance of slag blends.

This study investigated the combined influence of difference in slag composition and temperature on the performance of slag blends. Performance was evaluated in terms of strength and transport properties. Paste samples were characterised by calorimetry, TGA, XRD and SEM to follow hydration and microstructural development. Mortar samples were used to follow strength development and transport properties. All tests were carried out at temperatures of 20 and 38°C.

Curing at 38°C accelerated the early hydration, but not the later hydration. This led to higher early strengths and lower later strengths, and was attributed to the coarsening of the pore structure caused by the high temperature curing. Except at the early ages at 20°C, both slag blends showed better strength performance than the reference cement. The slag blends also showed better transport properties than the reference cement, especially at 38°C, and this was attributed to their finer pore structure and higher chloride binding capacity.

Of the two slags studied, the more reactive slag (slag 1) had better performance, especially at 38°C. Performance of the slag blends at 20°C was influenced mainly by the length of curing, and by the difference in chemical composition at 38°C.

Table of Contents

List of Figures

List of Tables

List of Abbreviations

Cement Nomenclature:

C = CaO	S = SiO_2	A = Al_2O_3
M = MgO	F = Fe_2O_3	$\overline{S}$ = SO_3
N = Na_2O	K = K_2O	H = H_2O

Techniques:

BSE	Back Scattered Electrons
DTA	Differential Thermal Analysis
EDS	Energy Dispersive X-ray Spectrometer
GGBS	Ground Granulated Blast Furnace Slag
IC/ICP	Ion Chromatography-Inductively Coupled Plasma
ICC	Isothermal Conduction Calorimetry
ITZ	Interfacial Transition Zone
MAS NMR	Magic Angle Spinning Nuclear Magnetic Resonance
MIP	Mercury Intrusion Porosimetry
PC	Portland Cement
PDF	Powder Diffraction File
PFA	Pulverised Fuel Ash
PONKCS	Partial Or No Known Crystal Structure
ppm	Parts per million
PSD	Particle Size Distribution
QXRD	Quantitative X-Ray Diffraction Analysis
RILEM TC	Reunion Internationale des Laboratoires et Experts des Materiaux Technical Committee
RCPT	Rapid Chloride Permeability Test
RH	Relative Humidity
SAI	Slag Activity Index

SCM	Secondary Cementitious Materials
SEM	Scanning Electron Microscope
STA	Simultaneous Thermal Analysis
TEM	Transmission Electron Microscope
TGA	Thermogravimetric Analysis
UCS	Unconfined Compressive Strength
w/b	Water/Binder ratio
w/c	Water/Cement ratio
w/s	Water/Solids ratio
XRD	X – Ray Diffraction
XRF	X – Ray Fluorescence

Clinker and hydrated phases:

Alite (C_3S)	$3CaO.SiO_2$
Belite (C_2S)	$2CaO.SiO_2$
Calcium Aluminate Silicate Hydrate (C-A-S-H)	$CaO\text{-}Al_2O_3\text{-}SiO_2\text{-}H_2O$
Calcium Hemicarboaluminate (Hc)	$3CaO.Al_2O_3.0.5Ca(OH)_2.0.5CaCO_3.11.5H_2O$
Calcium Monocarboaluminate (Mc)	$3CaO.Al_2O_3.CaCO_3.11H_2O$
Calcium Monosulphoaluminate (Ms)	$3CaO.Al_2O_3.CaSO_4.12H_2O$
Calcium Silicate Hydrate (C-S-H)	$CaO\text{-}SiO_2\text{-}H_2O$
Ettringite (AFt)	$3CaO.Al_2O_3.3CaSO_4.32H_2O$
Friedel’s salt	$3CaO.Al_2O_3.CaCl_2.10H_2O$
Gypsum	$CaSO_4.2H_2O$
Hydrotalcite (Ht)	$Mg_6Al_2(OH)_{16}.CO_3.4H_2O$
Kuzel’s salt	$3CaO.Al_2O_3.1/2CaCl_2.1/2CaSO_4.10H_2O$
Portlandite (CH)	$Ca(OH)_2$
Stratlingite	2CaO.Al2O3.SiO2.8H2O
Tetracalcium Aluminoferrite (C_4AF)	$4CaO.Al_2O_3.Fe_2O_3$
Tricalcium Aluminate (C_3A)	$3CaO.Al_2O_3$

Chapter 1
INTRODUCTION

Concrete is the most widely used construction material in the world as a result of its ability to resist penetration of water when used in marine environments, good fire resistance properties, versatility in forming various shapes, abundance of raw materials and low manufacturing and maintenance costs [1]. One very important feature regarding its use is the environmental concern regarding the production of Portland cement (PC) - the most common binder in concrete, which contributes significantly to the total global CO_2 emissions [2].

As a way to reduce the environmental footprint associated with concrete, it has become common practice to use secondary cementitious materials (SCM) as partial replacement for PC in the making of concrete. These SCMs are cheaper than PC and help to improve certain properties of concrete. There are a wide range of SCMs that are currently being used in the construction industry including fly ash, silica fume, metakaolin and ground granulated blast furnace slag (GGBS). Many of these SCMs are industrial by-products. Therefore, since convention in lifecycle analysis dictates that emissions follow the primary product; these SCMs offer a lower-carbon replacement for PC, while also diverting these materials from landfill and reducing abiotic depletion.

Thus, it is now common practice in the construction industry to use GGBS as a partial replacement for PC, in varying amounts ranging from as low as 6 per cent to as high as 95 per cent. While EN 197-1:2011 [3] may allow replacement levels of 6%, practically, replacement levels are much higher, typically around 20 to 40%. GGBS is a by-product from the making of iron and steel. The molten iron slag from the blast furnace is quenched with water or steam to produce a glassy and granular

material, which is grounded to a fine powder to produce GGBS. The material has almost the same fineness and specific surface area as PC [4]. It is glassy in nature and latently hydraulic [5].

When a blend of PC and GGBS is mixed with water, the GGBS portion reacts much more slowly with the water than the PC portion. Slag's hydraulicity – the term used to describe the ease with which GGBS reacts with water, depends mainly on its chemical composition, glass content, particle fineness, alkalinity of the reacting system and temperature at the early stages of hydration [6]. The chemical composition of GGBS can vary from plant to plant, depending on the nature of the ore, composition of the limestone flux, coke consumption and the type of iron being made [7].

The oxides of calcium, magnesium and aluminium are known to increase the hydraulicity of GGBS, while that of silicon decreases it [8]. Ratios of these oxides have been widely used to assess the hydraulicity of a slag. These ratios appear to vary from region to region. For example, in Britain, BS EN 197-1:2011 prescribes that for GGBS, the $(CaO + MgO)/SiO_2$ ratio by mass must exceed 1 [3]. In Germany, alumina is considered to play a positive role and is included in the hydraulicity index, to give $(CaO + MgO + Al_2O_3)/SiO_2$, which must exceed 1.0. In other countries like Japan and South Korea, it is recommended that the $(CaO + MgO + Al_2O_3)/SiO_2$ of GGBS must exceed 1.4 and 1.6 respectively, for it to be considered suitable for blending with PC [9]. Despite these prescriptions, several studies [10-13] have shown that these ratios do not necessarily give accurate prediction of a slag's performance.

In marine environments, chloride-induced corrosion of steel reinforcement has been identified as the major cause of premature deterioration and degradation of concrete

structures [14]. These chlorides may be introduced into concrete through a variety of routes, for example as admixtures, as de-icing salts, through the penetration of seawater, through the use of aggregates contaminated with chlorides or through the mix water [5]. The presence of chlorides in concrete may cause disruption to the passive film on the surface of steel reinforcement, thereby accelerating corrosion.

Chlorides in concrete usually exist either as free ions dissolved in the pore water, or bound. The bound chlorides are either chemically bound with the tricalcium aluminate (C_3A) phase in the form of Friedel's salt or physically bound to the surface of the hydration products (C-S-H phase). It is the free chlorides present in the pore water that are responsible for steel de-passivation, so when more chlorides are bound, less free chlorides will be available for de-passivation.

Several studies concerning the use of GGBS as partial replacements for PC in the making of concrete has shown that it improves the workability, long-term strength, thermal performance, and resistance to chemical attack from aggressive environments. Lower values of the chloride diffusion coefficient and longer corrosion initiation times have been reported for concretes made from blends of PC and GGBS. This has been largely attributed to their high alumina content [15-18], which increases the propensity for Friedel's salt formation and also enables them to form more of C-A-S-H phases that also contributes to chloride binding [19].

While at a first glance, it may appear to seem that slag blends have very good long-term strength and durability properties, there are still other aspects likely to have impact on the performance of slag blends that have not been fully studied. Firstly, it is known that the chemical composition of a slag is important as it may affect its performance. However, the relationship between composition and performance is not clear-cut.

Secondly, due to the variability in the use of GGBS as a SCM in different climates, like the tropical and temperate regions, temperature would be another factor that will have an effect on the performance of slag blended cements. For example, in a typical tropical marine environment, temperatures can vary from 22°C to 35°C [20]. Several studies [21-26] have shown that high temperature accelerates the hydration of slag, leading to high early strengths. However, how this will impact on other properties such as the microstructure and resistance to ingress of aggressive ions like chlorides, have not been fully explored.

Thirdly, it is known that the degree of hydration of cement and its blends depends on the initial curing conditions. Concrete structures made from blends containing GGBS require prolonged curing due to the slow reaction between GGBS and the calcium hydroxide. However, in practice this is hardly adhered to, especially for massive concrete structures. Hence, it will be of importance to investigate how shorter curing durations would impact on the performance of slag blends.

The main aim of this study was to investigate the combined influence of difference in slag chemical composition and temperature on the performance of slag blended cements. Performance in this sense is evaluated in terms of strength and durability properties, both of which are linked to the microstructure. The effect of shorter curing durations on the durability performance was also investigated. The specific objectives are highlighted below:

- To determine the influence of slag composition and temperature on the hydration and strength development of slag blends;

- To determine the influence of slag composition, curing duration and temperature on the microstructure, relating it to water transport properties of the slag blends;

- To determine the influence of slag composition and temperature on the chloride binding capacity of slag blends;

- To determine the influence of slag composition, curing duration and temperature on the resistance of slag blends to chloride ion penetration;

- To determine the influence of curing duration and difference in exposure conditions on the chloride ingress resistance of slag blends; and

- To assess the overall performance of slag blends in high and low temperature chloride environments.

The outcome of this research provides better understanding of the interplay between microstructural properties and engineering performance, and how these can be influenced by material and environmental factors. By this, one can better understand the strengths and limitations of using GGBS as SCM in different marine environments/applications.

The study is divided into the following chapters outlined below:

- Chapter 2 – comprises of an overview on the hydration of plain and blended cement systems, and a review of chloride ingress into concrete, with emphasis on the chloride ingress resistance of slag blends

- Chapter 3 – describes in detail the materials and the methods used in carrying out the study

- Chapter 4 – shows the impact of binder composition and temperature on hydration and strength performance

- Chapter 5 – shows the impact of binder composition, temperature and curing duration on the pore structure, relating it to water transport properties

- Chapter 6 – shows the impact of binder composition and temperature on chloride binding

- Chapter 7 – shows the impact of binder composition, temperature and curing duration on the resistance to chloride ingress

- Chapter 8 – discusses the findings and implications of the study

- Chapter 9 – conclusions and further work.

Chapter 2
LITERATURE REVIEW

2.1 Properties of cementitious materials

2.1.1 Portland cement

Portland cement (PC) is a hydraulic binder, which when mixed with water, undergoes hydration to form a paste, which after hardening can retain its strength and stability even under water [3].

The chemical composition of PC is often expressed in terms of oxides of the elements. The following oxides are typically found in PC: calcium oxide CaO (C), silica SiO_2 (S), alumina Al_2O_3 (A), iron oxide Fe_2O_3 (F), magnesium oxide MgO (M), sulphuric oxide SO_3 ($\overline{S}$), and water H_2O (H). Typical composition of PC in terms of oxides is shown in Table 2.1. Once the oxide analysis has been carried out, the compound composition can be determined either by quantitative X-ray diffraction (QXRD) or by using a set of equations developed by R. H. Bogue [7]:

$$\%C_3S = 4.071C - 7.600S - 6.718A - 1.430F - 2.850\overline{S} \quad (2.1)$$

$$\%C_2S = 2.867S - 0.7544C3S \quad (2.2)$$

$$\%C_3A = 2.650A - 1.692F \quad (2.3)$$

$$\%C_4AF = 3.043F \quad (2.4)$$

A limitation of using the above equations is that it does not account for the incorporation of foreign ions/elements within the structures [27], hence the use of QXRD is becoming more common.

The compound composition of the principal clinker corresponds approximately to alite or tricalcium silicate (C_3S), belite or dicalcium silicate (C_2S), tricalcium aluminate (C_3A) and calcium aluminoferrite (C_4AF).

Table 2.1: Typical composition of Portland cement (taken from [2])

Oxide	Amount present (%)
SiO_2	19 – 23
Al_2O_3	3 – 7
Fe_2O_3	1.5 – 4.5
CaO	63 – 67
MgO	0.5 – 2.5
K_2O	0.1 – 1.2
Na_2O	0.07 – 0.4
SO_3	2.5 – 3.5
LOI	1 – 5.0
IR	0.3 – 5.0
Free lime	0.5 – 1.5

LOI: Loss on ignition ($CO + H_2O$)

IR: Insoluble residue usually siliceous

2.1.2 Secondary cementitious materials (SCM)

Common SCMs used in blending PC include: fly ash, metakaolin, silica fume and ground granulated blast furnace slag (GGBS). These SCMs usually react at slower rates than that of the individual clinker phases.

2.1.2.1 Fly ash

Fly ash, also known as pulverised fuel ash (PFA), is the ash that is produced during the combustion of coal for electricity generation. It is captured from the flue gas as it rises, before it reaches the chimney at coal-fired power plants. Its particles are amorphous and spherical in shape, ranging in size between 10 and 100 μm [5]. Fly ash may either be siliceous or calcareous in nature. Siliceous fly ash has pozzolanic properties, while calcareous fly ash has both pozzolanic and hydraulic properties

[28, 29]. Fly ash is mainly rich in silica and alumina, as seen in Figure 2.1. When used as an SCM, it can replace PC in proportions ranging from 6 to 55% by weight of PC [3].

2.1.2.2 Silica fume

Silica fume, also known as microsilica, is a by-product collected from the production of silicon and ferrosilicon alloy. It is captured from the oxidised vapour at the top of the electric arc furnace. It is an amorphous, ultra-fine powder, spherical in shape with size averaging from 0.1 to 0.5 μm [5]. It is very rich in silica, as seen in Figure 2.1. As a result of its high degree of fineness (ranging from 15000 to 20000 m^2/kg), it is seen to increase the water demand of concrete when used as a SCM [28]. Hence, it is often used to replace PC in low proportions. For example, for a CEM II/A-D type cement, BS EN 197-1:2011 [3] specifies that the proportion of silica fume in cement should not be more than 10%.

2.1.2.3 Metakaolin

Metakaolin is obtained from the clay mineral kaolinite, by a process referred to as dehydroxilization (removal of chemically bonded hydroxyl ions). The clay mineral is placed in a rotary kiln, where it is fired externally to temperatures between 500 – 800°C, so that it loses water. In terms of particle size, they are finer than PC but not as fine as silica fume, and they are not amorphous (they have a two-dimensional order crystal structure). Metakaolin is rich in silica and alumina as seen in Figure 2.1. It is highly reactive, and several standards have specified that it can be used in cementitious systems [5].

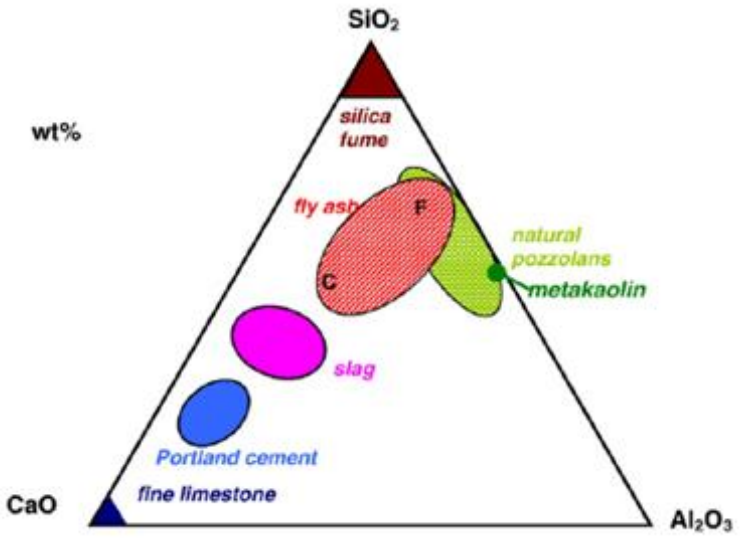

Figure 2.1: CaO-Al_2O_3-SiO_2 ternary diagram of cementitious materials (taken from [30])

2.1.2.4 Ground granulated blast furnace slag (GGBS)

GGBS is a non-metallic product, comprised mainly of silicates and aluminosilicates of calcium [9]. It is a by-product obtained from the making of iron and steel. In the production of iron, the iron oxide ore is reduced to metallic iron by means of a flux (limestone or dolomite) at temperatures of about 1400 to 1500°C [9]. During the heating process, the impurities in the iron ore comprising mainly of silica and alumina, combine with lime and magnesia to form a molten slag which is collected separately from the molten iron via the bottom of the blast furnace [31]. The molten slag collected from the blast furnace is quenched with water or steam to produce a glassy and granular material, which is grounded to a fine powder to produce GGBS.

2.1.3 Properties of GGBS that influence its reactivity

2.1.3.1 Structure

Slags that are cooled rapidly will contain a high amorphous glassy phase and minute crystalline phases. The glass fraction is generally considered to be very reactive while the crystalline part is considered to be inert [32]. The structure of the

amorphous glass phase comprise mainly of isolated or polymerised silica tetrahedral with bridging oxygen atoms (Figure 2.2). These silicates are mostly present as monomers and dimers [32]. Cations such as Ca^{2+} or Mg^{2+}, referred to as network modifiers, are often coordinated in the cavities of the network to neutralise the negative charges resulting from the Si-O-Si covalent bonds. The coordination of calcium atoms are considered as octahedral while that of magnesium atoms as either octahedral or both octahedral and tetrahedral [33]. Aluminium can also be coordinated as a network modifier, in the forms of Al^{3+}, AlO^{+} or AlO_4^{5-} [33-36]. The tetrahedral atoms are the network formers while the octahedral atoms are the network modifiers [37]. Higher number of network modifiers present in the structure will result in a smaller polymerisation degree, and higher reactivity of the slag [36].

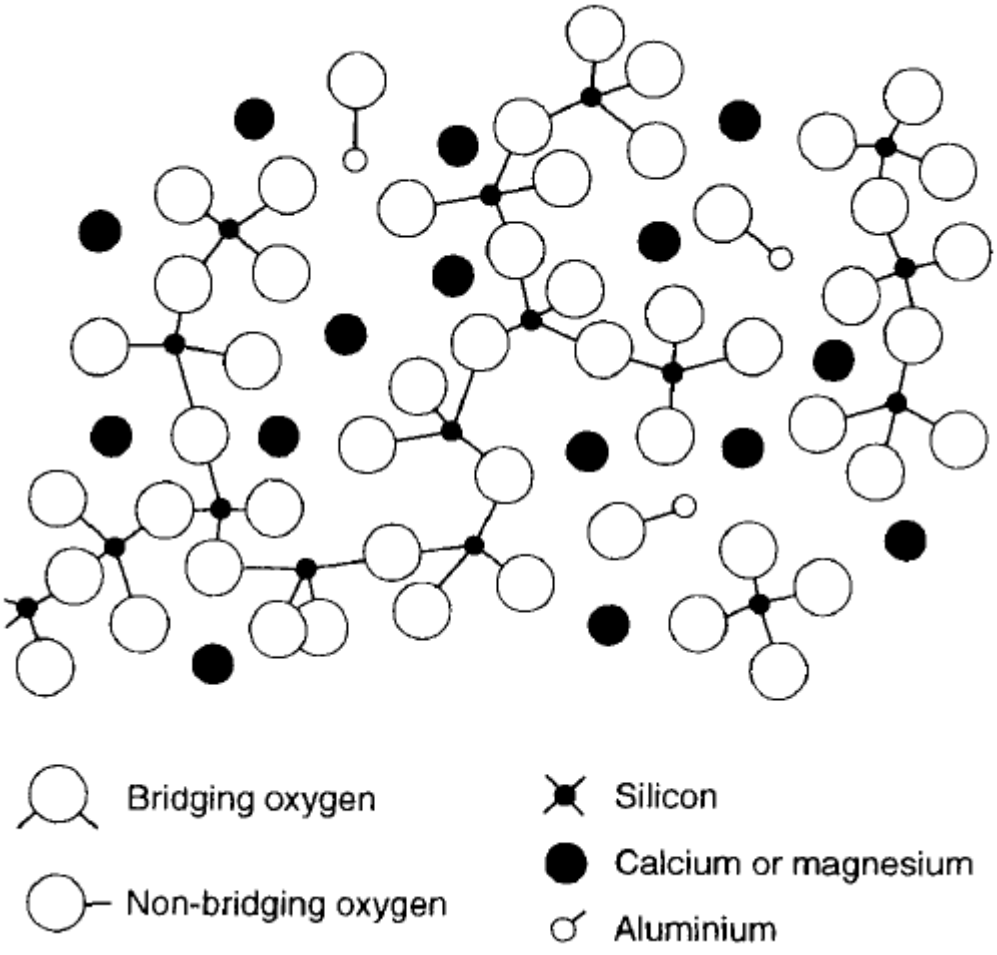

Figure 2.2: Schematic structure of a glassy slag (taken from [9])

2.1.3.2 Physical properties

The physical characteristic of GGBS is described mainly by its colour, fineness, glass content and bulk density. In terms of colour, it ranges from beige to dark to off-white depending on moisture content, but when ground it is usually white in colour. Its bulk density varies between 1200 – 1300 kg/m^3 [31]. GGBS has almost the same fineness and specific surface area as that of PC particles [4]. It is glassy in nature and latently hydraulic.

The fineness of GGBS is very important as it influences its reactivity. According to Swamy [38], an increase in fineness of slag to two or three times that of ordinary PC will lead to enormous improvement in a variety of engineering properties such as bleeding, setting time, heat of evolution, strength and durability.

The degree of fineness of GGBS depends on the efficiency of the method of grinding, which can be different for various countries. For instance, in the United Kingdom, GGBS is marketed at a surface area of 375–425 m^2/kg Blaine's, whereas some slags in the United States have a surface area in the range of 450–550 m^2/kg; Canadian slags are about 450 m^2/kg, while in India it is found to vary from 350 to 450 m^2/kg Blaine's [12]. According to Wan *et al.* [39], at the same composition of GGBS, grinding techniques becomes a primary factor that determines the particle geometric characteristics of the GGBS.

The glass content of GGBS also has considerable effect on its reactivity, and it is influenced by the rate of quenching of the molten slag. In a typical XRD pattern of a slag glass, the glassy part of the slag will appear as a large hump peaking at *d*-values of about 0.3 nm (Figure 2.3); while the crystalline fraction comprising mainly of melilite, merwinite, calcite and quartz, will appear as little peaks around the large

hump [33, 36]. Typical glass content of GGBS vary between 85 and 99% [31]. BS EN 197-1:2011 [3] specifies that at least two-third of the mass of the slag must be glassy, although research data show that slag samples with as little as 30 – 65% glass contents are still suitable [12].

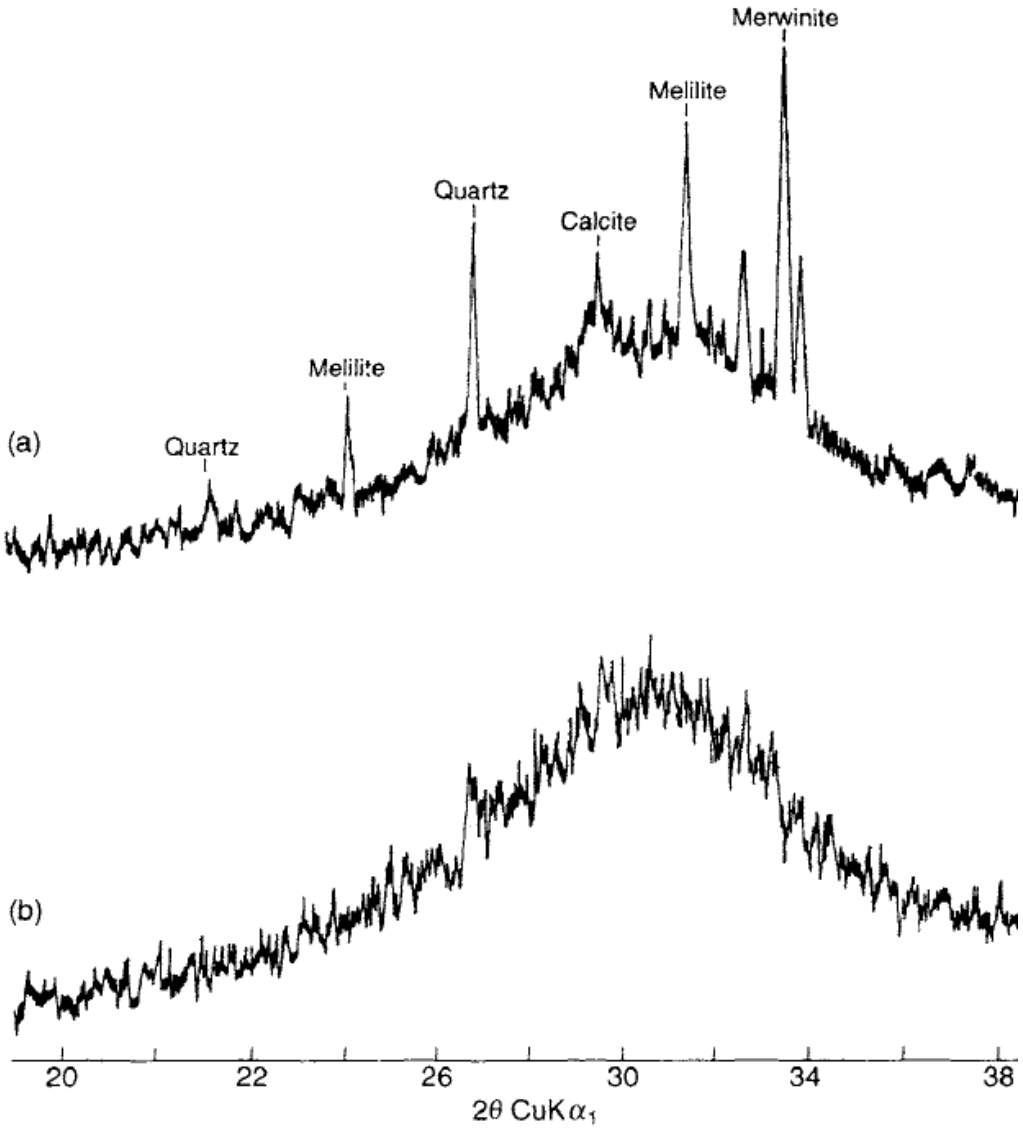

Figure 2.3: XRD patterns of two slags (a) glass + crystals (b) glass (taken from [9])

2.1.3.3 Chemical composition

The chemical composition of slag can vary over a wide range depending on the nature of the ore, the composition of the limestone flux, coke consumption and the

type of iron being made. It can also change over the years with alterations in the sources and types of ore being smelted [9].

Table 2.2 shows typical chemical composition of slags obtained from various sources. In general, the lime content may be in the range 30 – 50%, silica 28 – 38%, alumina 8 – 24%, magnesia 1 – 18%, sulphur 1 – 2.5% and ferrous and manganese oxides 1 – 3%. Other minor components are TiO_2, which is usually less than 4%, and $Na_2O + K_2O$, which is less than 2% [9].

Table 2.2: Typical oxide composition of GGBS (taken from [9])

Oxide	UK	Canada	France	Germany	Japan	Russia	S. Africa	USA
CaO	40	40	43	42	43	39	34	41
SiO_2	35	37	35	35	34	34	33	34
Al_2O_3	16	8	12	12	16	14	16	10
MgO	6	10	8	7	5	9	14	11
Fe_2O_3	0.8	1.2	2.0	0.3	0.5	1.3	1.7	0.8
MnO	0.6	0.7	0.5	0.8	0.6	1.1	0.5	0.5
S	1.7	2.0	0.9	1.6	0.9	1.1	1.0	1.3

2.1.3.4 Hydraulicity of slags

Hydraulicity is the term often used to describe the ease with which slag reacts with water. It depends mainly on its chemical composition, glass content, particle fineness, alkalinity of the reacting system and temperature at the early stages of hydration [6]. The oxides of calcium, magnesium and aluminium are known to increase the hydraulicity of GGBS, while that of silicon and manganese decreases it [8]. MgO has the same influence as CaO up to about 11% by weight [9]. The influence of P_2O_5 depends on the clinker type and test age, but generally has a

positive influence beyond 28 days of curing. Oxides of tin and iron, as well as sulphur, seem not to have any effect.

Increasing the Al_2O_3 content to 13% and above will result in an increase in early strength and a decrease in the later strength [37]. Wang *et al*. [40] observed a positive correlation between the Al_2O_3 content and the reactivity of the slags, for slags having a CaO content greater than 37%. In another study by Haha *et al.* [8, 41], it was observed that the reactivity of the slags increased with the magnesia content. As they increased the alumina content, the reactivity of the slags were reduced at early ages, but became similar at later ages beyond 28 days. Perhaps, the reason for the reduced reactivity observed in the study by Haha et al. [8], may be due to the CaO content of the high alumina slags, which in their case was less than 37%.

Ratios of some of these oxides have been used by various standards to assess the hydraulicity of a slag. For example, EN 197-1:2011 [3] prescribes that for GGBS, the $(CaO + MgO)/SiO_2$ ratio by mass must exceed 1. Several workers [9, 10, 12], have also suggested other oxide ratios, some of which are shown in Table 2.3. However, previous studies [10-13] have shown that these ratios do not necessarily give accurate prediction of a slag's performance.

Another parameter often used in assessing the reactivity of slags is the activity index (SAI). SAI is defined as the percentage ratio of the average compressive strength of slag cement (50 – 50%) mortar cubes to the average compressive strength of reference cement mortar cubes at a designated age [42]. It is expressed as SP/P x 100, where SP is the average compressive strength of the slag-reference cement mortar cubes and P is the average compressive strength of the reference cement

mortar cubes. SAI values recommended for slags at 7 and 28 days according to BS EN 15167-1:2006 [42] are also shown in Table 2.3.

Table 2.3: Formulas proposed for assessment of hydraulicity of GGBS

	Basicity/hydraulic index	Requirement for good performance	Remarks
P1	CaO/SiO_2	1.3 – 1.4 [12]	Mantel [11] proposed for medium-fine slags of 350 kg/m^2, P1 or P2 must be greater than 1.0
P2	$(CaO + MgO)/SiO_2$	> 1.0 [3]	
P3	$(CaO + MgO)/(SiO_2 + Al_2O_3)$	1.0 – 1.3 [12]	Here Al_2O_3 is assumed to have a negative influence
P4	$(CaO + MgO + Al_2O_3)/SiO_2$	≥ 1.0 [9]	In Japan, must be ≥ 1.4 [9]; while in S. Korea, must be ≥ 1.6 [43]
P5	$(CaO + 0.56Al_2O_3 + 1.4MgO)/SiO_2$	≥ 1.65 [12]	
P6	Al_2O_3/SiO_2	0.53 – 0.55 [44]	
	Activity index		
	7 day	> 45% [42]	
	28 day	> 70% [42]	

2.2 Overview of hydration of cementitious materials

2.2.1 Hydration of Portland cement

The hydration of PC involves the reactions between the individual clinker minerals (alite, belite, and tricalcium aluminate and calcium aluminoferrite), calcium sulphate and water. The reactions occur simultaneously, and at different rates to produce C-S-H as the main hydrate, intermixed with portlandite (CH), ettringite and the AFm phases. The rate and progress of this reaction is dependent on the dissolution rate of

the starting materials, the rate of nucleation and growth of the hydrates formed, and the rate at which water and dissolved ions diffuse through the hydrates formed [45].

The process starts as soon as the cement comes in contact with water. This initial reaction is exothermic resulting in a high heat output. During this period, a rapid dissolution of the individual clinker phases and calcium sulphate begins, yielding hydrated products. The dissolution of C_3S results in the precipitation of a layer of a C-S-H phase at the surface of the cement grain. C_3A and C_4AF also dissolve in like manner, reacting with calcium sulphate to form ettringite that is precipitated on the cement grain surface. This initial rapid reaction appears to slow down after a few minutes, resulting in a low heat output. After the slow reaction period, another period of accelerated hydration is seen, which is influenced mainly by the nucleation and growth of the hydration products. The heat output reaches its maximum during this acceleration period, and soon starts to decline due to a decrease in the hydration rate [45-51].

2.2.1.1 Alite or tricalcium silicate (C_3S)

Tricalcium silicate (C_3S) is the most abundant phase of Portland cement, constituting from 50 to 80% [52, 53]. It has different polymorphs, and its structure can vary from rhombohedral to monoclinic and to triclinic, depending on the transformation temperature [52]. Alite is an impure form of C_3S, which is what is often found in PC systems. The difference between pure C_3S and alite is due to the incorporation of minor elements in the solid solution, and to the cooling methods often used in the industrial production of clinker [53]. Minor elements or compounds such as magnesium, iron, aluminium, alkalis and sulphates, are often found in alite. The inclusion of these elements determine the stability, structure and reactivity of the alite phase [45]. For example, Maki and Goto [54] discovered that

the addition of large amounts of sulphates and magnesium to pure C_3S favoured the formation of M_1 and M_3 alite respectively.

Hydration of C_3S:

The reaction of C_3S with water is complex and has received a lot of attention in recent studies [50, 53, 55, 56]. The hydration of C_3S at temperatures ranging from 0°C to about 100°C, results in the formation of a poorly crystalline calcium silicate hydrate (C-S-H) and calcium hydroxide, according to the expression below:

$$3CaO.SiO_2 + (3 + m - n)H_2O \rightarrow nCaO.SiO_2.mH_2O + (3 - n)Ca(OH)_2$$

1. C-S-H phase

C-S-H has the general formula nCaO.SiO_2.mH2O. The numbers *n* and *m* denotes the CaO/SiO_2 (C/S) ratio and the water content of the C-S-H phase respectively. The published values for the C/S ratio of the C-S-H phase present in matured C_3S paste ranges from about 1.4 to 2.0 [57-59]. For a CEM I system, the C/S and H/S ratio of C-S-H has been found not to be dependent on the degree of hydration. The C/S ratio decreases with increasing water/solids (w/s) ratio [57, 58, 60], while at a particular degree of hydration, the H/S ratio will increase slightly as the w/s ratio increases [45].

The structure of the C-S-H phase resembles that of the crystalline phases of 1.4 nm tobermorite and jennite (shown in Figure 2.4). The chemical formula of 1.4 nm tobermorite is $[Ca_4(Si_3O_9H)_2]Ca.8H_2O$, while that of jennite is $[Ca_8(Si_3O_9H)_2(OH)_8]Ca.6H_2O$. Both have their SiO_4 tetrahedral compressed into linear chains that are interlocked in such a way that they repeat at constant intervals of three tetrahedral, in an arrangement referred to as ‘dreierkette’ [45]. Both also have similar structures, the main difference being the presence of

hydroxyl groups linked to the calcium atoms in jennite as opposed to oxygen atoms in the case of tobermorite.

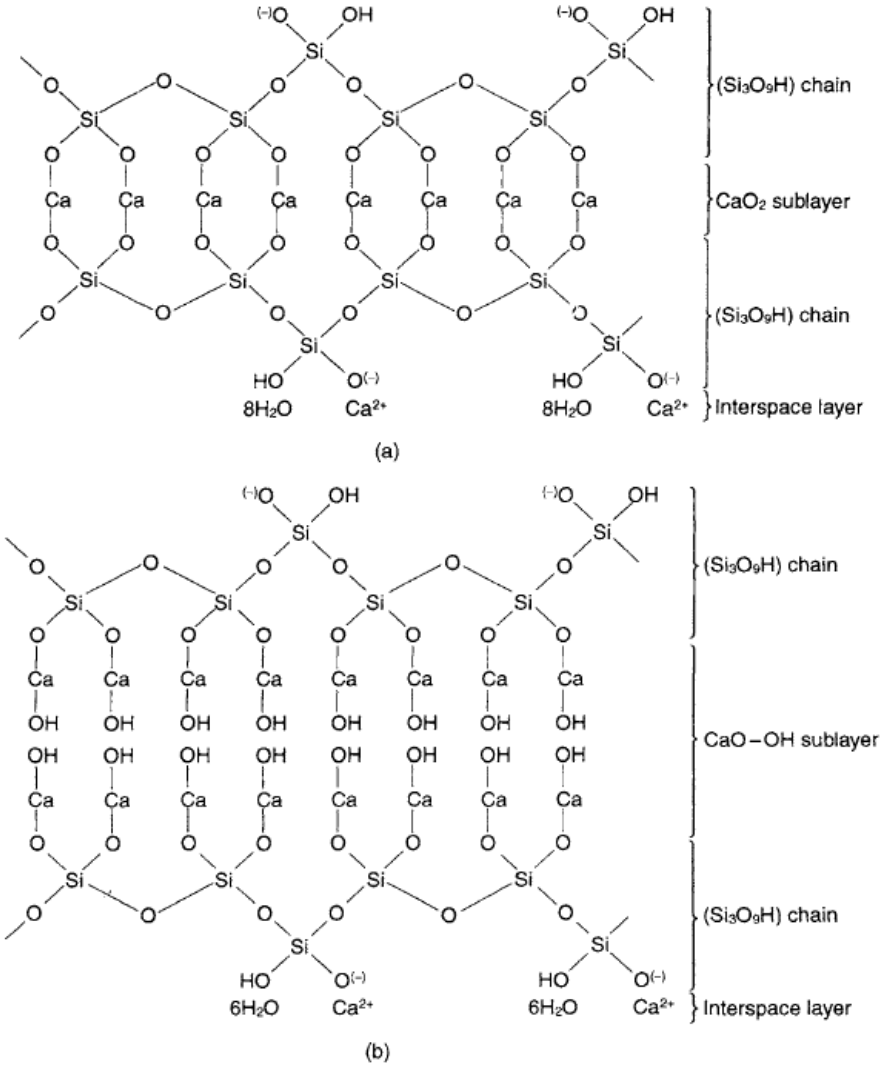

Figure 2.4: Idealised chemical structure of (a) 1.4nm tobermorite and (b) jennite (taken from [45])

C-S-H has an outer and inner product (Op and Ip respectively). The Op usually form within the spaces originally filled with water, while the Ip tend to form at the confines of the original C_3S grains [61]. In mature C_3S and neat cement pastes, the Op C-S-H as observed by TEM, adopts a fibrillary morphology that is influenced by the amount of space available. The fibrils adopts a coarse morphology when they form in large pore spaces, and appear as fine fibrils when

they form in smaller spaces [61]. On the other hand, the Ip C-S-H has a dense, fine and uniform morphology, consisting of only gel pores [61].

2. $Ca(OH)_2$ phase

Calcium hydroxide is the second hydration product formed from the hydration of C_3S. In C_3S or neat cement paste, it precipitates in the form of CH crystals, which are evenly dispersed within the hardened paste. The structure of CH is hexagonal, comprising of octahedral integrated calcium ion layers and tetrahedral integrated oxygen layers with hydrogen bound to oxygen [45].

Hydration kinetics and mechanism:

The rate of hydration of C_3S is affected by its intrinsic properties such as the presence of foreign ions in the system, and structural defects induced in the crystalline lattice due to rapid cooling at the stage of preparing C_3S [62, 63]. Mixing C_3S in water containing salts has also been reported to affect the kinetics of C_3S hydration. For example, chlorides accelerates the hydration of C_3S, whereas phosphates, borates and salts of Zn^{2+} and Pb^{2+}, retards it [45]. According to Montanaro *et al.* ([64] cited in [45]), the addition of anhydrite or gypsum and calcium carbonate can also accelerate the hydration of C_3S, as well as an increase in temperature [65, 66].

The hydration occurs in four main stages which are: a pre-induction or initial reaction period, an induction or slow reaction period, acceleration and a deceleration period, as shown below in Figure 2.5.

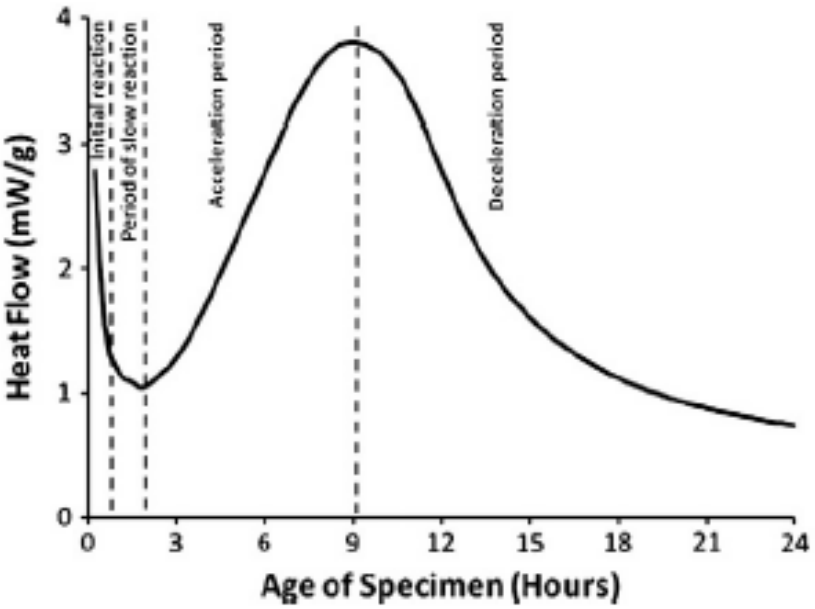

Figure 2.5: Isothermal calorimetry measurements showing the rate of alite hydration as a function of time (taken from [50])

Pre-induction period:

This period begins immediately after C_3S comes into contact with water. This stage only lasts for few minutes and is usually accompanied by an intense liberation of heat [45]. During this stage, the hydration rate reaches a value of about 5/day but immediately decreases to very low values (as shown in Figure 2.5).

There have been several debates on the mechanism governing this early deceleration of the hydration of C_3S, and many hypotheses have been postulated, two of which have been discussed here.

1. **Impermeable hydrate layer hypothesis**

   According to this hypothesis, the deceleration of the C_3S hydration is caused by a rapid formation of a thin protective hydrated layer on the surface of the C_3S grains. This layer acts as a barrier, which restricts the movement of water into the surface and the diffusion of ions away from the surface ([67, 68] cited in [50]). It is not very clear if this hydrated layer is C-S-H or a

modification of the anhydrous C_3S. A major issue with this theory was the lack of direct experimental evidence backing the existence of this layer [50, 53]. However, through the use of nuclear resonance reaction analysis, some researchers [69, 70] were able to verify the existence of this early hydrated layer. Despite this, there is still the challenge of demonstrating that this hydrated layer has the potential of creating a protective/passivating layer on C_3S that will explain the transition to the induction period.

2. **Slow dissolution step hypothesis**

This hypothesis stemmed out of an initial study by Barret *et al*. [71, 72], where it was proposed that a "superficially hydroxylated layer" forms on the C_3S surface when it comes into contact with water, and that ions dissociate from this layer at a very slow rate. Nonat *et al*. [73-76] used this explanation to formulate the mechanism governing the deceleration of C_3S hydration at the pre-induction period. They based it on a steady state balance between the slow dissolution of C_3S and the initial slow growth of C-S-H. The slow growth of C-S-H results in a decrease in the concentration of silicate in the solution and an increase in the C/S ratio. After a few minutes, a steady state condition (induction period) is reached, where the solution becomes supersaturated with C-S-H but under saturated with C_3S.

Induction period or dormant period:

This period begins immediately after the pre-induction period, and may last for a few hours, depending on the system. It can be shortened by incorporating prehydrated C_3S while mixing with water, increasing particle fineness by prolonged

grinding, and using higher w/s ratios; while it can be elongated by slow cooling of the sample, long lasting storage and doping with Al_2O_3 [63, 77].

In alite and C_3S systems, where retarders and heat treatment have not been used, the induction period is barely noticeable as seen in Figure 2.6. In such systems, the induction period is taken as the minimum in the hydration rate that is reached after the pre-induction period, and just before the start of the acceleration period [51].

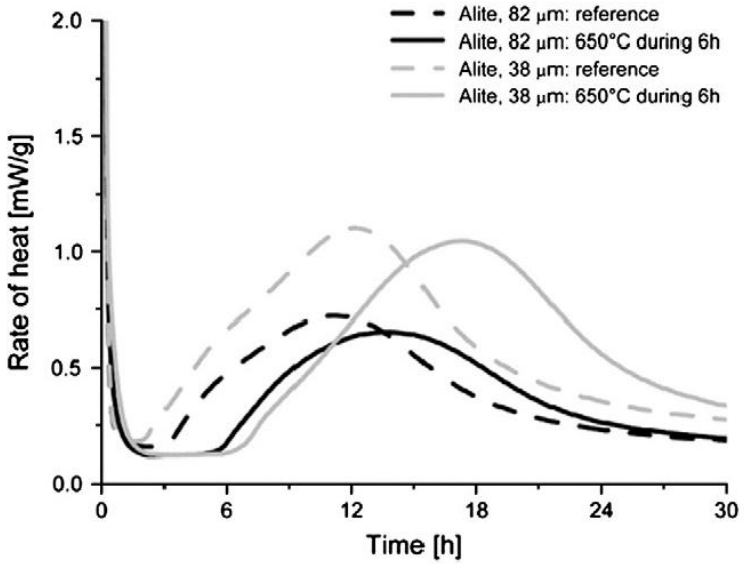

Figure 2.6: Heat evolution showing the effect of heat treatment and particle size distribution on the length of the induction period in the hydration of alite (taken from [50])

Acceleration period:

This follows the induction period, and is characterised by a sudden increase in the hydration rate, reaching values of about 1/day [45]. The start of this period coincides with the onset of the second main heat evolution peak (Figure 2.5).

While it is generally ascertained that the rate of hydration in the acceleration period is controlled by the nucleation and growth of C-S-H [45, 50], it is still not clear as to when this period actually begins. In an earlier study by Young *et al*. [78], it was shown that in paste systems having low w/s ratio, the beginning of the acceleration

period was associated with the precipitation of crystalline calcium hydroxide. This was confirmed later by studies done by [79, 80]. However, in paste systems having high w/s ratios, the acceleration period was seen to commence ahead of the precipitation of crystalline calcium hydroxide [80]. This implies that the commencement of the acceleration period is dependent on the w/s ratio of the system, but may also be influenced by other factors such as the particle fineness and heat treatment process as seen in Figure 2.6.

Deceleration period:

This period is characterized by a gradual decrease in the hydration rate, as the reaction slows down due to a complete consumption of the C_3S [6]. It is widely accepted that this later stages of the reaction is controlled by a diffusion process. However, recent studies have shown that it can also be influenced by several factors including: lack of space, lack of water, and the effect of particle size distribution [50, 81, 82].

2.2.1.2 Belite or dicalcium silicate (C_2S)

Pure C_2S also has different polymorphs, depending on the transformation temperature [45, 83]. The β-C_2S is the most common form found in PC clinker. In its impure form, it is referred to as belite [45]. Similar to alite, belite can also accommodate foreign ions such as Mg^{2+}, Al^{3+}, Fe^{2+}, K^{+}, B^{3+}, sulphates and phosphates, in its crystalline lattice [84-86].

The reactivity of belite is influenced mainly by the type and quantity of the foreign ion (dopant) incorporated during preparation. When the same dopant is used, the reactivity increases as the burning temperature [87] and decreases with repeated firing ([88] cited in [45]).

The reaction of C_2S with water yields similar products as C_3S as shown below:

$$2CaO.SiO_2 + (2 + m - n)H_2O \rightarrow nCaO.SiO_2.mH_2O + (2 - n)Ca(OH)_2$$

The rate of hydration of belite increases as the fineness of the C_2S grains, hydration temperature and the w/s ratio [88-90]. The mechanism of hydration is similar to that of C_3S, although the whole process occurs at a much slower rate [45].

2.2.1.3 Tricalcium aluminate (C_3A)

The crystal structure of pure tricalcium aluminate (C_3A) is cubic. However, it can take the form of orthorhombic or monoclinic, when it is doped with foreign elements like sodium [45]. The reactivity of C_3A depends on the type and quantity of the foreign ion it is doped with.

The reaction of C_3A with water in the absence of sulphate leads to flash set. As a result, calcium sulphate (gypsum) is usually added to PC clinker during grinding so as to delay the hydration and give more time for the placement of the concrete [91].

Hydration of C_3A in the absence of sulphate:

At ambient temperature, C_3A reacts with water in the absence of calcium hydroxide to form hexagonal crystals of C_2AH_8 and C_4AH_{19}. C_2AH_8 and C_4AH_{19} belong to the broad group of AFm phases with the general formula $[Ca_2(Al,Fe)(OH)_6]X.xH_2O$. Both phases later convert to a metastable hydrogarnet phase C_3AH_6, which has a cubic structure [92-95]. Several factors such as the hydration temperature, w/s ratio, and the fineness of the C_3A grains, affect the rate of conversion. At higher temperatures of about 80°C, the hydration of C_3A results in a direct formation of C_3AH_6 [45]. When calcium hydroxide is present, the rate of hydration of C_3A is

slowed down and C_4AH_{19} is the only product formed, which later converts to C_3AH_6.

Similar to the hydration mechanism of C_3S, the hydration rate of C_3A decelerates a few minutes after mixing with water. The reason for this is generally attributed to the formation of a protective layer of hexagonal hydrates (C_2AH_8 and C_4AH_{19}) at the surface of the C_3A grains, which acts as a barrier. However, as these hydrates are converted to the metastable cubic form C_3AH_6, this layer becomes disrupted and hydration continues at a much higher rate [93-95].

Hydration of C_3A in the presence of sulphate:

The reaction of C_3A with water in the presence of calcium sulphate results mainly in the formation of ettringite $C_6A\bar{S}H_{12}$ (trisulphate) as shown below [45]:

$$C_3A + 3C\bar{S}H_2 + 26H \rightarrow C_6A\bar{S_3}H_{32}$$

Ettringite is a member of the family of AFt phases having the general formula $[Ca_3(Al,Fe)OH_6]X_3.xH_2O$, where X denotes a formula unit of a doubly charged anion, e.g. SO_4^{2-}. The structure of ettringite is trigonal [45], while the morphology upon formation is dependent on the amount of free space available for crystal growth [45].

On depletion of the sulphate source, the initial ettringite formed reacts with any remaining unreacted C_3A to form a calcium aluminate monosulphate hydrate $C_4A\bar{S}H_{12}$ (monosulphate) as shown below [45].

$$C_6A\bar{S_3}H_{32} + 2C_3A + 4H \rightarrow 3C_4A\bar{S}H_{12}$$

The initial reaction with water in the presence of calcium sulphate is rapid, resulting in the release of a significant amount of heat, after which it is slowed down. This period where the reaction rate is slowed down is similar to the induction period in the hydration of C_3S, and its length is influenced by the amount of calcium sulphate present [91, 96-98].

Several hypotheses have been put forward to explain the kinetics of the hydration within this induction/dormant period. The most common of them postulates that the ettringite formed from the initial reaction accumulates on the surface of the C_3A grains and acts as a protective layer inhibiting further reaction of the C_3A [96-98]. This hypothesis was however questioned by the results from an earlier study by Mehta [99], which showed that the accumulated ettringite layer was not dense enough to inhibit hydration. In another study by Birchall *et al.* [100], it was assumed that the slowing down in the hydration process was due to the formation of an amorphous layer at the C_3A surface that acted as an osmotic membrane. In an earlier study by Skalny and Tadros [101], it was reported that C_3A dissolves incoherently in the solution, depositing a layer rich in aluminium on the surface of the unreacted C_3A. Calcium and sulphate ions are then adsorbed unto this layer, resulting in a reduction in the amount of dissolution sites. This was later confirmed in a study by Minard *et al.* [91], where the slow hydration rate in the induction period was attributed to the adsorption of sulphate ions on reactive sites, leading to a reduction in the dissolution rate of C_3A.

2.2.1.4 Calcium aluminoferrrite (C_4AF)

The composition of calcium aluminoferrite (commonly abbreviated as C_4AF) is generally of the form $C_2(A_xF_{1-x})_2O_5$. The structure comprises of layers of octahedral FeO_6 and tetrahedral FeO_4 bridged by Ca^{2+} ions. In impure form, it contains ions of

Mg^{2+}, Si^{4+}, and Ti^{4+}. The reactivity of C_4AF depends mainly on the Al/Fe ratio. It generally decreases as the Fe content increases, and increases with increasing fineness and temperature [102, 103].

The hydration products formed from the reaction of C_4AF with water are similar to those of C_3A, although the hydration rate is much slower as compared to that of C_3A. When C_4AF reacts with water in the absence of sulphates, $C_2(A,F)H_8$ and/or $C_4(A,F)H_x$, which are members of the AFm group, are formed as the initial products [102, 104-106]. These phases are later converted to an iron-containing hydrogarnet phase $C_3(A,F)H_6$ [102, 104, 105]. As in C_3A, at higher temperatures, this conversion does not occur, as $C_3(A,F)H_6$ is formed directly [102]. In the presence of sulphates, an AFt phase, $C_6(A,F)\overline{S}_3H_{32}$, is formed as the main hydration product [103, 106-109], which is later converted to an AFm phase $C_4(A,F)\overline{S}H_{12}$. The later reaction resulting in the formation of the AFm phase is usually initiated even before the complete depletion of the calcium sulphate, and at higher temperatures and low w/s ratios, the AFm phase may be formed directly [109].

2.2.1.5 Factors influencing PC hydration

There are several factors that affect the hydration kinetics of PC, including [45]:

- The phase composition and processing history of the clinker;
- The type and quantity of the calcium sulphate present in the cement;
- The fineness of the cement;
- The water/cement (w/c) ratio of the mix;
- The curing conditions (e.g. cured under water or ambient conditions);

- The hydration temperature; and
- The presence of admixtures or SCMs

2.2.1.6 Influence of temperature on PC hydration

Increasing the hydration temperature results in an increase in the rate of hydration of PC, this effect being more pronounced at the early stages of hydration than at the later stages [110-112]. In comparing the effect of high temperature curing on the individual clinker phases, Kjelson and Detwiler [113] found the hydration of C_2S to be significantly accelerated at higher temperatures even after months of mixing.

In terms of the hydration products, the hydration of C_3S and C_2S at temperatures ranging from 0 to 100°C results in the formation of an anhydrous C-S-H and calcium hydroxide. The composition of C-S-H is sensitive to temperature. Increasing the temperature from 5°C to about 60°C will result in a slight change in the C/S ratio, and a significant decrease in the H/S ratio, coupled with an increase in the degree of polymerisation [114, 115].

As the hydration temperature increases, the amount of SO_4^{2-} reversibly bound to the C-S-H phase increases. This leads to a reduction in the amount left to react with C_3A, and an increase in the amount of AFm formed in preference to AFt [111, 112, 116]. At temperatures of about 70°C, the concentration of SO_4^{2-} ions in the solution becomes so low that AFt is no longer formed. There is also an increase in the amount of Al^{3+} bound within the C-S-H phase as the hydration temperature increases [112, 115, 116].

A reduction in the bound water content of the C-S-H phase at higher temperatures, results in an increase in the capillary porosity of the paste. Gallucci *et al*. [114]

attributed this increase in capillary porosity to the apparent density of the C-S-H, which increases with temperature. Microstructural observations by several workers [113, 115, 117, 118], showed that the microstructure was coarser and more irregular at higher hydration temperatures. The presence of 'shells', whose density increased with increasing temperature, was also observed around the unreacted cement grains [113, 119].

2.2.1.7 Influence of the presence of SCMs on PC hydration

The hydration of blended systems is more complex than that of ordinary PC, as both constituents react simultaneously with water, and may even influence the reactivity of each other [30].

Influence on the hydration products formed:

The addition of SCMs to PC leads to the formation of a C-S-H phase having similar composition as that formed when SCMs are not used. However, the C-S-H formed has a lower C/S ratio and an increased mean silica chain length, due to the higher silica content of the SCMs [30]. The morphology of the C-S-H has also been reported to change from fibrillary to foil-like. This foil-like morphology is mainly the reason for the improved transport properties observed in composite systems [59]. Using SCMs rich in Al_2O_3, results in the formation of C-A-S-H, with the silicon atoms in the C-S-H replaced by aluminium atoms at the bridging sites [120, 121]. When such SCMs are used in high replacement levels, the quantity of aluminium atoms that can be incorporated in the C-S-H becomes exceeded, leading to the precipitation of stratlingite, which is often intermixed with the C-S-H [122, 123]. Figure 2.7 shows the hydrated phases present in the CaO-Al_2O_3-SiO_2 system.

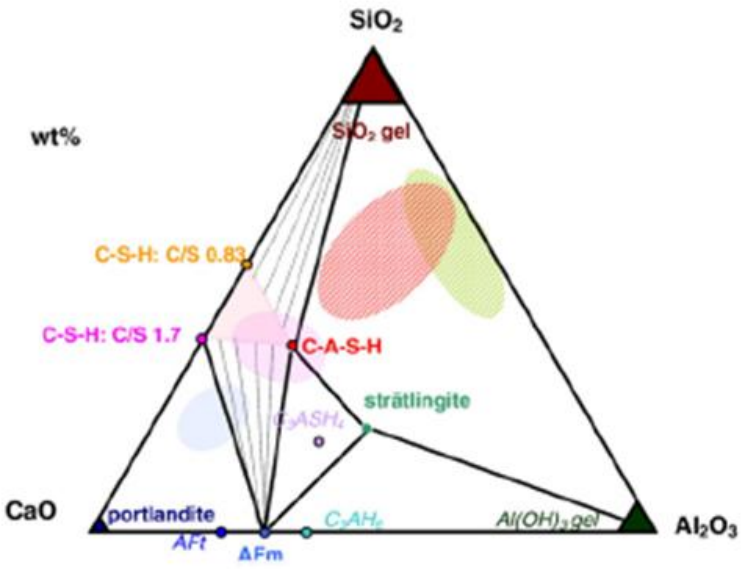

Figure 2.7: Hydrated phases present in the CaO-Al_2O_3-SiO_2 system (taken from [56])

Influence on the hydration kinetics:

It is generally agreed that the presence of SCMs alter the hydration kinetics of the individual clinker phases. At the initial stage of the hydration, usually within the first day, the SCMs do not react but mainly act as fillers. This filler effect is generally attributed to two main mechanisms [30]:

1. **Extra space**

   Since the SCMs do not react during the very early stages of hydration, given the same w/s ratio, the water/clinker ratio becomes higher and more space becomes available for the precipitation of the hydration products of the clinker phases.

2. **Enhanced nucleation**

   This occurs mainly in systems where the fineness of the SCM particles is greater than that of the cement. It is generally assumed that the extra surface provided by the SCM grains acts as nucleation sites for the

precipitation of the hydration products of the clinker phases. However, in a recent study by Berodier and Scrivener [124], it was shown that the acceleration caused by the filler effect is due mainly to the extra shearing produced by the presence of the SCM particles rather than the extra surface provided.

Figure 2.8 shows an illustration of the filler effect for a PC blend containing 10% of silica fume, taken from the study by Lothenbach *et al*. [30]. The heat evolution curve was normalized to the clinker content. It can be seen that in the blended system, the acceleration period commenced ahead of the neat system. Also, the peak of the heat curve was much higher for the blended system, as compared to the neat system. This was attributed to the finer particles of the silica fume acting as nucleation sites for the precipitation of the C-S-H and CH phases.

This same acceleration effect has been observed for the aluminate peak of PC slag blends, and this has been generally attributed to an early reaction of the slag itself [115, 125, 126]. However, in a recent study by Kocaba [44], it was suggested that the SCMs do not react but rather enhance the nucleation of the hydrates formed during the reaction of the aluminates. Other studies [127-129] have also reported different effects of SCMs on the hydration of the aluminate phases (C_3A and C_4AF). For example, Dittrich *et al*. [128] showed that soluble sulphates from fly ash may lead to a retardation in the reaction of the C_3A. The use of metakaolin [127] and zeolites [129] as SCMs was also observed to alter the amount of sulphate ions present in the solution, thereby resulting in undersulphation of the systems.

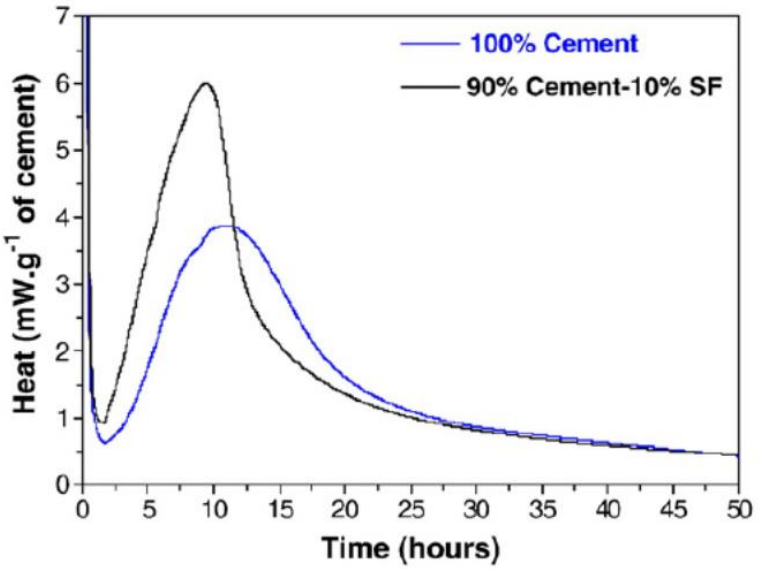

Figure 2.8: Heat evolution of a 100%PC paste compared to a 90% PC–10% SF blend, showing the filler effect (taken from [30])

2.2.2 Hydration of slag blended cements

In the hydration of PC slag blend, both constituents react simultaneously with the water to yield hydration products. The initial hydration of slag is much slower than that of PC [12], and usually no hydration product is observed to be formed when GGBS is placed alone in water. However, Regourd *et al.* [130], observed via X-ray photoelectron spectrometry (XPS) that the surface of the slag grains were modified upon contact with water, but it was not clear if these modifications were forms of hydrated products.

The hydration of slag involves activation of the GGBS by alkalis and sulphates to form its own hydration products. The crystalline part of the slag does not hydrate but interferes only as fine aggregate or crystallization seed [131]. Typical hydration products formed are C-S-H and hydrotalcite; however, some other hydration products have been reported. For example, C_4AH_{13} and C_2ASH_8 were formed as hydration products in slags activated by NaOH [132]. Slags rich in alumina formed

stratlingite [8, 30], while using sulphates as activator resulted in the formation of ettringite [133].

In terms of the nature of the hydration products formed, Richardson *et al.* [134] observed that the Op C-S-H of alkali activated slags had a foil-like appearance, and was partly crystalline. There was a difference in the morphology of the C-S-H found in the slag hydration rims compared to those found in the originally water filled space, the former having a finer morphology. The C/S ratios of the C-S-H formed were lower compared to those formed in the hydration of clinker, while the Al/Si ratios were higher [8, 61, 135]. Magnesium released from the slag hydration was not incorporated in the C-S-H, but reacted to form a hydrotalcite-like phase having a lower Mg/Al ratio [136-138]. The C-S-H in PC usually has a composition of 1.5-1.9CaO.SiO_2.nH_2O, with the number *n* depending on the relative humidity and temperature. The addition of GGBS, which is richer in silica compared to PC, as shown in Figure 2.1, results in the formation of C-S-H phases with lower C/S ratios, having a tobermorite-like structure $(CaO)_{0.83}SiO_2.(H_2O)_{1.5}$ [30].

Mechanism of slag hydration:

Tanaka *et al.* [139] carried out a study on the hydration mechanism of slag. In their study, glassy discs were zebra-coated with gold and hydrated. The hydrated glassy discs were inserted into PC paste. Cross-sections of the glassy discs were later observed under SEM. They found that there were three hydrated layers – a skeleton, inner and outer hydrated layer. The skeleton hydrated layer appeared porous, containing grains of type III C-S-H, while the inner hydrated layer appeared dense and crystalline. The explanation they gave was that the surface of the slag was first coated by PC hydrates, and then bombarded by Ca^{2+} ions from the supersaturated solution. As the Ca^{2+} and Al^{3+} ions of the slag dissolved in the solution, a skeleton

hydrated layer was formed which gradually transformed into an inner hydrated layer. Barker [140] also observed a type of hydrate zoning in PC slag blends that were hydrated at ambient temperature. Feng *et al.* [141] conducted studies on 60–40 and 50–50 PC-slag blends, and observed the formation of a gel-like layer surrounding the slag grains. This layer had higher silica content and was denser than the hydrates of the Portland cement, and its composition and microstructure changed with time.

In another study [142], synthetic glass having similar chemical composition to GGBS, was activated using a 0.1N KOH and observed by SEM and TEM. Similar to the findings of Tanaka *et al.* [139], three different zones were observed in the hydrated layer: an internal fibrous layer containing the residual glass together with some lamellae, a lamellar layer of hydrotalcite-like phase, and an outer layer comprising of granular C-S-H. It was suggested that the hydration kinetics was governed mainly by two processes: (1) nucleation growth of the calcium silicates, C-S-H and carbonates, and (2) a reordering of the remaining Si-Al hydrated glass by incorporation of Ca^{2+} and Mg^{2+} ions.

From the literature, the mechanism of slag hydration appears not to be very clear. Most of the studies [139, 140, 142], points to the formation of a hydrated layer comprising of three zones. However, as can be seen, the hydration of slag can be influenced by several factors including; the type of activator used, the hydration temperature, the fineness of the slag, the w/s ratio, and the proportion of the slag load.

2.2.2.1 Influence of activator type on the hydration of slag

Slag activators can either be alkaline in nature, such as sodium hydroxide, lime, sodium carbonate and sodium silicate; or sulphate-based, like calcium sulphates or phosphogypsum. The type of the activator influences the nature and type of the hydrates formed [9, 31]. Table 2.4 gives a summary of the hydration products obtained when different activators are used.

Table 2.4: Slag hydration products in the presence of different activators (taken from [143])

Nature of activator	Crystalline phases	Comments
NaOH, Na_2CO_3, sodium silicate	C-S-H, C_4AH_{13}, C_2AH_8, $Mg(OH)_2$	Some Si in C_3AH_{13}, C/S in C-S-H less than in OPC
$Ca(OH)_2$	C-S-H, C_4AH_{13}	C_2AH_8 absent
Sulphate e.g. gypsum, hemihydrates, phosphogypsum	C-S-H, AFt, $Al(OH)_3$	Sulphate in slag acts to some extent as an autoactivator
Portland cement	C-S-H, AFm, AFt, hydrogarnet, hydrotalcite-like phase	Not all phases are likely to be seen in the same paste

In a study by Ben Haha *et al.* [136], slags were activated by two different alkalis – NaOH and waterglass (sodium silicate). They observed that the NaOH activated slags were more reactive than the waterglass activated slags at the early stages. However, at ages beyond 7 days the trend was reversed. In terms of the impact on the microstructure, the initial fast reaction of the NaOH activated slags resulted in a more porous microstructure; whereas the slow hydration of the waterglass activated slag led to a more refined microstructure. Similar findings were reported by Jeong *et al.* [43], where they investigated the influence of four supplementary activators on $Ca(OH)_2$ activated slag system. They observed that the Na-based additives were less desirable, producing lower 28 day strengths.

In PC slag blends, the hydration of slag in the presence of the cement depends on the breakdown and dissolution of the glass slag structure by hydroxyl ions released during the hydration of the PC and also on the alkali content of the PC [131]. In contrast to alkali activated systems, using different types of PC as activator for slags does not seem to have any significant effect on the hydration of the slags [56, 137].

Whitaker *et al.* [135] studied the hydration kinetics of PC slag blends. The two slags they studied had the same fineness but different chemical composition and glass content. They observed that after 1 year of hydration of 60–40 PC slag blends, about 57% and 68% of the slags had reacted. The more reactive slag had higher alumina and glass contents. When they increased the slag loading from 40 to 70%, the degree of slag hydration dropped from 68% to 60%. In other similar studies, Luke and Glasser [144] observed that for 70–30 PC slag blends, about 41% and 65% of the slag had reacted after 1 month and 1 year of hydration respectively. Generally, the higher the slag proportion in the mix, the lower the degree of slag hydration [22].

2.2.2.2 Influence of particle size distribution and fineness on the hydration of slag

In PC slag blends containing between 50 – 60% of slag, the early strength seems to be influenced mainly by the clinker fineness and the later age strength by the slag fineness. For blends containing higher slag proportion, the fineness of the slag will have a major influence on strength at all ages; whereas in blends of lower slag proportion, the influence of the slag fineness on strength or hydration is more or less negligible, regardless of the age [9]. Table 2.5 shows a typical example of how the slag's fineness influences the strength of concrete.

Table 2.5: Influence of slag fineness on strength of concrete (taken from [9])

Blaine fineness	Compressive strength (MPa)				
(cm^2/g)	1 day	3 days	7 days	28 days	90 days
3095	0.72	2.48	5.90	16.96	27.23
3930	0.88	2.88	8.41	21.79	32.34
4850	1.05	3.60	10.58	24.82	36.34
6140	1.19	4.87	12.48	27.06	39.09

PC:GGBS = 30:70, Gravel concrete (1:2:4 by vol), w/b = 0.55, water cured

Wan *et al*. [39] reported the effect of specific surface area and particle size distribution (PSD) of GGBS on the hydration of PC slag blends. They observed that the compressive strength of mortar incorporating GGBS was related to both the fineness and the PSD of the GGBS. When GGBS mortar samples having the same degree of fineness were tested for strength, mortar samples containing particles less than 3 μm had high early strength, while mortars containing particles ranging between 3 to 20 μm, had high later strengths.

In another study, Gao *et al*. [145] investigated the hydration characteristics of slag blended systems using XRD and SEM. Two slags with the same chemical composition but different degree of fineness was used in their study, at replacement levels of 40%. They observed a higher degree of slag hydration for the finer slag, and concluded that slag hydration was a function of the specific surface area of the slag.

2.2.2.3 Influence of temperature on the hydration of PC slag blends

At higher temperatures, GGBS contributes more to the total heat of hydration than at lower temperatures [126, 146-148]. This has been attributed to the accelerating effect of temperature on the reaction of the slag.

In studies [125, 126, 146, 147] where heat evolved from hydration of PC slag blends was measured by isothermal calorimetry, a different peak was often observed to be formed after peak II (as shown below in Figure 2.9). The mechanism behind the formation of this peak is controversial, and has been debated on severally in the literature.

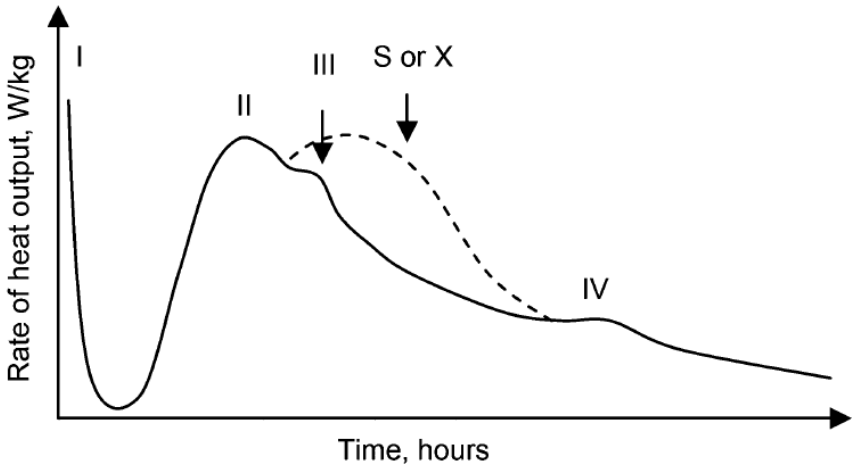

Figure 2.9: Typical heat evolution curve for the hydration of PC and slag blended cement (taken from [125])

Wu *et al.* [126] studied the influence of temperature on the early stage hydration of PC slag blends. They used three different PC slag blends comprising of 40, 50 and 65% of slag. All three slag blends were hydrated at temperatures of 15, 27, 38 and 60°C. They observed that the slag reacted more slowly at temperatures below 15°C and at an accelerated rate at temperatures above 27°C. Substantial portions of the slag had reacted within the first 24 hours at temperatures of 27°C and above. At the lower temperatures of 15 and 27°C, they observed a peak (similar to peak 'S' as seen in Figure 2.9) was formed after peak II. At the same temperature, this peak appeared at about the same time for all proportion of slag loading, and the intensity was seen to increase with the slag loading. They attributed the formation of this peak to the hydration of the slag portion. At 60°C, the reaction of the slag commenced very early and this peak was hidden in peak II.

Utton *et al.* [125], investigated four slag blended systems at temperatures of 12 and 25°C. Their observations was similar to that of Wu *et al.* [126]. There was a slight shoulder after peak II, which was attributed to the slag hydration. This shoulder was more visible at 25°C than at 12°C, and also became more obvious as the slag proportion was increased in the system. Escalante-Garcia and Sharp [146] reported similar findings, where they observed increased slag hydration at higher temperatures. However in their case, for PC slag blends containing 60% slag, peak 'S' was observed at all curing temperatures (10, 30 and 60°C).

Richardson *et al.* [147] studied the hydration mechanism of slag cements and observed that at higher temperatures, the reactions of the silicates and aluminates were accelerated. They also observed the formation of a slight shoulder to peak II. However, they identified the formation of this peak to be associated with the formation of secondary AFt.

2.2.2.4 Activation energy of PC slag blends

The reaction of slags is very sensitive to temperature, and several researchers [126, 149-151] have attempted to calculate the activation energy corresponding to the hydration of slag blended systems. Regourd *et al.* [150] applied Arrhenius law (Equation 2.5) to the heat evolved during hydration. They showed that at two different temperatures T_1 and T_2, provided that the degree of hydration is the same, the time of hydration, t, is related to the apparent activation energy (E) according to the expression shown in Equation 2.6.

$$k(T) = k_0 exp\left[\frac{-E}{RT}\right] \quad (2.5)$$

$$\frac{t_1}{t_2} = exp\frac{E}{R}(\frac{1}{T_1} - \frac{1}{T_2}) \quad (2.6)$$

Using Equation 2.6, values of 46 and 50 kJ/mol were calculated as the activation energy for PC and slag blends respectively.

Wu *et al*. [126] used another approach developed by Knudsen ([151] cited in [126]) to calculate the activation energy of PC and slag blends containing 50% GGBS. Knudsen [151] proposed that the kinetics of cement hydration can be followed by the expression below:

$$p = p_\infty \frac{t - t_0}{(t - t_0) + t_{50}} \quad (2.7)$$

Where p was related to the heat evolved, t_0 taken as the time at the end of the induction period, p_∞ is the ultimate heat evolved and t_{50} is the time taken to reach 50% degree of hydration. By plotting the reciprocal of the above expression, $1/p$ vs $1/(t-t_0)$, they were able to obtain values of t_{50} at various temperatures. Calculated t_{50} values were substituted into the Arrhenius equation to calculate E. They obtained values of 44.3 and 49.1 kJ/mol for PC and 50% PC slag blend. Table 2.6 shows values of activation energy calculated for slag blends obtained from different studies.

Table 2.6: Activation energy calculated for various slag blends

PC:GGBS	Activation energy (kJ/mol)	Reference
50:50	49.1	Wu *et al.* [126]
20:80	50	Roy and Idorn [152]
30:70	62.1	Barnett *et al.* [23]
50:50	48.0	-
65:35	47.0	-
80:20	35.2	-

2.2.3 Methods for determining the degree of hydration of slag

It is often difficult to apply the same methods used in determining the degree of hydration of PC to that of slag, as the reaction of slag with water is complex, and depends on several factors as already highlighted above. Several methods have been developed for following and/ or measuring the degree of slag hydration in slag blended systems, with each having their advantages and disadvantages.

Kocaba *et al.* [153] compared five methods for determining the degree of slag hydration in PC slag blends. The methods studied were selective dissolution, differential scanning calorimetry, SEM-BSE image analysis, cumulative heat evolved as measured by isothermal calorimetry and chemical shrinkage. They concluded that selective dissolution and differential scanning calorimetry were unreliable. SEM-BSE image analysis enabled the unreacted slag portion to be measured by a combination with EDS elemental mapping. However, it seemed to overestimate the degree of slag hydration at the early stages below 28 days. Cumulative heat measured by isothermal calorimetry gave a good correlation with chemical shrinkage, and both methods were able to isolate the reaction of the slag from that of the PC. However, there is the limitation of the length such experiments can go for, especially for isothermal calorimetry; and also how to obtain the value of

Q_∞ (ultimate heat evolved at time $t = \infty$), from which the degree of slag hydration can be obtained.

Pane and Hansen [154] used a combination of isothermal calorimetry and thermal analysis to determine the degree of slag hydration. They developed a relationship between Q_∞ and the maximum bound water content ($w_{b,\infty}$), which they used to determine the degree of hydration of the neat system. For the slag blends, they assumed that the decrease in the CH content of the slag blend was due to consumption by the slag reaction. They obtained plots relating the CH content to the bound water content for the neat and blended system, and from the use of a three-parameter hydration equation were able to develop an equation for calculating the degree of slag hydration. However, a limitation to this approach is the dependence of $w_{b,\infty}$ on temperature and water/binder (w/b) ratio.

Snellings *et al.* [155] combined XRD with partial or no known crystal structure (PONKCS) method to quantify the amount of unreacted slag present in a hydrated slag blend sample. The results they obtained were consistent, and were seen to be linearly correlated to the cumulative heat measured independently by isothermal calorimetry. However, a drawback to this approach is the difficulty in isolating the amorphous phases of C-S-H from that of slag, which often overlaps in hydrated systems [156].

Scrivener *et al.* [156] reviewed the methods that can be used for quantifying slag hydration. Based on some unpublished results of Skibsted ([157] cited in [156]), they stated that ^{27}Al MAS NMR can be used to determine the degree of slag reaction. This approach is based on the assumption that the slag dissolves congruently during hydration. It was seen to give results that matched well with those obtained from calorimetry and chemical shrinkage.

From the literatures reviewed, it can be seen that there is no ideal method for determining the degree of hydration of slag. However, from the recommendations given, isothermal calorimetry, chemical shrinkage, SEM-BSE combined with EDS, and ^{27}Al MAS NMR appear to be suitable methods that can be adopted.

2.2.4 Influence of GGBS on concrete's properties when used as a supplement

When GGBS is added as a partial replacement for PC in the making of concrete, it improves its properties in various ways, some of which have been discussed here:

Workability:

Increasing slag content at low w/b ratios can increase the water demand of the concrete, especially for slags of higher degree of fineness [158]. Also, the narrower the particle size distribution of the GGBS, the larger the fluidity of the mortar [39].

Setting times:

Increasing the slag proportion in concrete decreases the consistency and increases the setting time [159]. However, for slags of higher degree of fineness, increase in slag proportion may result in lower setting times [158].

Lower heat of hydration:

The heat of hydration of GGBS concretes is generally lower than that of plain concretes [160]. This makes the incorporation of GGBS in concrete to be advantageous for mass concreting in hot weather conditions, but on the other hand, disadvantageous in cold weather [9].

Compressive strength:

The addition of GGBS to PC in making concrete generally improves the later strength development of the concrete [23, 24, 161-166]. This is because, in comparison to PC, slag hydration does not begin early and therefore do not contribute to the densification of the concrete matrix at the early ages. Although, this may also be influenced by other factors such as the proportion of slag in the mix, the w/b ratio, the hydration temperature, the curing conditions, etc.

Porosity:

Pores in concrete can be classified as either gel pores (<0.01 μm) or capillary pores (0.01 to 10 μm). The quantity, characteristics and connectivity of the pores in a concrete determines its properties in terms of strength and durability [167]. Slag blends exhibit similar porosities as ordinary PC at early ages. However, at later ages when substantial portions of the slag have reacted, the porosities of the slag blends becomes less than that of the ordinary PC [164, 168, 169]. In terms of pore connectivity, the pore structure of slag blends comprises of large discontinuous thin-walled pores, as compared to that of the ordinary PC which is continuous [170].

Permeability/ Sorptivity:

As seen from above, the addition of GGBS to concrete results in the formation of a hardened cement paste having smaller gel pores and fewer large capillary pores. This finer pore structure makes GGBS concretes to exhibit lower permeability than concretes made from PC [31, 131].

2.3 Chlorides in concrete

Chloride-induced corrosion of steel reinforcement is one of the major causes of premature deterioration and degradation of concrete structures built in marine environments. The mechanisms by which this corrosion affects the load carrying capacity of marine concrete structures are: loss of reinforcement section, loss of steel–concrete bond, concrete cracking and delamination [171] as shown in Figure 2.10. The presence of chloride ions in concrete tend to accelerate the corrosion of the steel reinforcement and according to Saassouh [172], this occurs in three stages namely:

- Disruption of the passive film;
- Reduction of the pH level; and
- Catalyst of oxidation.

The rate of chloride ingress into concrete is often expressed as the chloride diffusion coefficient of concrete, and it is an indicator of concrete's durability. The magnitude of this value for a concrete structure depends mainly on the concrete's pore structure and on all the factors that determine it such as w/c ratio, type of cement, proportion of mineral admixtures or SCM, curing conditions, etc. It also depends on the chloride exposure condition (submerged, splash or tidal, atmosphere, etc.), length of exposure, and partly on the hydration of slow reacting constituents such as GGBS or fly ash [173].

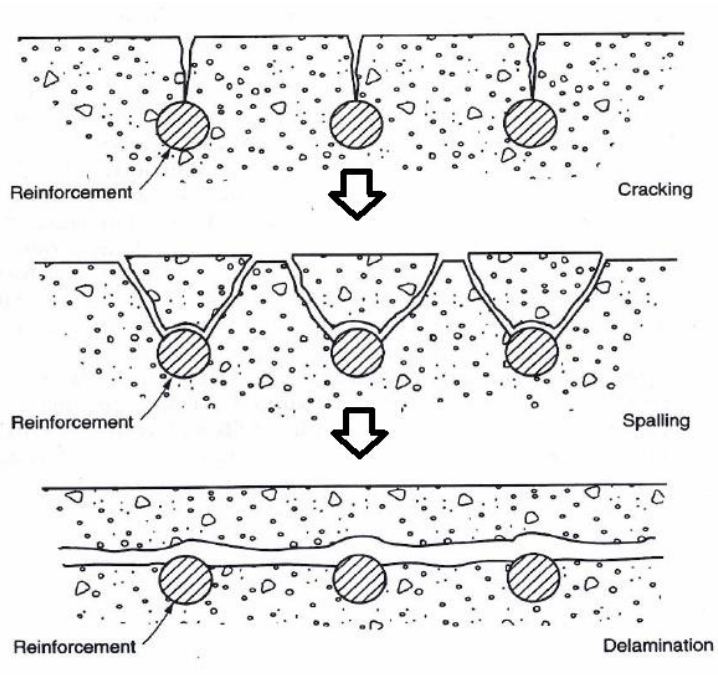

Figure 2.10: Schematic diagram showing the damage caused by chloride-induced corrosion (taken from [174])

Chlorides may enter into through various routes [175]:

- Either as admixtures;
- As de-icing salts as in bridge decks;
- Through penetration of seawater as in marine structures;
- Using mix ingredients (fine and coarse aggregate) contaminated with chlorides; or
- Through the mix water.

The chlorides which enter into the concrete from the admixtures or mix water or mix ingredients are referred to as internal chlorides, whereas those which enter from outside sources like de-icing salts and seawater during the service life of the structures, are referred to as external chlorides.

Figure 2.11 shows the various mechanisms through which chloride ions can penetrate into a concrete structure [14].

- From airborne salts raised from the sea by turbulence, carried by wind and deposited on the surface of the concrete. Nireki ([176] cited in [177]), reported that such salts can travel up to 2 km and even more depending on wind and topography.

- Under a hydraulic pressure, water containing chlorides penetrates into concrete. This mechanism is known as permeation or chloride ingress due to pressure gradient. This occurs mainly in dams and underground facilities.

- When water containing chlorides comes in contact with a dry concrete surface, it gets drawn into the porous microstructure due to capillary suction. This mechanism is known as absorption. In this case, the force driving the chloride ions into the concrete is the moisture gradient between the surface and the bulk.

- When a concrete member is in contact with chloride contained water at one surface, while its other surface is exposed to drying, chloride ions move from the wet surface towards the dry surface in a process called wicking. In this case too, the moisture gradient between the two surfaces is the potential that drives chlorides inside the member.

- Another mechanism is diffusion or the movement of chlorides under a concentration gradient. For this to occur concrete must have a continuous liquid phase (i.e., continuous pores filled with pore solution), and there

must be a concentration gradient that drives chlorides toward the zones of lower concentrations.

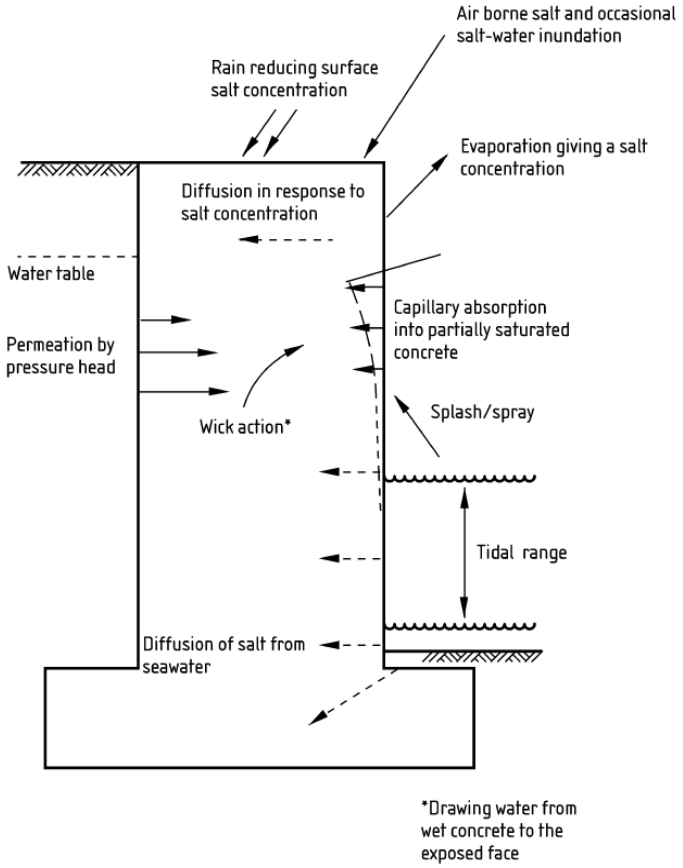

Figure 2.11: Mechanisms of chloride ingress into marine concrete (taken from [14])

Generally, chlorides exist in concrete basically in two forms [178]:

- Bound – either chemically with hydration products in the C_3A or C_4AF phases of the cement, or physically with the C-S-H phase; and
- Free – as ions within the pore solution.

2.3.1 Mechanisms governing chloride ingress into concrete

Concrete in a marine environment can either be in saturated or unsaturated condition. The mechanism of chloride ingress into concrete in a marine environment is different for each of these conditions.

Saturated condition:

For saturated concrete (e.g. concrete continuously submerged in seawater), this mechanism is governed by pure diffusion and can be modelled and described by Fick's laws of diffusion [179, 180].

Fick's first law is usually applicable to steady state conditions, where it is assumed that there is no change in flow. It is usually expressed as shown below [180]:

$$J = -D\frac{dc}{dx} \tag{2.8}$$

For conditions where the flow of ions is not constant (ion concentration can change over time), Fick's second law is more applicable. It is expressed as shown below [179]:

$$\frac{\partial C_i}{\partial t} = D\frac{\partial^2 C_i}{\partial x^2} \tag{2.9}$$

The above equation is often expressed in a more general form as [179]:

$$C(x,t) = C_s\left[1 - erf\left(\frac{x}{2\sqrt{D_c t}}\right)\right] \tag{2.10}$$

Where J is the flux, $C(x,t)$ is the chloride concentration at a given time and position, C_s is the surface chloride concentration, D_c is the chloride diffusion coefficient, t is the time, x is the depth in the diffusion direction and *erf* is the error function.

Fick's second law is often applied in most chloride ingress studies involving saturated conditions such as in laboratory ponding tests and field conditions where the samples are continuously immersed in seawater.

Laboratory ponding tests are close to field exposures, but are often slow, requiring longer periods. Therefore, to increase the rate of chloride ingress, an external electrical potential is sometimes applied, e.g. in electrical migration or accelerated tests. In such instances, the diffusion is described by a part of Nernst-Planck equation as shown below [180, 181]:

$$J(x) = -D\left[\frac{\partial c(x)}{\partial x} + \frac{ZFE}{RT}c\right] \qquad (2.11)$$

Where Z is the valence of the ion (-1 for Cl^-), F is Faraday's constant, E is the electrical field, R is the universal gas constant, and T is the temperature.

Unsaturated condition:

In the case of unsaturated concrete (concrete partially submerged in seawater or exposed to alternate wetting and drying cycles of seawater), the mechanism governing chloride transport is complex. For instance, in the case of unsaturated concrete exposed to alternate wetting and drying cycles, the chlorides diffuse alongside seawater into the concrete during the wetting period by liquid pressure gradient. In the drying period, only water evaporates from the concrete surface while the salts remain in the concrete leading to an accumulation of chlorides [182], which then increases capillary suction [183]. Thus, deterioration caused by chloride-induced corrosion is usually higher for unsaturated concrete compared to saturated concrete structures.

The mechanism governing chloride ingress in such conditions is a combination of diffusion of chlorides as in the saturated condition, and capillary absorption or convection of seawater [171, 184]. To account for both mechanisms in the assessment of chloride ingress for unsaturated condition, a convective term is added to Fick's second law of diffusion [171, 185]:

$$\frac{\partial C_{tc}}{\partial t} = \underbrace{\mathrm{div}\left(D_c w_e \underset{\nabla}{\rightarrow}\left(C_{fc}\right)\right)}_{\text{diffusion}} + \underbrace{\mathrm{div}\left(D_h w_e C_{fc} \underset{\nabla}{\rightarrow}(h)\right)}_{\text{convection}} \qquad (2.12)$$

Where C_{tc} is the total chloride concentration, t is the time, D_c is the effective chloride diffusion coefficient, w_e is the evaporable water content, C_{fc} is the concentration of chlorides dissolved in the pore solution (free chlorides), D_h is the effective humidity diffusion coefficient and h is the relative humidity.

2.3.2 Factors influencing chloride ingress

There are several factors which influence the ingress of chloride ions into concrete, some of which have been briefly discussed here.

2.3.2.1 Porosity

Generally, the finer the pore structures of a concrete, the higher the resistance to chloride ingress and vice versa [164, 186]. Al-Amoudi *et al*. [161] conducted a study on the long-term corrosion resistance of plain and blended cement concretes immersed in 5% NaCl solution for a period of 7 years. The results they obtained for both plain and blended cement concretes showed strong correlation between porosity and the corrosion resistance of the concretes. Aldea *et al*. [187] also found a correlation between the continuous pore diameter and the initial current measured by rapid chloride penetration test. In the case of Yang *et al*. [188, 189], a linear

relationship was observed between the capillary pore volume and the steady-state and non-steady state chloride migration coefficient, as shown in Figure 2.12.

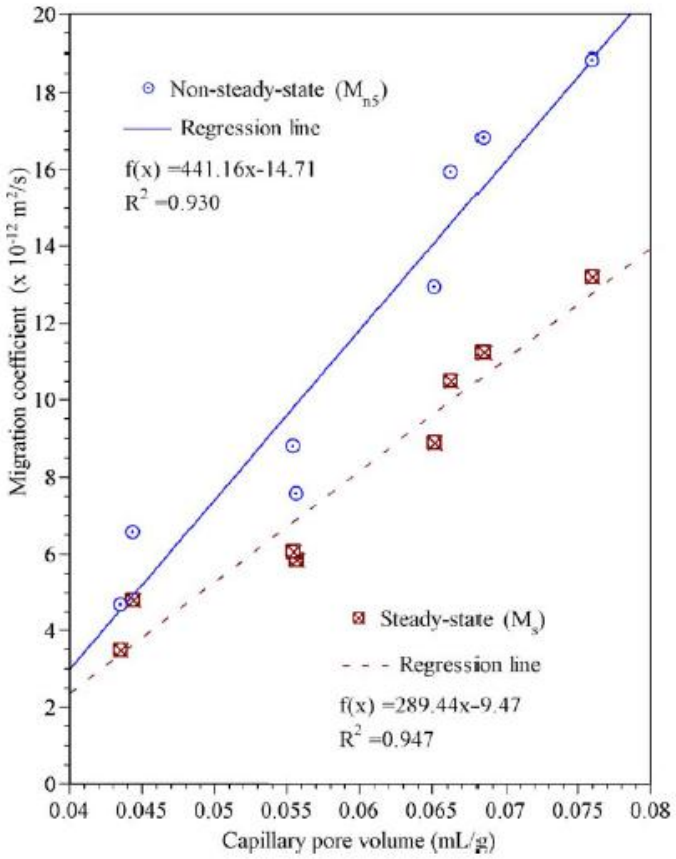

Figure 2.12: Relationship between chloride migration coefficients and capillary pore volume (taken from [188])

2.3.2.2 Relative humidity

Several studies [179, 190, 191] have shown that chloride ingress is greatly influenced by the relative humidity (RH). Ben Fraj *et al.* [182] observed an increase in the chloride diffusion coefficient of unsaturated concretes subjected to wet-dry cyclic chloride exposure, when the relative humidity was decreased from 90 to 50%. They attributed the increase to a combination of diffusion and capillary absorption.

2.3.2.3 Cation type

The source of the chloride ions or the associated cation usually affects the rate of chloride ingress or binding. Arya *et al.* [192] reported higher diffusion rates for

magnesium chloride, compared to sodium chloride. Angst *et al.* [193] reported that calcium chloride led to more chloride binding than sodium chloride.

2.3.2.4 Water/cement ratio

At a given temperature, the higher the w/c or w/b ratio, the higher the rate of chloride ingress and vice versa [188, 194-196]. This appears to be more significant at higher w/b ratios, as shown in the study by Page *et al.* [196]. They observed that at a temperature of 25°C, increase in w/c ratio from 0.4 to 0.5 resulted in an increase of about 70% in the chloride diffusion coefficient; compared to an increase of about 170% when the w/c ratio was increased from 0.5 to 0.6.

In unsaturated exposure conditions, this can also be influenced by the relative humidity. Olsson *et al.* [197] observed that at higher RH, chloride ingress was greater for samples having higher w/b; whereas at lower RH, the trend was reversed.

2.3.2.5 Exposure condition

Higher chloride diffusivities have been reported for concrete exposed to unsaturated or partially submerged conditions (tidal and splash zones) than those subjected to saturated or submerged conditions [171, 182, 183]. This is because in unsaturated conditions like tidal and spray zones, chlorides will diffuse into the concretes during the wetting period because of a liquid pressure gradient, while in the drying period only the water will evaporate out of the concrete, leaving behind an accumulation of chlorides [182].

2.3.2.6 Time/duration of exposure

Several studies have shown that chloride diffusion is time dependent. Longer periods of exposure will result in lower values of D_c. The reason for this can be

simply explained. As time progresses, more hydration products are formed and the microstructure becomes denser making it more difficult for chloride ions to permeate.

Thomas and Bamforth [198] proposed a model relating D_c to time. They showed that D_c was time dependent and changes significantly with time, especially for blended systems. Their model is as shown below:

$$D_t = D_{28}\left(\frac{t_{28}}{t}\right)^m \qquad (2.13)$$

Where D_t is the chloride diffusion coefficient at time t, D_{28} is the chloride diffusion coefficient at time t_{28} = 28 days, and m is a constant.

2.3.2.7 Curing condition

The curing medium (water or air), length of curing, and temperature of curing, affects the rate of chloride ingress. Longer curing duration in water at a temperature of about 20°C enhances the chloride ingress resistance of concretes [5, 164, 199-201]. On the other hand, shorter curing durations or curing in ambient conditions results in higher rates of chloride ingress. This can be attributed to the impact of curing on the microstructural development. Prolonged moist curing will generally result in a finer pore structure that will be more resistant to the penetration of chloride ions [164].

Güneyisi *et al*. [202] studied the influence of curing conditions on the chloride ingress and corrosion resistance of plain and blended cements. The concrete samples were subjected to three initial curing regimes – air curing for 28 days, 7 days wet curing followed by 21 days air curing, and 28 days wet curing. After

curing, the samples were immersed in a 4% NaCl solution, and tested for chloride penetration at various periods. The results they had showed that initial curing had significant impact on the rate of chloride ingress, especially for the blended cements. They concluded by suggesting that 7 days of wet curing was not enough for blended cements.

2.3.2.8 Cement type

The C_3A phase plays an important role in chloride binding. Type V cements, which have lower C_3A contents than Type I cements, generally shows less resistance to chloride penetration than Type I cements [175, 203-205]. Hussain [204] observed that an increase in the C_3A content from 2.43 to 14% resulted in an increase of about 2.65 and 2.85-fold in the chloride binding capacity and chloride threshold respectively. In another study by Rasheeduzzafar [206], it was reported that Type I cements having C_3A contents of 9.5%, bound about 1.6 times more chloride than those having C_3A contents of 2.8%. Although, in that same study it was reported that when the C_3A content was increased beyond a certain amount, the impact on the chloride ingress resistance became very little. In the study by Al-Khaja [207], it was reported that concretes made from ordinary PC were more resistant to chloride ingress than those made from sulphate resistant cements.

2.3.2.9 Presence of sulphates

Feldman *et al.* [208] immersed concrete samples prepared from PC and slag blends in a combined chloride and sulphate solution. After 12 months, they observed a decrease in chloride ion ingress compared to samples that were immersed in chloride solutions. Similar findings were reported by Tumidajski and Chan [209] for plain

concretes, but for slag blended concretes they observed an increase in chloride ingress in the presence of sulphate ions.

In another study by Zuquan *et al.* [210], the presence of sulphate ions was seen to decrease the rate of chloride ingress at early exposure period, while increasing it at later exposure periods. They attributed the early decrease in chloride ingress to the gradual formation of ettringite crystals, which led to a compaction of the microstructure; and the later increase to the presence of expansive ettringite crystals in the pores and ITZ, which resulted in the formation of cracks. Similar findings were also reported by Luo *et al.* [17], where 5% gypsum was added to slag blends containing 65% GGBS. They observed that this resulted in a significant increase in the chloride diffusion coefficient, and argued that the increase was as a result of the expanding reaction between the sulphates and C_3A.

It seems that the effect of the presence of sulphates on the rate of chloride ingress is unclear, and tend to depend on the length of exposure, the cement type and the source of the sulphate (whether it is admixed as in the case of adding gypsum or it is external as in the case of a combined mixture of sulphate and chloride solution). For both sources, the presence of sulphate seems to decrease the later resistance to chloride ingress.

2.3.2.10 Presence of carbonates

Carbonation generally increases the rate of chloride ingress into concrete. This has been attributed to two main factors. The first is that carbonation coarsens the pore structure, this effect being more pronounced on blended systems [209]. The second effect is due to a reduction in chloride binding. Friedel's salt is usually destabilized at low pH, which can be caused by carbonation [211, 212].

The effect of carbonation on chloride ingress tends to be different for plain and blended systems. Chindaprasirt *et al.* [213] studied the effects of CO_2 on the chloride diffusion coefficient of plain and blended cement mortars. They reported that for PC mortars, exposure to CO_2 did not have any significant effect on the resistance to chloride ingress; whereas for the blended cement mortars, exposure to CO_2 resulted in a significant decrease in the resistance to chloride ingress. The reason for this can be linked to the coarsening of the pore structure as mentioned above.

2.3.2.11 Use of SCMs

SCMs such as fly ash (PFA), metakaolin, GGBS, when used as additives also reduce the rate of chloride ingress [164, 186, 214-216]. Dhir *et al*. [217] found that substituting PC with PFA up to 50% greatly increased the chloride binding capacity, and reduced the chloride permeability of concrete. Song *et al*. [218] reported that silica fume reduced the permeability of concrete by refining its microstructure through physical and chemical processes. For concretes incorporating metakaolin, Badogiannis and Tsivilis [219] reported that the replacement of cement or fine aggregates by metakaolin up to 20% significantly reduced the chloride permeability, gas permeability and sorptivity of the concretes.

Detwiler *et al*. [199] studied the effect of SCM on the chloride ingress resistance of concretes cured at elevated temperatures. In their study, they used GGBS to partially replace PC at 30%, at w/c ratio of 0.4 and 0.5, and varied the curing temperature from 23°C to 50°C to 70°C. They observed that the use of SCM such as GGBS was more effective than lowering the w/c ratio when trying to improve the durability of concrete in high temperature environments.

Bai *et al*. [216] reported significant reduction in chloride ingress when ternary blends of PFA and metakaolin were used to partially replace PC. They observed the chloride diffusion coefficient to decrease with increasing level of SCM replacement and exposure time. They attributed this to the formation of pozzolanic reaction products within the capillary pore spaces resulting in a finer pore structure, and also to an increase in chloride binding capacity of the paste. Similar trends of results were also obtained by Goñi *et al*. [220], in ternary blended systems containing thermally activated paper sludge and fly ash.

2.3.3 Chloride ingress resistance of slag blended cements

Majority of studies in the literature has shown that the incorporation of GGBS in concrete enhances the resistance to chloride ingress. This has been attributed mainly to their finer pore structure and higher chloride binding capacity. A study by Boutellier *et al*. [221], where plain and GGBS concretes containing 70% GGBS were subjected to cyclic chloride exposure, showed that the D_c value of GGBS concretes were much lower than that of plain concretes. This was attributed to the higher chloride binding capacity of the GGBS concretes. Similar findings have also been reported by others [173, 182, 201, 222, 223].

Apart from enhancing chloride ingress resistance, the incorporation of GGBS in concrete can affect the pH of the pore solution, which might have impact on the corrosion risk of the embedded steel reinforcement. Cheng *et al.* [16] observed that the addition of GGBS to concrete resulted in a decrease in the pH of the pore solution. They measured a pH of 12.8 and 12.4 for blends containing 40 and 60% slag respectively. This decrease in pH is due to the consumption of CH by slag hydration, and would result in the lowering of the buffering effect provided by the alkaline medium surrounding the reinforcing steel. While some believe that this may

have a negative effect on the corrosion risk of steel reinforcement in slag concretes, others do not. For example, Gouda and Halaka [224] obtained lower chloride threshold values for slag concretes as compared to plain concretes, Schiessl and Breit [225] reported the opposite while Oh *et al*. [226] did not observe any significant difference. The bulk of findings from the literature still points to the fact that GGBS concretes are more resistant to chloride ingress than plain concretes. This has even been reflected in standards, e.g. BS EN197-1:2011 [3], where CEM IIA/B-S and CEM III A/B/C cements are commonly used for marine construction.

The chloride diffusion coefficient (D_c) is often used as measure of the resistance to chloride ingress. Table 2.7 gives a summary of D_c values obtained from the literature for concrete or mortar samples prepared from slag blends. The wide variability in the data is due to the different testing methods and conditions. For slag blends, D_c can be influenced by several factors including:

- the proportion of slag in the mix;
- the w/b ratio;
- the curing duration before exposure;
- the exposure condition, saturated or unsaturated;
- temperature;
- salinity; and
- chemical composition of the slag

Table 2.7: D_c values of slag blends obtained from literature

Slag proportion (%)	w/b	Curing length	Exposure temperature (°C)	Exposure condition	Period of exposure	Salt solution type	D_c ($x10^{-12}$ m^2/s)	Reference	Remarks
40	0.42	28 days	20 ± 2	RCPT	6 hrs	5.0M NaCl	1.1	Yeau and Kim [227]	Concrete samples
70	0.6	28 days	-	Submerged	6 months	Marine water	1.95	Luo et al. [17]	Mortar samples
70	0.5	28 days	20	RCPT	15 days	1.0M	6.47	Andrade and Bujak [228]	Mortar samples
70	0.48	28 days	NS	Splash zone	6 months	Seawater	7.5	Thomas and Bamforth [198]	Concrete samples
65	0.45	63 days	20	Submerged	50 days	165 g/L NaCl	1.1	Loser et al. [229]	Concrete samples
50	0.52	See remarks	20 ± 1	1 day wet, 6 days dry	12 months	0.55M NaCl	2.8	Basheer et al. [230]	Concrete samples were wet-cured for 14 days followed by 14 days drying at 40°C
45	0.36	1 day	25 ~ 28	Submerged	90 days	Seawater	4.823	Chen et al. [164]	Concrete samples
60	0.48	90 days	20°C and 90% RH	6 hrs wet, 6hrs dry	30 days	30 g/L NaCl	35	Ben Fraj et al. [182]	Concrete samples

Slag proportion (%)	w/b	Curing length	Exposure temperature (°C)	Exposure condition	Period of exposure	Salt solution type	D_c ($x10^{-12}$ m^2/s)	Reference	Remarks
30	0.60	28 days	20 ± 2	3 days wet, 4 days dry	90 days	Artificial seawater	90	Jau and Tsay [231]	Concrete samples
50	0.45	90 days	20	RCPT	Not stated	3% NaCl + 1% NaOH	10.9	Shi et al. [173]	Mortar samples
50	0.51	See remarks	13 ~ 20	Tidal zone	12 months	Seawater	2.7	Mackechnie and Alexander [223]	Concrete samples were moist cured for 7 days followed by 21 days under mild conditions (9-18°C and 70-95% RH)

At a given w/b ratio and RH, increasing the slag proportion will result in a decrease in the chloride diffusion coefficient [197, 227]. Yeau and Kim [227] conducted rapid chloride permeability tests (RCPT) and accelerated chloride ion diffusion tests on concrete samples made from GGBS and plain cements. They used concrete mixes containing 0, 25, 40 and 55% of GGBS by weight of PC at a constant w/b ratio of 0.42. Irrespective of the curing duration before exposure, they observed that the chloride penetrability decreased as the proportion of the slag in the concrete mixes was increased, with the 55% GGBS having the lowest chloride penetrability. Jau and Tsay [231] prepared concrete specimens from slag blends containing up to 50% GGBS, and subjected them to a cyclic chloride exposure for periods up to 1 year. They carried out various tests such as compressive strength, electrical resistance, total chloride concentrations, permeability and corrosion potential. They concluded that slag blends containing 20 to 30% GGBS had the best corrosion resistant performance.

In the same study by Yeau and Kim [227], they observed that the chloride penetrability decreased as the curing period was increased from 28 to 56 days. This was attributed to the effect of prolonged curing on the microstructure, which resulted in a more refined pore structure that had better resistance to the ingress of chloride ions. In another study by Ramezanianpour and Malhotra [201], slag concrete specimens prepared with a w/b ratio of 0.5 were subjected to four different curing regimes – continuous moist curing, 2 days moist curing followed by air curing, continuous air curing and curing at 38°C and 65% RH. The samples were cured for various lengths of 7, 28 and 180 days before testing for chloride diffusion using RCPT. They observed that the slag concretes were more sensitive to poor curing than the plain concretes, with this effect increasing with greater slag

replacements. In terms of resistance to chloride diffusion, samples that were moist cured for longer periods had better resistance to chloride penetration.

Mackechnie and Alexander [223] exposed concrete specimens to different marine conditions. The concrete specimens were prepared from slag blends containing 50% GGBS at w/b ratios of 0.35, 0.51 and 0.80. The samples were exposed in two different marine zones (tidal and splash zones). They observed that for both zones, the chloride diffusion coefficient increased as the w/b ratio. Olsson *et al*. [197] reported similar findings for mortar samples prepared from slag blends using w/b ratios of 0.38 and 0.53, and exposed at higher RH. However, as the RH was lowered, they observed that at some point chloride diffusion was greater for samples having lower w/b ratios. They attributed this to an increased number of gel pores present in the lower w/b mortar samples.

Concrete structures exposed to repeated wetting and drying by seawater are generally more susceptible to degradation as compared to those that are submerged continuously in seawater [183]. This same applies to concretes made from slag blends. Ben Fraj *et al*. [182] investigated the effects of cyclic wetting and drying with NaCl solution on chloride ingress into GGBS concrete. The concretes were prepared using w/b ratios of 0.7 and 0.48, and were cured for a period of 3 months before exposure to a 6 hour wet – 6 hour dry cycle for a period of 30 days at different RH of 50%, 75% and 90%. The results they obtained showed increase in chloride ingress as the number of cycles and w/b ratio increased, and as the relative humidity was decreased.

Very few studies [165, 166, 232] have highlighted the impact a difference in chemical composition of slag can have on its chloride ingress resistance properties. The first two studies were carried out by the authors and are parts of this study. The

third study by Otieno *et al*. [232], showed that particle fineness, as well as difference in chemical composition of slags, had impact on their chloride ingress resistance. However, amongst the three types of slags they studied, only one of them was GGBS. The other two were by-products of the Corex process and FeMn arc-furnace slag.

2.3.4 Chloride binding

Chloride binding is beneficial to the durability of a concrete structure in that it removes chloride ions from the pore solution that would have been available to initiate chloride-induced corrosion of the steel reinforcements [5]. The binding of chloride ions result in the formation of Friedel's salt, which can act as pore blockers, slowing down the rate of chloride ingress [220, 233, 234]. For concrete mixes having high chloride binding capacities, the chloride profile usually appear block-shaped. These block-shaped profiles are characterised by very high chloride concentrations at the surface, which decreases to much lower values within a short distance [235].

The higher the chloride binding capacity of cement, the more durable the cement will be. However, some researchers [236-238] have reported that under certain conditions such as drop in the pH of the pore solution to values below 12, it is possible for bound chlorides to become unbound, dissolving into the pore solution and thus increasing the risk of corrosion of the embedded steel. As a result, the total chloride concentration is often used in service-life prediction models to determine the time-to corrosion. Several factors have been reported to affect chloride binding. A summary of some of these factors and their effects on chloride binding is presented in Table 2.8.

Table 2.8: Factors influencing chloride binding

Factor	Effect	References
Cement type	The higher the C_3A content, the higher the chloride binding capacity	[175, 204, 239]
Salt type	$CaCl_2$ results in more bound chlorides than NaCl	[192, 240-242]
Chloride concentration	The higher the chloride concentration of the solution, the higher the amount of bound chlorides	[15, 18, 217, 243-245]
w/c ratio	The higher the w/c or w/b ratio, the greater the chloride binding capacity	[243, 245-247]
pH/alkalinity of the pore solution	Increase in pH or alkalinity of the pore solution decreases the chloride binding capacity	[204, 248-250]
Presence of other anions	The presence of sulphates and carbonates decreases chloride binding capacity	[17, 211, 212, 241, 244, 251]
SCMs	Blending PC with fly ash and GGBS increases chloride binding, while blending PC with silica fume decreases it	[18, 192, 217, 244, 252-254]

2.3.4.1 Phases associated with chloride binding

Bound chlorides in concrete are either chemically bound to the tricalcium aluminate (C_3A) and the calcium aluminoferrite (C_4AF) phases in the form of Friedel's salt or Kuzel's salt, or physically bound to the surface of the hydration products (C-S-H gel). Kuzel's salt is mainly found in solutions containing low chloride concentrations or in systems undergoing external sulphate attack, as its stabilization requires high concentrations of sulphate [255, 256].

The formation of Friedel's salt occurs in the AFm phases. It involves an ionic interaction/exchange mechanism between sulphate, hydroxyl, carbonate and chloride ions [257-259]. Suryavanshi *et al*. [239] proposed that the formation of

Friedel's salt involved two separate mechanisms – an adsorption mechanism that accounts for the binding of bulk of the chlorides, and a second mechanism involving the exchange of anions. They argued that in the adsorption process, the chloride ions present in the pore solution would be adsorbed on the interlayers of the AFm structure to balance the charge. Then, in order to restore the charge neutrality of the pore solution, an equivalent amount of sodium ions would have to be bound onto the C-S-H phase. While this is theoretically possible, in the study however, there was no sufficient evidence to back this argument.

As mentioned earlier, C_4AF reacts at a much slower rate than C_3A. Nevertheless, some researchers [203, 260] have reported that C_4AF can also contribute to chloride binding by chemically reacting with chlorides to form a chloro-complex, having similar chemical formula as Friedel's salt but with the aluminium replaced by iron ($3CaO.Fe_2O_3.CaCl_2.10H_2O$). In the study by Csizmadia *et al*. [260], C_4AF systems, in which gypsum was incorporated, was hydrated and subjected to cyclic chloride exposure with NaCl. They observed the formation of a Friedel-type salt of the form $C_3/AF/CaCl_2.H_{10}$. However, this form of Friedel's salt is unlikely to be stable in normal PC systems, due to the interaction with other hydration products. Also, the availability of iron in hydrated PC systems is usually low to be able to sustain the formation of an iron-type Friedel's salt.

Apart from the chemical binding of chlorides by the aluminate phases, the physical binding of chlorides by the C-S-H phase has also been reported by several workers [19, 244, 261-264]. The ability of C-S-H to bind chlorides is attributed to its morphology, which comprises of numerous nanopores, unto which the chlorides can be adsorbed. Hirao *et al.* [264] studied the chloride binding of C-S-H obtained from hydration of alite, and they observed that the amount of chlorides bound increased as

the chloride concentration of the host solution was increased. The bound chloride content followed a Langmuir-type binding isotherm, and reached a maximum value of about 0.4 mmol/g of C-S-H at a chloride concentration of 2.0M, and 0.6 mmol/g when corrected for $Ca(OH)_2$ (as seen in Figure 2.13).

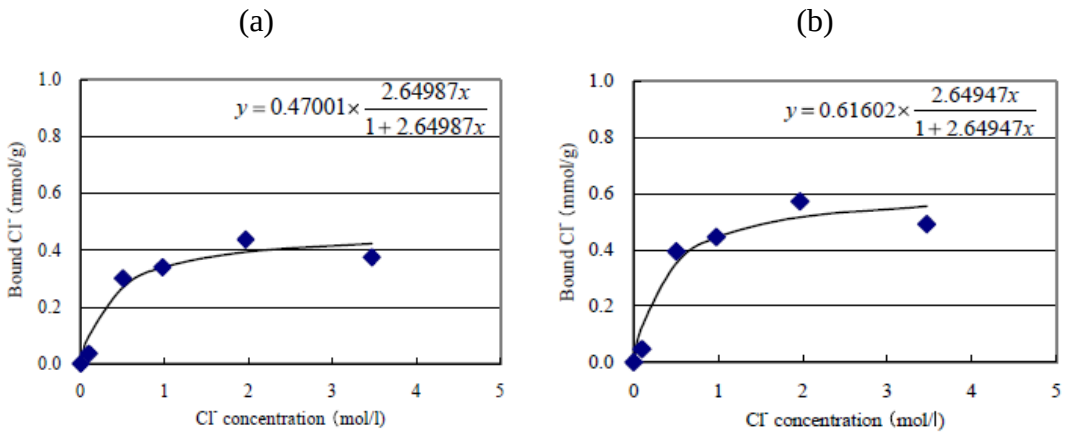

Figure 2.13: Chloride binding curve for C-S-H (a) uncorrected for $Ca(OH)_2$ (b) corrected for $Ca(OH)_2$ (taken from [264])

The role of AFt in chloride binding is not very clear. Birnin-Yauri and Glasser [257] argued that it was possible for ettringite to bind chlorides, but they did not show any experimental data to sustain the argument. In another study by Elakneswaran *et al*. [261], it was reported that ettringite binds chlorides by a physical adsorption of the chlorides onto its hydrated surface and that the chloride binding capacity of ettringite was intermediate between that of AFm and C-S-H. However, since the amount of ettringite in a hydrated paste is usually very small compared to C-S-H, the contribution of ettringite to chloride binding will be very minimal. Conversely, Hirao *et al*. [264] did not measure any bound chlorides for ettringite subjected to external chloride.

In terms of the CH phase, Hirao *et al*. [264] did not also observe any chloride binding with the CH phase. Meanwhile, Elakneswaran *et al*. [265] argued that it was possible for CH to adsorb chloride ions unto its surface, in a similar way as Friedel's

salt. Through XRD, they detected the presence of CaOHCl, which they claimed was formed by chloride ions being adsorbed on the positive surfaces of dissociated CH.

2.3.4.2 Chloride binding isotherms

Chloride binding isotherms have been developed relating free chlorides to bound chlorides. The two most commonly used ones are the Freundlich and Langmuir isotherms. The Freundlich isotherm is more applicable at free chloride concentrations higher than 0.01 mol/l, and is represented by [243, 245]:

$$logC_b = alogC_f + b \qquad (2.14)$$

Or by Thomas *et al*. [18]:

$$C_b = \alpha . C_f^{\beta} \qquad (2.15)$$

Where C_b and C_f are the concentrations of the bound and free chlorides in mol/l, while a and b or α and β are adsorption constants, which vary for different cement types.

The Langmuir isotherm, according to Luping and Nilsson [243] is more suitable for free chloride concentrations lower than 0.05 mol/l. It is given as [18]:

$$C_b = \frac{\alpha . C_f}{(1 + \beta . C_f)} \qquad (2.16)$$

2.3.4.3 Chloride binding in slag blended cements

The use of GGBS to partially replace Portland cement in the making of concrete has been shown to be beneficial in terms of chloride binding. This has been attributed to their high alumina content [15-18], which increases the propensity for Friedel's salt formation and also the formation of more C-A-S-H phase, that is responsible for the binding of about two-thirds of the chloride [19].

Higher levels of slag replacement will result in higher chloride binding [15, 18, 266]. Dhir *et al*. [15] observed increase in the chloride binding capacity of slag blends containing 33.3, 50 and 66.7% of GGBS. They observed that irrespective of the concentration of the host chloride solution, the chloride binding capacity increased as the GGBS content increased, with the 66.7% GGBS content having a chloride binding capacity of about 5 times that of the control. They attributed the increase in chloride binding of the slag blends to an increase in the alumina content, enabling it to form more of Friedel's salt. They proposed a model relating chloride binding capacity to GGBS content and concentration of chloride exposure solution as shown below.

$$C_b = (-22.21G^2 + 39.45G + 3.36)X + (6.84G^2 - 6.40G + 3.64) \qquad (2.17)$$

Where, C_b is the chloride binding capacity in mg/g of sample, G is the GGBS/total binder ratio, and X is the chloride exposure concentration in mol/litre.

Similar findings were also reported elsewhere [18, 266]. However, in the study by Kayali *et al*. [266], the increase in chloride binding observed at higher slag proportions was attributed to increase in the amount of hydrotalcite (Ht) formed, which they claimed plays a significant role in the binding of chloride ions. In their

study, plain forms of calcined Ht were subjected to chloride solutions. They observed that about 40% of the chloride ions were removed from the chloride solution after 1 hour, and about 54% after 24 hours. Theoretically, this is possible because the structure of Ht consists of positively charged layers that are formed by the incorporation of divalent or trivalent cations in the octahedral layers [267]. Between these positively charged layers are negatively charged anions that can be replaced by a wide range of other anions like chlorides [268, 269].

Xu [241] investigated the chloride binding properties of ordinary PC and a blend of PC – slag containing 65% of slag. Sodium and calcium sulphates were added to all the cements at varying proportions from 2 to 9% by weight of binder. They observed that the higher chloride binding capacity of the slag blends disappeared when the sulphate content was increased to similar levels as that of the ordinary PC. In a previous study by Holden *et al*. [251], it was observed that the addition of sulphates to slag blends and ordinary PC had more negative effect on the paste samples of the slag blends than those of the ordinary PC. This implies that in slag blends, it is possible that the higher chloride binding property observed may be as a result of the lower sulphate content in the blends.

Although, it has been established that using GGBS as partial replacement for PC enhances chloride binding, studies have not really focused on the influence chemical composition of slag would have on its chloride binding capacity. In the study by Thomas *et al*. [18], where they investigated the effect of SCMs on chloride binding in hardened cement paste. Their results showed that the chloride binding capacity was jointly influenced by the chemical composition of the binder and the w/c ratio. The chloride binding capacity was found to increase as the alumina content of the binder.

In general, the higher chloride binding capacity observed in slag blends as seen from the literature can be attributed either to the role of Ht in chloride binding for slag blends containing high proportions of slags or to a lower sulphate or higher alumina content as compared to ordinary PC. In regards to the later, the chemical composition of the slags in all these studies was not varied. It would be interesting to see how much effect, varying the sulphate or alumina or magnesia content would have on the chloride binding capacity of slag blends.

2.3.5 Methods for measuring chloride contents in concrete

2.3.5.1 Free chloride content

The determination of free chloride content usually involves two stages – extraction and analysis.

Extraction:

There are two main methods that have been reported for use in extracting free chlorides from concrete specimens. The first approach involves placing cylindrical specimens on a pore press, and applying a load until the pore fluids are squeezed out. This approach seems to give the exact representation of the free chloride content [270]. However, a major setback to this approach is that pore presses are not readily available; hence they have to be constructed as a special rig.

The second approach involves leaching the free chlorides from concrete specimens. The free chlorides obtained by this process are usually referred to as ‘water-soluble chloride’. Arya *et al*. [270] reported that free chloride contents obtained from leaching experiments gave an underestimation of the free chloride content of the pore solution as obtained from pore solution expression. However, several leaching

techniques have been reported [271-273] concerning the extraction of free chlorides, and the accuracy of each technique tends to depend on several factors such as the solvent type, exposure time, and temperature. Arya *et al.* [273] used several leaching methods and observed that the methods were dependent on the total chloride content. Amongst the methods used were:

- 48 hour standing at 20°C – suitable for total chloride content of 1.0 to 1.5% by weight of cement
- 72 hour standing at 20°C – suitable for total chloride content of 1.5 to 2.0% by weight of cement
- 6 hour continuous stirring – was suitable for total chloride content of 1.5 to 2.5% by weight of cement
- 5 mins boiling and allow to stand for 55 mins – was suitable for total chloride content of 2.0 to 2.5% by weight of cement.

In a subsequent study, Arya *et al.* [270] observed that the extraction technique which involved boiling for 5 mins and allowing to stand for 55 mins gave similar free chloride contents to that of the expressed pore solution. However, there is the tendency for boiling to liberate some of the chemically bound chlorides, thereby increasing the free chloride content. Since chloroaluminate compounds are known to be insoluble in cold water, the extraction techniques carried out at room temperature is expected to liberate only the free or water soluble chlorides and is therefore preferable.

Analysis:

After the free chlorides have been extracted, they can be analysed either by the use of a potentiometric titration device [164, 182, 270] or by the use of an ion chromatography-inductively coupled plasma (IC/ICP) device [173, 265, 274].

2.3.5.2 Total chloride content

The approach adopted for the determination of the total chloride content in concrete depends on whether the chlorides are allowed to diffuse naturally into the concretes or accelerated by the application of electrical fields.

Natural diffusion:

These natural diffusion test methods are also referred to as 'salt ponding tests'. It can take different forms, but the two most common forms are shown below in Figure 2.14. In the first arrangement, the salt solution is placed on top of the concrete specimen so that the chlorides can diffuse unto the concrete specimen unidirectional under gravity. In the second arrangement, the concrete sample is immersed completely into the salt solution but all sides of the concrete sample except the exposed face is coated with a substance that is impermeable by chlorides. In both arrangements, the concrete samples would usually be exposed for periods up to 90 days, for a 3% NaCl solution [275]. BS EN 12390:2015 [275] also prescribes a duration of 35 days for a 16.5% NaCl solution.

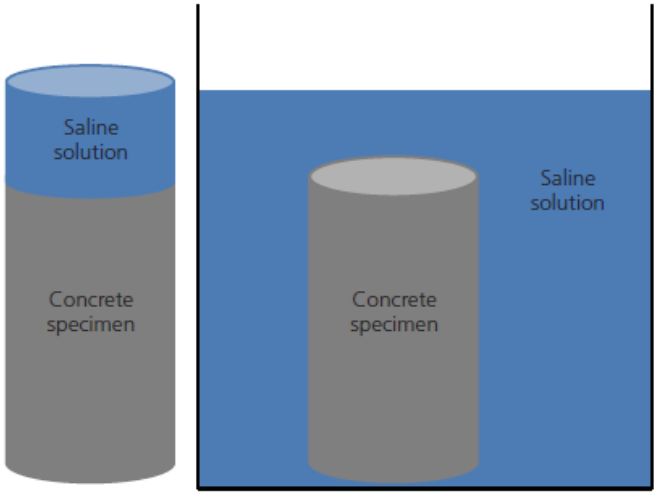

Figure 2.14: Typical set-ups for salt ponding test (taken from [181])

At the end of the ponding period, powders are either drilled from various depths or slices of concrete are collected from the exposed face downwards. The drilled powders or ground concrete slices can then be analysed for total chloride contents using the method specified in BS 1881-124:1988 [276] or RILEM TC 178-TMC [277] for determining acid-soluble chlorides. Dhir *et al.* [278] reported that the acid extraction technique underestimated the total chloride content. They observed that using different acid concentrations, temperature and exposure times resulted in different total chloride contents, and recommended that for accurate determination of the total chloride content, XRF should be used. However, the method recommended by RILEM TC 178-TMC [277] was based on the results from a round-robin test that involved 30 laboratories and 64 independent measurements.

When the total chloride contents at various depths from the exposed face of the sample have been obtained, a chloride profile is plotted and fitted into Fick's 2nd law of diffusion to obtain the non-steady state chloride diffusion coefficient.

Accelerated diffusion:

Accelerated diffusion usually involve the use of electric fields to drive chlorides through concrete, in which case, the concrete acts as a diffusion membrane between a chloride solution and a neutral solution (see Figure 2.15 below). There are several variants of this method. In some instances, the current flowing through the concrete is measured [279, 280], or the charge passed [281], the resistivity [282, 283] or conductivity [284] of the diffusion membrane or the electrical impedance [285]. The Nernst – Planck equation shown previously in Section 2.3.1, is mostly applied in calculating the chloride diffusion coefficient in accelerated diffusion tests.

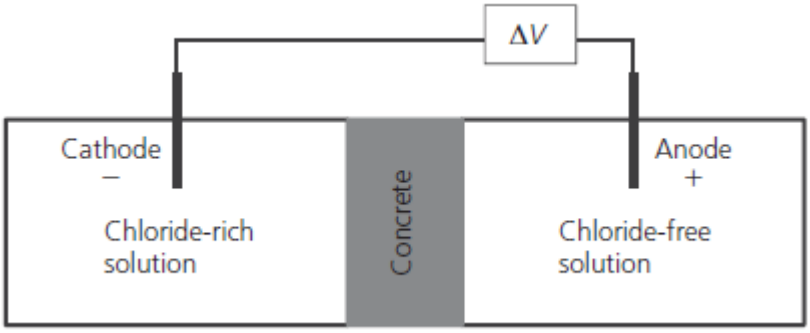

Figure 2.15: Typical set-up for an accelerated chloride migration test (taken from [181])

2.3.5.3 Bound chloride content

Tang and Nilsson [243] developed a method for determining bound chloride content. This method is based on the principle of equilibrium and has been used by several researchers [18, 182, 245]. The method involves wet-crushing mortar or cement paste samples to particles ranging in size from 0.25 to 2.0 mm, saturating the crushed specimens with NaCl solution and allowing the resulting solution to stand for a period between 10 to 14 days to reach equilibrium. After equilibrium is reached, the chloride concentration of the resulting solution is determined. Knowing

the initial concentration of the NaCl solution, the content of bound chlorides can then be determined using the expression:

$$C_b = \frac{35.45V(C_0 - C_1)}{W} \qquad (2.18)$$

Where C_b is the bound chloride content in mg/g-sample, V is the volume of solution in ml, C_0 is the initial concentration of the chloride solution in mol/l, C_1 is the equilibrium concentration of the chloride solution in mol/l, and W is the weight of the dry sample in grams.

Another method that can be used for determining bound chlorides content is QXRD. Arya and Newman [270] showed that QXRD can detect the presence of Friedel's salt. However, this method may not give an entire representation of the bound chlorides in the concrete, since the C_4AF and C-S-H are also capable of binding some of the chlorides.

2.4 Influence of temperature on concrete's properties

Curing or exposure of concrete to higher temperatures affects several properties of concrete such as the workability, setting times, hydration reaction, compressive and tensile strengths, permeability, pore structure, durability in terms of resistance to aggressive ions, etc. The influence of temperature on hydration reaction for both PC and PC-blended systems has been discussed in previous sections. So here, only the effect on some of the properties relevant to the study has been discussed.

2.4.1 Compressive strength

Hogan and Meusel [163] investigated the compressive strength of slag blended cements subjected to varying curing temperatures. They observed that at ambient temperature, the mortar strengths of the slag blends developed at a slower rate than that of the neat system for the first 3 days and at a higher rate at ages of 7 days and above. When they increased the curing temperature, the slag blends had higher strengths than the neat system at all curing ages.

Similar findings were made by Barnett *et al.* [23], where they investigated the strength development of mortars prepared by replacing PC with GGBS at 0, 20, 35, 50 and 70% by weight of the PC. The w/b ratio was varied from 0.25 to 0.60, and the mortars were cured at temperatures ranging from 20 to 50°C. They observed that the early age strength development of the mortars containing GGBS was highly dependent on temperature. At 20°C, the rate at which the GGBS mortars gained strength was slower than the PC mortars, but as the curing temperature was increased; the strength gain of the GGBS mortars became more rapid. At 40 and 50°C, the strength development of the GGBS mortars after 3 days was more or less the same as that of the PC mortars at all levels of replacement.

Çakir and Aköz [24] also had similar observations from flexural strength test performed on GGBS mortars at 20 and 40°C. They observed that elevated curing temperature increased the early age strength of mortar but decreased their later age strengths, and that it was more significant for the GGBS mortars than the PC mortars.

From the literatures reviewed, it can be seen that increase in curing temperature results in increase in the early strength and a subsequent decrease in the later

strength. More so, this effect appears to be more pronounced on slag blended systems as compared to neat systems.

2.4.2 Chloride ingress

Like most chemical reactions, increase in exposure temperature leads to an increase in the rate of chloride ingress [196, 205, 207, 286, 287]. Samson and Marchand [288] proposed a model that related chloride diffusion coefficient to temperature, as shown below:

$$D_i = D_i^{ref}\, e^{\alpha\left(T - T^{ref}\right)} \qquad (2.19)$$

where D_i is the chloride diffusion coefficient, the subscript *ref* corresponding to a reference value taken as the value at room temperature, and α is a parameter depending on material type. The model correlated well with their experimental results. However, they observed that α was independent of the cement type or the w/c ratio.

Page *et al*. [196] studied the influence of temperature and w/c ratio on chloride ingress of ordinary PC pastes, and observed that at a given w/c ratio, the chloride diffusion coefficient significantly increased with temperature. At a w/c ratio of 0.5, the chloride diffusion coefficient increased by about 100% between the temperatures of 7 and 25°C, compared to an increase of about 300% between 25 and 44°C.

Similar findings were reported by Oh and Jang [205], where they measured the total chloride contents of concrete samples exposed to chloride environments at temperatures of - 5°C, 25°C and 40°C, for a period of 10 years. From their results

shown in Figure 2.16, it can be seen that increase in exposure temperature results in a significant increase in the depth of chloride penetration.

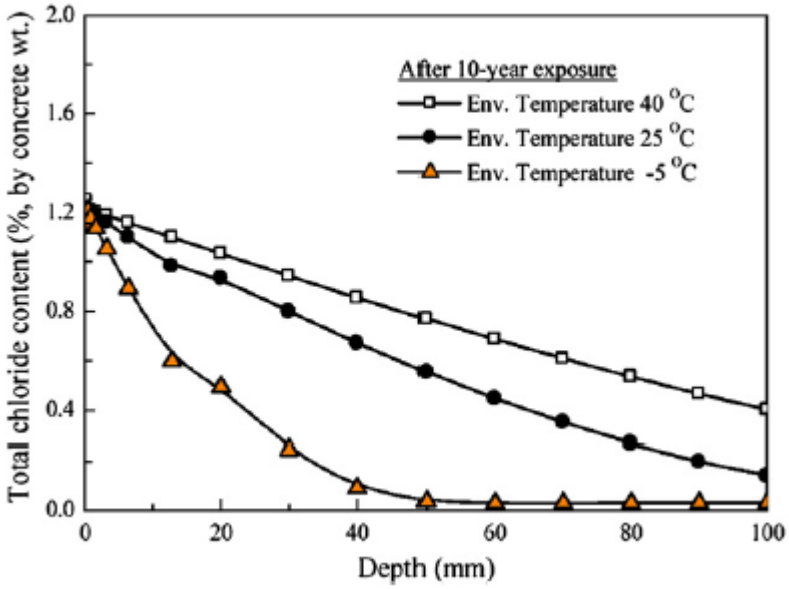

Figure 2.16: Influence of exposure temperature on chloride ingress (taken from [205])

Lindvall [286] compared the influence of temperature and salinity on the chloride ingress of samples exposed in laboratory and field conditions. In the laboratory conditions, they observed that chloride ingress was more influenced by the salinity and only to a small extent by the temperature; whereas in the field conditions, temperature was the dominating factor influencing chloride ingress.

In ordinary PC concretes, it is clear from the literature that an increase in temperature results in an increase in the rate of chloride ingress. However, the lack of studies on slag blends makes such a comment difficult to prove or disprove.

Detwiler *et al*. [199] investigated the effect of SCMs on the resistance to chloride ion penetration of concretes cured at elevated temperatures. They prepared concretes from PC and slag blends containing 30% GGBS, using w/b ratios of 0.4 and 0.5. All samples were cured at temperatures of 23, 50 and 70°C, for varying periods to attain

a 70% degree of hydration before subjected to chloride ingress tests. They observed that at a given w/b ratio, increasing the curing temperature resulted in an increase in the rate of chloride ingress. The slag blended concretes had much better performance than the plain concretes. The negative influence of high temperature curing on the resistance to chloride ingress was more pronounced on the plain concretes than the slag blended concretes, despite both being at the same degree of hydration.

In another study by Chini and Acquaye [289], slag blends containing 50% GGBS were cured at temperatures of 23, 71 and 93°C for periods of 28 and 91 days, and tested for resistance to chloride penetration using rapid chloride tests and time to corrosion tests. The results of the rapid chloride penetration tests showed that the elevated curing temperatures improved the durability of the slag blends, whereas the time to corrosion test showed the reverse.

The results of the rapid chloride tests and time to corrosion test conducted by Chini and Acquaye [289] appear to contradict each other and therefore cannot be trusted. Also, it has been stated before that high temperature curing results in a coarser pore structure [290, 291]. This coarse pore structure should imply greater ingress of chloride ions as observed by Detwiler *et al*. [199]. However, in the study by Detwiler *et al*. [199], it took the PC pastes 5 days to attain 70% degree of hydration at temperature and w/b ratio of 50°C and 0.5 respectively, compared to 17 days for the slag pastes. This longer curing time allowed for the slag pastes must have resulted in a more refined pore structure. This suggests that the pore structure might be the main factor controlling the ingress of chloride ions as observed by Shi *et al*. [173], and not necessarily the degree of hydration. However, more work will need to be done to verify this for slag blended systems.

2.4.3 Chloride binding

At temperatures below 0°C:

Very few studies [292, 293] have looked at chloride binding at temperatures below 0°C. Dousti and Shekarchi [293] observed that more chlorides were bound at -4°C than at 3°C. Similar trends were reported by Panesar and Chidiac [292], for temperatures of – 3 and 5°C. While Dousti and Shekarchi [293] could not find any explanation for this, Panesar and Chidiac [292] attributed it to a simultaneous occurrence of multiple mechanisms – a physical binding mechanism combined with an increase in the chloride content of the solution due to partial freezing of the pore solution.

At temperatures above 0°C:

There seem to be controversy on the effect increasing temperature has on chloride binding, at temperatures above 0°C. Some studies [192, 240, 244, 292] have reported increase in the amount of bound chlorides as temperature was increased, while others [293-296] have reported the opposite. Panesar and Chidiac [292] observed an increase in the amount of bound chlorides as the temperature was increased from 5 to 22°C, for neat pastes and pastes containing GGBS at 25, 50 and 60% by weight of PC.

Wowra and Setzer [240] considered temperatures between 0 and 40°C, and observed that chloride binding increased as the temperature was increased. Similar trends were observed by Arya *et al*. [192]. However, in their case, the chlorides were introduced at the time of mixing. In both studies, the increase in chloride binding with temperature was attributed to faster reaction rates at the higher temperature.

Zibara [244] investigated the effect of temperature on the binding of external chlorides for various PC blends at temperatures ranging from 7 to 38°C. They observed that at lower chloride concentrations between 0.1 and 1.0M, increase in temperature resulted in a decrease in chloride binding; whereas at higher chloride concentrations of 3.0M, increase in temperature led to an increase in chloride binding.

Hussain and Rasheeduzzafar [294] prepared cement pastes with ordinary PC having C_3A contents of 2.43, 7.59 and 14%, at a w/c ratio of 0.6. Three levels of chloride (0.3, 0.6 and 1.2%) were added through the mix water. The paste samples were allowed to cure for 180 days at temperatures of 20 and 70°C, after which they were subjected to pore solution expression tests. They observed that the amount of unbound chlorides were significantly higher at 70°C than at 20°C. Similar trend of results were reported by Maslehuddin *et al*. [295], at temperature range of 25 to 70°C for admixed chlorides. This may be due to a partial release of the bound chlorides occurring at the higher temperature, as observed in a recent study by Xu *et al*. [297].

Mejlhede Jensen *et al*. [296] studied the influence of cement constitution and temperature on the chloride binding capacity of cement pastes. They used a white PC and replaced it with various amounts of C_3S, C_2S and C_3A. The chlorides were from an external source. Crushed paste samples that had been cured for about 46 days (28 days at 20°C followed by 18 days at 35°C), were exposed to NaCl solutions of different concentrations, at temperatures of 4, 20 and 35°C. They observed that the bound chloride content calculated from the equilibrium solution, decreased with increase in temperature. However, the impact of temperature was little compared to that of the cement constitution.

Dousti and Shekarchi [293] reported decrease in the binding of external chlorides with increasing temperature. They considered various temperatures, relating to the climatic conditions of south of Iran. The chloride binding capacity was observed to decrease in the order of 22°C > - 4°C > 3°C > 35°C > 50°C > 70°C. They attributed this to increase in the solubility of Friedel's salt at the higher temperatures, and increase in the thermal vibrations of the absorbents, which would result in the release of the chlorides physically bound to the C-S-H phase.

The studies [192, 240] that have reported an increase in chloride binding with increasing temperature, have generally attributed it to an increase in the rate of reaction at the higher temperatures. However, considering the effect of higher temperature on hydration, which was discussed in a previous section, the amount of sulphate ions bound reversibly to the C-S-H phase increases. This leads to a reduction in the amount of sulphates left to react with C_3A, and an increase in the amount of AFm formed in preference to AFt [111, 112, 116]. Since the AFm phase is associated with chloride binding, an increase in the amount of AFm formed at higher temperatures should result in increased chloride binding.

The higher the concentration of the external chloride solution, the higher the chloride concentration of the pore solution, which in turn results in more chlorides being, bound [229, 298, 299]. So at elevated temperatures, due to evaporation, the chloride concentrations of the external chloride solutions would increase. As a result, in such conditions, evaporation losses should be accounted for when estimating the bound chloride content. This was considered in the study by Zibara [244], but not in the ones by [293, 296].

In summary, the effect of temperature on chloride binding is not clear-cut, and may be influenced by other factors such as the source of the chlorides (whether internal

or external), correction for evaporation losses occurring at elevated temperatures as pointed out by Zibara [244], the w/b ratio, total chloride content, and temperature range, as pointed out by Xu *et al*. [297].

2.5 Summary

This chapter concerned a review of published studies on the mechanism and factors influencing the hydration and chloride ingress resistance of plain and slag blended cements. It was seen that GGBS undergoes hydration, though at a slower rate when compared to PC. The hydraulicity of GGBS was seen to be influenced mainly by the degree of fineness, glass content, chemical composition and hydration temperature. Higher hydration temperature was seen to increase the early reactivity of the slags, giving rise to higher early strengths. Concerning the performance of slag blended cements, combining GGBS with PC to make concrete was generally seen to improve certain properties of the concrete such as the long-term compressive strength, workability, permeability and resistance to the ingress of chloride ions. The better resistance to chloride ingress exhibited by slag blended cements was generally attributed to their higher chloride binding abilities, which was a function of their higher alumina content. Increasing the slag proportion, lowering the w/b ratio, and prolonged moist curing, was seen to improve the chloride ingress resistance of slag blended cements.

However, there are certain aspects listed below that are likely to affect the performance of slag blended cements, which have not been looked at, and more studies should be carried out to address these.

1. It is known that the chemical composition of GGBS affects its hydraulicity, but only few studies have investigated how this will affect the performance

of slag blended cements, and of these few studies, most have been focused on strength performance.

2. Although, it was seen that temperature influences the hydraulicity of GGBS, the question of how slag blends of differing chemical compositions would perform in different climates was not answered. The impact of higher temperature curing and exposure on the chloride ingress resistance of slag blended cements is not very clear.

3. It was also seen that slag blended cements performed better when they were cured for longer periods under normal conditions. However, the effect shorter curing durations will have on the performance of slag blended cements is not very clear, especially when higher curing temperatures are considered.

Chapter 3
Materials and Methods

This chapter gives a description of the materials and methods that were used for the study. The tests methods adopted for the study have been grouped into three as shown below:

- Hydration and microstructural studies on cement paste samples using: isothermal calorimetry, thermal analysis, X-ray diffraction, and back-scattered electron image analysis
- Compressive strength development on mortar samples
- Transport properties on mortar samples using: sorptivity (unidirectional water penetration), water absorption, chloride binding and diffusion

3.1 Materials

3.1.1 Cementitious materials

3.1.1.1 Cement

Two CEM I type cements (42.5 R and 52.5 R), designated as C1 and C2 respectively were used for the study. C2 was replaced partially by 30 per cent by weight of GGBS. The chemical composition of the cement, as obtained by XRF, and the clinker phases present as obtained by XRD are shown in Table 3.1 and Table 3.2 respectively, and the physical properties are shown in Table 3.3.

C1 was used as the reference cement in assessing the performance of the slag blends. This is a common industrial practice. Cement producers usually prepare

blends using CEM I 52.5R at replacement levels ranging from 20 to 40%, to produce cement products with similar performance as a CEM I 42.5R type cement.

3.1.1.2 Slag

Two slags (S1 & S2) with similar physical properties yet different chemical compositions were used for the study. Both were supplied by a European cement company. In order to limit the difference between the slags to just the chemical composition, slag 2 was ground to similar fineness as slag 1 using a Gyromill. The chemical composition and crystalline phases of the slags as obtained by XRF and XRD are shown in Table 3.1 and Table 3.4 respectively, and their physical properties are shown in Table 3.3. The X-ray diffraction patterns showing the amorphous and crystalline phases; and the particle size distribution of the slags, are shown in Figure 3.1 and Figure 3.2 respectively.

3.1.1.3 Anhydrite

In some instances, anhydrite was added to the slag blends to keep the sulphate content of the slag blends same as that of the CEM I 52.5R. The chemical composition and properties of the anhydrite used is given in Table 3.1 and Table 3.3 respectively.

Table 3.1: Chemical composition of cementitious materials

Property	Unit	C1	C2	Slag 1	Slag 2	Anhydrite
LOI at 950°C	%	2.20	2.54	(+1.66)	(+0.40)*	
SiO_2	%	19.71	19.10	36.58	40.14	2.04
Al_2O_3	%	5.08	5.35	12.23	7.77	0.60
TiO_2	%	0.26	0.25	0.83	0.30	0.03
MnO	%	0.03	0.03	0.64	0.64	0.00
Fe_2O_3	%	2.97	2.95	0.48	0.78	0.23
CaO	%	63.16	62.38	38.24	37.9	38.32
MgO	%	2.19	2.37	8.55	9.51	1.45
K_2O	%	1.08	1.05	0.65	0.55	0.16
Na_2O	%	0.06	0.05	0.27	0.36	0.00
SO_3	%	2.97	3.34	1.00	1.47	52.24
P_2O_5	%	0.20	0.10	0.06	0.02	0.02
Sum at 950°C	%	99.90	99.50	99.88	99.43	98.76

* The sample was oxidized with HNO_3 before the determination of LOI

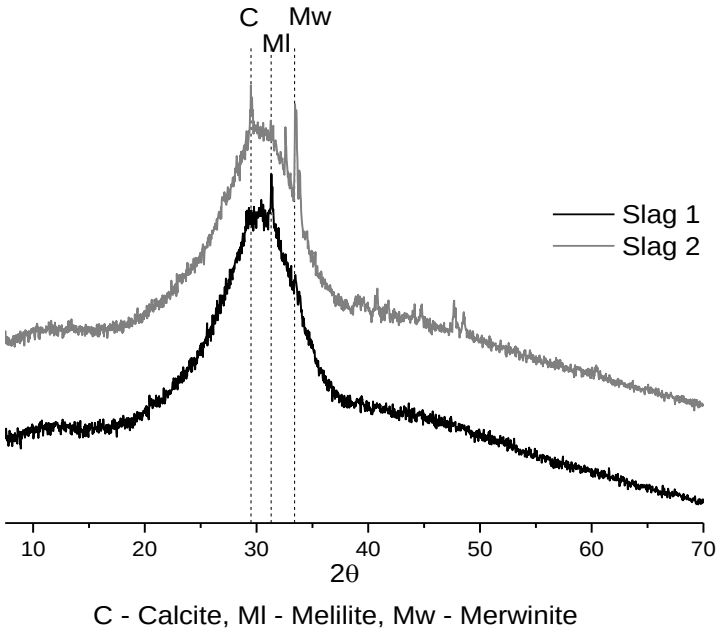

Figure 3.1: XRD patterns of the as-received slags

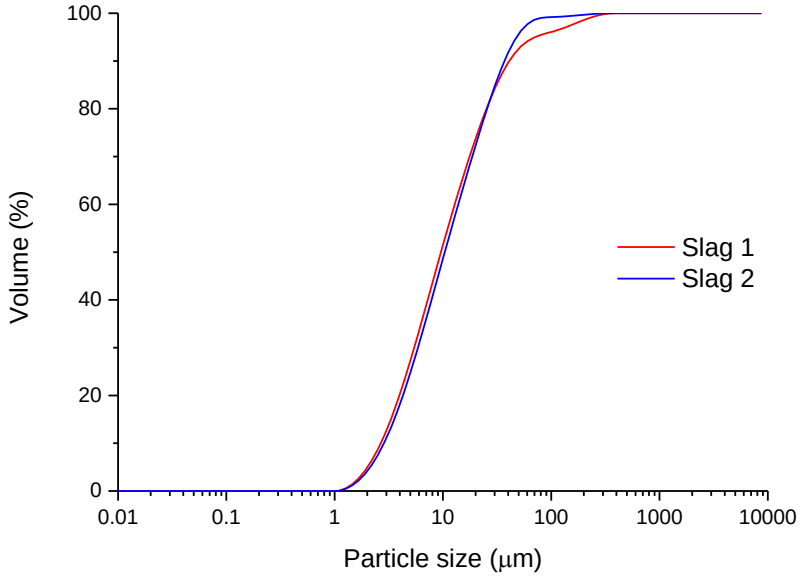

Figure 3.2: Particle size distribution of slag 1 and slag 2

Table 3.2: Clinker phases identified in the CEM Is

Phase	Unit	C1	C2
Alite, C_3S	%	58.9	62.1
Belite, C_2S	%	13.1	8.9
Aluminate, C_3A	%	7.4	9.1
Ferrite, C_4AF	%	8.5	8.5
Calcite	%	3.6	1.8
Anhydrite, AH	%	2.7	0.6
Hemihydrate, HH	%	0.6	2.4
Gypsum	%	0.0	1.7
Others	%	5.3	5.0

The clinker phases were determined by the suppliers of the cements

Table 3.3: Physical properties of the cementitious materials

Property	Unit	C1	C2	Slag 1	Slag 2	Anhydrite
Density	g/cm^3	3.23	3.18	2.94	2.95	2.94
Blaine	cm^2/g	3510	5710	4490	4090	4720
Particle size, d50	µm	-	-	11.0	11.9	-

Table 3.4: Crystalline phases identified in Slag 1 and Slag 2

Phase	Unit	Slag 1	Slag 2
Calcite	%	0.3	0.5
Merwinite	%	<0.1	2.3
Akermanite	%	0.2	<0.1
Illite	%	0.2	<0.1
Gehlenite	%	<0.1	<0.1
Quartz	%	<0.1	<0.1
Glass content	%	99.3	97.1

The crystalline phases were determined by the suppliers of the slags

3.1.2 Fine aggregate

The fine aggregate used complied with the specification for fine aggregates as given in EN 12620:2002+A1 [300]. The particle size distribution is shown in Table 3.5.

Table 3.5: Particle size distribution of fine aggregate

Sieve size	Percentage passing	Specification limit
8mm	100	100 – 100
6.3mm	100	95 – 100
4mm	89	85 – 99
1mm	46	40 – 80
0.500mm	30	30 – 70
0.250mm	19	10 – 50
0.063mm	3	0 – 3
Moisture content (%)	9.4	not specified
Uniformity coefficient	11	5 – 15

3.1.3 Water

Distilled or de-ionised water was used for the mixing of the sodium chloride solution and for the preparation of paste samples. Normal drinking water as obtained

from the University's main supply was used for the mixing of the mortar samples. This complied with the specifications given in EN 196-1:2005 [301].

3.1.4 Sodium chloride solution

Sodium chloride (NaCl) solutions were prepared in the laboratory using distilled water and in accordance with the recommendation in EN 12390:2015 [275]. A 3% NaCl solution was used for the chloride ingress studies as specified by EN 12390:2015 [275]. This has similar chloride concentration as that of Atlantic seawater as shown in Table 3.6. The solution was prepared by mixing 30 grams of NaCl in 970 grams of distilled water, to get an approximate concentration of 30.93 g/L or 0.53M.

Table 3.6: Typical composition of seawater in g/L (taken from [7])

Constituent		Mediterranean	Atlantic	Mean sea water
Sodium	Na	11.56	9.95	11.00
Potassium	K	0.42	0.33	0.40
Magnesium	Mg	1.78	1.50	1.33
Calcium	Ca	0.47	0.41	0.43
Chloride	Cl	21.38	17.83	19.80
Bromide	Br	0.07	0.06	-
Sulphate	SO_4	3.06	2.54	2.76

3.2 Mix design

Three series of mixes were used for this study. A water/binder ratio (w/b) of 0.5 was used for all mixes. The details of the mixes are shown in Table 3.7. C2S1$ and C2S2$ indicates mixes containing extra anhydrite.

Table 3.7: Mix ratios for the mortar specimens

Mix	w/b	C1	C2	Slag 1	Slag 2	Anhydrite	Water	Fines
C1	0.5	1	0	0	0	0	0.5	3
C2S1	0.5	0	0.7	0.3	0	0	0.5	3
C2S2	0.5	0	0.7	0	0.3	0	0.5	3
C2S1$	0.5	0	0.70	0.28	0	0.02	0.5	3
C2S2$	0.5	0	0.70	0	0.28	0.02	0.5	3

The blends were prepared by mixing the various portions of the slag, cement and anhydrite (where applicable) in a laboratory ball mill using polythene balls as charges. Mixing was done for about 4 hours, which was suitable to obtain a homogeneous blend.

3.3 Sample preparation

3.3.1 Mortar

Mortar samples were prepared in accordance to EN 196-1:2005 [301]. The samples were prepared by mixing one part of binder with three parts of fine aggregates in a Hobart-type mixer, using a w/b of 0.5. After mixing, the mortar samples were poured into moulds of 40 x 40 x 160 mm prisms or 50 mm cubes, depending on the tests they were used for.

3.3.2 Cement paste

Cement paste samples were prepared by manual mixing of the cementitious materials and water. After mixing, the resulting paste was poured into 14 or 25 mm ϕ cylindrical plastic vials, depending on the tests they were used for.

3.4 Details of curing conditions

Two temperature regimes were chosen in order to study the effect of temperature on the performance of the slag blends. 20°C was chosen as a reference temperature, which is typical of laboratory conditions. 38°C was chosen as a representative temperature for tropical, arid or semi-arid zones. The details of both curing regimes are described below, and summarized in Table 3.8.

3.4.1 Curing at 20°C

The cast mortar samples were covered with thin polythene sheets and left to cure under laboratory air for a period of 20 to 24 hours. After this initial curing, the samples were de-moulded and placed under water in curing tubs at 20°C until the day of testing. For the paste samples, after casting, the top of the plastic vials were sealed with polythene and allowed to rotate vertically at 20 rpm for 24 hours so as to prevent bleeding. After 24 hours, the paste samples were removed from the plastic vials and cured in saturated lime water at 20°C until testing.

3.4.2 Curing at 38°C

Mixing and casting was done at room temperature, but the materials and moulds used were preconditioned in an oven set to 38°C so as to minimise the temperature difference. After casting, the mortar samples were covered with thin polythene sheets and transferred immediately to a preheated oven at 38°C, for a period of about 20 to 24 hours. Thereafter, the mortar samples were demoulded and transferred to water baths set to 38°C, where they were left to cure until the test day.

The paste samples were treated in the same way except that they were not rotated vertically at 20 rpm, as was the case of the samples cured at 20°C. Rather, immediately after casting, they were transferred to the preheated oven. For analysis

involving these samples, only the central portions of the samples were used, so as to minimise effect of bleeding and segregation.

Table 3.8: Curing regimes

Curing regime	Temperature (°C)	Relative humidity (%)
1	20	99.9
2	38	99.9

3.5 Details of exposure conditions

Mortar samples that was used for the chloride ingress studies were cured under curing regime 1 and 2, for periods of 7 and 28 days respectively, before they were exposed to two different laboratory-modelled chloride exposure conditions described below.

3.5.1 Saturated or submerged chloride exposure

This exposure condition is similar to the XS2 exposure classification as defined in BS 6349-1:2000 [14] for chlorides. In this exposure condition, the samples were submerged in 3% NaCl solutions kept at temperatures of 20 and 38°C, for a period of 90 days. For the samples exposed at 20°C, the solutions were renewed every 4 weeks to maintain the salinity of the solution, and the liquid to solid ratio was kept above 12.5 millilitres per square centimetre of exposed surface as specified in EN 12390:2015 [275]. For the samples exposed to the sodium chloride solution at 38°C, the solutions were renewed every fortnight so as to minimise the effect of evaporation on the salinity of the solutions.

3.5.2 Cyclic chloride exposure

This exposure condition is similar to the XS3 exposure classification as defined in BS 6349-1:2000 [14] for chlorides. In this exposure condition, the samples were subjected to continuous cycles of wetting and drying. A cycle consisted of 6 hours of wetting during which the samples were submerged in a 3% NaCl solution, followed by 6 hours of drying. This cycle was chosen as according to Ben Fraj *et al.* [182], this represents the daily application of salts that a reinforced concrete structure will be subjected to in a tidal zone. A schematic of the setup for this exposure condition is shown in Figure 3.3.

The setup shown in Figure 3.3 consists of a pump, solenoid valve, water level switch, stainless steel mesh and supports, and a timer switch (not shown). The operations of the solenoid valve was controlled by the timer switch, while that of the pump was jointly controlled by the timer switch and the water level switch. The exposure chamber was left opened all through the duration of the exposure period so as to keep the samples under atmospheric conditions, and the temperature and RH of the room was about 20°C and 50% respectively.

At the start of the cycle, the salt solution is pumped unto the upper tank containing the samples, to a level of about 25 mm above the samples. On reaching this level, the water level switch comes on and the pump is automatically turned off. After 6 hours, the timer switch opens the valve and the salt solution flows out to the lower tank. The samples are then allowed to dry for 6 hours. This completes one cycle. At the end of the drying period, the pump switch comes on and salt solution is then pumped from the lower tank to the samples in the upper tank. The whole process was allowed to run continuously till 180 cycles (90 days) was reached.

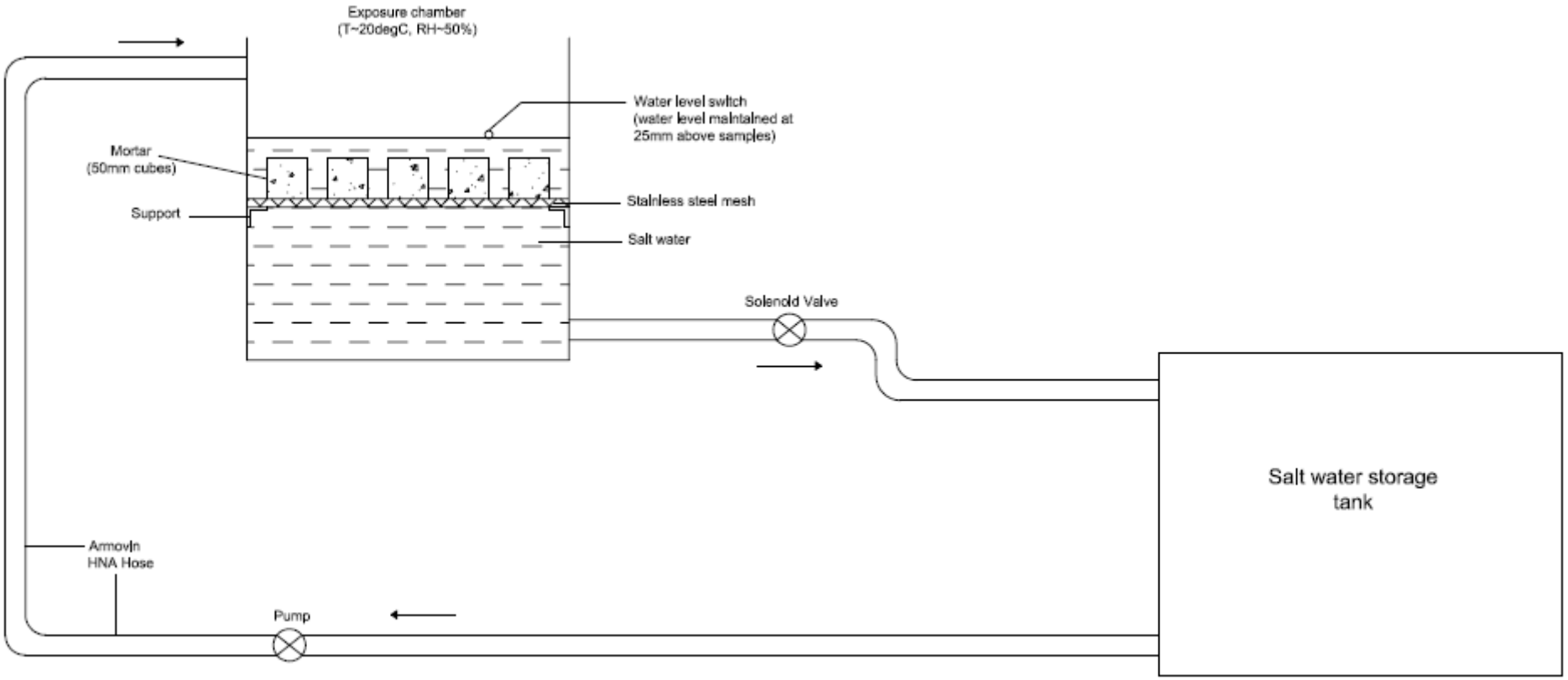

Figure 3.3: Schematic of the setup for the unsaturated exposure condition

3.6 Test Methods

3.6.1 Methods for studying hydration process and microstructure

3.6.1.1 Isothermal conduction calorimetry

Principle:

The reaction of cement and water, otherwise known as hydration, is an exothermic process. Heat released during the process of the reaction can be measured using Isothermal Conduction Calorimetry (ICC) [302]. Most modern calorimeters usually have twin channels, which enables the heat released from a hydrated sample to be compared to that of a reference sample. The reference sample should have similar thermal properties to that of the sample being measured so as to reduce the amount of noise or drift generated [303]. Quartz is often used as a reference material when measuring the hydration of cement. It has a specific heat capacity of 0.8 J/gK compared to that of cement, which is 0.75 J/gK [304].

Calorimetry measures the overall heat evolution, which is the sum of the heat evolved by all the reactions occurring at a particular time. So if for instance, an exothermic reaction is occurring at the same time as an endothermic reaction, the overall heat evolved might be negligible even when the reactions are occurring at a high rate. As a result, calorimetry is mainly used as a global measure of the degree of hydration [44].

Experimental procedure:

The heat flow generated during hydration was measured for cement pastes, using a TAM Air 8 twin channel calorimeter. 6 grams of binder and 3 grams of deionised water was placed in a 20 ml plastic ampoule, and shaken on medium speed for 2

minutes using a vortex shaker. The reference sample (quartz) was prepared in the same way and placed in the reference position, while the paste samples to be measured was placed in the measuring position. Measurements were taken at 20 and 38°C respectively, for periods up to 30 days (720 hrs).

Measuring the degree of slag reaction:

Calorimetry was used qualitatively to measure the degree of reaction of the slag [44]. This was done by replacing the slag component in the slag blends with quartz. This enabled the heat contributed by the slag's hydration to be separated from that of the cement (Figure 3.4). The difference between the total heat evolved by the neat cement paste and that containing quartz is attributed to the filler effect, while the difference between the heat evolved by the paste containing quartz and that containing slag is attributed to the hydration of the slag (Figure 3.4a). Figure 3.4b shows the heat evolved as a result of the slag hydration normalized to the cement content, while Figure 3.4c shows the heat evolved by the slag's hydration normalized to the slag content and the positive contribution of the slag's hydration to the total heat evolved. Figure 3.4b showed initial drops in the heat evolved by the slag, which was attributed to the differences in the hydrates formed between the cement paste containing quartz and that containing slag. As stated in the studies by [44, 305], it was assumed that the slag's hydration had not commenced at that stage.

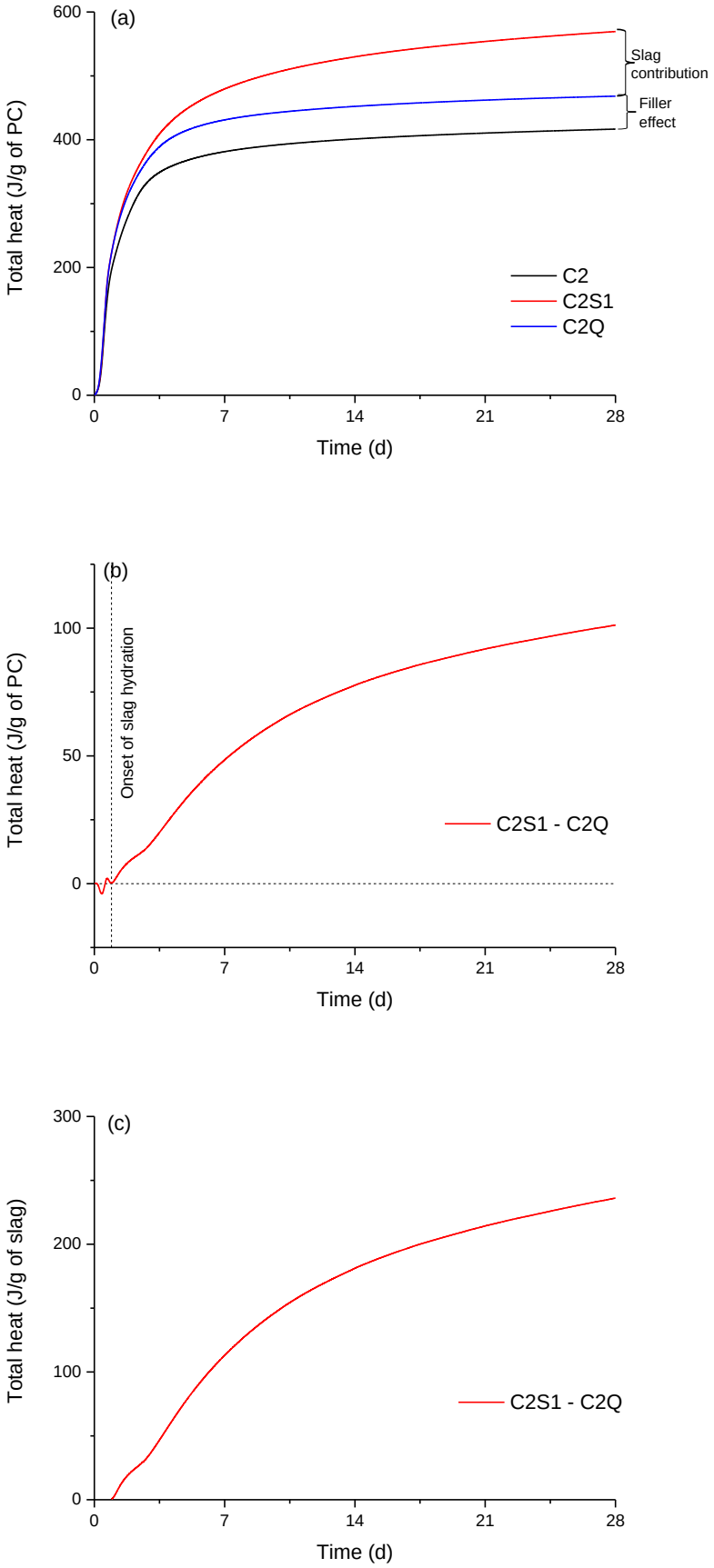

Figure 3.4: Measuring the degree of slag hydration by calorimetry

3.6.1.2 Hydration stopping for cement paste samples

There are various techniques for stopping/ arresting the hydration of cement. The ones commonly used include: solvent exchange, freeze drying, oven drying and vacuum drying. Each of these techniques has their own advantages and disadvantages. Some have been reported to affect the microstructure of the hardened cement paste resulting in the structural and physical collapse of some of the cement hydrates, especially ettringite (AFt), monosulphate (AFm) and C-S-H [306]. The suitability of any technique depends on various factors such as: type of specimen – cement paste, mortar or concrete; size of specimen; age of specimen; and test to which specimen will be subjected to – scanning electron microscopy (SEM) or mercury intrusion porosimetry (MIP).

For example, Galle [307] suggested that freeze drying was an adequate drying technique for use with MIP but that it generates significant damage to C-S-H. Konecy and Naqvi [308] found that the pores of hardened cement pastes were damaged by freeze drying. Collier *et al*. [306] observed that for samples having high porosity the method of arresting cement hydration did not appear to have any effect on the crystalline phase composition and microstructure, while Zhang and Scherer [309] found that for electron microscopy and pore structure analysis, solvent exchange with isopropanol best preserved the microstructure.

For this study, hydration was stopped for the cement paste samples using the solvent exchange technique, as it best preserves the microstructure [308, 309]. Isopropanol was used as the first solvent and was replaced by another solvent (diethyl ether). Diethyl ether has a lower density than isopropanol and boils at about 35°C, and would therefore displace isopropanol from the pores of the hardened cement paste.

Also, the initial exchange with isopropanol does not have an irreversible effect on the length change as observed by Beaudion *et al*. [310].

The samples used for the hydration studies were cement paste discs having a diameter of 14 – 16 mm and a thickness of 2 mm. The samples were placed in isopropanol for at least 24 hours. Hughes [311] tracked the weight change of hardened cement paste discs of diameter 33 mm and thickness 3 mm, using solvent exchange and found that after 1000 mins (about 17 hrs) of soaking, the weight reached equilibrium. A solution to sample ratio of about 100:1 was used as suggested by Aligizaki [312]. After soaking for 24 hours, the isopropanol was removed completely and replaced with diethyl ether, and left for about 2 hours. The samples were then dried in a preconditioned oven at 40°C to remove the diethyl ether.

3.6.1.3 X-ray diffraction (XRD)

Principle:

X-ray diffraction is defined as the elastic scattering of x-ray photons by atoms in a lattice plane [313]. It is a technique that is often applied in the identification and quantification of mineral or phase composition in cement based materials. It involves focusing a beam of x-rays unto a sample, while changing the angle between the incident beam and the reflecting lattice plane. When the scattered monochromatic x-rays reflected by the atoms in a lattice plane are in phase, constructive interference occurs, and by application of Bragg's law the characteristic spacing between the crystal planes (*d)* can be determined as follows:

$$n\lambda = 2d\ sin\,\theta \qquad (3.1)$$

Where:

n integer called the order of reflection

λ wavelength of x-rays

d characteristic spacing between the crystal planes of a given specimen, and

θ angle between the incident beam and the normal to the reflecting lattice plane

To identify the composition of the crystalline phases in an unknown material, the XRD pattern is obtained on a powdered sample of the material. This is then compared to the standard line patterns available for various compounds in the powder diffraction file (PDF) database, from which the crystalline phases in the material can be identified. In this study, XRD was only used for qualitative purposes – for the identification and characterisation of the crystalline phases present in the hydrated cement paste samples.

Experimental setup:

XRD patterns were obtained on hydration stopped cement paste samples that had been ground to particle sizes less than 63 microns. In order to minimise the effect of preferred orientation, care was taken when preparing the samples and minimal pressure was applied when backloading the samples onto the sample holders [314, 315]. Measurements were obtained via a D2 Phaser Bruker diffractometer, using a CuK_{α} radiation in a θ-θ configuration with a fixed divergence split size of 0.5° and a

sample stage set to rotate at 15°/min. The samples were scanned over a range of 2θ values (7 to 70°), at a step size of 0.034° and a dwell time of 3 secs, resulting in a total scan time of 100 mins per sample.

3.6.1.4 Simultaneous thermal analysis (STA)

Principle:

Simultaneous thermal analysis (STA) is a technique in which two or more types of measurement are made on a single sample at the same time [316]. This technique is particularly useful for carrying out quantitative and qualitative thermal analysis for materials such as cement paste that undergo physical or chemical changes as heat is applied to them. Thermogravimetric analysis (TGA) which involves the measurement of mass loss can be used for quantitative analysis, while differential thermal analysis (DTA), which involves the measurement of the difference in temperature between a sample and a reference, can be used for both qualitative and quantitative analysis.

When a hydrated cement paste sample is heated, the phases will decompose releasing either water from hydrates, or CO_2 from calcite [317]. Figure 3.5 shows a typical thermogravimetry curve (TGA) for a cement sample with its corresponding differential curve (DTA). The unreacted gypsum (calcium sulphate) decomposes at temperatures between 140 and 170°C, ettringite at temperatures of 120 – 130°C, while C-S-H gel decomposes at temperatures below 150°C [317]. Portlandite (CH) decomposes to CaO between 420 and 550°C, releasing water in the process [44]. This is often seen as a sharp drop in the TGA and DTA curves as shown in Figure 3.5. At higher temperatures of 650 to 800°C, calcium carbonate decomposes to CaO, releasing CO_2.

The data is usually affected by the type and size of the sample as well as the rate of heating. A powdered sample will result in a more even distribution of the heat within the sample compared to a lump. Too big a sample mass will result in an increase in the time required to fully decompose a phase. The use of fast heating rates will also affect the decomposition temperature as some phases present in low concentrations will not be detected on the TGA and DTA curves.

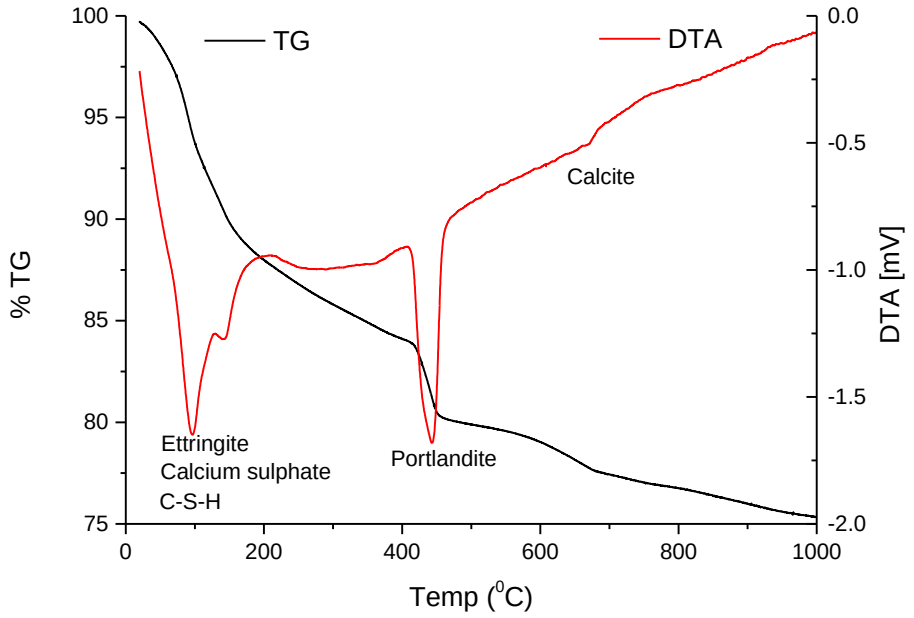

Figure 3.5: Typical TGA and DTA curves for a hydrated cement paste

Experimental setup:

STA was carried out using a Stanton Redcroft 780 series. About 15 to 18 mg of hydration stopped cement paste samples were placed in an empty platinum crucible. A corresponding empty platinum crucible was used as the reference. Both the sample and the reference were heated under a nitrogen atmosphere from 20 to 1000°C at a constant rate of 10°C/min.

Measuring the Portlandite and bound water content:

The CH content was determined using the tangent method as shown in Figure 3.6. Tangents were drawn on the TGA curve at the points where inflection occurred on the DTA curve. A line was then drawn along the slope of the TGA curve between the inflection points. The mass loss due to the water bound to CH *(CH_w)*, is taken as the length of the vertical line drawn through the midpoint of this line connecting the tangent lines. The CH content was then calculated using Equation 3.2. In some cases, where the CH content is corrected for carbonation, Equation 3.2 becomes modified to Equation 3.3 [44]. Although, there is the difficulty of accounting for the unreacted calcite and the carbonation of the C-S-H phase [44], both of which can also contribute to the total calcite content. In this study, the drying method adopted did not lead to any additional carbonation of the samples. Hence, the CH content was not corrected for carbonation.

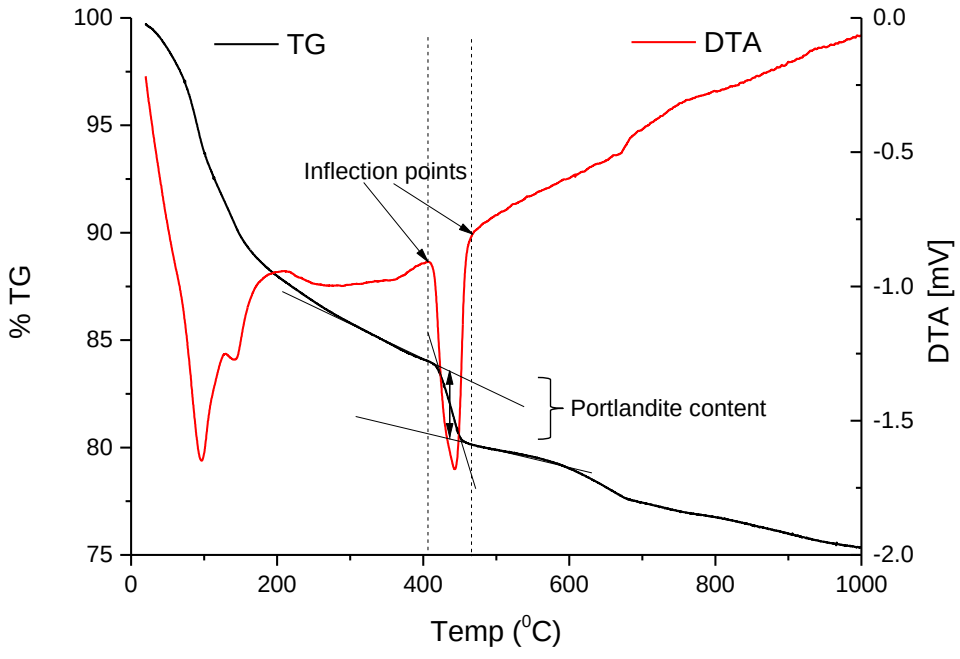

Figure 3.6: Determining portlandite content using the tangent method

The bound water content (W_n) was taken as the difference between the mass loss at 50 and 550°C, at which point it was assumed that all the phases containing water had fully decomposed. W_n, normalised to the total mass loss at 550°C was calculated using Equation 3.4.

$$\%CH = CH_w \times \frac{M_{CH}}{M_{H_2O}} \quad (3.2)$$

$$\%CH = CH_w \times \frac{M_{CH}}{M_{H_2O}} + CC_c \times \frac{M_{CH}}{M_{H_2O}} \quad (3.3)$$

$$W_n = \left(\frac{W_{50} - W_{550}}{W_{550}}\right) \times 100 \quad (3.4)$$

where:

CH_w mass loss of water bound to CH

M_{CH} molar mass of CH, taken as 74 g/mol

M_{H2O} molar mass of water, taken as 18 g/mol

CC_c mass loss due to decarbonation of calcite

W_{550} mass loss at 550°C

W_{50} mass loss at 50°C

3.6.1.5 Scanning electron microscope (SEM)

Principle:

Scanning electron microscope (SEM) is a well-known technique that is used to investigate the microstructure of materials. It has been used by several researchers [30, 135, 318-320] to study the microstructural evolution of hydrated cementitious materials, both quantitatively and qualitatively. In an SEM, a beam of electrons is

focussed over the sample surface and scattered electrons are collected by detectors and used to construct an image.

Depending on the way the electrons interact with the sample, secondary electrons, backscattered electrons (BSE) or X-rays will be produced. Secondary electrons are low-energy electrons and they give information relating to the topography of the sample. BSE are high-energy electrons from the primary incident beam that are ejected back out from the sample. These BSE are used to produce a different kind of image. Such an image uses contrast to give information about the average atomic number of the sample. As the atomic number of a feature increases, more electrons are reflected and appear brighter. Features having low atomic numbers appear dark grey or black [321]. As a result, different phases can be identified according to greyscale and this can be used for the characterisation and quantification of the various phases present in the sample. This study involved the use of BSE imaging.

Sample preparation:

Sample preparation is a very important aspect of the SEM technique. For determining degree of hydration of hydrated cement paste samples using BSE, it is better to use flat polished samples so as to reduce edge effects [322]. 2 mm thick discs were cut from the central portions of 14 mm ϕ cylindrical hydrated cement paste samples. The samples were hydration stopped, followed by resin impregnation using an epoxy based resin and a hardener. The resin impregnated samples were polished to obtain flat surfaces using silicon carbide paper. This resulted in scratches developing on the surface of the polished samples, which were removed by further polishing using various diamond pastes (6, 3, 1 and 0.25 μm).

Experimental procedure:

BSE-SEM images were collected for the polished samples using a Carl Zeiss EVO SEM. An accelerating voltage of 15 keV was used, combined with a spot size of 500. Electron images were collected at a magnification of x800 and a working distance of 8 – 8.5 mm, and were analysed to determine the degree of porosity. In determining the degree of hydration of the slags, magnesium maps were collected using an Oxford Instrument Xmax SDD detector at a minimum acquisition time of 90 secs.

Image analysis:

Image analysis was done using a software – ImageJ, on BSE–SEM images to determine the degree of porosity and hydration. In the analysis, it was assumed that the volume fraction in a three dimensional surface is equal to the area fraction of a two dimensional surface. This assumption is based on the principle of stereology, which uses two dimensional sections to interpret three dimensional structures [312].

Pores in the microstructure appear as dark spots on the electron images and can be easily distinguished from the hydrated phases – C-S-H and CH, as shown in Figure 3.7. C-S-H appears as dark grey; however, the grey level varies depending on the C/S ratio, temperature, water content and microporosity [114, 319, 320]. In a typical histogram for a hydrated neat paste (Figure 3.8), the CH phase is brighter than the C-S-H phase and appears as light grey while the anhydrous cement appears as the brightest.

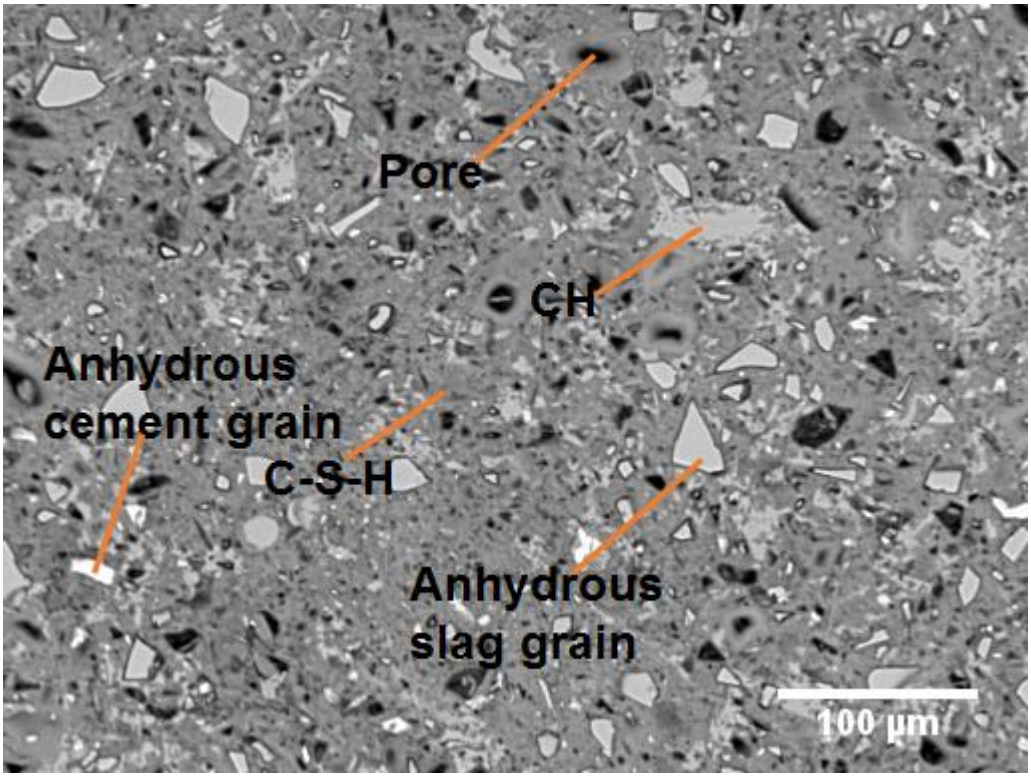

Figure 3.7: Typical BSE-SEM image of a 28 day old paste sample of a slag blend

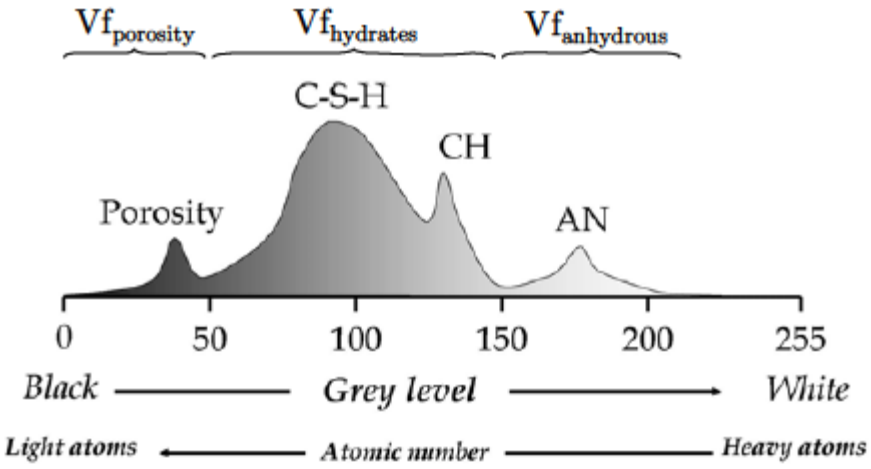

Figure 3.8: Typical histogram for a hydrated neat paste showing the grey levels of the various hydrated phases (taken from [44])

Degree of porosity:

The degree of porosity was determined for 7 and 28 day old samples. It was taken as the area fraction corresponding to the pores present in an electron image. A total of 50 electron images were collected at random and analysed, and the average was taken as the degree of porosity.

It is important to state here that the degree of porosity measured by this technique depends largely on the resolution of the electron images. It can also be affected by overlap between the pores and the C-S-H phase on the greyscale, and other factors associated with the instrument e.g. filament brightness. For slag blends, the hydrated dark rim surrounding the anhydrous slag grains can also interfere while thresholding for porosity. This was corrected for by careful adjustment of the brightness and contrast of the images, while the aspects concerning the instrument was dealt with by using the same settings each time measurements were being taken. The other aspects not involving the instrument are discussed as follows:

- **Image resolution:** Images of 1024 x 768 pixels were collected at a magnification of x800. Based on this resolution, 1 pixel is approximately 0.17 x 0.17 µm [135]. If it is assumed that the smallest feature that can be captured at this resolution is 2 pixels [135, 323], then only pores greater than 0.3 µm will be visible at this resolution. This implies that a fraction of the capillary pores (those ranging from 0.01 to 0.3 µm), will not be captured. Thus, the degree of porosity measured is that of pores greater than 0.3 µm, and this will be referred to as 'coarse porosity' in this study.

- **Overlap between the pores and the C-S-H phase:** This often occurs at later ages, where sufficient portion of the anhydrous materials have reacted, resulting in lower porosity and pore size. In such instances, it becomes difficult to distinguish the pores from the C-S-H phase on the greyscale. This was only observed for the 28 day samples, and the porosity was measured following the technique developed by Scrivener et al. [324]. The porosity was taken at the point of intersection between tangents drawn to the lower leg and the rising leg of the C-S-H peak, as shown below in Figure 3.9.

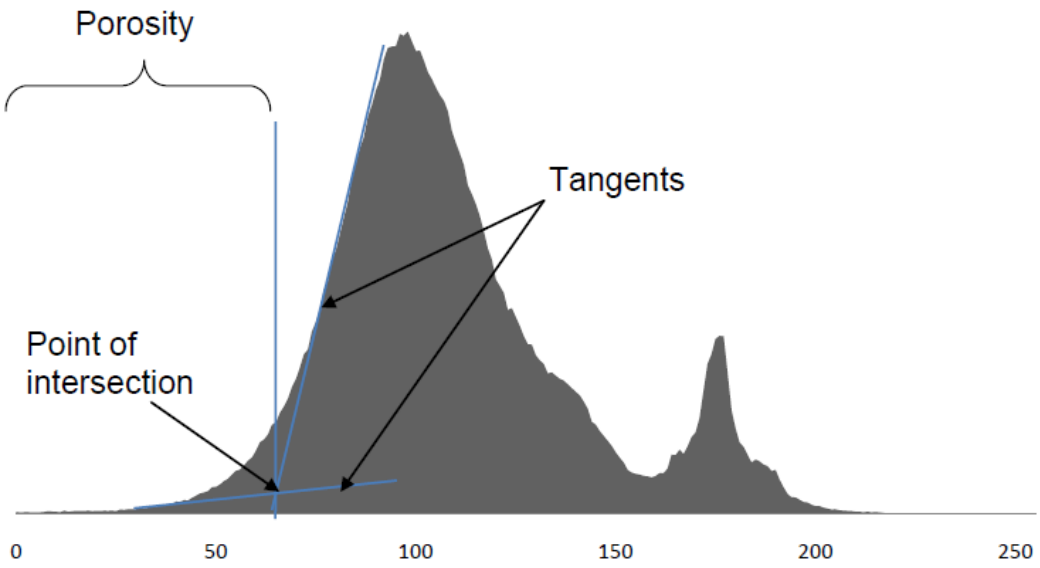

Figure 3.9: Determination of porosity by tangent method

Degree of slag hydration:

The degree of hydration was determined for 7 and 28 day old samples using the expressions below [44, 318] for the neat and slag blended systems.

$$DH_{SEM}^{cem}(t) = 1 - \frac{V_{(t)cem}}{V_{(0)cem}} \quad (3.5)$$

$$DR_{SEM}^{SCM}(t) = 1 - \frac{V_{(t)SCM}}{V_{(0)SCM}} \quad (3.6)$$

where:

$V_{(0)cem}$ is the volume fraction of cement before hydration,

$V_{(0)SCM}$ is the volume fraction of unreacted SCM before hydration,

$V_{(t)cem}$ is the volume fraction of unhydrated cement at hydration time *t*, and

$V_{(t)SCM}$ is the volume fraction of unreacted SCM at hydration time *t*.

For a slag blended cement paste, it is often difficult to distinguish between the unreacted slag grain and the CH phase, as they have similar grey levels (as can be seen from Figure 3.7) and tend to overlap on the histogram. As a result, in determining the degree of hydration of a slag blended system by image analysis, chemical elemental mapping by EDS is often combined with BSE-SEM imaging [44, 153, 318].

Slags are rich in magnesium, and due to the element's low mobility, magnesium maps will reveal the initial position of the unreacted slag grains. As the slags undergo hydration, a dark rim is formed around the slag grain, which can be removed by applying a threshold on the map to show only the unreacted slag grains. The resulting map is then overlaid on the original BSE-SEM image to indicate the position, shape and size of the unreacted slag grains.

This approach has been used by various researchers [44, 305, 318] to determine the degree of slag hydration. The technique is described in Figure 3.10. Figure 3.10a shows the original BSE-SEM image while Figure 3.10b shows the magnesium map obtained from EDS. Threshold was applied to Figure 3.10a to highlight the unreacted slag grains. However, during the process of thresholding, some clinker and portlandite phases were also captured as seen in Figure 3.10c. To isolate the unreacted slag grains, the magnesium map (Figure 3.10b) was overlain on Figure 3.10c to obtain Figure 3.10d. The area fraction corresponding to the unreacted slag grains can then be obtained from Figure 3.10d. Due to the limitation of the resolution, slag grains smaller than 0.3 μm will not be captured. However, from the particle size distribution of the slags shown in Figure 3.2, we can see that this will not have any impact on the measurement.

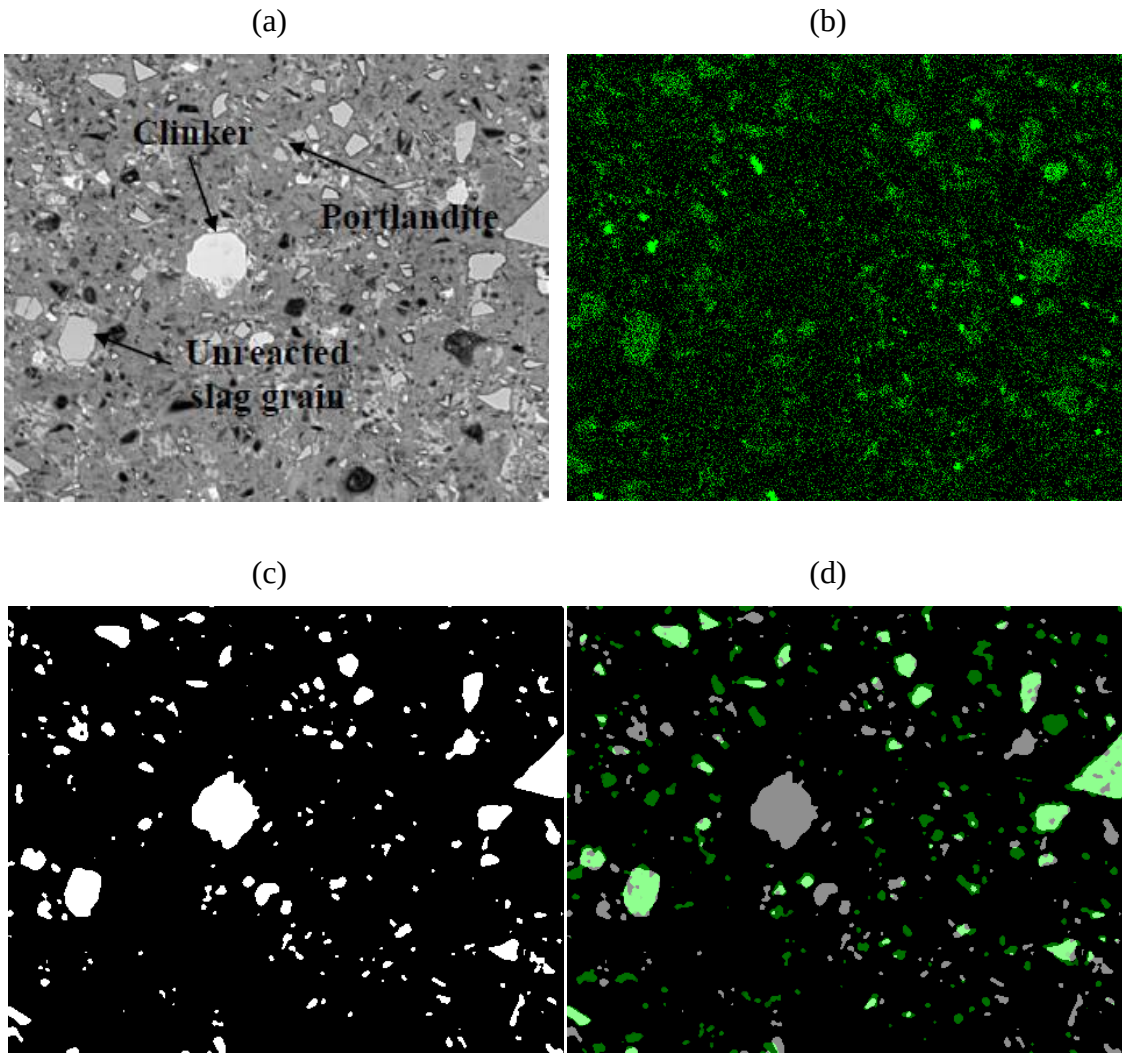

Figure 3.10: Determination of degree of hydration of slag by SEM combined with EDS (a) original BSE-SEM image (b) EDS Mg map (c) threshold of original image showing unreacted slag grains, portlandite and clinker (d) thresholded image overlain by Mg map

3.6.2 Unconfined compressive strength development

Compressive strength was determined in accordance with the procedure outlined in EN 196-1:2005 [301] for mortar samples. Compressive strength was determined at 1, 7, 28, 90 and 180 days. Except for the 1 day old samples, the samples were brought out from the curing tubs at the test date, and cleaned with a dry cloth before testing. Each mortar prism was split into two halves to produce six samples, having an approximate size of 40 x 40 x 80 mm. Thereafter, the split samples were tested

for compressive strength using a Tonipact 3000 concrete cube crusher. The compressive strength was taken as the average of six measurements.

3.6.3 Methods for studying transport properties

3.6.3.1 Water penetrability

The degree of capillary porosity, which was determined on 7 and 28 day old paste samples, enabled the effect of temperature on the early stages of the microstructural development to be studied. In order to study similar effects on mortar samples, water penetration tests were carried out. Both techniques complement each other. While the degree of capillary porosity does not give any indication as to the connectivity of the pores, it does give information regarding the microstructure. The water penetration tests on the other hand, does not give any information on the microstructure, but can be used to assess the connectivity of the pore system, and in some cases it is often linked to durability.

Drying or preconditioning of samples is a very important aspect that should be considered in determining the water transport properties of mortars or concretes. Drying at 50°C is considered to be less damaging to the microstructure [131], however, it usually takes longer periods for the samples to reach constant mass during which hydration and pore refinement will still be going on. On the other hand, drying at 105°C reaches equilibrium faster but induces microcracks [325] and creates irreversible microstructural alterations [326], which will also have effects on the transport properties. While drying at 50°C might seem to be the best option, there is the possibility that microcracks could also be formed as reported by Wu *et al.* [327].

Since the scope of the study did not involve looking at the effect of the drying technique on water penetrability, two different methods – sorptivity and water absorption, involving the use of different drying techniques were used to study the water transport property. In terms of the age of the samples, 7 day old samples were considered unsuitable for the tests. This was as a result of the longer times required to dry the samples to constant mass. For 7 day old samples, where the microstructure is not fully developed and hydration is still on-going, drying would interfere with the hydration process and microstructural development thus affecting the results. Hence, the tests were only conducted on 28 and 90 day old samples. Also, mortar samples were used instead of concrete so as to be able to relate the results to other aspects of the study.

Sorptivity:

Sorptivity was determined using similar methods as used by Tasdemir [328], and Gӧneyesi [131]. 50 mm mortar samples were used for the test. The test was conducted on triplicate samples. The samples were cured for 28 and 90 days at 20 and 38°C, after which they were dried to constant mass in an oven at 50°C. Depending on the mix, it took about 20 – 35 days for the samples to dry to constant mass, with the slag blends taking longer times to dry than the neat system. After drying, the sides of the samples were coated with paraffin and weighed to obtain the initial mass before they were placed in a trough of water at 20°C. The water level was maintained at about 5mm from the base of the samples (Figure 3.11), all through the experiment. This was achieved by occasionally topping-up the water in the trough. The mass of the samples were recorded at predetermined times (1, 4, 9, 16, 25, 36, 49 and 64 mins). At each of these times, the mass of water absorbed by each specimen was calculated by subtracting the initial mass from the recorded

mass, and from this the sorptivity coefficient (*k)* can be determined using the following expression:

$$k = \frac{Q}{A\sqrt{t}} \qquad (3.7)$$

where:

Q amount of water absorbed in m^3, which was calculated by dividing the mass of the water absorbed in kg, by the density of water (1000 kg/m^3)

t time in seconds

A cross-sectional area of the specimen that was in contact with the water in m^2

k sorptivity coefficient in $m^3/m^2s^{1/2}$.

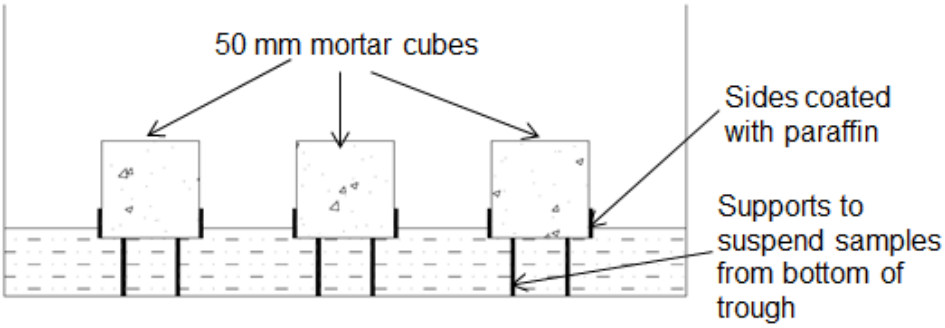

Figure 3.11: Schematic of setup used for sorptivity test

In determining *k*, values of *Q/A* were plotted against $\sqrt{t}$, and *k* was taken as the slope of the straight line fitted through the origin to the data points as shown below in Figure 3.12.

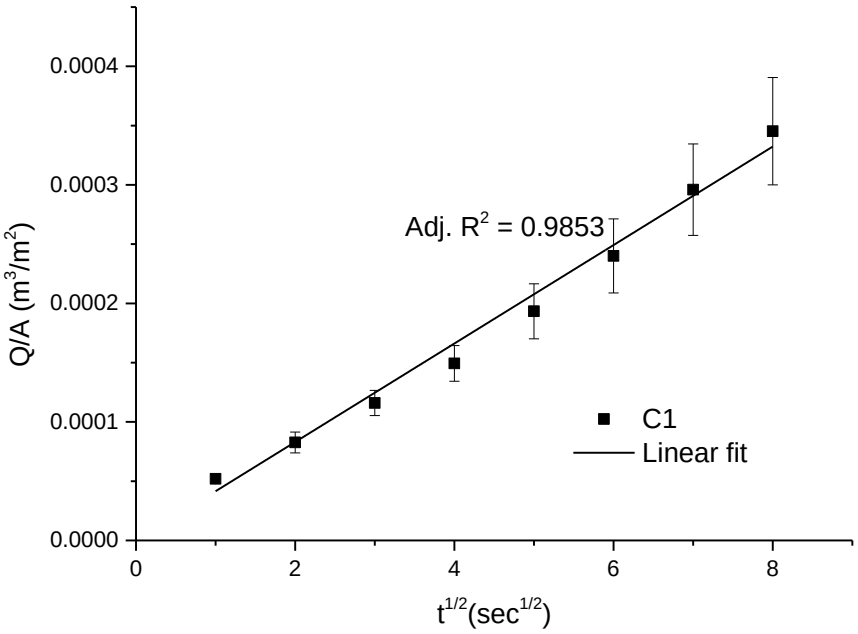

Figure 3.12: Linear fit for the determination of sorptivity coefficient for a C1 mortar sample cured for 28 days at 20°C

Water absorption:

Water absorption was determined according to the procedure outlined in BS 1881-122:2011 [329]. However, mortar samples were used in place of concrete. The mortar samples were prepared and cured in similar ways as the samples used for the sorptivity test. At the end of the curing period, the samples were dried in an oven for 72 hours at 105°C to remove all the evaporable water. After drying, the samples were placed in a desiccator and left to cool for 24 hours at room temperature before testing. The samples were weighed to obtain a dry mass M_d, after which they were completely immersed in a water tank at 20°C. The water level in the tank was maintained at 25 mm above the samples throughout the duration of the test by occasionally topping-up with water. The mass of the samples were recorded at 10, 30, 60 and 120 mins. The water absorbed (W_a) as a percentage was calculated using Equation 3.8 and plotted against time *t*.

$$W_a = \frac{K(M_t - M_d)}{M_d} \times 100 \qquad (3.8)$$

where:

M_d dry mass of the sample in grams

M_t mass of the sample after time *t*, in grams

K correction factor for the shape of the samples, which is equal to 0.667 [329]

W_a water absorbed in %

3.6.3.2 Depth of chloride penetration by silver nitrate colorimetric technique

The depth of chloride ion penetration was determined using the silver nitrate ($AgNO_3$) spray technique. 50 mm mortar cubes were exposed to a 3% NaCl solution after they had been initially cured for 7 and 28 days respectively, at temperatures of 20 and 38°C. The samples were subjected to two chloride exposure conditions (saturated and cyclic, as described in Section 3.5) at 20°C and only the saturated exposure condition at 38°C. The samples were withdrawn periodically, at 14, 28, 56 and 90 days, to determine the depths of chloride ion penetration. The withdrawn samples were split in half and the surfaces of the freshly split samples were sprayed with a 0.1M $AgNO_3$ solution. The presence of free chlorides was indicated by the formation of a white precipitate of silver chloride (AgCl), while in the absence of free chlorides the reaction between silver nitrate and portlandite resulted in a brown coloration, due to the formation of silver hydroxide (Figure 3.13). By taking linear measurements from the edge of the specimen up to the colour change boundary, the depth of free chloride penetration can be determined.

Although, this technique has its limitations in that it can only indicate the presence of free chloride ion if the concentration is greater than 0.15% by weight of cement [200], it has been widely used by several researchers [200, 202, 274, 330, 331].

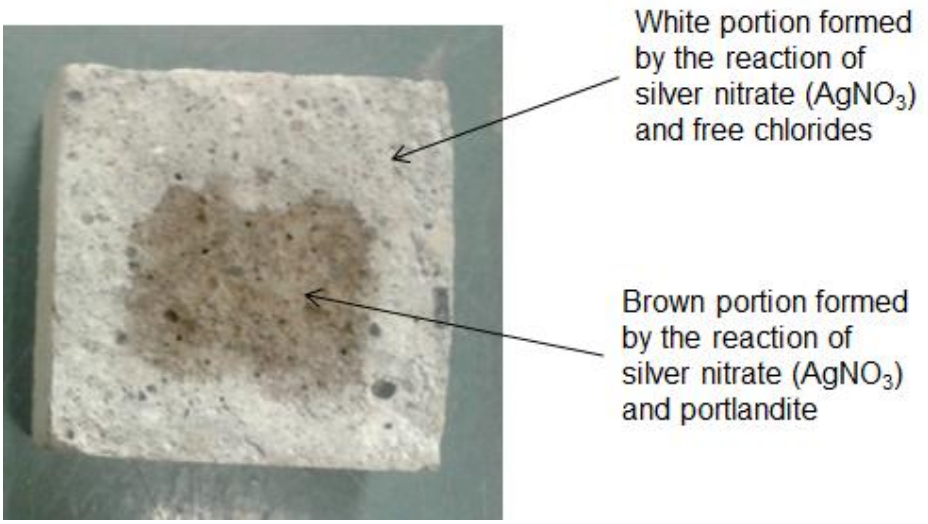

Figure 3.13: Colour changes for chloride ingress sample sprayed with 0.1M $AgNO_3$ solution

3.6.3.3 Total chloride content

Sample preparation:

40 x 40 x 160 mm mortar samples were cast and cured for 7 and 28 days respectively at temperatures of 20 and 38°C. After curing, a slice, about 20 mm thick, was sawn off from one end of the samples so as to obtain a fresh surface. An epoxy – based paint was used to coat all the sides of the sample except the fresh surface so as to allow for unidirectional chloride ingress. The coated samples were left in the laboratory for 2 days to allow for proper curing of the paint, after which they were saturated in deionised water for 24 hours.

Exposure to chloride solution:

The saturated samples were then immersed in a tub containing 3% NaCl solution for a soaking period of 90 days. The liquid to solid ratio was kept above 12.5 millilitres

per square centimetre of exposed surface as recommended in EN 12390:2015 [275], all through the exposure period.

Extraction of layers/ grinding:

At the end of the exposure period, the samples were removed from the tub and wiped dry with a clean cloth. Layers were extracted from the sample by dry cutting using an Erbauer tile cutter (Figure 3.14). The thickness of the cutting blade was approximately 3 mm. A total of 7 layers (approximately 5 mm thick) were cut from each sample. After cutting, each of the layers was placed in separate polythene bags for grinding. Grinding was done for most of the samples using a mortar and a pestle. The samples were ground to particles passing through a 300 microns sieve. The ground samples were further dried in an oven at 105°C for 24 hours before they were analysed for total chloride content.

(a) (b)

Figure 3.14: (a) Dry cutting of sample into layers (b) Layers marked on sample prior to cutting

Determining total chloride content:

Total chloride content was determined for each layer using the procedure recommended by RILEM [277]. About 1 gram of the dried samples was weighed

and placed in a beaker. 50 ml of concentrated nitric acid (HNO_3) diluted to 1 in 2 parts was added to the sample. After the effervescence had stopped, the solution was heated and allowed to boil for about 1 min. 5 ml of 0.1N silver nitrate solution ($AgNO_3$) was added to the beaker and the resulting solution was allowed to boil for another 1 min. After this, the solution was allowed to cool down to room temperature and filtered over a filter paper under vacuum. The filter paper and beaker were washed with diluted HNO_3 (diluted to 1 in 100 parts), and collected alongside the filtrate. The final volume of the filtered solution was made up to 200 ml by adding diluted HNO_3. This was titrated against a 0.05M ammonium thiocyanate solution (NH_4SCN). A blank test was also run using the same procedure outlined above, but without any sample. The total chloride content per mass of the dried sample was determined using the expression below:

$$\%Cl = \frac{3.5453 V_{Ag} M_{Ag} (V_2 - V_1)}{m V_2} \qquad (3.9)$$

where:

V_{Ag} volume of $AgNO_3$ added in cm^3

M_{Ag} molarity of the $AgNO_3$ solution

V_1 volume of NH_4SCN used in the sample in cm^3

V_2 volume of NH_4SCN used in the blank test in cm^3

m mass of the dried sample used for the test in grams

Two or three measurements were taken per layer, depending on the amount of ground sample obtained from the cutting and grinding process. The average total

chloride content obtained per layer was plotted against the distance of the centre of each layer from the exposed face, to obtain total chloride profiles.

Chloride diffusion coefficient:

The non-steady state chloride diffusion coefficient D_c and the chloride content at the surface C_s were determined by performing a non-linear regression analysis on the total chloride profiles, using the expression below [275]:

$$C_x = C_s\left(1 - erf\left[\frac{x}{2\sqrt{D_c t}}\right]\right) \qquad (3.10)$$

where:

C_x chloride content measured at average depth x and exposure time t, % by mass of sample

C_s calculated chloride content at the exposed surface, % by mass of sample

x depth below the exposed surface to the mid-point of the ground layer, in metres

D_c calculated non-steady state chloride diffusion coefficient, in square metres per second (m^2/s)

t exposure time, in seconds (s)

erf error function

The regression analysis was done using Excel solver function. The first set of data (the chloride content of the first layer, obtained very close to the exposed surface)

were not included in the regression analysis (Figure 3.15) as recommended in EN 12390:2015 [275].

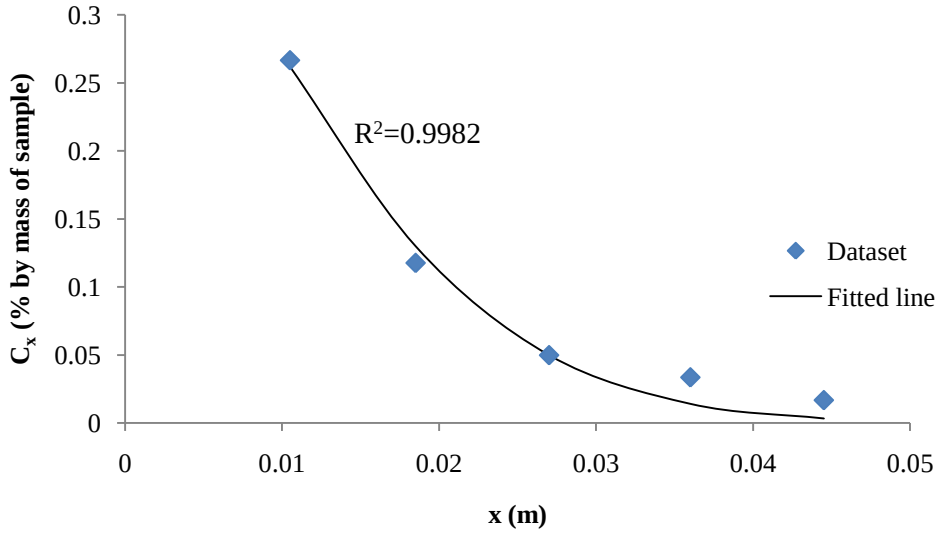

Figure 3.15: Determining the non-steady state chloride diffusion coefficient D_{nss} by non-linear regression

3.6.3.4 Water-soluble chloride content

Water-soluble chloride content is defined here, as the amount of chloride ion in a concrete specimen which can be leached out by water at room temperature [332]. This is not the same as the free chloride content, which is taken as the amount of chloride ion dissolved in the pore solution that can be obtained by squeezing concrete samples at high pressures [332].

Several leaching methods have been proposed by various researchers for the extraction of water-soluble chlorides (see Section 2.3.5.1). Amongst the various methods, 72 hour standing in water at 20°C was selected for this study, as according to Arya *et al*. [273], this was seen to be more suitable for total chloride contents of 1.5 to 2.0% by weight of cement.

Experimental procedure:

5 grams of ground samples was taken from each layer of the same samples used for the total chloride content determination test. This was placed in a plastic bottle. A solid to liquid ratio of 1:20 was used [273], hence 100 ml of distilled water was added to the sample and the plastic bottle was sealed and left to stand for 72 hours at 20°C. At the end of the standing period, the solution was filtered off and the chloride concentration of the filtrate was determined using an ion chromatography device.

The water-soluble chloride content, which was taken as the chloride concentration of the filtrate, was expressed in parts per million (ppm) and plotted against the distance of the centre of each layer from the exposed face, to obtain the water-soluble chloride profile.

3.6.3.5 Chloride binding capacity

Sample preparation:

Paste samples were prepared and cured in sealed plastic moulds at 20 and 38°C, for a period of 8 weeks. The central portions of the cured samples were wet-crushed and water-sieved to particles ranging in size from 0.25 to 2.0 mm. The particulate samples were vacuum dried in a desiccator at room temperature to remove most of the water, then stored in a desiccator with decarbonized air at 11% RH kept by saturated lithium chloride solution for 14 days.

Bound chloride content:

Bound chloride content was measured using the equilibrium method. This method was developed by Luping and Nilsson [243] and has been used by several researchers [15, 18, 245]. About 20 grams of the particulate sample dried at 11% RH

was put in a plastic cup and filled with approximately 50 ml of a given concentration of NaCl solution saturated with $Ca(OH)_2$. Five different concentrations of NaCl solution was used – 0.1, 0.5, 1.0, 2.0 and 3.0M. The filled plastic cup was sealed and stored at temperatures of 20 and 38°C for a period of 6 weeks to attain equilibrium. After equilibrium was reached, the chloride concentration of the resulting solution was determined using an ion chromatograph. Knowing the initial concentration of the NaCl solution, the content of bound chlorides was determined using the expression:

$$C_b = \frac{35.45V(C_i - C_f)}{W} \qquad (3.11)$$

where:

C_b bound chloride content in mg/g-sample

V volume of solution in ml

C_i initial concentration of the chloride solution in mol/l

C_f equilibrium concentration of the chloride solution in mol/l

W weight of the dry sample in g, which is calculated from the difference in weight of the sample dried in a desiccator at 11% RH and in an oven at 105°C.

Correction for temperature effect on C_b:

Evaporation occurred at rates ranging from 3 – 12% at 38°C (as shown in Appendix D) and this was corrected for using the method adopted by Zibara [244] as shown in Equations (3.12 – 3.14). The correction is based on two assumptions:

- The ratio of the initial and equilibrium volume of the chloride solutions is equal to the ratio of the initial and equilibrium weight of the chloride solutions
- The evaporation does not affect the equilibrium between the bound and free chlorides

$$\frac{V_i}{V_{ee}} = \frac{W_i}{W_{ee}} \qquad (3.12)$$

$$C_e \times V_i = C_{ee} \times V_{ee} \qquad (3.13)$$

$$C_e = C_{ee} \times \frac{V_{ee}}{V_i} = C_{ee} \times \frac{W_{ee}}{W_i} \qquad (3.14)$$

where:

V_i initial volume of host solution (without evaporation) in ml

V_{ee} volume of host solution after evaporation occurred in ml

W_i initial weight of host solution in grams

W_{ee} weight of host solution after evaporation occurred in grams

C_e chloride concentration at equilibrium (without evaporation) in mol/l

C_{ee} measured chloride concentration at equilibrium after evaporation occurred in mol/l

Chloride binding isotherms:

The bound chloride content *(C_b)* was plotted against the equilibrium concentration *(C_f)*. The chloride binding coefficients (α and β) of the mixes were then determined

using Freundlich and Langmuir binding isotherms [18] as shown below in Equations 3.15 and 3.16.

$$C_b = \alpha C_f^{\beta} \tag{3.15}$$

$$C_b = \frac{\alpha C_f}{(1 + \beta C_f)} \tag{3.16}$$

Figure 3.16 shows the chloride binding coefficients α and β obtained for one of the mixes using Freundlich and Langmuir binding isotherms. The Freundlich binding isotherm has been widely used by several researchers [18, 292, 296, 333], and from Figure 3.16, it is seen that it gives the best fit to the data; hence it was used in determining the chloride binding coefficients of all the mixes.

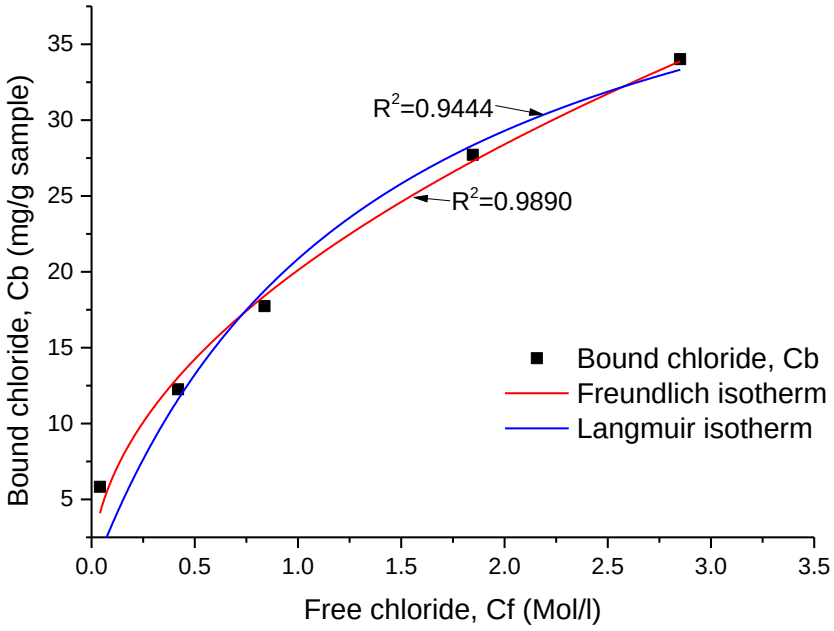

Figure 3.16: Best fit binding isotherm for determining chloride binding coefficients

Chapter 4
Effects of Binder Composition and Temperature on the Hydration of CEM I and Slag Blends

4.1 Hydraulicity of the slags

There are several indices that have been proposed for use in assessing the potential of a slag to form cementitious hydration products [3, 9, 10, 12, 44], as discussed previously in Section 2.1.3.4. Table 4.1 shows those used here for the initial classification of the slags.

Table 4.1: Basicity and activity indices of the slags

Basicity index	Slag 1	Slag 2
CaO/SiO_2	1.05	0.94
$(CaO + MgO)/SiO_2$	1.28	1.18
$(CaO + MgO + Al_2O_3)/ SiO_2$	1.61	1.37
Activity index (%)		
7 day	58.8	53.6
28 day	84.3	84.3

From the table, it is seen that slag 1 has a higher basicity index and should be more reactive than slag 2. The activity index of the slags at 20°C, which were obtained in accordance with EN 15167-1 [42], indicates that slag 1 would have better early age strength than slag 2, but similar later age strength.

4.2 Compressive strength development

Figure 4.1 shows the unconfined compressive strength (UCS) development of all the mixes at 20°C. The CEM I 42.5R (C1) mix had higher strength up to 7 days but this trend reversed at 28 days and beyond with the slag blends having higher strengths.

The poor early age performance can be attributed to the lower reactivity of the slags as observed previously by Al-Amoudi *et al*. [161]. At early ages, the degree of slag hydration is considerably less than that of the cement clinker. Whittaker *et al*. [135] reported that, in 40% slag blends, approximately 40% of slag had hydrated after 7 days at 20°C, compared with about 80% of the clinker.

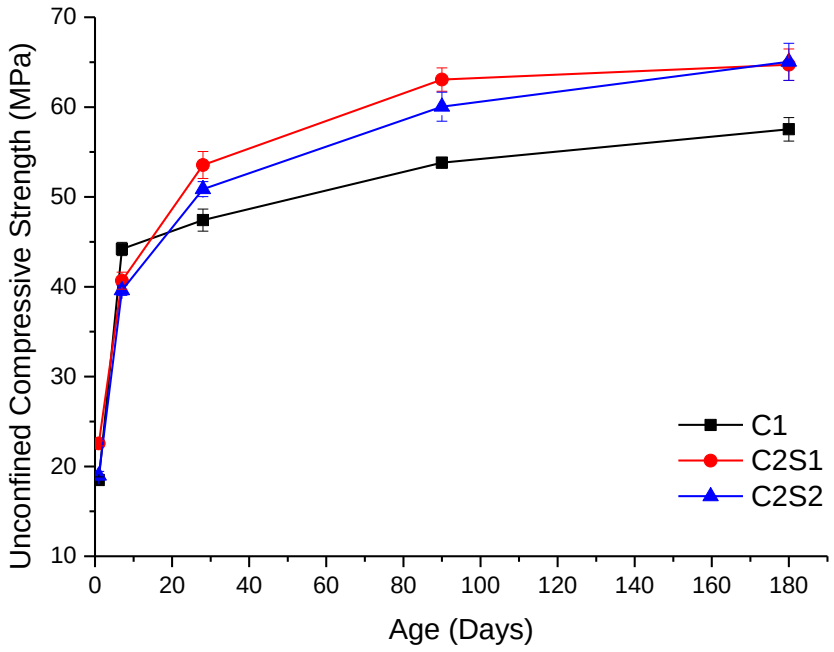

Figure 4.1: Compressive strength development at 20°C

The UCS development of all the mixes at 38°C is shown in Figure 4.2. High temperature curing was seen to increase the early strength of all the mixes up to 7 days, except the neat C1 mix. While the 1 day UCS of the C1 mix was greater at 38°C, the 7 day UCS was slightly lower at 38°C than at 20°C. After 28 days, there was minimal strength gain for the samples cured at 38°C as compared to those cured at 20°C. This can be attributed to the effect of high temperature curing, which would result in a high initial rate of hydration and slower subsequent hydration rates [23, 290]; and shows the deleterious impact of high temperature curing on the later-age strength development. At 38°C, the UCS of the slag blends was higher than that of

C1 at all ages indicating that the slag blends had better strength performance. This agrees with similar findings by [23, 24, 163].

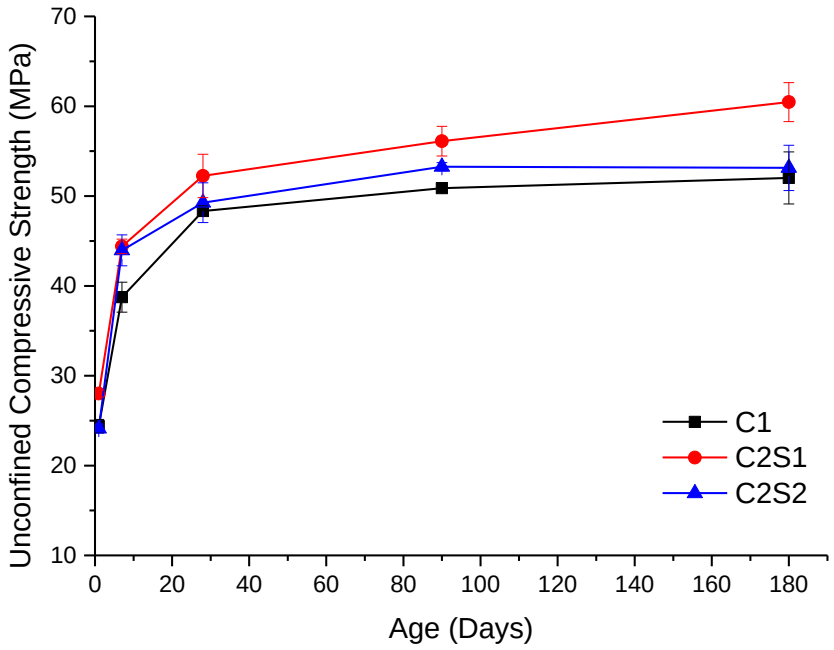

Figure 4.2: Compressive strength development at 38°C

At 20°C there was no significant difference in the UCS of the two slag blends, especially at later ages; whereas at 38°C, there was a clear distinction in their UCS with slag 1, the more basic of the 2 slags, performing better than slag 2 at all ages. Comparing this with the indices shown in Table 4.1, it can be seen that the strength performance of the slag blends at 20°C did not tally with the prediction of the basicity index, which predicted that slag 1 should have better strength performance due to its higher reactivity. This is in agreement with previous studies [10, 11, 334] which showed that at 20°C, there was no correlation between basicity indices and the properties of slag blends. However, at 38°C there was a correlation between the strength performance of the slag blends and the basicity indices. On the other hand, the strength performance was seen to tally with the prediction of the activity index,

which indicated that slag 1 would have better early age strength performance than slag 2, but similar later age strength performance.

4.3 Heat of hydration by isothermal calorimetry

4.3.1 Heat flow

Figure 4.3 and Figure 4.4 shows the rate of heat flow at 20°C and 38°C, as determined by isothermal calorimetry, normalised to the cement content. The addition of quartz and slag to C2 resulted in a slight acceleration of the alite hydration, as can be observed from Figure 4.3 and Figure 4.4, where the curves of C2S1, C2S2 and C2Q appeared slightly earlier than that of C2. This can be attributed to the filler effect of the quartz and the slags [30, 124, 153, 335]. At the start of the reaction, the quartz and the slags do not react, and as a result more space becomes available for the hydrates of the clinker [124, 153].

The main difference between Figure 4.3 and Figure 4.4 is seen within the early stages of the reaction (0 to 20 hrs). The high temperature of 38°C resulted in an increase in the rate of reaction of all the mixes, especially at the early ages, as was observed in previous studies [110-112]. Peaks II and III corresponding to the formation of C-S-H and secondary ettringite [83, 147], are observed after about 15 hours from the start of the reaction at 20°C compared to after about 7 hours at 38°C. Peaks II and III appeared to be merged together at 20°C; whereas at 38°C, there was a clear distinction between both peaks. The reason for this is because at higher temperatures, there is an increase in the amount of sulphate ions reversibly bound to the C-S-H phase, such that fewer sulphates are available to react and form AFt [111, 112, 116]. This was clearly reflected in Figure 4.4, where the intensity of peak III was much lower than that of peak II; whereas in Figure 4.3, both peaks had similar

intensities. The formation of the AFm phases, which is represented by peak IV [83], was visible at 20°C, but not at 38°C. This indicates that at the higher temperature, the AFt to AFm conversion occurred very early on such that peak IV was hidden underneath peaks II and III. This can be attributed to the accelerating effect of temperature on the early stages of hydration [45, 111], and explains the reason for the initial higher strengths observed at 38°C in Figure 4.2.

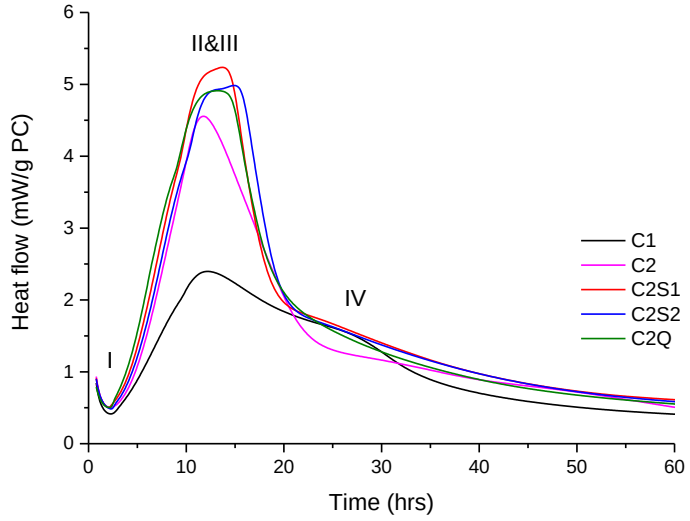

Figure 4.3: Heat flow at 20°C normalised to the cement content

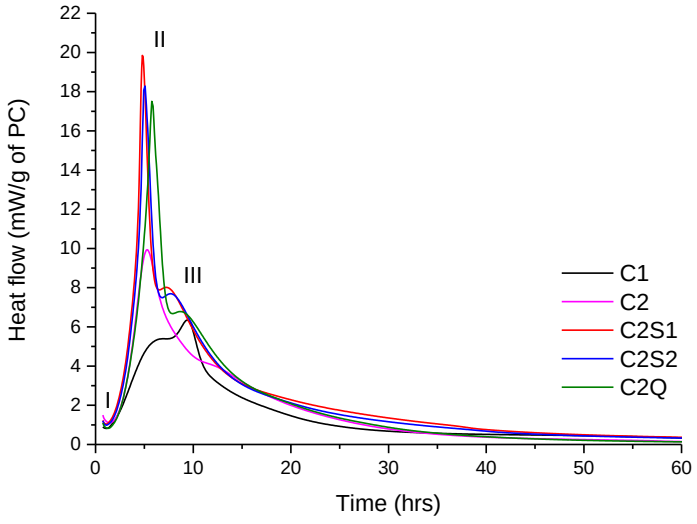

Figure 4.4: Heat flow at 38°C normalised to the cement content

Table 4.2 shows the maximum peak heat flow (q_{max}) for all the mixes and the time taken to reach q_{max}. At 20°C, the C1 sample was the first to reach its maximum peak heat, followed by C2S1. However, at the higher temperature, both slag blends reached their maximum peak heat ahead of the C1 mix. As the temperature rose from 20 to 38°C, there was an increase of about 164% in the q_{max} of C1 at 38°C, compared to about 300% for the slag blends. This can be attributed to the accelerating effect of temperature; with the effect being greater on the slag blends than the C1 mix. This indicates that at 38°C the slags reacted more rapidly and contributed to the heat released in the system, hence the lower times taken to reach q_{max}. This agrees with previous findings [126, 146-148], where it was reported that at higher temperatures, GGBS contributes more to the total heat of hydration than at lower temperatures. At both temperatures, the q_{max} of C2S1 was higher than that of C2S2. Since the level of replacement was the same for both mixes, the higher values of q_{max} obtained for C2S1 indicates that slag 1 had reacted more. This correlates with the compressive strength results shown in Figure 4.1 and Figure 4.2.

Table 4.2: Maximum peak heat flow (q_{max}) and time taken to reach q_{max}

	20°C		38°C	
	q_{max} (mW/g of PC)	Time (hrs)	q_{max} (mW/g of PC)	Time (hrs)
C1	2.40	12.21	6.35	8.79
C2S1	5.24	13.70	19.85	4.55
C2S2	4.98	14.95	18.29	4.81

4.3.2 Cumulative heat flow

The cumulative heat flow at 20°C and 38°C normalised to the cement content is shown in Figure 4.5 and Figure 4.6 respectively. Similar trends were observed in the total heat curves for both temperatures. There was positive heat contribution all

through the period of measurement. Also, at the end of the measurement period (at about 700 hrs), for a given mix, temperature did not greatly affect the total heat.

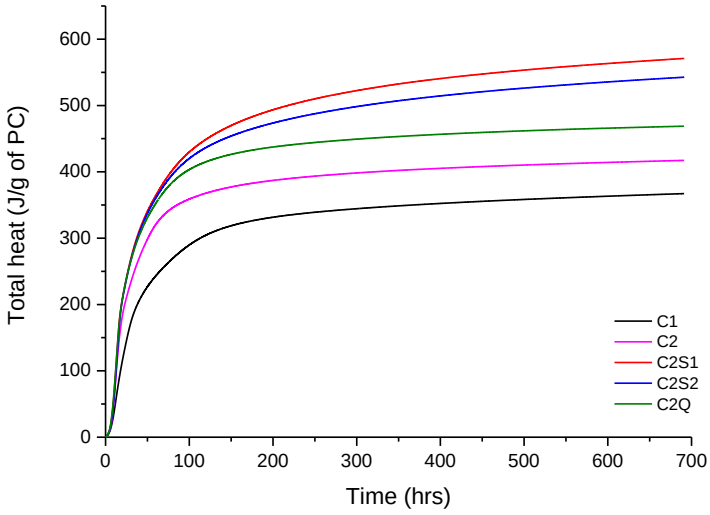

Figure 4.5: Total heat at 20°C normalised to the cement content

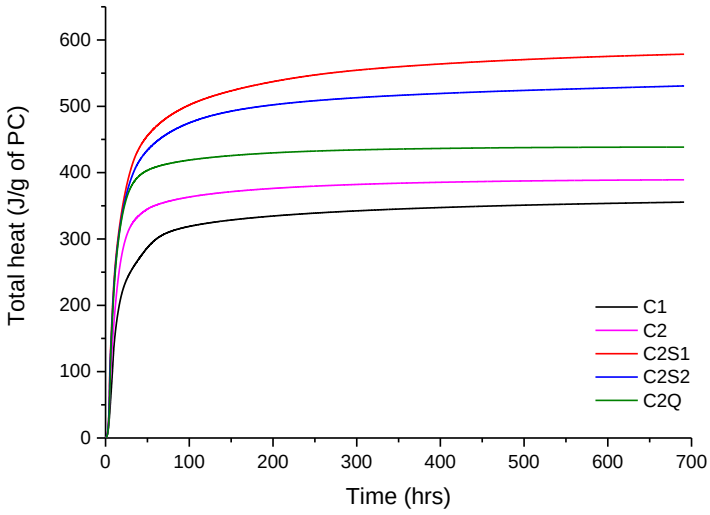

Figure 4.6: Total heat at 38°C normalised to the cement content

A major difference was however seen at the early stages of the reaction, where the 38°C heat curves were steeper over 0 to 100 hrs, due to the accelerating effect of temperature on the hydration reaction. This is similar to the trends observed in the compressive strength results (Figure 4.1 and Figure 4.2). After about 700 hrs, the

heat curves of the C1 mix were relatively at the same level at both temperatures; whereas that of the C2 and C2Q mixes appeared to be slightly lower at 38°C as compared to 20°C. This indicates that the high temperature only accelerated the early hydration (0 to 100 hrs) of C2 but not the later hydration (at about 700 hrs). This agrees with previous studies [110-112], which reported that higher temperature curing increases the rate of hydration of PC, but the effect is more pronounced at the early stages of hydration than at the later stages.

The cumulative heat evolved by the slag blends, normalised to the cement content, was greater than that of C2 at both temperatures as seen in Figure 4.5 and Figure 4.6. This can be attributed to two reasons. The first being the hydration of slag, which has been shown to be exothermic [154, 336]; and the second, due to the filler effect [30, 153, 335]. At both temperatures, the total heat evolved by C2S1 (the blend containing the more reactive slag) was greater than that of C2S2. However, the difference was seen to be much higher at 38°C than at 20°C, thus indicating that slag 1 had reacted much more at 38°C. This is in correlation with the compressive strength results (Figure 4.1 and Figure 4.2), where it was observed that the difference between the UCS of the slag 1 and 2 blend was much higher at 38°C than at 20°C.

4.3.3 Degree of slag reaction

Figure 4.7 shows the positive contribution of the slag hydration to the total heat evolved. The procedure followed in obtaining this has been described previously in Section 3.6.1.1.

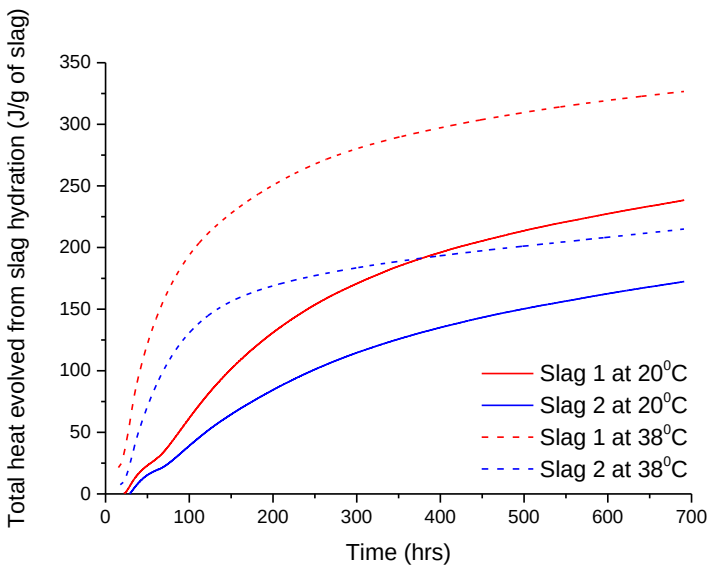

Figure 4.7: Total heat evolved from the slag hydration

From Figure 4.7, it can be seen that the contribution to the total heat from the hydration of the slags was far greater at 38°C than at 20°C. However, this was not clearly reflected on the overall total heat evolved by the slag blends at 38°C, as seen at the later stages (at about 700 hrs) in Figure 4.3 and Figure 4.4. This is because the total heat evolved by C2 at about 700 hrs, is greater at 20°C than at 38°C, thus masking the increased contribution from the slag hydration at the higher temperature. This would explain why towards the later stages of the measurement, the total heat curve of each slag blend appeared to be at the same level, at both temperatures. This indicates that high temperature favours the reactivity of slags more than that of clinker, and is in agreement with previous findings [21, 22, 26, 291].

In terms of the reactivity of the slags, slag 1 had a higher degree of reaction than slag 2 at both temperatures, as was predicted by the basicity index in Table 4.1. However, the difference in reactivity was much greater at 38°C than at 20°C. This correlates with the compressive strength results and is in agreement with previous studies [337, 338]. The reason for this can be attributed to two aspects. The first

being the lower activation energy of the slag 1 blend, which is discussed in the next section, and the second being the higher alumina content of slag 1. Richardson *et al.* [147] observed for slag blends that the reaction of the silicates and aluminates were accelerated at higher temperatures. Since slag 1 has a higher alumina content than slag 2 (as seen in Table 3.1), the higher temperature would accelerate its reaction more than that of slag 2.

4.3.4 Activation energy of the slag blends

The activation energy of the slag blends was determined from the cumulative heat flow, by applying Arrhenius equation as shown below [9, 126]:

$$k(T) = k_0 exp\left[\frac{-E}{RT}\right] \quad (4.1)$$

$$\frac{t_1}{t_2} = exp\frac{E}{R}\left(\frac{1}{T_1} - \frac{1}{T_2}\right) \quad (4.2)$$

where $k(T)$ is the rate constant (rate of hydration), k_0 is the pre-exponential term, t_1 and t_2 = time at 50% degree of hydration (t_{50}) at temperatures T_1 and T_2 respectively, E = activation energy in kJ/mol, and R = gas constant taken as 8.314 $JK^{-1}mol^{-1}$.

Equation 4.2 was used to calculate the activation energy of the slag blends. In determining the values of t_1 and t_2, the total heat evolved (Q) was plotted against the inverse of time $(1/t)$, as seen in Figure A9 and Figure A10 in Appendix C. Q_∞ was extrapolated from the data at $1/t = 0$. The degree of hydration was approximated as Q/Q_∞, and plotted against time (t). t_{50} was taken as the time when the degree of hydration was 50%.

Values of 43.65 and 44.57 kJ/mol were obtained as the activation energy for the slag 1 and slag 2 blend respectively. These values fall within the range reported for slag blends [9, 23, 126]. Contrary to what was observed in Figure 4.7, there was no significant difference between the activation energy of the slag 1 blend and that of the slag 2 blend. The reason for this is can be seen from Equation 4.1, which shows that the rate of hydration is influenced jointly by the pre-exponential term *(k_0)* and the activation energy *(E)*. This implies that why both slag blends have similar activation energies, there may be a significant difference between their k_0 values. Although, this inference cannot be drawn as the k_0 values were not determined, values of Q_∞ obtained for the slag blends (shown in Table A1 in Appendix C), shows significant difference in the Q_∞ of the slag blends at 20 and 38°C.

4.4 XRD analysis

XRD analysis was carried out to examine the influence of temperature on the hydration of the clinker phases present in the mixes. Figure 4.8a and Figure 4.8b shows the XRD patterns obtained for 1, 7 and 28 day old paste samples of the various mixes at 20 and 38°C respectively. As observed in the calorimetry results, the high temperature accelerated the early hydration of the clinker phases. This can be seen by comparing Figure 4.8a and Figure 4.8b. For the neat C1 system, the reflections due to C_3S and C_3A were less pronounced after 1 day upon curing at 38°C. However, at 7 and 28 days, the reflections due to C_3S and C_2S were at similar levels at both temperatures. The peak due to portlandite (CH), a product of hydration of C_3S [45], was more intense at the higher temperature of 38°C for the C1 mix, thus indicating that more of these phases had reacted at the higher temperature. This agrees with earlier observations made by [110-112].

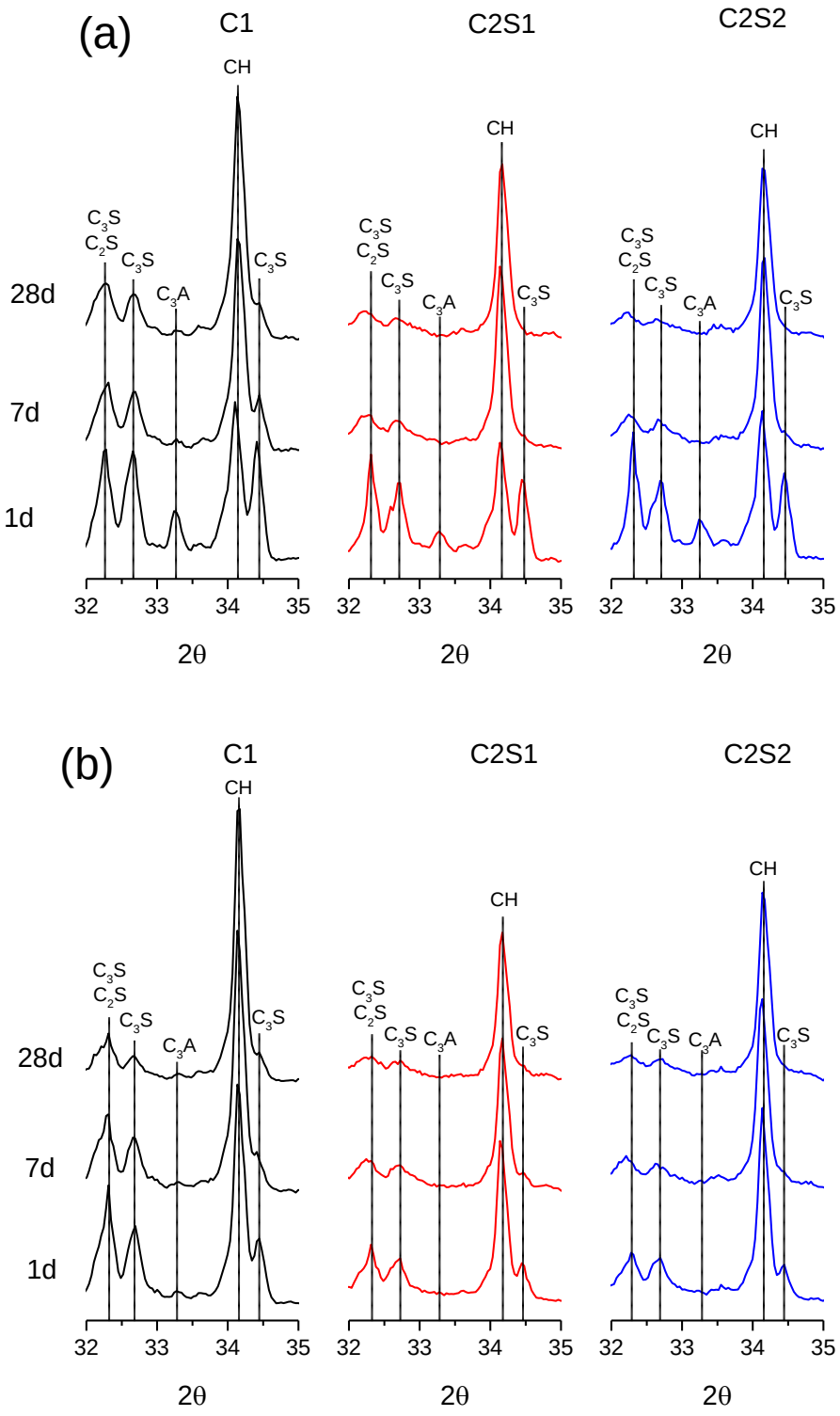

Figure 4.8: XRD patterns of paste samples showing the influence of temperature on the hydration of the clinker phases (a) 20°C (b) 38°C

For the slag blends, after 1 day there was no trace of C_3A in the samples cured at 38°C and the peaks of C_3S and C_2S were much lower than that of the samples cured at 20°C. At later ages of 7 and 28 days, the C_3S and C_2S peaks were also similar at

both temperatures. Also Figure 4.8 indicated that, at both temperatures, the blends containing slag 1 contained less CH than those containing slag 2. Assuming that the degree of clinker hydration was similar in the two blends, this will imply that slag 1 had reacted more than slag 2. This is in line with the results of the isothermal calorimetry shown in Figure 4.7, and will be discussed further in Section 4.6.

Figure 4.9a and Figure 4.9b shows the impact of temperature on the evolution of the AFt and AFm phases for all the mixes at 20 and 38°C. Ettringite (E), which is the main AFt phase had lower reflections at the higher temperature for all the samples, as was observed by Lothenbach *et al.* [291]. This is because at higher temperatures, more AFm phases are formed in preference to AFt [111, 112, 116]. This can be seen from Figure 4.9, where the reflections due to the AFm phases (calcium monosulfoaluminate – Ms, calcium hemicarboaluminate – Hc, calcium monocarboaluminate – Mc) are higher at 38°C than at 20°C, and supports the earlier observation in the heat flow measurements (Figure 4.3 and Figure 4.4).

The accelerating effect of temperature on the early hydration of C_3A can be seen by comparing Figure 4.9a and Figure 4.9b, where, after 1 day, the reflections due to the AFm phase appeared more prominent at 38°C than at 20°C. This indicates that the reaction of C_3A with SO_4^{2-} occurred earlier, and at a faster rate at the higher temperature. This explains why peak IV was not clearly visible in the heat flow curve (see Figure 4.4) at 38°C.

For the neat C1 system, the higher temperature resulted in an increase in the amount of Ms and a decrease in the amount of AFt. The reflections for Hc and Mc after 1 day were more prominent at 38°C than at 20°C, but this reversed after 7 days. Beyond 7 days, the amount of Hc decreased while that of Mc increased at both

temperatures, indicating that the Hc was gradually being converted to Mc, as was also observed in previous studies [305, 339-341].

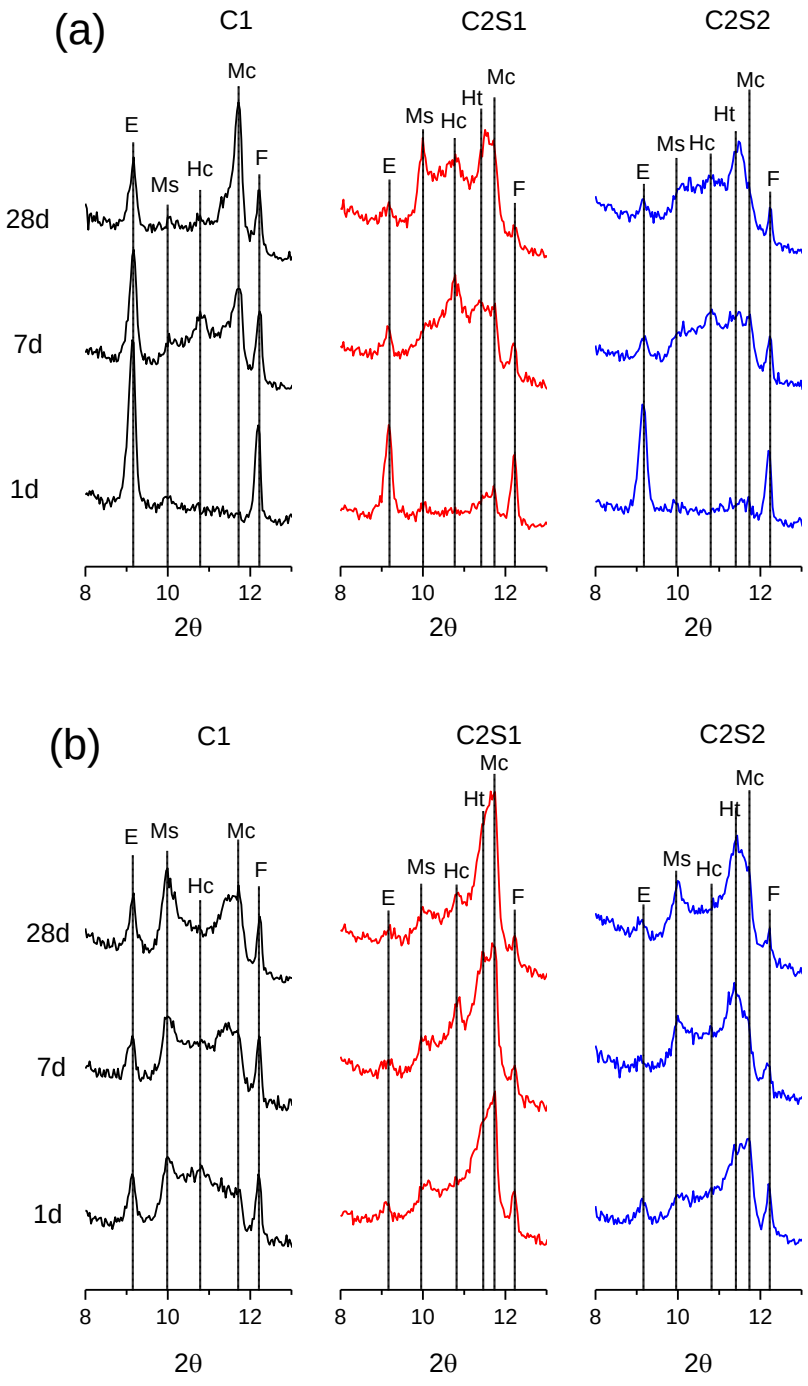

E – Ettringite, Ms – Calcium monosulfoaluminate, Hc – Calcium hemicarboaluminate, Ht – Hydrotalcite, Mc – Calcium monocarboaluminate, F - Ferrite

Figure 4.9: XRD patterns showing the Aft and AFm phase for all mixes at (a) 20°C (b) 38°C

For the slag blends, there was less AFt formed after 1 day at the higher temperature. The reflection for hydrotalcite (Ht), a product of slag hydration [136-138], was seen to overlap with that of Mc, and was more prominent after 1 day at the higher temperature, indicating that the early hydration of the slags was accelerated at the higher temperature. This correlates with the calorimetry results (Figure 4.7).

The reflections for Hc was more prominent in the aluminium-rich slag blend (C2S1) as observed by Whitaker *et al* [135], and temperature did not seem to have any impact on the amount formed except at 1 day. At 38°C, Mc was formed at the expense of Ms for the slag 1 blend. For the slag 2 blend, the amount of Hc decreased progressively and was barely noticeable after 28 days especially at the higher temperature, due to the conversion of Hc to Mc. The reflection for Ms and Ht was more prominent at 38°C than at 20°C for the slag 2 blend. The higher temperature did not have any significant effect on the amount of Mc formed for the slag 2 blend, as compared to the slag 1 blend.

Overall, in terms of the hydration products formed in both slag blends, the reflections due to Ms were slightly lower in C2S1 than in C2S2, but the reflections due to Ht and Mc was more prominent in C2S1 than in C2S2 at both temperatures, especially at the higher temperature. This indicates that the degree of hydration of slag 1 was much higher than that of slag 2 at 38°C, and correlates with the calorimetry and compressive strength results shown in Figure 4.7 and Figure 4.2 respectively.

4.5 Degree of slag hydration by BSE-SEM image analysis

Table 4.3 shows the degree of hydration determined by BSE-SEM image analysis of 7 and 28 day old paste samples cured at 20 and 38°C. The results followed the same

trend as the calorimetry and XRD (Figure 4.7 and Figure 4.9), where it was seen that the higher temperature increased the reaction rate of the slags. The higher temperature resulted in an increase in the degree of slag hydration, especially at early age. At 7 days, the degree of hydration of slag 1 and slag 2 at 38°C was greater than that of 20°C by about 14 and 11 percentage points respectively. Meanwhile, at 28 days, this difference fell, to about 8 and 5 percentage points for slag 1 and slag 2 respectively.

Table 4.3: Degree of hydration (%) of the slags

Age		Degree of slag hydration (%)	
		20°C	38°C
7 day	C2S1	39.6 ± 1.29	53.3 ± 1.12
	C2S2	31.8 ± 1.84	42.4 ± 1.76
28 day	C2S1	54.9 ± 1.00	62.4 ± 1.01
	C2S2	43.8 ± 1.55	48.9 ± 1.50

In terms of the impact of the chemical composition of the slags, the more reactive slag 1 had hydrated to a greater extent than slag 2, at both ages and curing temperatures. At 20°C, the degree of hydration of slag 1 was about 8 and 11 percentage points higher than that of slag 2 at 7 and 28 days respectively; while at 38°C, this became about 11 and 13 percentage points at 7 and 28 days respectively. At 38°C, as the curing duration was increased from 7 to 28 days, the degree of hydration of slag 1 was increased by about 9 percentage points compared to about 6 percentage points for slag 2. This indicates that slag 1 reacted more at the high temperature as was previously observed in the calorimetry and XRD results.

4.6 Portlandite content from thermogravimetric analysis

Figure 4.10 and Figure 4.11 shows the CH content calculated from thermogravimetric analysis (TGA) for all the samples cured at 20 and 38°C respectively.

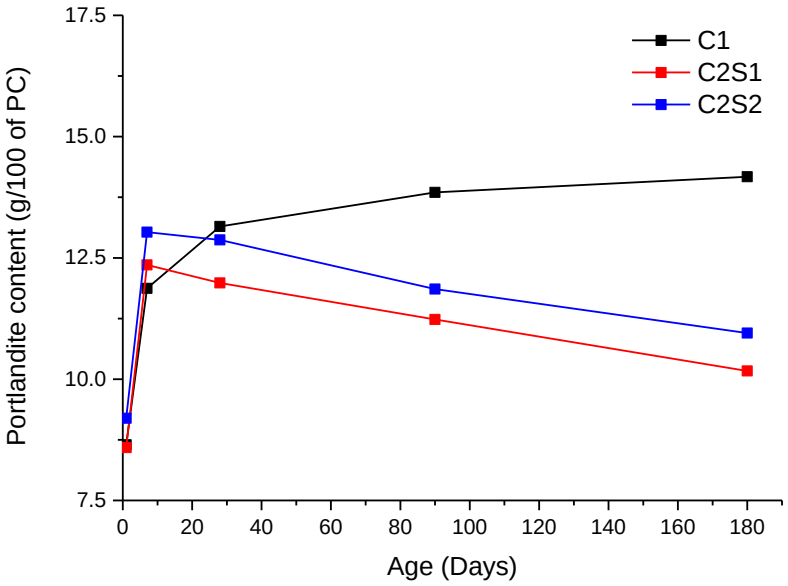

Figure 4.10: Portlandite content from STA at 20°C

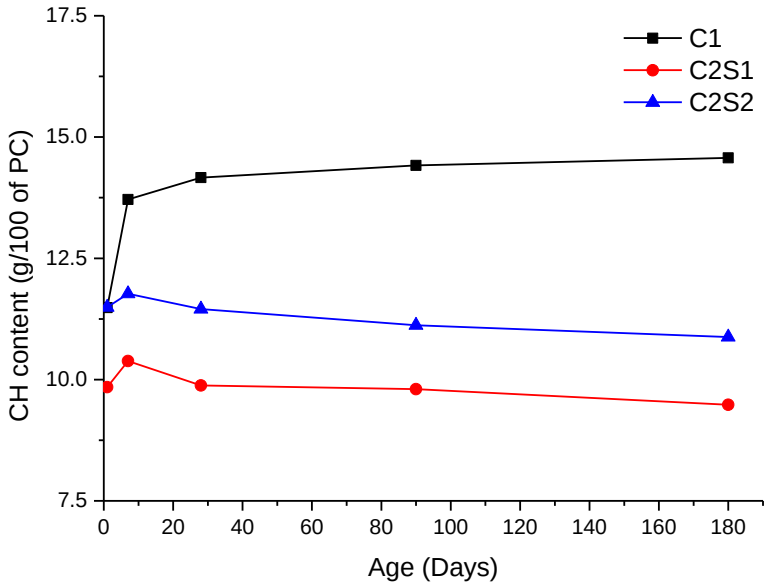

Figure 4.11: Portlandite content from STA at 38°C

As CH is a hydration product of cement, the CH content of the slag blends was normalised to the PC content so as to produce comparable results with the neat C1 system. At 20°C, the CH content of C1 increased rapidly up to 28 days and continued at a slower rate up to 180 days; whereas at 38°C, it remained relatively constant beyond 28 days. This indicates that most of the CH was formed within the first 28 days, and explains the early strength gain observed within this period as seen in Figure 4.1 and Figure 4.2.

In the early ages up to 7 days, the CH content of C1 was much higher at 38°C than at 20°C, indicating that more CH was formed at 38°C. This is in agreement with the XRD patterns shown in Figure 4.8, and can be attributed to the accelerating effect of temperature on the early hydration of the clinker phases. At the later ages of 28 days and beyond, there was no significant difference between the CH content of C1 at 20 and 38°C. This is in agreement with previous studies [110-112], and correlates with the calorimetry results (shown in Figure 4.5 and Figure 4.6), where it was seen that after about 28 days the total heat evolved by the C1 mix was already at the same level at 20 and 38°C. This indicates that the degree of hydration was similar at the later ages and supports the earlier observation that the higher temperature only accelerated the early degree of hydration. Despite the degree of hydration of the C1 mix being similar at the later ages at both temperatures, this did not reflect in the compressive strength results. From Figure 4.1 and Figure 4.2, it can be seen that the later strengths of the C1 samples were lower at 38°C than at 20°C. The reason for this can be attributed to the effect of high temperature curing on the microstructure, which is discussed in the next chapter.

The CH content of the slag blends was much lower than that of the neat system, and was seen to decrease steadily over time up to 180 days. This can be attributed to the

consumption of the CH by the hydration of the slag [13, 25, 154]. This implies that the hydration of the slags continued up to 180 days, and supports previous observations [135, 153, 342] that slag hydration is gradual and continues for longer periods. This also correlates with the calorimetry results (over the first 28 days), where Figure 4.7 show that slag is still hydrating at 28 days (the slope being positive at this time).

After 7 days and beyond, the CH contents were lower following curing at higher temperatures, reflecting the greater degree of slag hydration. C2S1 had lower CH contents than C2S2 at both temperatures, with the difference appearing to be much greater at 38°C. This reflects the increased reactivity of slag 1 over slag 2 at the higher temperature as observed previously in the calorimetry results (Figure 4.7), XRD patterns (Figure 4.8) and SEM results (Table 4.3). This explains the significant difference observed in their strength development at 38°C, as seen in Figure 4.2.

4.7 Bound water content

The bound water content is often used to study hydration of cementitious materials, as it gives an indication of the progress of hydration [135, 154]. Figure 4.12 and Figure 4.13 shows the bound water content calculated for all the mixes at 20 and 38°C respectively, using the procedure described previously in Section 3.6.1.4. At 20°C and at ages up to 28 days, there was no significant difference between the bound water content of the slag blends and the neat C1 mix. However, at later ages up to 180 days, the slag blends had higher bound water contents. This correlates with the compressive strength results (Figure 4.1 and Figure 4.2) and also supports the increased degree of slag hydration as determined from the portlandite contents (Figure 4.10 and Figure 4.11) and SEM (Table 4.3).

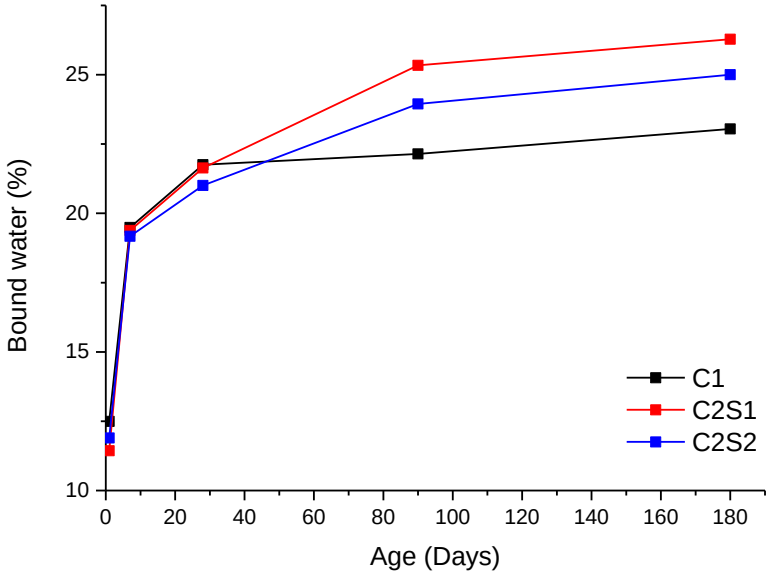

Figure 4.12: Bound water content from STA at 20°C

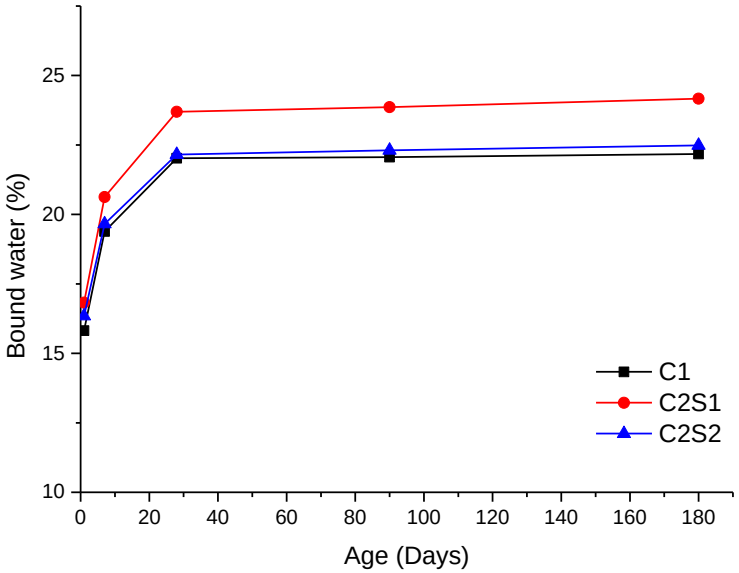

Figure 4.13: Bound water content from STA at 38°C

The impact of temperature on the hydration of the neat C1 system is seen by comparing Figure 4.12 and Figure 4.13. Bound water content at 1 day was much greater at 38°C, due to the acceleration effect of temperature on the early age hydration. However, the difference reduced at intermediate ages, such that bound

water contents determined at 20 and 38°C were similar. Prolonged hydration then led to lower bound water content at later ages in the samples cured at 38°C.

It should be noted that the bound water content at 38°C was not corrected for temperature effect. Gallucci *et al.* [114] observed that the bound water content of C-S-H was reduced by about 14.5% when the temperature was increased from 5 to 60°C. If we take this into consideration at 38°C, and ignore minor contributions to the bound water content due to CH and AFt, the degree of hydration at the later ages would be similar at both temperatures, as was observed in the CH content.

At 38°C the impact of temperature on the hydration of the slag blends resulted in the slag blends having higher bound water contents than the neat C1 mix at all ages. More so, the difference between the bound water content of C2S1 and C2S2 was much higher at 38°C than at 20°C, highlighting the impact of temperature on the reactivity of the slag 1 blend, as previously shown in Figure 4.7 and Figure 4.11. This also correlates with the compressive strength results.

4.8 Summary

This chapter has looked at the combined effect of binder composition and temperature on the strength development and hydration process of the neat CEM I 42.5R mix and the slag blends. High temperature curing was seen to increase the early strength of all the mixes, but not the later strength. Beyond 28 days, there was minimal strength increase at 38°C while the samples cured at 20°C continued to gain strength. This was attributed to the effect of high temperature curing on hydration, which would accelerate the early hydration, and slow down subsequent hydration.

The various techniques (isothermal calorimetry, XRD, SEM and TGA) used to study hydration showed that the early hydration of the mixes was accelerated at the higher

temperature. However, this accelerating effect of temperature on hydration was seen to be more pronounced on the slag blends than the neat CEM I 42.5R mix. At 20°C, the neat CEM I 42.5R mix had higher strengths than the slag blends up to 7 days, but beyond 28 days, the trend was reversed; whereas at 38°C, the slag blends had better strength performance than the neat CEM I 42.5R mix at all ages.

In terms of the strength performance of the slag blends, at 20°C, both slag blends showed similar strength development, especially at later ages; whereas at 38°C, there was a clear distinction in their UCS with slag 1, the more basic of the 2 slags, performing better than slag 2 at all ages. Although, the higher temperature increased the reactivity of the slags, the effect was seen to be greater on slag 1 (the more reactive slag). This was attributed to the slag 1 blend having a lower activation energy and higher alumina content, than the slag 2 blend. The strength performance of the slag blends tallied with the predictions of the slag activity index and basicity index at 20°C and 38°C respectively.

Chapter 5
Effects of Temperature and Curing Duration on the Microstructure of CEM I and Slag Blends

5.1 Degree of capillary porosity by BSE – SEM image analysis

Figure 5.1 and Figure 5.2 shows selected BSE-SEM images obtained from 7 and 28 day old paste samples, which had been cured under saturated lime water at 20 and 38°C respectively. 7 and 28 day old paste samples were chosen for characterisation because they represented the times at which the mortar samples were immersed in chloride solutions.

Regardless of the temperature, the neat C1 paste samples cured for 28 days had lower apparent porosities than those cured for 7 days. The samples cured at the higher temperature appeared to have a coarser pore structure. In the previous chapter, although it was seen that the higher temperature resulted in an increase in the initial degree of hydration, this did not reflect on the compressive strength, especially for the neat C1 mix. The reason for this can be attributed to the impact of high temperature curing on the microstructure. When hydration occurs at higher temperatures, the hydration rims formed around the cement grains are usually denser [113, 119, 291]. The acceleration of the early hydration coupled with the formation of denser rims at higher temperatures, gives rise to a non-uniform distribution of the hydration products [113, 343]. This non-uniform distribution of the hydration products will result in a coarser pore structure [21, 113, 291]. At lower temperatures, the distribution of the hydration products are more homogenous, giving rise to the formation of smaller gel pores and better interlocking between the hydrated phases [291].

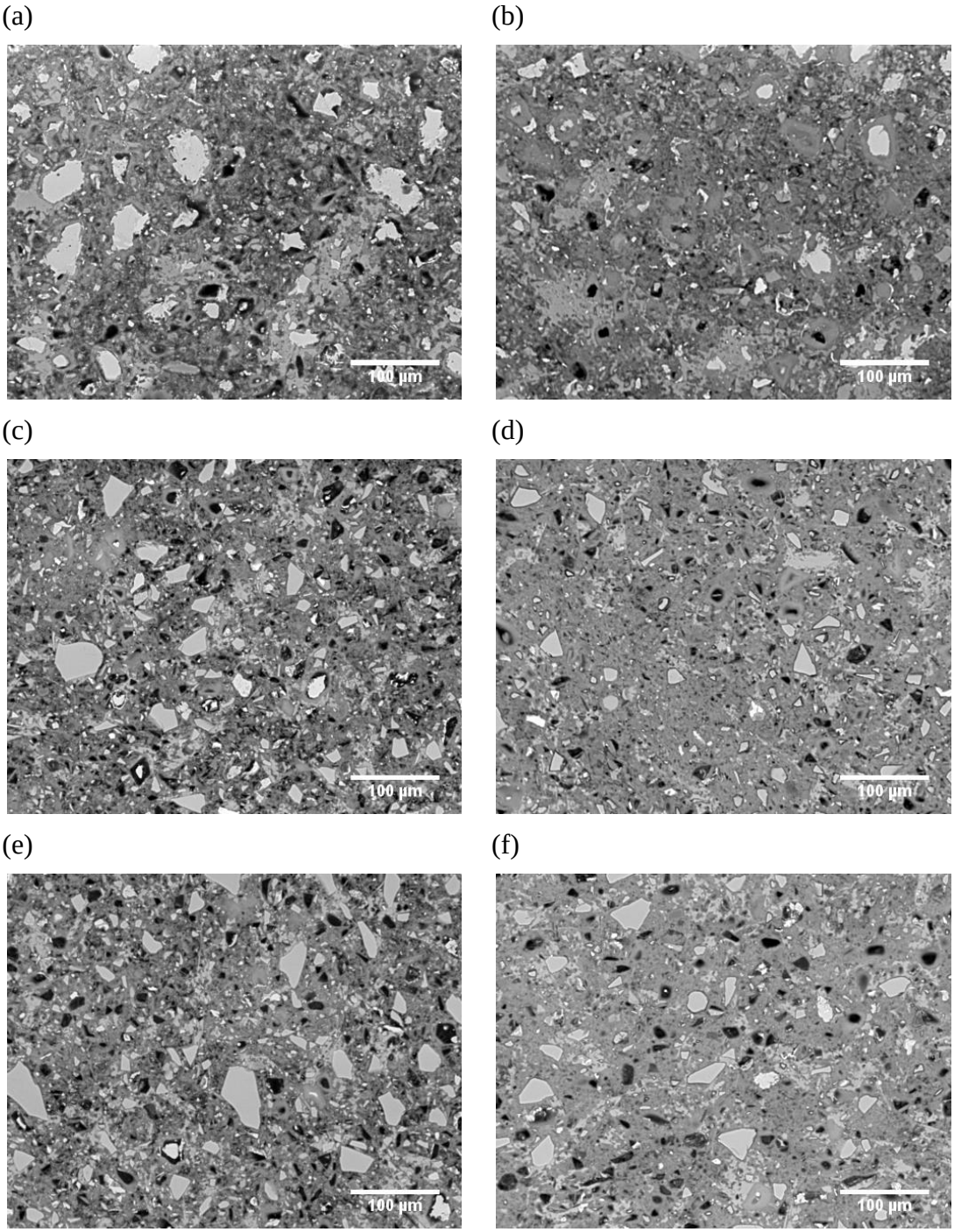

Figure 5.1: BSE – SEM images of paste samples at 20°C (a) C1 – 7 day (b) C1 – 28 day (c) C2S1 – 7 day (d) C2S1 – 28 day (e) C2S2 – 7 day (f) C2S2 – 28 day

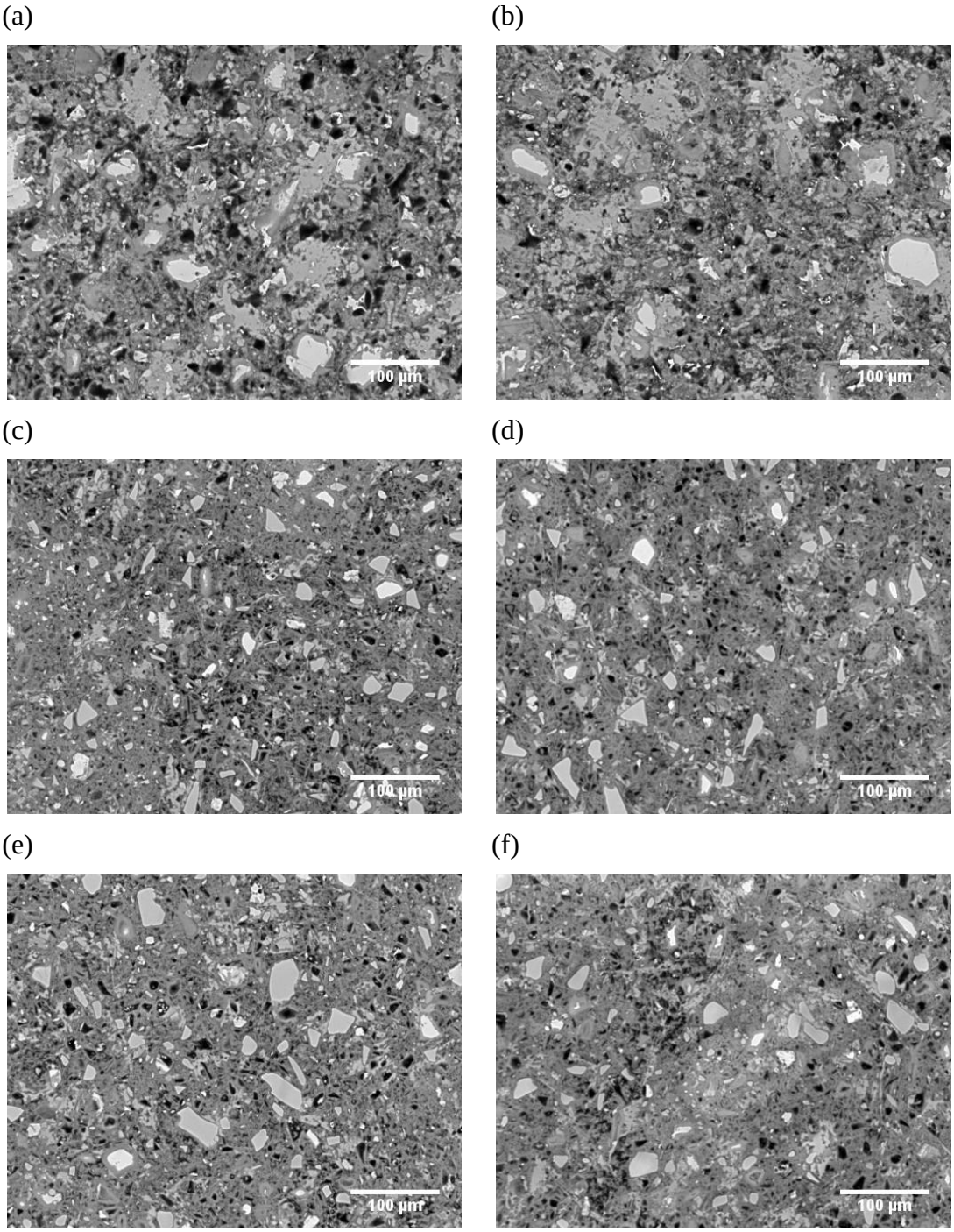

Figure 5.2: BSE – SEM images of paste samples at 38°C (a) C1 – 7 day (b) C1 – 28 day (c) C2S1 – 7 day (d) C2S1 – 28 day (e) C2S2 – 7 day (f) C2S2 – 28 day

For the slag blends, the samples cured at 38°C for 7 days showed lower porosities than the ones cured at 20°C. The reason for this can be attributed to the increased reactivity of the slags at 38°C as was discussed in the previous chapter, and as was reported by [337]. Anguski da Luz and Hooton [337] observed that paste samples

made from super sulphated cements and cured for 7 days at higher temperatures had lower porosities than the ones cured at lower temperatures. After 7 days (as shown in Table 4.3), the degree of slag hydration in the samples cured at 38°C was about 53% and 42% for slag 1 and 2 respectively, compared to about 40% and 32% at 20°C. This would lead to the formation of more hydration products at the early stages, that will have a pore blocking effect on the microstructure [31]. This reduced porosity at 7 days observed for the slag blends at 38°C was indeed reflected in the strength results (Figure 4.1 and Figure 4.2), where it can be seen that the slag blends had greater early age strengths at 38°C than at 20°C. However, on prolonged curing for 28 days, the slag blended samples cured at 38°C had greater apparent porosities than those cured at 20°C. The reason for this can also be linked to the reactivity of the slags at 38°C. From Table 4.3, after 28 days, we can see that there was no much difference in the degree of hydration of the slags at 20 and 38°C. This, coupled with the effect of prolonged high temperature curing on the microstructure, would explain why the porosity of the slag blended samples cured for 28 days at 38°C became greater than those cured at 20°C.

The coarse porosities, as determined from the electron images according to the method described in Section 3.6.1.5, are shown in Table 5.1. At the lower temperature of 20°C, increasing the curing duration from 7 to 28 days resulted in a significant decrease in the coarse porosity, especially for the slag blends. The coarse porosity dropped by 1.9 percentage points for C1 and by over 5.2 percentage points for the slag blends. At 7 days, the coarse porosity of C1 was lower than that of the slag blends but at 28 days, the trend was reversed. Similar observations were made by [164, 168, 169], where it was seen that slag blends exhibited similar porosities as ordinary PC at early ages, but at later ages when substantial portions of the slag had

reacted, the porosities of the slag blends became less than that of the ordinary PC. This indicates that prolonged curing at the lower temperature was beneficial for the microstructural development of the slag blends. Slags are latently hydraulic [4], and so require prolonged moist curing for better performance. This explains why in the compressive strength results shown in Figure 4.1 for 20°C, the 7 day strength of the C1 samples were greater than that of the slag blends, but at later ages beyond 28 days, the samples made from the slag blends became stronger.

Table 5.1: Effect of curing age and temperature on coarse porosity

Age		Coarse porosity (%)	
		20°C	38°C
7 day	C1	9.0 ± 0.16	10.4 ± 0.16
	C2S1	11.8 ± 0.10	9.2 ± 0.14
	C2S2	12.3 ± 0.12	9.9 ± 0.11
28 day	C1	7.1 ± 0.13	9.9 ± 0.13
	C2S1	6.5 ± 0.11	8.9 ± 0.08
	C2S2	7.0 ± 0.07	9.5 ± 0.09

At the higher temperature of 38°C, prolonged curing for 28 days did not seem to have any significant improvement on the coarse porosity of the samples. Only a drop of about 0.5 and 0.4 percentage points was observed in the coarse porosity of the C1 and slag blends respectively. From the calorimetry (Figure 4.6), XRD (Figure 4.8b and Figure 4.9b) and TGA (Figure 4.11) results, it was seen that prolonged curing at 38°C did not change the degree of hydration much between 7 and 28 days, and so there were no significant changes in the microstructure. Also, the coarse porosity of the C1 samples was always greater than that of the slag blends, indicating that the microstructure of the slag blends were better than that of the neat C1 mix at the higher temperature. This can also be related to the compressive strength results

(Figure 4.1 and Figure 4.2), where at 38°C, the strength performance of the slag blends were better than that of the neat C1 mix at all ages.

Comparing the two slags, the blends prepared with slag 1 always showed a lower coarse porosity than the equivalent blend prepared with slag 2. Furthermore, the difference in performance between the two slags increased with increasing temperature. This correlates with the previous results and further explains why samples prepared with slag 1 had higher strengths than those prepared with slag 2.

5.2 Relationship between compressive strength and coarse porosity

Several studies [135, 344-347] have showed that there is a negative correlation between porosity and compressive strength. Although, the coarse porosity measurements were made on paste samples, it can also be related to mortar samples. Figure 5.3 shows a scatter plot of compressive strength against coarse porosity, using the 7 and 28 day strength and coarse porosity at both temperatures. From the figure, it can be seen that for most of the data points, there was a negative correlation between the compressive strength and the coarse porosity. This suggests that the coarse porosity is the main factor that dominates the compressive strength, irrespective of the degree of hydration or the type of binder.

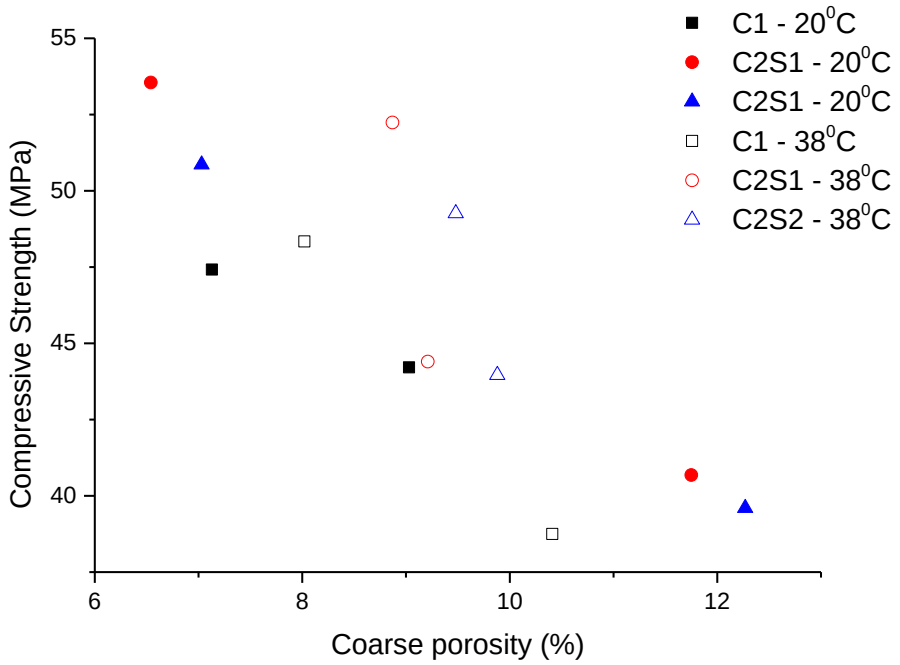

Figure 5.3: Relationship between compressive strength and coarse porosity

5.3 Water penetrability

As mentioned previously in Section 3.6.3.1, 7 day old samples were considered unsuitable for the water penetration tests, so 28 and 90 day old samples were used.

5.3.1 Sorptivity

Table 5.2 shows the sorptivity of 28 and 90 day old samples which had been cured at 20 and 38°C. At the lower temperature, increasing the curing duration from 28 to 90 days resulted in a significant decrease in the sorptivity of all the mixes. The sorptivity coefficient of the C1 mix was seen to decrease by about 80%, compared to about 50% and 80% for the slag 1 and 2 blend respectively. These results are similar to those obtained by Güneyisi and Gesoğlu [131], and can be attributed to the formation of a more developed and dense microstructure, upon prolonged curing from 28 to 90 days.

At 38°C, prolonged curing also resulted in a decrease in the sorptivity, although the impact was not as significant as was observed at 20°C. There was a drop of about 30% in the sorptivity coefficient of the C1 mix, compared to about 12% and 14% for the slag 1 and 2 blend respectively. This implies that prolonged curing at 20°C was more beneficial for the resistance to water penetration of all the mixes, and can be related to the compressive strength results.

At 38°C, there was minimal decrease in the sorptivity between 28 and 90 days, hence the minimal increase in the compressive strength observed between 28 and 90 day (Figure 4.2). Meanwhile, at 20°C the significant decrease in the sorptivity between 28 and 90 days resulted in a significant increase in the compressive strength between 28 and 90 days (Figure 4.1). As observed in the coarse porosity results, there was a negative correlation between the sorptivity coefficient *(k)* obtained at 28 and 90 days, and the 28 and 90 day UCS at both temperatures. These are shown as scatter plots in Figure A7 and Figure A8 in Appendix B.2.

Table 5.2: Effect of curing age and temperature on sorptivity

Age		Sorptivity, k ($m^3/m^2s^{1/2}$)x10^{-5}	
		20°C	38°C
28 day	C1	4.1 ± 0.08	9.9 ± 0.07
	C2S1	2.1 ± 0.05	4.0 ± 0.07
	C2S2	3.3 ± 0.09	6.34± 0.04
90 day	C1	2.3 ± 0.05	7.7 ± 0.07
	C2S1	1.4 ± 0.04	3.6 ± 0.08
	C2S2	1.9 ± 0.07	5.6 ± 0.04

On the effect of temperature on water sorptivity, high temperature curing resulted in an increase in the sorptivity of all the mixes. This effect was more pronounced on

the neat C1 mix, with an increase in sorptivity over the values obtained at 20°C by about 2.4 and 3.4 folds at 28 and 90 days respectively. For the slag blends, at 28 days, the sorptivity of the samples cured at 38°C was about 1.9 folds higher than those cured at 20°C. After 90 days, this became higher by about 2.6 and 3.0 folds for the slag 1 and 2 blend respectively, indicating that the high temperature curing was more detrimental to the microstructure of the less-reactive slag 2. This supports the compressive strength results and explains the lower later strengths observed for the samples cured at 38°C (Figure 4.2), and the larger difference observed between the compressive strength of the slag blends cured at 38°C.

Overall, the slag blends showed better resistance to the penetration of water than the neat system at both temperatures, as has been seen previously [348]. The addition of GGBS to concrete results in the formation of a hardened cement paste having smaller gel pores and fewer large capillary pores [59]. Also, as stated by Feldman [170], the pore structure of slag blends comprises of large discontinuous thin-walled pores, as compared to that of plain PC, which is continuous. This finer pore structure is what makes GGBS concretes to exhibit lower permeability than concretes made from PC [31, 164].

As was observed with coarse porosity, the sorptivities of blends prepared with slag 1 were lower than those for slag 2 blends at both temperatures. This can be attributed to the higher reactivity of slag 1 enabling the formation of more hydration products that resulted in a more refined pore structure, as was observed by [164]. At 20°C, the 28 day sorptivity of C2S2 was about 60% greater than that of C2S1, but at 90 days this reduced to about 35%; whereas at 38°C, the slag 2 blend's sorptivity was about 60% higher at both 28 and 90 days. This highlights the impact of prolonged curing at the lower temperature on the microstructural development of the slag 2

blend, and would explain why both slag blends had similar later strengths at 20°C (as seen in Figure 4.1).

5.3.2 Water absorption

The results obtained for the water absorption tests carried out at 20 and 38°C, on similar samples used for the sorptivity tests are shown in Figure 5.4 and Figure 5.5 respectively. While the sorptivity is a measure of the unidirectional penetration of water (i.e. only one face of the sample is exposed), the water absorption test is a measure of the total amount of water absorbed by the samples when completely immersed in water, as described in Section 3.6.3.1. As observed in the results of the sorptivity test, the high temperature of 38°C resulted in more water being absorbed into the samples. The impact was also more pronounced on the neat C1 system as compared to the slag blends, and slag 1 showed better resistance to the absorption of water than slag 2, at both temperatures.

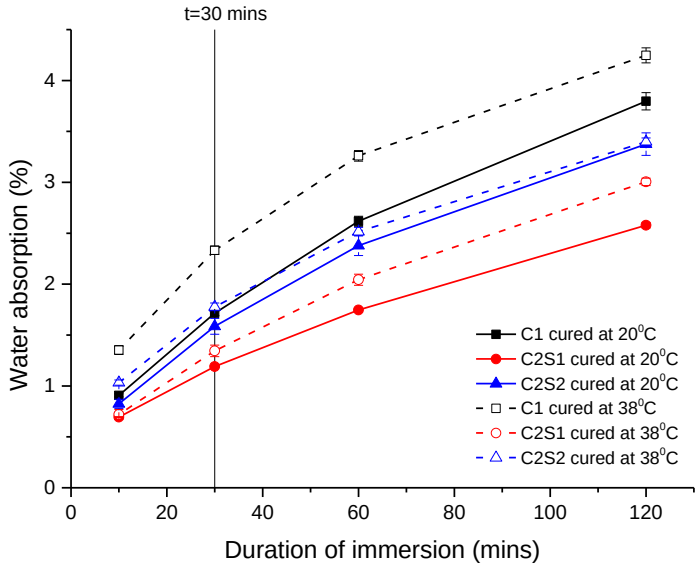

Figure 5.4: Effect of temperature on the water absorption for 28 day old samples

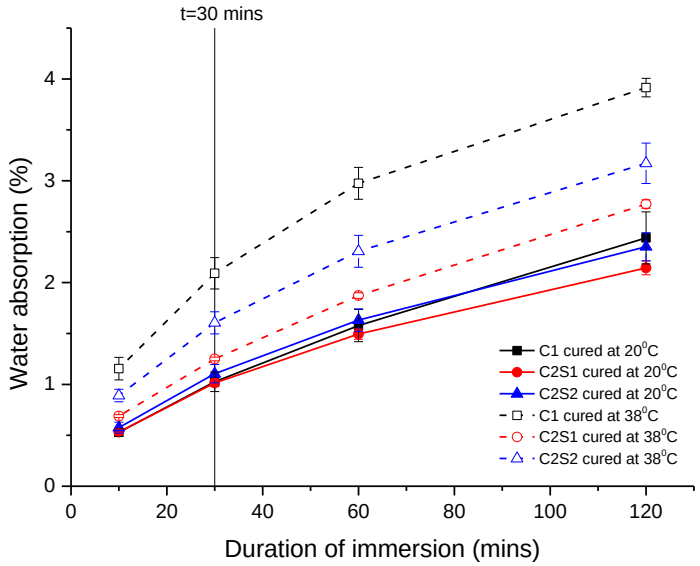

Figure 5.5: Effect of temperature on the water absorption for 90 day old samples

The 30 mins water absorption, which is given as the standard duration for water absorption test in BS 1881-122 [329], was obtained for all the mixes as shown in Table 5.3. At all curing ages and temperature, the slag blends had lower water absorption values than the neat system, indicating that they had a finer pore structure. This correlates with the sorptivity results. The reduction in the 30 mins water absorption, when the curing duration was increased from 28 to 90 days, was much greater at 20°C than at 38°C. This is because the degree of hydration at the higher temperature did not change significantly from 28 to 90 days, while it did at 20°C. There was a decrease of about 66% for the C1 mix as compared to about 18% and 45% for the slag 1 and 2 blends. This is similar to the trends observed in the sorptivity results. Also, as was observed in the sorptivity results, prolonged curing at the higher temperature resulted only in a minimal decrease in the 30 min water absorption, thus confirming that the lower temperature was more beneficial for the later development of the microstructure of all the mixes.

Table 5.3: 30 mins water absorption for all the mixes

Age		30 mins water absorption (%)	
		20°C	38°C
28 days	C1	1.7 ± 0.02	2.3 ± 0.04
	C2S1	1.2 ± 0.01	1.3 ± 0.06
	C2S2	1.6 ± 0.08	1.8 ± 0.04
90 days	C1	1.0 ± 0.09	2.1 ± 0.10
	C2S1	1.0 ± 0.04	1.3 ± 0.02
	C2S2	1.1 ± 0.09	1.6 ± 0.11

5.4 Summary

Increased degrees of hydration are known to reduce porosity. However, the results have shown that the degree of hydration alone cannot explain porosity and transport properties. Rather, temperature has been shown to have a great impact. For all the samples studied, high temperature curing was seen to increase the degree of capillary porosity and rate of water penetration. The effect of the high temperature curing was more pronounced on the neat C1 mix, as compared to the slag blends. Samples that were cured for longer periods exhibited lower porosities and better resistance to water penetration, especially those cured at the lower temperature.

Apart from the early ages at 20°C, when the degree of hydration of the slags was low, the slag blends had lower porosities and better water resistant properties than the neat C1 mix. Regardless of the temperature and curing duration, the slag 1 blend had lower porosities and exhibited better transport properties than the slag 2 blend. This was attributed to the higher reactivity of slag 1. Prolonged curing at 20°C led to significant improvements in the microstructure and transport properties of the slag blends. However, this impact was seen to be greater for the slag 2 blend.

Chapter 6
Effects of Binder Composition and Temperature on the Chloride Binding Capacity of CEM I and Slag Blends

6.1 Bound chloride content (C_b)

The bound chloride content obtained from samples exposed to 5 different concentrations (*Ci*) of NaCl solution at 20 and 38°C is shown in Figure 6.1 and Figure 6.2. At both temperatures, there was an increase in the amount of chlorides bound by all the mixes as the chloride concentration of the host solution was increased. This can be seen from Figure 6.3 and Figure 6.4, where chlorides bound as Friedel's salt, as evidenced by TGA data are greater for samples exposed to host chloride solutions of 2.0M than those exposed to 0.5M.

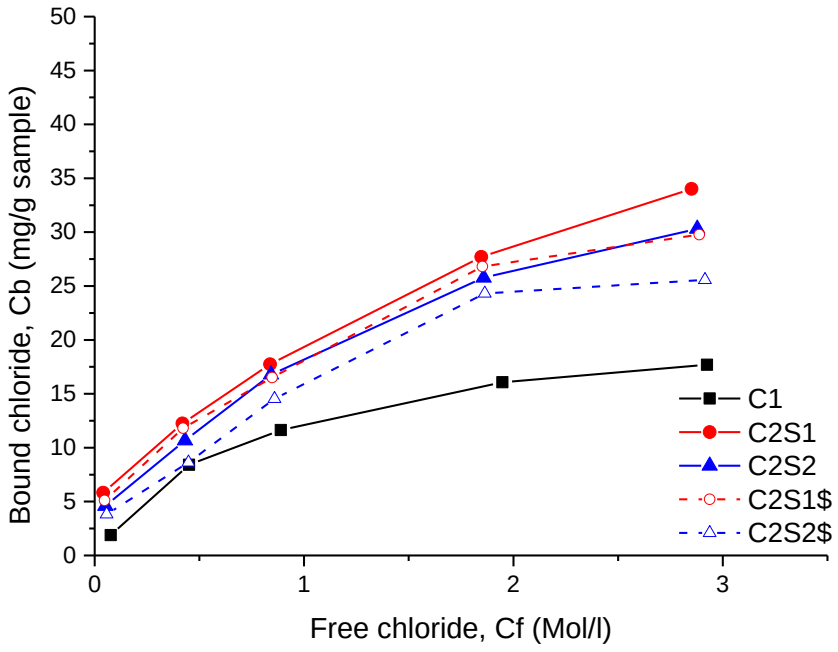

Figure 6.1: Chloride binding relationship for all mixes at 20°C

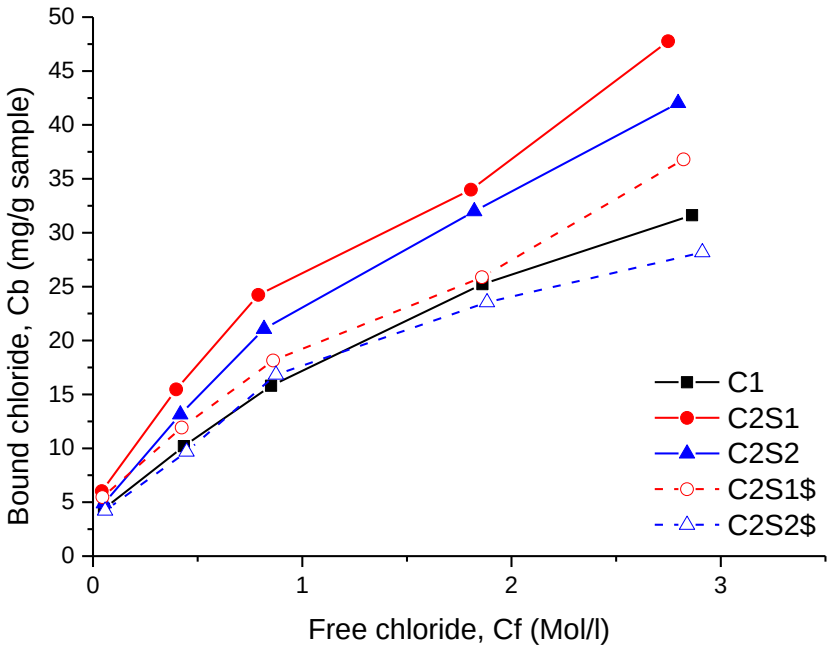

Figure 6.2: Chloride binding relationship for all mixes at 38°C

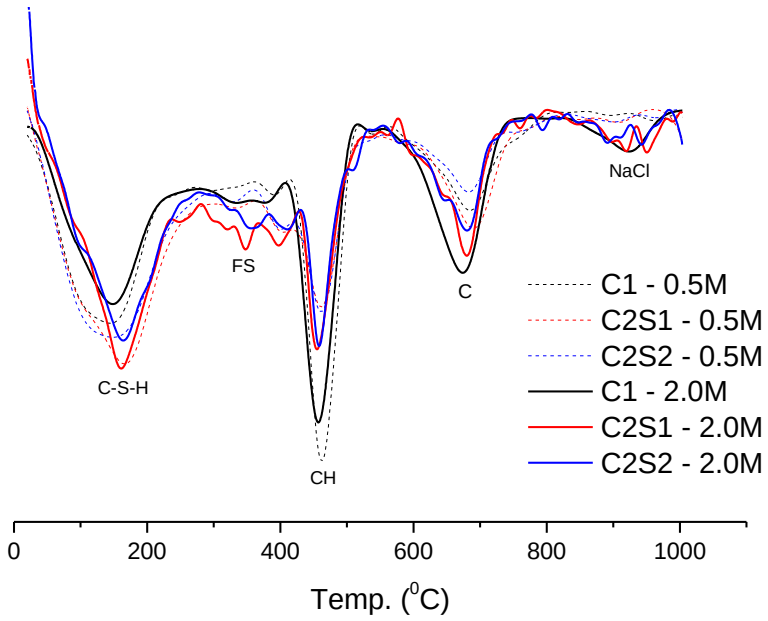

E - Ettringite, FS - Friedel salt, CH - Portlandite, C - Calcite

Figure 6.3: DTG plots showing peaks of Friedel salt (FS) for paste samples after immersion in 0.5 and 2.0M NaCl solution at 20°C

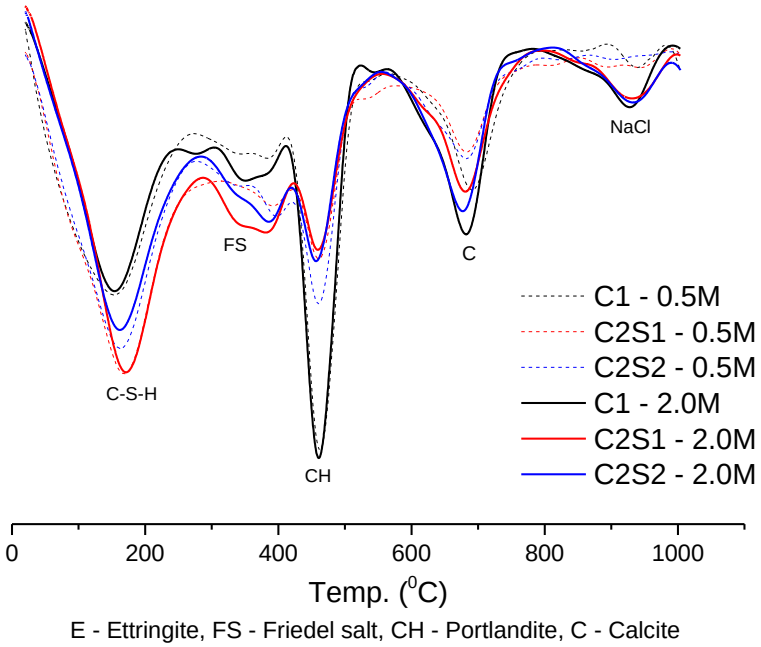

Figure 6.4: DTG plots showing peaks of Friedel salt (FS) for paste samples after immersion in 0.5 and 2.0M NaCl solution at 38°C

6.1.1 Effect of binder composition on chloride binding

At both temperatures (as seen in Figure 6.1 and Figure 6.2), the bound chloride contents of the slag blends were greater than that of the neat C1 mix. This can be attributed to the high alumina content of the slag blends [15-18], which will increase the propensity for Friedel's salt formation, and enable more of C-A-S-H phases to be formed. A study by Florea and Brouwers [19] showed that the C-A-S-H phase was responsible for the binding of about two-thirds of the chloride. From Table 6.1, it can be seen that the main difference in the oxide compositions of all the mixes is in the alumina content, and that the bound chloride content at a *Ci* of 3.0M increased as the alumina content. Also, from Figure 6.3 and Figure 6.4, it can be seen that the reflections due to the C-S-H phase is greater for the slag blends, than the neat C1 mix. This is in agreement with previous studies [15-18], and explains the higher bound chloride contents of the slag blends as compared to the neat C1 system. In

comparing both slag blends, C2S1 had higher bound chloride contents than C2S2 at both temperatures, and this can also be attributed to its higher alumina and C-S-H content (as seen in Table 6.1, Figure 6.3 and Figure 6.4).

Table 6.1: Relationship between bound chloride content and alumina and sulphate content at NaCl solution of Ci = 3.0M

Mix	Bound chloride content (C_b) (mg/g-sample)		Al_2O_3 (%)	SO_3 (%)
	20°C	38°C		
C1	16.69	31.62	5.08	2.97
C2S1	34.01	47.76	7.41	2.64
C2S2	30.31	42.03	6.07	2.78
C2S1$	29.77	36.81	7.16	3.64
C2S2$	25.57	28.18	5.92	3.77

The addition of extra sulphate to the slag blends resulted in a decrease in the bound chloride content as seen in Figure 6.1, Figure 6.2 and Table 6.1. At 20°C, the amount of chlorides bound by C2S2 was very similar to that of the slag 1 blend containing extra sulphate (C2S1$). At the higher temperature, the effect of the added sulphate became more pronounced such that the C1 mix having the lowest alumina content had slightly higher bound chloride contents than the slag 2 blend containing extra sulphate (C2S2$). This agrees with previous findings [17, 241, 349, 350], and can be attributed to the preferential reaction of sulphates with C_3A [17]. In the presence of additional sulphates, more of the C_3A reacts with the sulphates to form ettringite [45, 351, 352], which is more thermodynamically stable than Friedel's salt. This reduces the amount left to chemically bind the chlorides. XRD patterns (Figure 6.5) and DTG plots (Figure 6.6) show more intense reflections for ettringite, for the mixes containing extra sulphate compared to those without, thus confirming that more ettringite was formed.

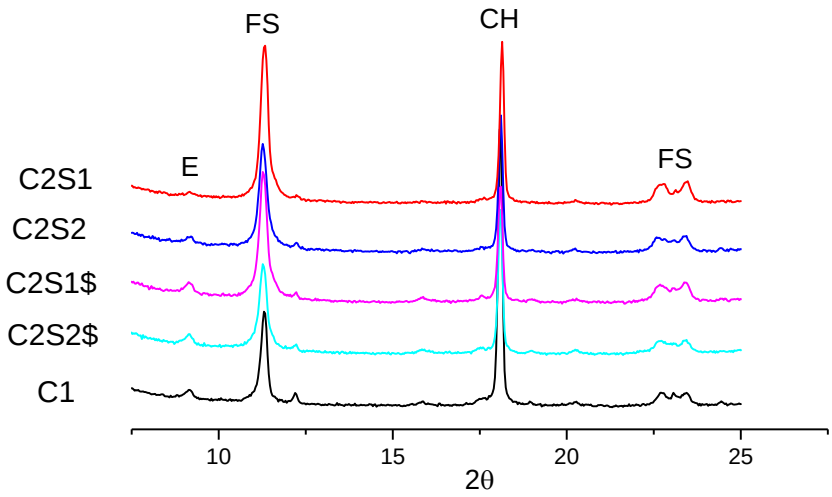

Figure 6.5: X-ray diffraction pattern for paste samples after immersion in NaCl solution (Ci = 2.0M) at 20°C

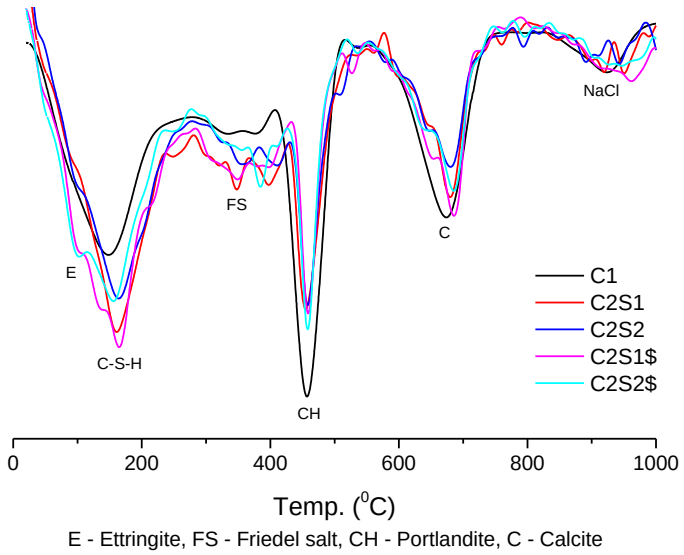

Figure 6.6: DTG plots showing peaks of Friedel salt (FS) for paste samples after immersion in NaCl solution (C_i = 2.0M) at 20°C

6.1.2 Effect of temperature on chloride binding

The effect of temperature on chloride binding is seen by comparing Figure 6.1 and Figure 6.2. At C_i = 0.1M, there was no significant difference in the bound chloride contents obtained at 20 and 38°C but at C_i of 0.5M and beyond, bound chloride contents were higher for samples cured and exposed at 38°C. XRD patterns (Figure

6.7) and DTG plots (Figure 6.8), showed that there were increased signals due to Friedel's salt (FS) for the 38°C samples, thus confirming that there was higher chloride binding at 38°C. This agrees with previous findings by [192, 292], but appears to be slightly different from those obtained by [244]. Zibara [244] observed that an increase in temperature from 23 to 38°C resulted in a decrease in the amount of bound chlorides for host chloride solutions having low concentrations between 0.1 and 1.0M, and an increase in the amount of bound chlorides at a concentration of 3.0M. However, the difference at 1.0M was minor compared to the increase at 3.0M. Also, it is important to point out that all their test samples were cured at the same temperature of 23°C and tested for chloride binding at temperatures ranging from 7 to 38°C. In this study, the samples were cured and tested for chloride binding at temperatures of 20 and 38°C.

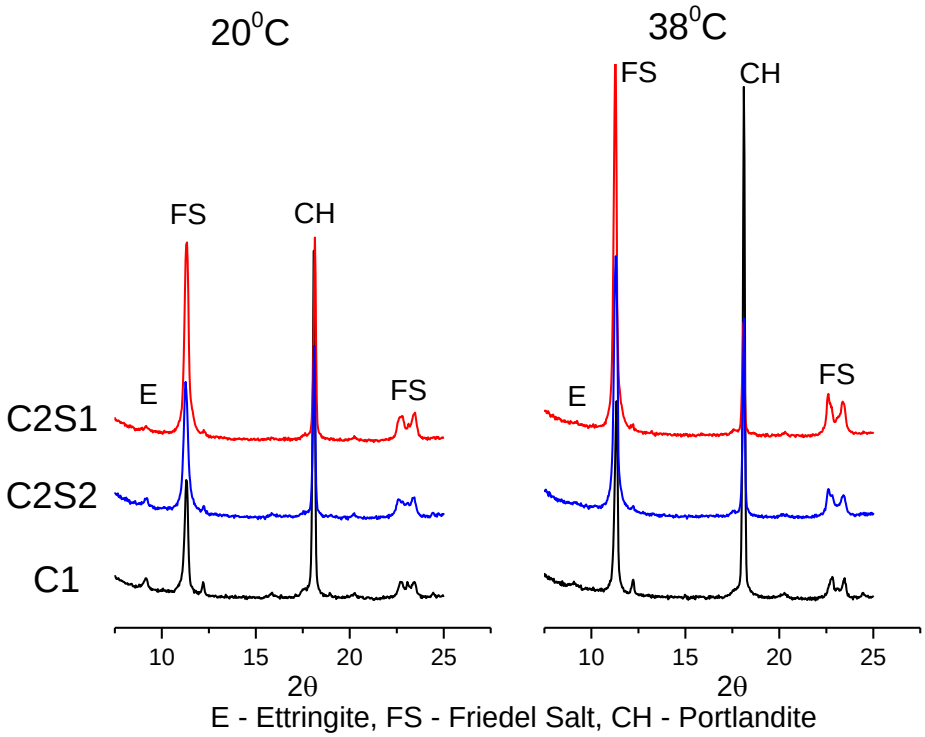

Figure 6.7: X-ray diffraction pattern for paste samples after immersion in NaCl solution (Ci = 2.0M) at 20 and 38°C

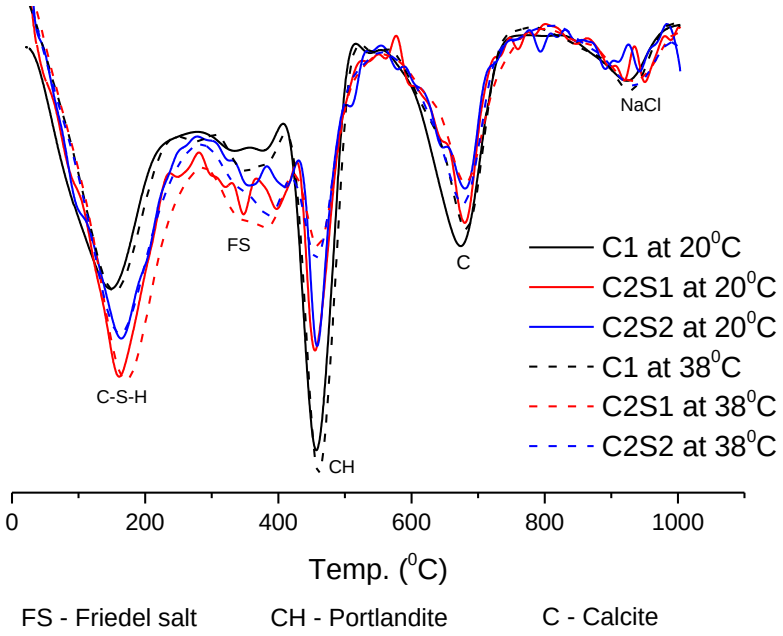

Figure 6.8: DTG plots showing peaks of Friedel salt (FS) for all mixes at 20 and 38°C after immersion in NaCl solution (C_i = 2.0M)

The reason for the increased chloride binding observed at 38°C can be attributed to an increase in the amount of C-A-S-H and AFm phases, due to the impact of high temperature curing on hydration. At higher temperatures, there is increase in the amount of sulphate ions bound reversibly within the C-S-H phase, and less calcium sulphate remains available for a reaction with C_3A [45]. Gallucci *et al.* [114] observed that at higher temperatures, AFm phases were formed in preference to AFt phases, and more sulphate and aluminium ions were incorporated into the C-S-H phase. The XRD patterns shown in Figure 6.5 indeed confirmed this, as the reflections due to ettringite were barely visible in the 38°C samples. This shows that there was more AFt to AFm conversion at the higher temperature, in line with previous observation in Figure 4.9.

Also, from the XRD patterns (Figure 6.7), it can be seen that the reflections due to CH were lower for the slag blends and higher for the C1 mix at 38°C, indicating that

the degree of hydration was greater at 38°C than at 20°C, as was observed in the TGA plots shown in Figure 4.10 and Figure 4.11. DTG plots of the same samples shown in Figure 6.8 also confirmed this, and even showed slightly greater intensities for the C-S-H phase at 38°C. This implies that at 38°C, more C-S-H or C-A-S-H and AFm phases was available for the physical and chemical binding of the chloride ions. Thus, the higher bound chlorides observed at 38°C can be related to the higher degree of hydration of the slags and the cement at 38°C, as was observed in the study by Loser *et al.* [229], where it was shown that chloride binding was strongly related to the hydration degree of the cement and of the mineral admixtures.

6.2 Binding isotherms

The chloride binding capacity of the mixes was obtained using Freundlich binding isotherms as described previously in Section 3.6.3.5. The chloride binding coefficients α and β obtained for the mixes are shown in Table 6.2. These coefficients don't have any physical meaning as they are not material properties, but can be used to give an indication of the chloride binding capacities of the cementitious materials.

Table 6.2: Chloride binding coefficients obtained at 20 and 38°C using Freundlich's binding isotherm

Mix	20°C			38°C			Al_2O_3	SO_3
	α	β	Adj. R^2	α	β	Adj. R^2	(%)	(%)
C1	11.41	0.45	0.9596	17.49	0.56	0.9949	5.08	2.97
C2S1	20.11	0.50	0.9890	26.46	0.55	0.9839	7.41	2.64
C2S2	18.07	0.51	0.9908	23.00	0.58	0.9972	6.07	2.78
C2S1$	18.68	0.47	0.9815	19.71	0.56	0.9762	7.16	3.64
C2S2$	15.62	0.52	0.9523	16.74	0.50	0.9856	5.92	3.77

The values of α and β shown here are somewhat higher than those reported by Thomas *et al.* [18] for similar samples at 23°C. The reason for this can be related to the type of samples used. They used 3mm thick disc paste samples for their chloride binding test, but here ground samples were used. Zibara [244] showed that the amount of chlorides bound by ground samples were higher than that of disc samples.

The chloride binding coefficient *(α)* increased by about 53%, 32% and 27% for the C1, C2S1 and C2S2 mixes respectively, when the temperature was raised from 20 to 38°C. The highest value obtained for α was that of C2S1 at 38°C. For the slag blends containing anhydrite, the increase in α from 20 to 38°C was about 7%. At 20°C, the values of α was seen to decrease in the order of C2S1 > C2S2 > C2S1$ > C2S2$ > C1, which also links to the alumina content of the binders. A similar order of decrease was observed at 38°C, except that the C1 mix had a slightly higher chloride binding capacity than C2S2$. This can be attributed to the effect of the additional sulphate, as previously explained.

In terms of the performance of the slag blends, the α-value of C2S1 was greater than that of C2S2 at both temperatures. An interesting observation was that the difference between the α-value of C2S1 and C2S2 increased as the temperature was raised from 20 to 38°C (as seen in Table 6.2). At 20 and 38°C, the α-value of C2S1 was higher than that of C2S2 by about 11% and 15% respectively. This indicates that it is not just the alumina content of the slag which is important, but also the degree of hydration. The impact of temperature on the degree of hydration of the slags was greater for the aluminium-rich slag, as seen in the calorimetry (Figure 4.7), XRD (Figure 4.8 and Figure 4.9), portlandite (Figure 4.10 and Figure 4.11) and bound water content results (Figure 4.12 and Figure 4.13). Also from Figure 6.8, while both slags seemed to have similar portlandite contents at 20°C, the portlandite

content of C2S1 was lower than that of C2S2 at 38°C, indicating that slag 1 had reacted more. Alumina is the principal compound within the slag which can contribute to chloride binding [353]. Thus, at the high temperature of 38°C, due to increased reactivity of the slags, there would be more reactive alumina in the system and this would be more beneficial for the slag 1 blend in forming C-A-S-H. This relates to the findings of Gallucci *et al.* [114], where it was observed that more aluminium was incorporated into the C-S-H phase at higher temperatures, and explains why the C2S1 had a much greater chloride binding capacity than C2S2 at 38°C.

6.3 Relationship between chloride binding coefficient (α) and the alumina and sulphate contents

A multiple linear regression model of the form $(y = Ax_1 + Bx_2 + C)$ was fitted to the values of α, and the Al_2O_3 and SO_3 contents shown in Table 6.2, at both temperatures. A summary of the results obtained from the fit is shown below in Table 6.3.

Table 6.3: Multiple linear regression model relating the chloride binding coefficient (α) to the Al_2O_3 and SO_3 content at 20 and 38°C

Temperature	Model	Adj. R^2
20°C	$\alpha = 3.27678Al_2O_3 - 0.70703SO_3 - 1.72322$	0.72355
38°C	$\alpha = 2.7379Al_2O_3 - 5.6382SO_3 + 21.17129$	0.93335

The model indeed showed that there was a relationship between the chloride binding coefficient (α) and the alumina and sulphate contents, at both temperatures. The model showed that the α-value would increase as the alumina content increases and decrease as the sulphate content increases. However, the model had a stronger correlation at 38°C. At 20°C, the model showed that the alumina content was the

dominating factor, whereas at 38°C the sulphate content was seen as the most dominating factor.

6.4 Summary

The results presented in this chapter have shown that chloride binding is influenced by the chemical composition of the binder, as well as temperature. Regardless of the temperature, chloride binding was seen to increase with the alumina content, and decrease with the sulphate content. Also, regardless of the binder type, more chlorides were seen to be bound at the higher temperature.

The slag blends were seen to bind more chlorides than the neat C1 mix, and this was attributed to higher alumina contents, enabling them to form more Friedel's salt and C-A-S-H phases. Adding extra sulphate to the slag blends significantly decreased their chloride binding capacity, and this impact was seen to be greater at the higher temperature. The chloride binding capacity of the mixes decreased in the order of C2S1 > C2S2 > C2S1$ > C2S2$ > C1 at 20°C, and in a similar way at 38°C, except that the slag 2 blend containing extra sulphate was seen to have the lowest chloride binding capacity.

The chloride binding capacity of the slag 1 blend was greater than that of the slag 2 blend, especially at the higher temperature. This was attributed to the higher alumina content of C2S1 and the greater degree of hydration of C2S1 at 38°C. A multi-linear regression model, which was developed to relate chloride binding capacity to binder composition, showed that chloride binding was more influenced by the alumina content at 20°C, and by the sulphate content at 38°C.

Chapter 7
Chloride Ingress Resistance of the CEM I and slag blends: Effects of Binder Composition, Temperature, Curing and Exposure Conditions

7.1 Depth of penetration of free chlorides

Figure 7.1 to Figure 7.6 shows the depth of penetration of free chlorides, measured on mortar samples that had been pre-cured for 7 and 28 days under water before exposure to a 3% NaCl solution. As mentioned in the description of the test method (Section 3.6.3.2), all samples were cured and exposed at temperatures of 20 and 38°C.

7.1.1 Effect of pre-curing duration

Figure 7.1 shows the chloride penetration depths measured on samples that were cured and exposed at 20°C.

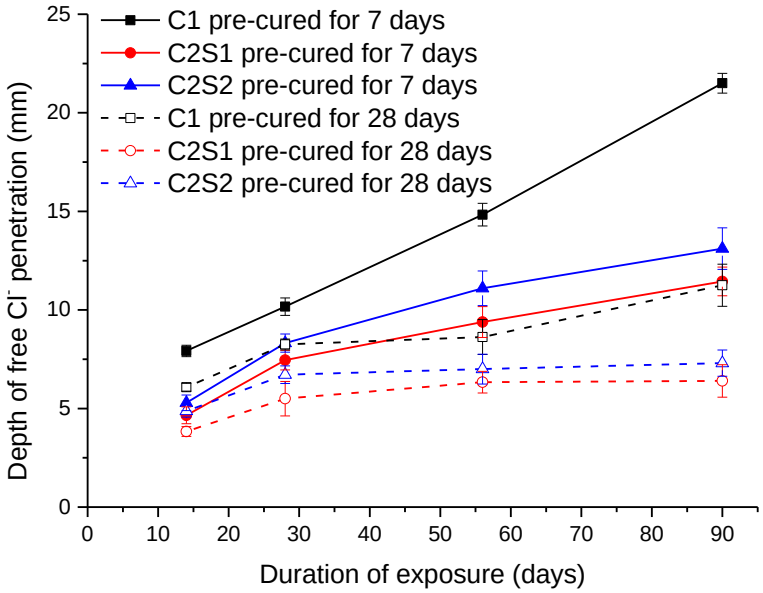

Figure 7.1: Effect of pre-curing duration on depth of chloride penetration at 20°C

The depth of free chloride penetration for samples that were pre-cured for 7 days were significantly greater than those pre-cured for 28 days before exposure. Beyond about 28 days of exposure, the depth of free chloride penetration did not increase much for samples that were pre-cured for 28 days, as compared to those that were pre-cured for 7 days before exposure. This agrees with previous studies that has shown that longer curing duration in water at a temperature of about 20°C, enhances the chloride ingress resistance of concretes [5, 164, 199-201].

At the end of the exposure period, the chloride penetration depth was about 90% higher for the C1 samples that had been pre-cured for 7 days compared to those that were pre-cured for 28 days before exposure. For the slag blends, the difference was about 80%. This can be attributed to two factors. The first can be attributed to the coarseness of the pore structure, which was seen to be reduced significantly when the curing duration was increased from 7 to 28 days at 20°C (as seen in Table 5.1). This will imply that the samples pre-cured for 28 days had a less coarse pore structure and was more resistant to the ingress of chloride ions. The second factor can be attributed to chloride binding. Chloride binding is related to the degree of hydration of the cement and the admixtures [21, 291], as shown in the previous chapter. The degree of hydration at 28 days was greater than at 7 days, as shown in the calorimetry (Figure 4.5 and Figure 4.7), XRD (Figure 4.8a and Figure 4.9a), SEM (Table 4.3) and TGA (Figure 4.10 and Figure 4.12) results. This implies that more chlorides were bound by the 28 day pre-cured samples, and explains the reason for the lower chloride penetration depths observed for the 28 day pre-cured samples.

Although, the coarse porosity results (Table 5.1) at 20°C showed that at 7 days, the slag blends had a coarser pore structure than the neat C1 mix, this did not reflect in the chloride penetration results. The chloride penetration depths measured for the

slag blends were seen to be much lower than that of the neat C1 mix for samples pre-cured for 7 days before exposure. This can be attributed to the higher chloride binding capacities of the slag blends, as observed by [15-18] and as shown in the previous chapter. This also implies that chloride binding plays a greater role in resistance to chloride ingress, than the coarseness of the pore structure.

In comparing the performance of the slag blends at 20°C, C2S1 showed better resistance to the penetration of chloride ions than C2S2, especially for samples that were pre-cured for 7 days prior to exposure. This agrees with the results obtained by Otieno *et al.* [232], and can be attributed to the higher reactivity of slag 1 as predicted by the activity index (shown in Table 4.1), and the higher chloride binding capacity of C2S1 (as seen in Figure 6.1). For the samples that were pre-cured for 28 days before exposure, there was minimal difference in the chloride penetration depths measured for both slag blends, especially at later ages. This can be attributed to the impact of prolonged curing at 20°C on the microstructure, which was seen to significantly improve the resistance to water penetration of the slag 2 blend as seen from the sorptivity and water absorption results shown in Table 5.2 and Table 5.3 respectively.

At 38°C (Figure 7.2), similar trends were observed as at 20°C. The overall depth of chloride penetration was greater for samples that were pre-cured for 7 days than those pre-cured for 28 days before exposure. For the period of exposure up to 28 days, except for the C1 mix, there was not much difference in the chloride penetration depth for the samples pre-cured for 7 days as compared to those pre-cured for 28 days.

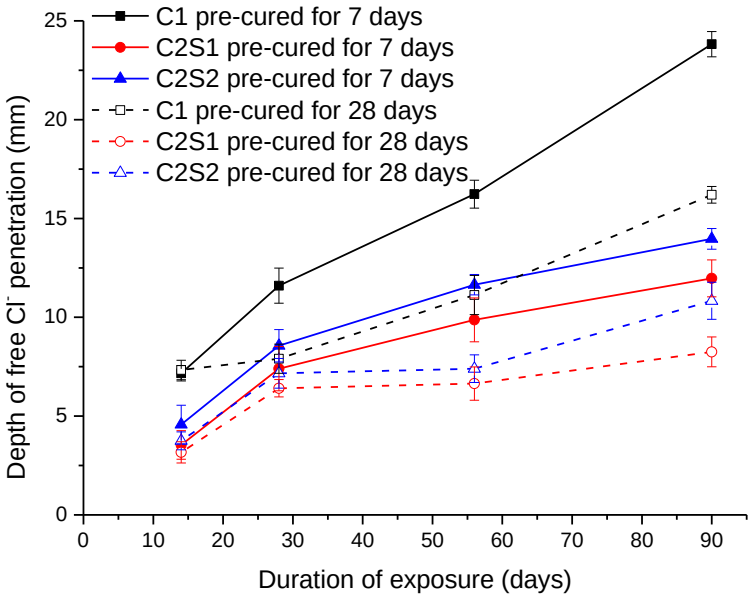

Figure 7.2: Effect of pre-curing duration on depth of chloride penetration at 38°C

The explanation for this can also be linked to the role of chloride binding and porosity on chloride ingress. From Table 4.3 and Table 5.1, it can be seen that at 38°C, prolonged curing did not have much impact on the degree of hydration and coarse porosity of the samples. Since chloride binding is related to the degree of hydration, it implies that at 38°C the chloride binding capacity of the samples pre-cured for 7 and 28 days were similar. Hence, the minimal difference observed in the chloride penetration depths measured within the period up to 28 days of exposure. However, on prolonged exposure, samples that were cured for 28 days before exposure showed better resistance to chloride penetration.

At the end of the 38°C exposure, the chloride penetration depth of the C1 samples that were pre-cured for 7 days before exposure was about 47% greater than those that were pre-cured for 28 days before exposure. For the slag 1 and 2 blend, the difference was about 45% and 29% respectively. Comparing these values to the previous ones at 20°C, it can be seen that prolonged curing at the higher temperature

before exposure did not improve the chloride ingress resistance as it did at 20°C. This is because the degree of hydration at 38°C was high, even after 7 days, so prolonged curing before immersion had less effect. It should also be noted that of the two slag blends, the slag 2 blend had the lowest decrease of 29% in the chloride penetration depth, due to prolonged curing at the high temperature. This correlates with the water penetration results (shown in Table 5.2 and Table 5.3), and also supports the earlier observations made in the sorptivity and UCS results that prolonged curing at the higher temperature was detrimental to the performance of the slag 2 blend.

7.1.2 Effect of temperature

Figure 7.3 and Figure 7.4 shows the effect of temperature on the depth of chloride penetration into samples pre-cured for 7 and 28 days respectively, before immersion in a 3% NaCl solution. As can be seen from both figures, irrespective of the pre-curing duration before exposure, samples cured and exposed at 38°C always had greater chloride penetration depths. This agrees with previous studies [196, 205, 207, 286, 287] that has shown that increase in exposure temperature leads to an increase in the rate of chloride ingress.

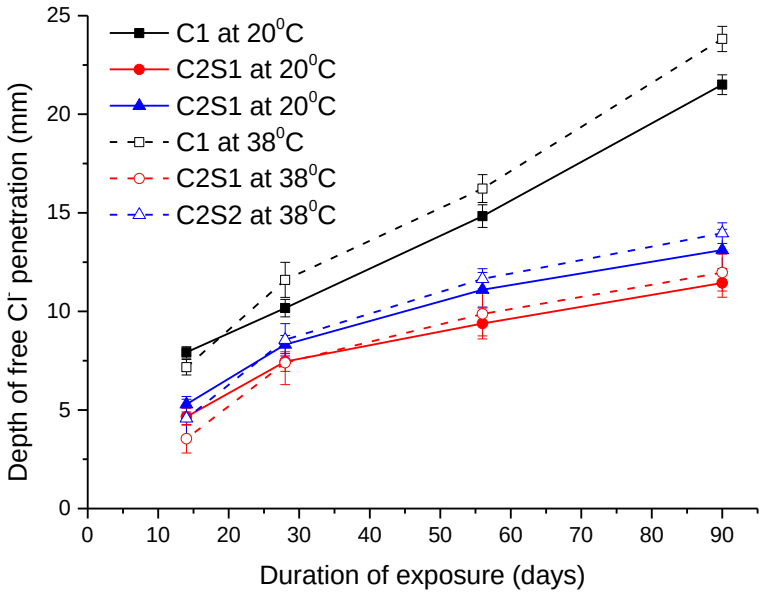

Figure 7.3: Effect of temperature on depth of chloride penetration for samples wet-cured for 7 days before exposure to 3% NaCl solution

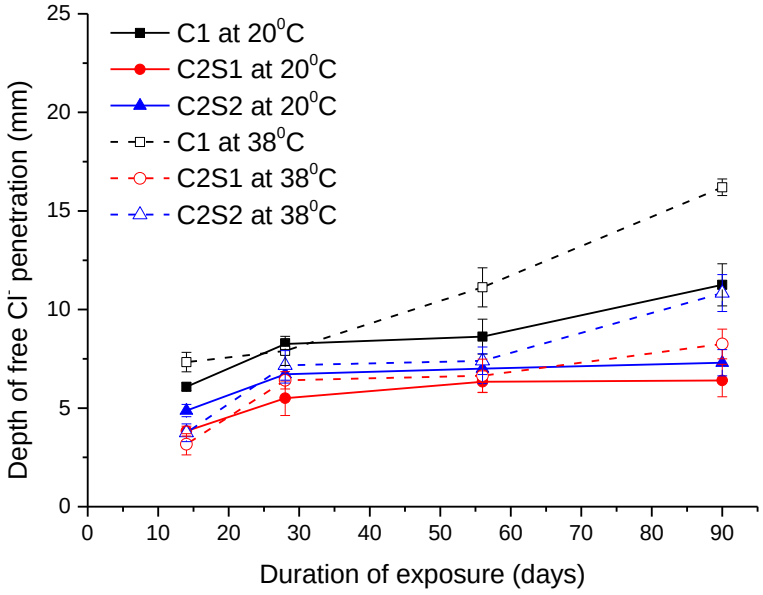

Figure 7.4: Effect of temperature on depth of chloride penetration for samples wet-cured for 28 days before exposure to 3% NaCl solution

For samples pre-cured for 7 days before exposure, the difference in temperature did not appear to have much significant impact on the initial rate of chloride ingress, especially for the slag blends. As explained before, this may be due to the influence

of temperature on the porosity and chloride binding capacity of the samples. Table 5.1 showed that slag blended samples cured at 38°C for 7 days had a less coarse pore structure than those cured at 20°C. Also, from Figure 6.2, it was seen that chloride binding was greater at 38°C due to a higher degree of hydration of the samples. This would explain the similar depths of chloride penetration observed within the first 28 days of exposure (as seen in Figure 7.3). However, at prolonged exposure periods beyond 28 days, the chloride penetration depths were greater for samples exposed at 38°C than those exposed at 20°C, especially for the neat C1 mix. This indicates that the pore structure became coarser on prolonged exposure at the higher temperature, allowing the ingress of more chloride ions. This is similar to the results obtained by Detwiler *et al*. [199], for slag blends containing 30% GGBS. They observed that at a given w/b ratio, increasing the curing temperature resulted in an increase in the rate of chloride ingress, and that the effect was more pronounced on the plain concretes than the slag blended concretes.

For the samples pre-cured for 28 days before exposure (Figure 7.4), there was no difference in the chloride penetration depths measured at both temperatures within the first 14 days. However, as the exposure period lengthened, the samples cured and exposed at the higher temperature showed greater chloride penetration. This may be attributed to two aspects. The first, due to the pore structure being coarser at 38°C. As mentioned before, high temperature curing results in a high initial rate of hydration, retarding subsequent hydration. This produces a non-uniform distribution of hydration products compared with the case of a lower curing temperature [290, 291]. The samples exposed at 38°C had hydrated to a greater degree but had a much more open microstructure as seen in the results of the degree of capillary porosity (Table 5.1). The second may be attributed to continued curing under exposure to the

salt solution, as shown in previous studies by [164, 165]. Goñi *et al.* [220], cured paste samples in demineralised water for 28 days at 20°C before exposing them to NaCl solutions. They observed that the ingress of sodium and chloride ions into the paste caused the formation of Friedel's salt in the pores that resulted in a denser microstructure. This denser microstructure resulted in a decrease in the rate of subsequent chloride ingress.

Overall, the effect of the high temperature curing and exposure was more pronounced on the neat C1 mix than the slag blends, especially for the samples that were pre-cured for 7 days before exposure. This highlights the benefit of using slag cements in high temperature marine environments. In terms of the effect of temperature on the chloride ingress resistance of the slag blends, C2S1 performed better than C2S2 at all pre-curing durations and temperature. This can be attributed to the higher chloride binding capacity and finer pore structure of the slag 1 blend.

7.1.3 Effect of exposure condition

Figure 7.5 and Figure 7.6 shows the depth of chloride penetration for samples that were continuously immersed in a 3% NaCl solution, and samples that were subjected to a cyclic chloride exposure of 6-hr wetting in a 3% NaCl solution followed by 6-hr drying, after initially pre-cured under water for 7 and 28 days respectively.

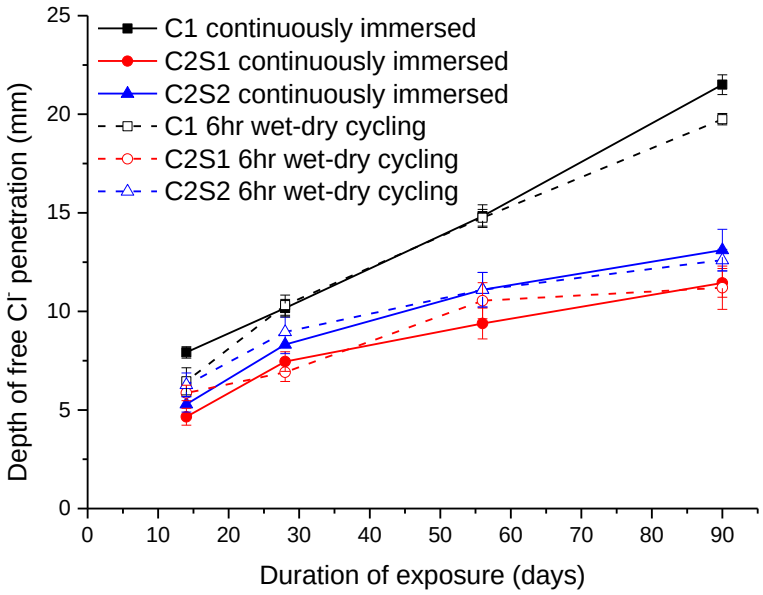

Figure 7.5: Effect of exposure condition on chloride ingress for 7 days pre-cured samples

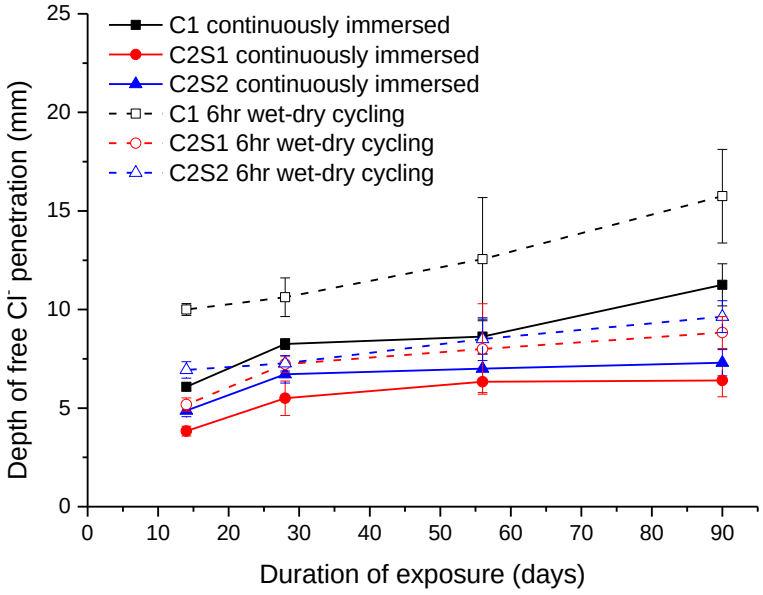

Figure 7.6: Effect of exposure condition on chloride ingress for 28 days pre-cured samples

For samples that were pre-cured for 7 days before exposure (Figure 7.5), the difference in the exposure condition did not have any significant impact on the depth of chloride penetration. However, from Figure 7.6, longer curing durations appeared

to amplify the effects of the exposure condition on chloride ingress. Samples which were cured for 28 days prior to exposure showed greater chloride ingress depths upon cyclic exposure than when exposed continuously. This effect was more pronounced for the neat C1 samples compared to the slag blends, and implies that the immature 7 day samples allowed rapid ingress, so capillary suction was less important. This is similar to results obtained by Ben Fraj *et al.* [182] where they investigated the effect of saturation rate of concrete on chloride ingress by subjecting concrete specimens to wetting/drying cycles at 75% RH and continuously in contact with sodium chloride solution of 30g/l for 1 month. They observed greater chloride ingress for the samples exposed to the wetting/drying cycles, and attributed it to the combined effect of diffusion and capillary suction. For unsaturated concrete exposed to alternate wetting and drying cycles, the chlorides diffuse into the concrete during the wetting period by liquid pressure gradient. In the drying period, only water evaporates from the concrete surface while the salts remain in the concrete leading to an accumulation of chlorides [182], which then increases capillary suction [183, 184, 205].

From Figure 7.5 and Figure 7.6, it can be seen that in the cyclic exposure condition the slag blends performed better than the neat C1 mix. The slag 1 blend having a higher chloride binding capacity, performed better than the slag 2 blend, especially for the shorter pre-curing duration. However, when the pre-curing duration was increased to 28 days, the difference in performance between the two slag blends became minimal. This is in correlation with the strength and water penetration results, which showed that prolonged curing at 20°C improved the performance of the slag 2 blend.

7.2 Total and water-soluble (free) chloride content

Total and water-soluble chloride profiles obtained for samples immersed completely in a 3% NaCl solution for a period of 90 days (as described in Section 3.6.3.3 and 3.6.3.4), at 20 and 38°C are shown in Figure 7.7 and Figure 7.8 respectively. Here, total chloride means both free and bound chloride, while water-soluble chloride means free chloride.

7.2.1 Effect of pre-curing duration

At 20°C and at the region within 10mm from the exposed face (Figure 7.7a), samples that were pre-cured for 7 days had similar total chloride contents as those pre-cured for 28 days before exposure. However, at further depths from the exposed face, the total chloride content was greater for samples pre-cured for 7 days compared to those pre-cured for 28 days before exposure. This was especially true for the neat C1 samples. This indicates that samples pre-cured for 28 days before exposure were more resistant to the ingress of chloride ions due to their lower porosity as seen from the coarse porosity results (Figure 5.1 and Table 5.1). This agrees with previous studies [5, 164, 199-201], and is also similar to the trend observed in the chloride penetration results (Figure 7.1), where it was seen that the depth of chloride penetration into samples pre-cured for 28 days were lower than those that were pre-cured for 7 days before exposure.

(a)

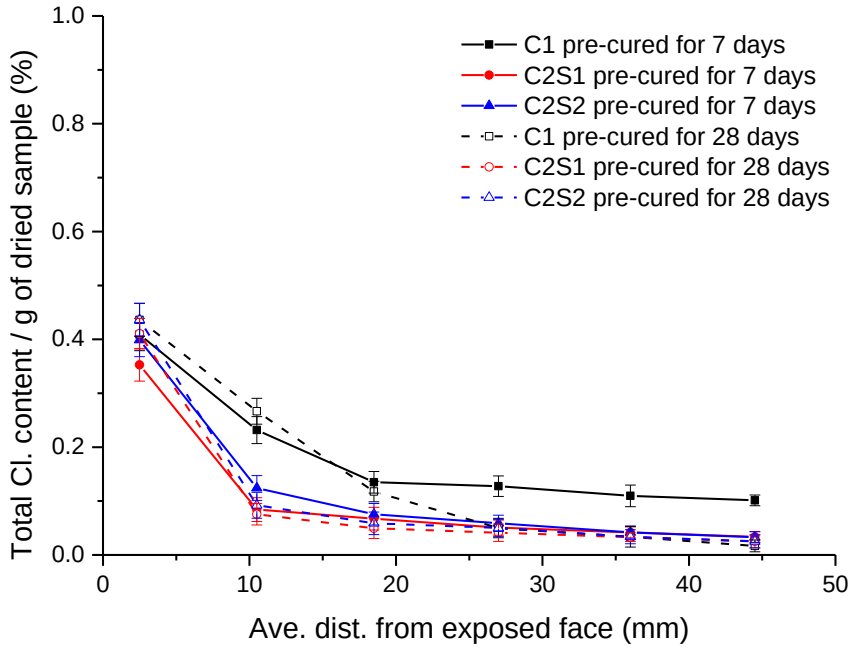

(b)

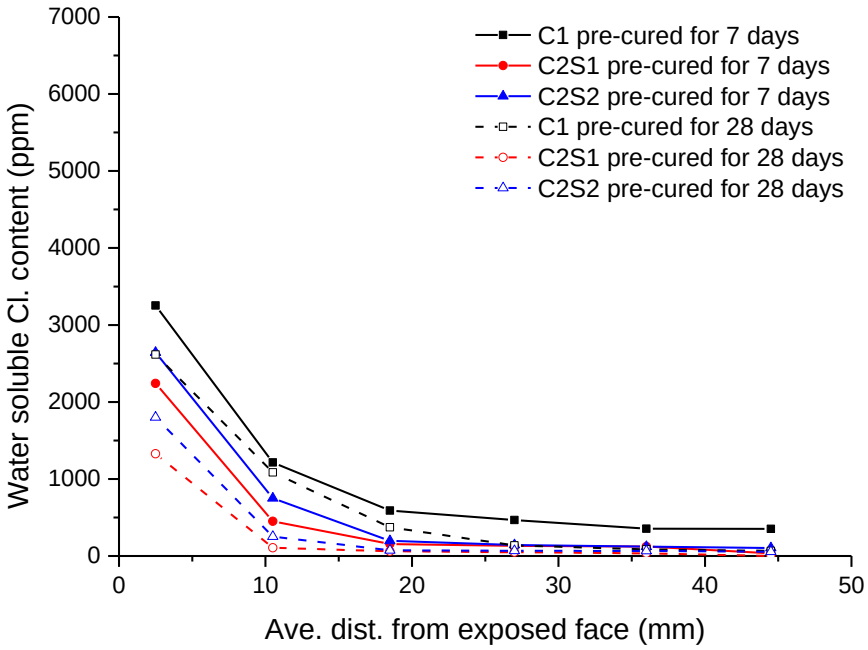

Figure 7.7: (a) Total chloride profile and (b) water-soluble chloride profile for samples pre-cured for 7 and 28 days at 20°C

However, comparing Figure 7.7a and Figure 7.1, we see that the difference between the total chloride contents of the samples pre-cured for 7 and 28 days, is not as

significant as the difference between the chloride penetration depths measured for these samples. The reason for this can be seen by observing Figure 7.7b, which shows the water-soluble (free) chloride content obtained from the same samples used for the determination of the total chloride content. In Figure 7.7b, we see a clear difference in the free chloride content of the samples pre-cured for 7 days compared to those pre-cured for 28 days before exposure, especially at the region close to the exposed surface. This can be attributed to chloride binding as previously discussed in Section 7.1.1. The samples pre-cured for 28 days before exposure had a higher degree of hydration and were able to bind more of the chlorides, hence their lower free chloride content. The results shown in Figure 7.7b correlates with those shown in Figure 7.1, and thus confirms the benefit of prolonged curing on the resistance to the ingress of free chloride ions. This is significant, as it is the free chlorides present in the pore solution that can induce corrosion of steel reinforcement.

Figure 7.8 shows the total and free chloride profile obtained for samples that were immersed in the 3% NaCl solution at 38°C for a period of 90 days. In contrast to what was observed in Figure 7.7a at the region close to the exposed face, samples that were pre-cured for 28 days had greater total chloride contents than those pre-cured for 7 days before exposure. The reason for this can be attributed to the greater porosity of the samples pre-cured for 7 days compared to those pre-cured for 28 days as seen in Figure 5.2 and Table 5.1, where at 38°C, paste samples cured for 7 days had a more porous microstructure than those cured for 28 days. Also, as seen later in Section 7.2.3, samples pre-cured for 7 days had higher chloride diffusion rates, as compared to those pre-cured for 28 days. This would mean that the chlorides permeating into the 7 day pre-cured samples migrated faster unto further

depths within the samples, without reaching higher concentrations at the surface region. This is similar to findings by Maes *et al.* [180], where they observed that samples having lower chloride diffusion rates had greater chloride concentrations at the surface. This explains why in the 28 day pre-cured samples (having a less coarse pore structure and lower chloride diffusion rate); more of the chlorides permeating into the samples remained within the region close to the exposed face. Since total chloride is a measure of the free and bound chlorides, this indicates that most of the chlorides found within this region in the 28 days pre-cured samples, would exist in the form of bound chlorides. Figure 7.8b, which shows the free chloride content profile indeed confirmed this, and showed that the free chloride content measured in this region was greater for samples pre-cured for 7 days than those pre-cured for 28 days. At further depths into the samples, as seen in Figure 7.8, the total and free chloride contents of the samples pre-cured for 7 days were always greater than those pre-cured for 28 days before exposure. This is in agreement with the chloride penetration results (Figure 7.2).

(a)

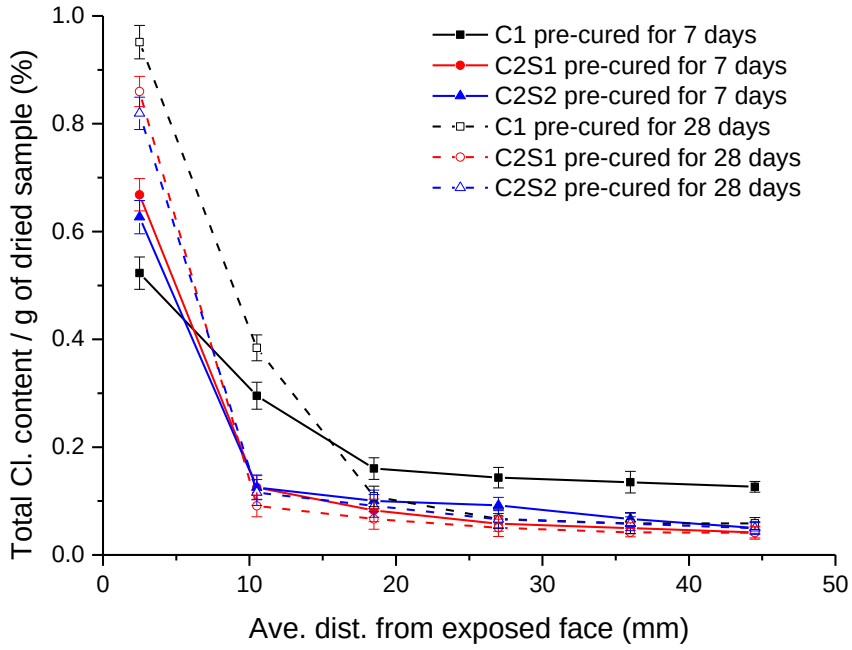

(b)

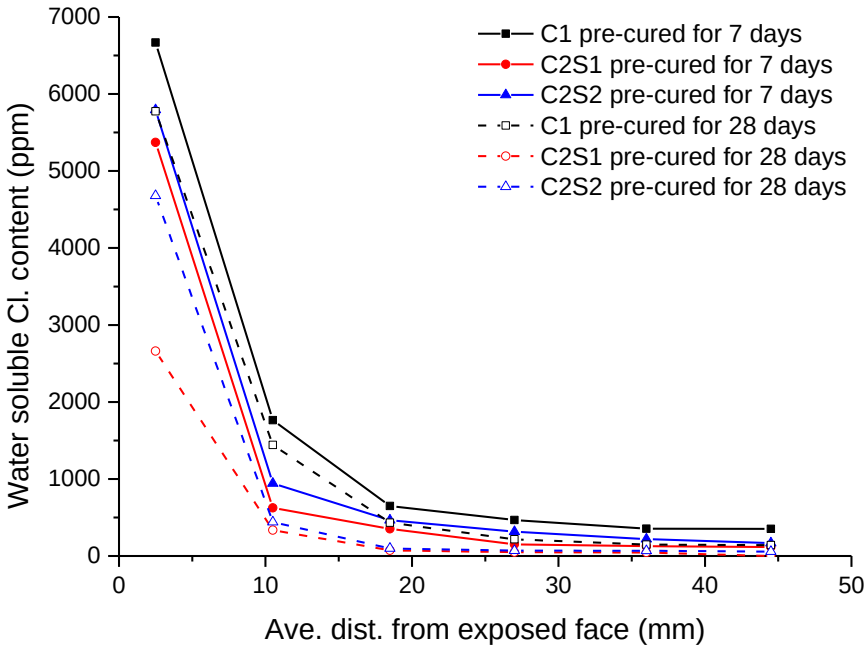

Figure 7.8: (a) Total chloride profile and (b) water-soluble chloride profile for samples pre-cured for 7 and 28 days at 38°C

From Figure 7.7 and Figure 7.8, it can be seen that the total chloride contents of the C1 samples were much greater than that of the slag blends at both pre-curing durations. This indicates that the slag blends had better resistance to the ingress of chloride ions, due to their finer pore structure [164, 168, 169] and higher chloride binding capacities [15-18]. This correlates with the chloride penetration (Figure 7.1 and Figure 7.2) and chloride binding (Figure 6.1 and Figure 6.2) results and is also in agreement with previous studies [17, 221, 228, 354]. The aluminium-rich slag blend (C2S1) had lower total and free chloride contents than C2S2 at both pre-curing durations. This is in agreement with the results of the chloride penetration depth (Figure 7.1), degree of capillary porosity (Figure 5.1 and Table 5.1) and sorptivity (Table 5.2). This confirms that the slag 1 blend had a higher chloride binding capacity and finer pore structure than the slag 2 blend.

7.2.2 Effect of temperature

The effect of temperature on the diffusion of chloride ions into the samples can be seen from Figure 7.9 and Figure 7.10, for samples pre-cured for 7 and 28 days respectively.

(a)

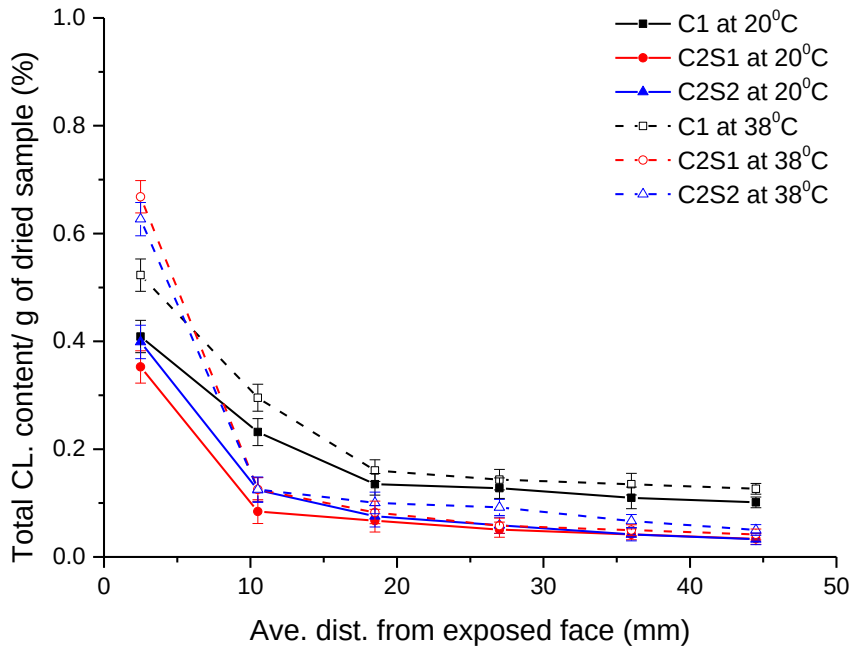

(b)

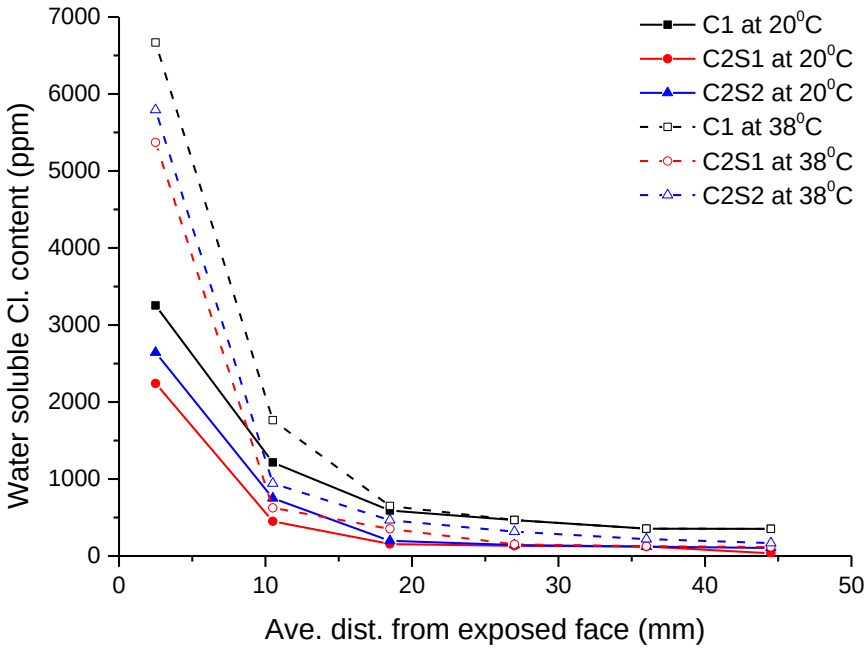

Figure 7.9: Effect of temperature on (a) total and (b) water-soluble chloride content for samples wet-cured for 7 days before exposure to 3% NaCl solution

(a)

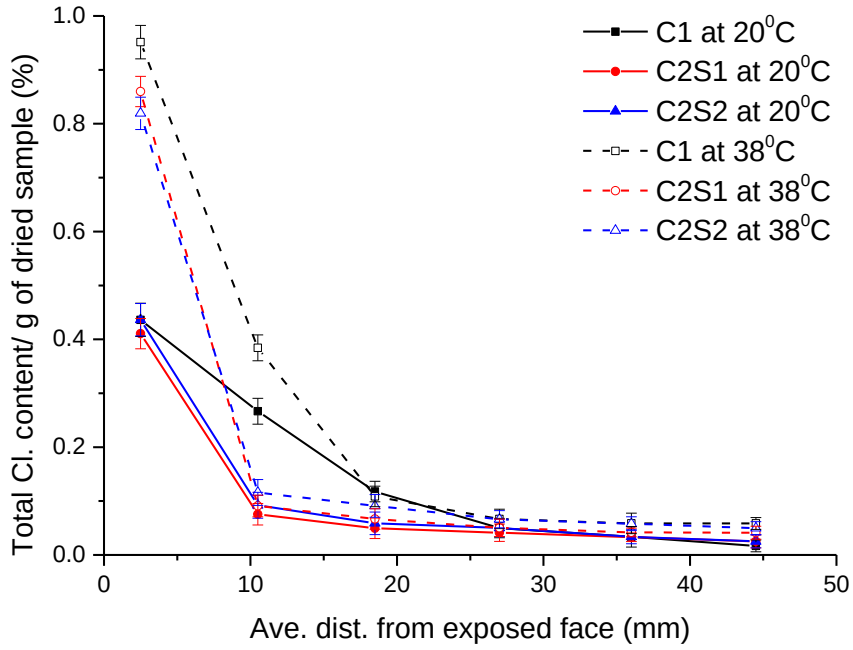

(b)

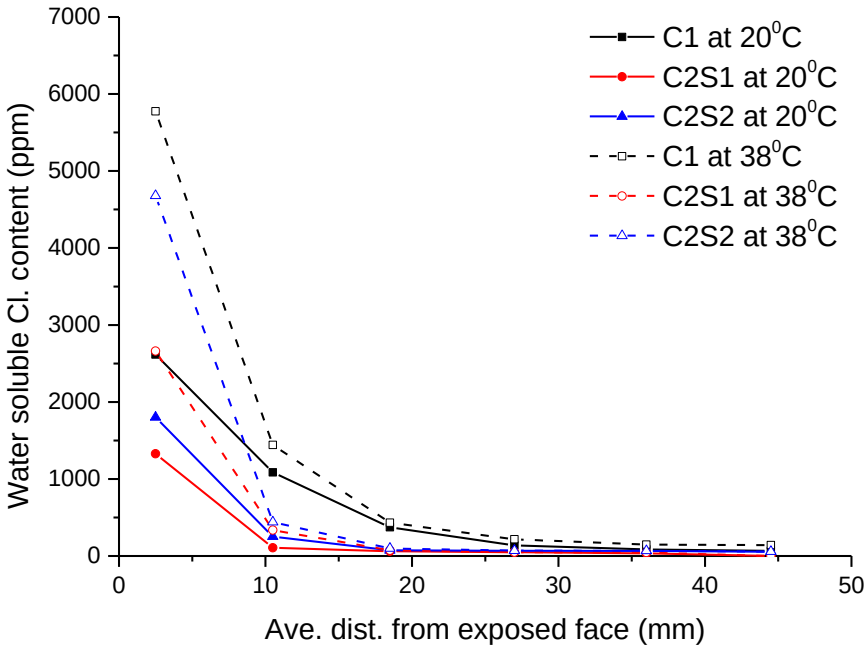

Figure 7.10: Effect of temperature on (a) total and (b) water-soluble chloride content for samples wet-cured for 28 days before exposure to 3% NaCl solution

The total chloride profiles at 38°C appear more as block-shaped, when compared to those at 20°C. These block-shaped profiles are characterised by very high chloride concentrations at the surface, which decreases to much lower values within a short distance [235], and are characteristics of mixes having high chloride binding capacities. Indeed, the chloride binding results shown in Figure 6.1 and Figure 6.2 showed that there was higher chloride binding at 38°C.

The trend observed in both figures was similar. Irrespective of the pre-curing duration, the total and water-soluble chloride content of samples cured and exposed at the higher temperature of 38°C was greater than those at 20°C, especially at the region close to the exposed face. This agrees with results from previous studies [205, 207, 287, 355], and supports the chloride penetration results which showed that there was greater chloride penetration at 38°C (as seen in Figure 7.3 and Figure 7.4). The difference in temperature only had a significant effect on the total and water-soluble chloride content at the region close to the surface. At further depths within the samples, there was no significant difference between the total and water-soluble chloride contents for the samples exposed and cured at 20°C as compared to those at 38°C, despite the increased porosity of the 38°C samples. The reason for this can be linked to chloride binding. Since chloride binding was greater at 38°C, this implies that more Friedel's salt was formed. These can act as pore blockers, slowing down the rate of chloride ingress [220, 233, 234].

7.2.3 Chloride diffusion coefficient (D_c)

Table 7.1 and Table 7.2 shows the chloride diffusion coefficient (D_c) and the chloride concentration at the surface (C_s) obtained at 20 and 38°C respectively, from the samples by a non-linear regression fit of Fick's 2nd law of diffusion, as described previously in Section 3.6.3.3.

Table 7.1: *Cs* and D_c of the slag blends obtained by non-linear regression fit of Fick's 2nd law of diffusion to the total chloride profile of all the mixes at 20°C

		C_s (% mass of sample)	D_c (m^2s^{-1})	Adj. R^2
7 days pre-cured	C1	0.38	5.15×10^{-11}	0.9135
	C2S1	0.44	5.41×10^{-12}	0.9796
	C2S2	0.47	7.70×10^{-12}	0.9816
28 days pre-cured	C1	0.50	1.75×10^{-11}	0.9980
	C2S1	0.55	3.87×10^{-12}	0.9936
	C2S2	0.58	4.00×10^{-12}	0.9916

Table 7.2: *Cs* and D_c of the slag blends obtained by non-linear regression fit of Fick's 2nd law of diffusion to the total chloride profile of all the mixes at 38°C

		C_s (% mass of sample)	D_c (m^2s^{-1})	Adj. R^2
7 days pre-cured	C1	0.50	4.41×10^{-11}	0.9156
	C2S1	0.90	3.56×10^{-12}	0.9939
	C2S2	0.83	4.02×10^{-12}	0.9859
28 days pre-cured	C1	1.15	7.92×10^{-12}	0.9976
	C2S1	1.25	2.47×10^{-12}	0.9979
	C2S2	1.17	2.73×10^{-12}	0.9954

At both temperatures, the D_c values of the samples pre-cured for 28 days were lower than those pre-cured for 7 days before exposure. However, the trend was reversed for the values of C_s. This can be attributed to the finer pore structure and higher chloride binding capacity of the 28 days pre-cured samples. This would lead to an accumulation of chloride ions at the region close to the exposed face, resulting in the higher values obtained for C_s.

It was expected that increased chloride ingress at the higher temperature would result in greater D_c values. However, the results in Table 7.1 and Table 7.2 showed a

slight decrease in the chloride diffusion coefficient *(D_c)*, but a significant increase in the total chloride concentration at the surface *(C_s)*, when the temperature was increased from 20 to 38°C. This can be explained by the block shape of the total chloride profiles at 38°C, as discussed in the previous section. Similar observations were also made in previous studies by [286, 355]. Lindvall [286] observed that for samples subjected to laboratory chloride exposure, the rate of chloride diffusion was more influenced by the salinity and only to a small extent by the temperature; while Song *et al.* [355] showed that exposure in tropical areas resulted in increased values of C_s with similar levels of D_c. This indicates that chloride diffusion was influenced jointly by the pore structure and chloride binding, both of which were also influenced by temperature. The coarsening of the pore structure caused by the high temperature curing, led to the ingress of more chloride ions, some of which were bound as Friedel's salt and made to act as pore blockers slowing down the rate of subsequent chloride ingress [220, 233, 234]. Hence, the significant increase in the values of C_s, and the slight decrease in D_c as the temperature increased from 20 to 38°C.

Although, the C_s values of the neat C1 mix was less than that of the slag blends, the values of D_c was seen to be higher at both temperatures and for all pre-curing durations. This can be attributed to the finer pore structure and higher chloride binding capacity of the slag blends. This would result in higher total chloride contents at the surface, as explained previously. Similar results were also reported by [180, 356]. For the slag blends, the D_c values of C2S1 were lower than those obtained for C2S2 at both temperatures and for all pre-curing durations. At 20°C, the difference between the D_c value of C2S1 and C2S2 was greater for samples pre-cured for 7 days than those pre-cured for 28 days. This links to the activity index of

the slags (Table 4.1), which showed better early performance for slag 1 and similar later performance for both slags. This is also in correlation with the previous results shown above, and indicates that less chlorides had diffused into the samples of the more basic, high alumina slag blend.

7.3 Summary

The results of this chapter have shown that chloride ingress is influenced jointly by the chloride binding capacity of the binder and the coarse porosity. The greater the former, the lower the rate of chloride ingress; while the greater the later, the higher the rate of chloride ingress. Chloride binding and capillary porosity can also be influenced by the curing temperature, binder type and length of curing duration as shown in the previous chapters.

Regardless of the exposure condition, increasing the curing duration from 7 to 28 days resulted in a significant reduction in the rate of chloride ingress, especially for the samples cured and exposed at the lower temperature. Samples cured for longer periods at 20°C would have a higher chloride binding capacity and less coarse pore structure, hence lower chloride ingress. While those cured at 38°C, although they would have a higher chloride binding capacity, they would also have a more coarse pore structure, which will be more open to the ingress of chloride ions.

The CEM I 42.5R samples had the least resistance to chloride ingress at both temperatures, and for all pre-curing durations. This was attributed to its lower chloride binding capacity as compared to the slag blends. For the slag blends, the aluminium-rich slag 1 blend had better chloride ingress resistance than the slag 2 blend, for all exposure and pre-curing durations. This was attributed to the higher chloride binding capacity and finer pore structure of the slag 1 blend. Prolonged

curing at 20°C was seen to improve the chloride ingress resistance of the slag 2 blend; such that there was minimal difference between the D_c values and chloride penetration depths measured for both slag blends. This is significant as it highlights the importance of prolonged curing on the performance of slag blends in low temperature chloride environments, especially for slags of lower reactivity.

Chapter 8
Discussion

As mentioned in Chapter 3, the performance of the slag blends was measured against that of C1 (CEM I 42.5R) and not C2 (CEM I 52.5R). Looking at the chemical compositions of C1 and C2 (see Table 3.1), we can see that C2 contains more alumina and sulphate than C1. The addition of the slags to C2 will result in blends containing more alumina and less sulphate. The results of the chloride binding and ingress studies showed that alumina and sulphate were the primary compounds influencing chloride binding, hence the better chloride ingress resistance observed for the slag blends as compared to that of the neat C1.

If C2 had been used as the reference cement, the slag blends would have still showed better chloride ingress resistance properties because of their higher alumina and lower sulphate content. The only difference, perhaps would have been in the strength performance, and it is generally known that slag blends have inferior early age strength but similar or superior later age strength as compared to neat systems. Hence, while it would have been better to compare the performance of the slag blends against that of C2, the outcome would probably still be the same as comparing against C1.

In this section, the performance of the slag blended cements, which was evaluated in terms of the strength and durability (water and chloride transport) properties, was compared against that of C1. Various factors such as chemical composition of the slag, exposure/ curing temperature, and the curing duration, were seen to influence the performance of the slag blends. These various factors are discussed here, as well as the implications this may have on the practical applications of slag blended cements.

8.1 Performance of the slag blends at 20°C

Table 8.1 shows the strength performance of the slag blends relative to that of the reference cement (C1), at each temperature. At 20°C, the C1 mix had better strength performance than the slag blends at 7 days, but this reversed at 28 and 180 days.

Table 8.1: Strength performance index of the slag blends

Age	C2S1		C2S2	
	20°C	38°C	20°C	38°C
7 days	0.92	1.15	0.90	1.13
28 days	1.13	1.08	1.07	1.02
180 days	1.12	1.16	1.13	1.02

The calorimetry (Figure 4.7), SEM (Table 4.3) and TGA (Figure 4.10 and Figure 4.11) results showed that the degree of hydration of the slags at the early ages was low at 20°C, as compared to at 38°C. The degree of capillary porosity obtained by SEM at 20°C (Table 5.1) showed that the slag blends had a coarser pore structure than the C1 mix at 7 days. This implies that at 20°C, the slag hydration did not contribute much to the densification of the microstructure at the early ages. It is generally known that the hydration of slags occurs over a long period of time, and at a slower rate than that of PC. Thus, as the curing duration was increased to 28 days, the slags hydrated more leading to the formation of a denser microstructure, hence the higher strengths observed beyond 28 days.

This denser microstructure of the slag blends resulted in a better resistance to the penetration and absorption of water, as compared to the neat C1 mix (see Table 5.2 and Table 5.3). When considering the resistance to the ingress of chloride ions, the higher alumina content of the slag blends also played an important role, in terms of chloride binding. The slag blends were seen to bind more of the chlorides

penetrating into the samples, resulting in lower chloride penetration depths and lower chloride diffusion coefficients, as seen in Figure 7.1 and Table 7.1 respectively.

So overall, in comparing the performance of the slag blends to that of the C1 mix at 20°C, while the early strength of the slag blends were lower than that of the C1 mix, the slag blends had better later strength performance. For the durability performance, regardless of the curing duration, the slag blends were seen to perform better than the C1 mix.

In terms of the individual performance of the slags, Table 8.1 shows that at 20°C, the strength performance of the slag 2 blend was similar to that of the slag 1 blend at the later ages. This was contrary to what was expected as predicted by the basicity index of the slags (shown in Table 4.1), which showed that slag 1 is more basic and should be more reactive than slag 2. However, the strength performance of the slag blends matched well with the predictions of the activity index of the slags, which showed that slag 1 should have higher early reactivity than slag 2, but at later ages both slags would show similar levels of reactivity. This improved performance of the slag 2 blend at the later ages can also be linked to the impact of prolonged curing on the microstructural development. The capillary porosity (Table 5.1), sorptivity (Table 5.2) and water absorption (Table 5.3) results, all showed that prolonged curing improved the pore structure of the slag 2 blend more significantly than that of the slag 1 blend.

It was seen from the chloride binding results that at 20°C, the alumina content was the chief dominating factor influencing chloride binding. The aluminium-rich slag 1 blend was seen to bind more chlorides than the slag 2 blend. However, when considering the chloride ingress resistance of the slag blends, the slag 1 blend only

outperformed the slag 2 blend at the shorter curing duration of 7 days, as seen in Figure 7.1 and Table 7.1. As the curing duration was increased to 28 days, despite the higher chloride binding capacity of slag 1, there was minimal difference in the chloride ingress resistance of the two slag blends (see Figure 7.1 and Table 7.1).

Considering the performance of the slag blends at 20°C, it is obvious that except at the early ages, the difference in basicity of the slags did not have much impact on the performance of the slag blends; rather it was the duration of curing. Prolonged moist curing was seen to be essential for the performance of the slag blends, especially for the blend prepared from the lower reactive slag.

8.2 Performance of the slag blends at 38°C

Referring to Table 8.1, it can be seen that at 38°C, the slag blends showed better strength performance than the C1 mix at all ages. Also, as observed at 20°C, the slag blends had better resistant to the ingress of water and chloride ions, as well as higher chloride binding capacities, than the neat C1 mix at 38°C.

As mentioned before, the hydration of slag in the presence of PC depends on the breakdown and dissolution of the glass slag structure by hydroxyl ions released during the hydration of PC [12, 22], both of which are accelerated at higher temperatures. At 20°C, the reactivity of the slags was lower at the early ages, but as the temperature was increased to 38°C, the reactivity of the slags increased greatly, resulting in higher degrees of slag hydration as seen in the calorimetry (Figure 4.7), SEM (Table 4.3) and TGA (Figure 4.10 and Figure 4.11) results. This higher degree of slag hydration led to the formation of a more refined microstructure, as seen by comparing Figure 5.1 and Figure 5.2, where at 7 days, the microstructure of the slag blends were less coarser at 38°C than at 20°C. This explains why at 38°C, the slag

blends were seen to have better early strength performance than the C1 mix, as against what was observed at 20°C.

Although, it was seen that the higher temperature curing resulted in higher degree of slag hydration, this was not reflected on the long-term strength and transport properties of the slag blends. This was mainly because prolonged curing at the higher temperature resulted in a coarser pore structure as seen in the capillary porosity (Table 5.1), sorptivity (Table 5.2) and water absorption (Table 5.3) results. This coarser pore structure was the reason why the slag blends had lower later strengths and poorer transport properties at 38°C than at 20°C. Figure 5.3 showed a negative correlation between compressive strength and capillary porosity. Similar relationships were drawn relating the degree of hydration and sorptivity, to compressive strength at both temperatures. These are shown in Appendix A and B respectively. The figures clearly show that at the higher temperature, the pore structure is the most dominating factor influencing performance, and not the degree of hydration. While the higher temperature resulted in a higher degree of hydration and hence, increase in chloride binding, it also resulted in a coarser microstructure that was more open to the ingress of chloride ions.

Comparing the individual performances of the slags at 38°C, the more basic slag 1 had higher reaction rates and was much better in terms of early- and later-age strength, resistance to water and chloride ions penetration, and chloride binding. The reason for this was partly attributed to the higher amount of CH available from PC hydration, at the high temperature of 38°C (Figure 4.11), which will be used for the early activation of the slags. Slag 1, having a higher basicity and slightly higher glass content than slag 2, would benefit more from the availability of the CH, as we see from Figure 4.7 where the reaction of slag 1 commenced earlier and more

rapidly than that of slag 2. Also, for slag blends, the reaction of silicates and aluminates are accelerated at higher temperatures [147], and slag 1 is richer in alumina than slag 2 (Table 3.1). This increased early reactivity of slag 1 led to the formation of more hydration products, and a more developed microstructure that was more resistant to the ingress of water and chloride ions, as compared to that of slag 2.

So, at 38°C, the performance of the slag blends was influenced mainly by the difference in basicity of the slags, which is a function of the chemical composition of the slags, and not the curing duration as was observed at 20°C. Prolonged curing at 38°C resulted in a non-uniform distribution of the hydration products and a coarser pore structure. Slag 2 being the lower reactive slag, suffered more from this effect, as compared to slag 1. Hence, the poor performance observed for the slag 2 blend at 38°C.

8.3 Practical implications of this study

The results of this study imply that at lower temperatures, longer curing durations is essential for good performance of slag blends. However, if shorter curing durations of 7 days is to be adopted, as often seen in practice, then to achieve good early performance, slags richer in alumina or more basic in nature should be used in preparing the blends.

Secondly, in hot climates like the tropical regions, the findings of this study indicates that to achieve good performance, slag blends should be prepared from slags of higher basicity or higher alumina contents. This pinpoints the drawbacks in relying on the European standards in the design and choice of construction materials, as are often the case in Nigeria and other developing countries in tropical

regions. While both slags used in the study met with the requirements as specified in BS EN 197-1:2011 [3] and BS EN 15167 [42], and performed well at the lower temperature, the results clearly showed that the high temperature exposure was less favourable to the lower reactive slag. Nevertheless, the slag blends prepared from the CEM I 52.5R still performed better than the equivalent CEM I 42.5R at the high temperature, regardless of the curing or exposure condition.

Chapter 9
Conclusions and Further Works

9.1 Conclusions

This study has investigated the influence of slag composition and temperature on the performance of slag blended cements in chloride environments. In conclusion, the following points are highlighted in relation to the findings of the study, and the contribution to knowledge.

- ***Influence of slag composition and temperature on the hydration and strength development of slag blends:***

  It is known from previous studies that higher temperature curing accelerates the early hydration of slags, leading to higher early strengths of the slag blends. This was also observed in this study. At 20°C, the early strength performance of the slag blends was inferior to that of the reference cement; but at 38°C, it became the opposite.

  Curing at 38°C accelerated the early hydration of the slags, leading to higher early strengths. This effect was more pronounced on the more reactive slag 1 blend (C2S1). At 20°C, difference in slag composition did not have much impact on the later degree of hydration and strength development of the slag blends. This has not been reported in previous studies.

- ***Influence of slag composition, curing duration and temperature on the microstructure, relating it to water transport properties of the slag blends:***

  The results of this study showed that prolonged curing at lower temperatures enhances the transport properties of slag blends. This confirms existing knowledge.

  The results also showed that slags of higher basicity will give better resistance to water penetration than those of lower basicity, especially at higher temperatures. This has not been reported in previous studies.

  It was observed that curing for 28 days at 20°C was more beneficial for the microstructural development of slag blends as compared to curing for 7 days. On the other hand, curing for 28 days at 38°C did not result in any significant improvement on the microstructure of the slag blends. In both cases, the effects were more pronounced on the blend prepared from the lower reactive slag.

- ***Influence of slag composition and temperature on the chloride binding capacity of slag blends:***

  In relation to slag composition, the study has shown that chloride binding in slag blends is dependent on the chemical composition of the slag. High alumina content will result in an increase in the amount of bound chlorides and vice versa, while high sulphate content will result in a decrease. This has not been clearly highlighted in previous studies.

  The results also showed that higher temperature increases chloride binding. The chloride binding of the slag blends was far greater at 38°C than at

20°C. In previous studies, it was unclear as to whether chloride binding increases or decreases at higher temperatures.

- ***Influence of slag composition, curing duration and temperature on the resistance of slag blends to chloride ion penetration:***

  This study showed that irrespective of the curing duration or temperature, slags of higher alumina contents will have better chloride ingress resistance properties. Slag 1 having an alumina content of 12.23%, bound and resisted more chlorides than slag 2 having an alumina content of 7.77%. This confirms the findings of previous studies that have attributed the better chloride resistance properties of SCMs to their higher alumina content.

  On the influence of curing duration, it is generally known that slag blends require prolonged moist curing for better chloride ingress resistance properties. The results of this study confirmed this. In addition, it was shown that the beneficial effect of curing for longer duration was more pronounced at 20°C than at 38°C.

  On the influence of temperature, it is generally known that higher temperature increases the rate of chloride ingress. This was observed in this study. Curing and exposure at 38°C resulted in significant increase in the C_s values, with minimal changes in the D_c values.

- ***Influence of curing duration and difference in exposure conditions on the chloride ingress resistance of slag blends:***

  It is generally known that subjecting samples to a cyclic chloride exposure will result in greater chloride ingress than if the samples were completely immersed in the chloride solutions. This was also observed in this study.

  The results of this study further showed that the negative impact of cyclic chloride exposure is greater for samples cured for longer periods of 28 days than those cured for shorter periods of 7 days. The reason for this was because the main factor influencing chloride ingress at the early ages was the porosity, whereas that of the later ages was capillary suction. This has not been looked at in previous studies.

Overall, in assessing the performance of slag blends in high and low temperature environments, the findings of this study implies that it is important to consider the temperature of the environment as well as the chemical composition of the slag, when selecting the type of slag to be used. For low temperature environments, irrespective of the slag composition, prolonged curing is essential for good strength and durability performance. On the other hand, to achieve good strength and durability performance in high temperature environments, slag blends should be prepared from slags of higher reactivity.

9.2 Further works

There are several factors that can affect the performance of slag blends. This study has focused mainly on the impact of slag composition, hydration temperature and curing duration. It would be interesting to see how variations in the degree of fineness and proportion of slag loading would impact on the performance of the slag

blends. For example, there is a possibility that increasing the degree of fineness of the lower reactive slag would improve its performance, such that it may perform better than the higher reactive slag.

Other techniques such as SEM-EDS and ^{27}Al NMR, coupled with thermodynamic modelling can be used to study how the hydration kinetics and phase assemblage changes with time and temperature, for slag blends prepared from slags of different chemical compositions. This would give more understanding as to the reason for the significant difference in performance observed at the higher temperature, between the slag blends.

In hot climates, sulphates are usually added to slag blends to regulate the setting times and give more time for concrete placement. Literature shows that at higher temperatures, the amount of sulphates reversibly bound to the C-S-H phase increases, resulting in a decrease in the $\overline{S}$/Al ratio, and the preferential formation of AFm phases. It would be interesting to see how this impacts on the hydration and performance of slag blended systems, which are already rich in aluminium. This would give a clearer explanation to the observations in the chloride binding results, where it was seen that at higher temperatures, the chloride binding capacity of the slag blends was significantly reduced by the addition of extra sulphates.

In this study, durability performance was assessed only by resistance to the ingress of chloride ions. Furthermore, samples were only subjected to a 3% NaCl solution. This does not replicate typical field conditions, where seawater can contain other ions such as K^+, Mg^{2+}, Ca^{2+}, Br^- and SO_4^{2-}. Artificial seawater containing similar ionic concentrations as that of seawater could have been used in the chloride ingress

experiments. Then, one would have been able to study the interaction between sulphate and chloride ions, and how it impacts on the durability of slag blends.

References

[1] Mehta P. K. and Monteiro P. *Concrete: Microstructure, properties and materials*. 3rd ed. New York: McGraw-Hill, 2006.

[2] Bye G. C. *Portland cement*. 3rd ed. London: ICE publishing, 2011.

[3] EN197-1:2011. Composition, specifications and conformity criteria for common cements. *Brussels*: BSI.

[4] Hadj-sadok A., Kenai S., Courard L. and Darimont A. Microstructure and durability of mortars modified with medium active blast furnace slag. *Construction and Building Materials*. 2011, **25**, 1018-1025.

[5] Shi X., Xie N., Fortune K. and Gong J. Durability of steel reinforced concrete in chloride environments: An overview. *Construction and Building Materials*. 2012, **30**, 125-138.

[6] ACI-233R-03. Slag Cement in Concrete and Mortar *Farmington Hills, MI*: American Concrete Institute; 2003.

[7] Hewlett P. C. *Lea's chemistry of cement and concrete*. 4th ed. Oxford: Elsevier Butterworth-Heinmann, 2004.

[8] Haha M. B., Lothenbach B., Le Saout G. and Winnefeld F. Influence of slag chemistry on the hydration of alkali-activated blast-furnace slag — Part II: Effect of Al2O3. *Cement and Concrete Research*. 2012, **42**, 74-83.

[9] Moranville-Regourd M. Cements Made from Blastfurnace Slag. *Lea's Chemistry of Cement and Concrete*, 2003, pp. 637-678.

[10] Smolczyk M. G. Effect of the chemistry of the slag on the strengths of blast furnace slags. Zement-Kalk-Gips. Wiesbaden, 1979, pp. 294-296.

[11] Mantel D. G. Investigation into the hydraulic activity of five granulated blast furnace slags with eight different portland cements. *ACI Materials Journal*. 1994, **91**, 471-477.

[12] Pal S. C., Mukherjee A. and Pathak S. R. Investigation of hydraulic activity of ground granulated blast furnace slag in concrete. *Cement and Concrete Research*. 2003, **33**, 1481-1486.

[13] Bougara A., Lynsdale C. and Milestone N. B. Reactivity and performance of blastfurnace slags of differing origin. *Cement and Concrete Composites*. 2010, **32**, 319-324.

[14] BS6349-1:2000. Maritime structures - Part 1: Code of practice for general criteria. *London*: BSI; 2000.

[15] Dhir R. K., El-Mohr M. A. K. and Dyer T. D. Chloride binding in GGBS concrete. *Cement and Concrete Research*. 1996, **26**, 1767-1773.

[16] Cheng A., Huang R., Wu J. K. and Chen C. H. Influence of GGBS on durability and corrosion behavior of reinforced concrete. *Materials Chemistry and Physics*. 2005, **93**, 404-411.

[17] Luo R., Cai Y., Wang C. and Huang X. Study of chloride binding and diffusion in GGBS concrete. *Cement and Concrete Research*. 2003, **33**, 1-7.

[18] Thomas M. D. A., Hooton R. D., Scott A. and Zibara H. The effect of supplementary cementitious materials on chloride binding in hardened cement paste. *Cement and Concrete Research*. 2012, **42**, 1-7.

[19] Florea M. V. A. and Brouwers H. J. H. Modelling of chloride binding related to hydration products in slag-blended cements. *Construction and Building Materials*. 2014, **64**, 421-430.

[20] Chorley R. J. and Barry R. G. *Atmosphere, weather and climate*: Routledge Ltd, 2009.

[21] Escalante-García J . I. and Sharp J. H. Effect of temperature on the hydration of the main clinker phases in portland cements: part ii, blended cements. *Cement and Concrete Research*. 1998, **28**, 1259-1274.

[22] Escalante J. I., Gómez L. Y., Johal K. K., Mendoza G., Mancha H. and Méndez J. Reactivity of blast-furnace slag in Portland cement blends hydrated under different conditions. *Cement and Concrete Research*. 2001, **31**, 1403-1409.

[23] Barnett S. J., Soutsos M. N., Millard S. G. and Bungey J. H. Strength development of mortars containing ground granulated blast-furnace slag: Effect of curing temperature and determination of apparent activation energies. *Cement and Concrete Research*. 2006, **36**, 434-440.

[24] Çakır Ö. and Aköz F. Effect of curing conditions on the mortars with and without GGBFS. *Construction and Building Materials*. 2008, **22**, 308-314.

[25] Kolani B., Buffo-Lacarrière L., Sellier A., Escadeillas G., Boutillon L. and Linger L. Hydration of slag-blended cements. *Cement and Concrete Composites*. 2012, **34**, 1009-1018.

[26] Wang Q., Miao M., Feng J. and Yan P. The influence of high-temperature curing on the hydration characteristics of a cement - GGBS binder. Advances in Cement Research, 2012, pp. 33-40.

[27] Crumbie A., Walenta G. and Füllmann T. Where is the iron? Clinker microanalysis with XRD Rietveld, optical microscopy/point counting, Bogue and SEM-EDS techniques. *Cement and Concrete Research*. 2006, **36**, 1542-1547.

[28] Jackson P. J. Portland Cement: Classification and Manufacture In: Hewlett P. C., editor. *Lea's Chemistry of Cement and Concrete*. 4th ed. Oxford: Butterworth-Heinemann, 1998, pp. 25-94.

[29] Massazza F. Pozzolana and Pozzolanic Cements In: Hewlett P. C., editor. *Lea's Chemistry of Cement and Concrete*. 4th ed. Oxford: Butterworth-Heinemann, 1998, pp. 471-635.

[30] Lothenbach B., Scrivener K. and Hooton R. D. Supplementary cementitious materials. *Cement and Concrete Research*. 2011, **41**, 1244-1256.

[31] Siddique R. and Bennacer R. Use of iron and steel industry by-product (GGBS) in cement paste and mortar. *Resources, Conservation and Recycling*. 2012, **69**, 29-34.

[32] Mehta P. K. Pozzolanic and cementitious by-products in concrete--another look. *ACI Special Publication*. 1989, **114**.

[33] Regourd M. Slags and slag cements. *Cement replacement materials Department of Mechanical Engineering, University of Sheffield*. 1986, 73-99.

[34] Schroder F. Blastfurnace slags and slag cements. In: *Proc 5th Intern Symp Chemistry of Cement, Tokyo*, 1968, pp. 149-207.

[35] Yuan R., Ouyang S. and Gao Q. Structure and hydraulic activity of slags in the system CaO-MgO-Al_2O_3-SiO_2. *Silicates Industriels*. 1983, **1**, 3-6.

[36] Smolczyk H. G. Slag structure and identification of slags. In: *7th International Congress on the Chemistry of Cement*, *Paris*, 1980, pp. 3-17.

[37] Satarin V. Slag portland cement. In: *The proceedings of the sixth internatinal congress of Chem Cem(VI ICCC), Moscow*, 1974, pp. 1-51.

[38] Swamy R. N. Design for durability and strength through the use of fly ash and slag in concrete. In: *CANMET/ACI International Workshop on Supplementary Cementing Materials, Superplasticizers and Other Chemical Admixtures in Concrete*, *Toronto, Canada*, American Concrete Institute, 1998, pp. 1-72.

[39] Wan H., Shui Z. and Lin Z. Analysis of geometric characteristics of GGBS particles and their influences on cement properties. *Cement and Concrete Research*. 2004, **34**, 133-137.

[40] Wang P. Z., Trettin R., Rudert V. and Spaniol T. Influence of Al2O3 content on hydraulic reactivity of granulated blast-furnace slag, and the interaction between Al2O3 and CaO. *Advances in Cement Research*. 2004, **16**, 1-7.

[41] Haha M. B., Lothenbach B., Saout G. L. and Winnefeld F. Influence of slag chemistry on the hydration of alkali-activated blast-furnace slag - Part I: Effect of MgO. *Cement and Concrete Research*. 2011, **41**, 955-963.

[42] EN15167-1:2006. Definitions, specifications and conformity criteria: Ground granulated blast furnace slag for use in concrete, mortar and grout. *Brussels*: BSI.

[43] Jeong Y., Oh J. E., Jun Y., Park J., Ha J.-h. and Sohn S. G. Influence of four additional activators on hydrated-lime [Ca(OH)2] activated ground granulated blast-furnace slag. *Cement and Concrete Composites*. 2016, **65**, 1-10.

[44] Kocaba V. *Development and evaluation of methods to follow microstructural development of cementitious systems including slags.* PhD Thesis. Lausanne, Switzerland, Ecole Polytechnique Federale De Lausanne, 2009.

[45] Odler I. Hydration, Setting and Hardening of Portland Cement. *Lea's Chemistry of Cement and Concrete*, 2003, pp. 241-297.

[46] Gartner E. M. and Gaidis J. M. Hydration mechanisms: I. *Materials Science of Concrete III, I, 1 pp*. 1989, **95**.

[47] Gaidis J. and Gartner E. Hydration mechanisms: II. *Materials Science of Concrete II*. 1991, 9-39.

[48] Chen Y. and Odler I. On the origin of Portland cement setting. *Cement and Concrete Research*. 1992, **22**, 1130-1140.

[49] Ylmén R., Jäglid U., Steenari B. M. and Panas I. Early hydration and setting of Portland cement monitored by IR, SEM and Vicat techniques. *Cement and Concrete Research*. 2009, **39**, 433-439.

[50] Bullard J. W., Jennings H. M., Livingston R. A., Nonat A., Scherer G. W., Schweitzer J. S., Scrivener K. L. and Thomas J. J. Mechanisms of cement hydration. *Cement and Concrete Research*. 2011, **41**, 1208-1223.

[51] Gartner E. M., Young J. F., Damidot D. A. and Jawed I. Hydration of portland cement. In: Bensted J., Barnes P., editors. *Structure and performance of cements*. 2nd ed. New York: Spon Press, 2002, pp. 57-113.

[52] Macphee D. E. and Lachowski E. E. Cement Components and Their Phase Relations. *Lea's Chemistry of Cement and Concrete*, 2003, pp. 95-129.

[53] Scrivener K. L., Juilland P. and Monteiro P. J. M. Advances in understanding hydration of Portland cement. *Cement and Concrete Research*. 2015, **78, Part A**, 38-56.

[54] Maki I. and Goto K. Factors influencing the phase constitution of alite in portland cement clinker. *Cement and Concrete Research*. 1982, **12**, 301-308.

[55] Stark J. Recent advances in the field of cement hydration and microstructure analysis. *Cement and Concrete Research*. 2011, **41**, 666-678.

[56] Scrivener K. L. and Nonat A. Hydration of cementitious materials, present and future. *Cement and Concrete Research*. 2011, **41**, 651-665.

[57] Odler I. and Dörr H. Early hydration of tricalcium silicate II. The induction period. *Cement and Concrete Research*. 1979, **9**, 277-284.

[58] Parrott L. J., Patel R. G., Killoh D. C. and Jennings H. M. Effect of Age on Diffusion in Hydrated Alite Cement. *Journal of the American Ceramic Society*. 1984, **67**, 233-237.

[59] Richardson I. G. and Groves G. W. Microstructure and microanalysis of hardened ordinary portland cements. *Journal of Material Science*. 1993, **28**, 265-277.

[60] Taylor H. F. W., Barret P., Brown P. W., Double D. D., Frohnsdorff G., Johansen V., Ménétrier-Sorrentino D., Odler I., Parrott L. J., Pommersheim J. M., Regourd M. and Young J. F. The hydration of tricalcium silicate. *Matériaux et Construction*. 1984, **17**, 457-468.

[61] Richardson I. G. The nature of the hydration products in hardened cement pastes. *Cement and Concrete Composites*. 2000, **22**, 97-113.

[62] Fierens P., Kabuema Y. and Tirlocq J. Influence du millieu de trempe sur la cinetique d'hydratation du silicate tricalcique. *Cement and Concrete Research*. 1982, **12**, 191-198.

[63] Odler I. and Schüppstuhl J. Early hydration of tricalcium silicate III. Control of the induction period. *Cement and Concrete Research*. 1981, **11**, 765-774.

[64] Montanaro L., Negro A. and Regourd M. Action de CaCO3, CaSO4 et CaSO4 · 2H2O sur l'hydratation de C3S. *Cement and Concrete Research*. 1988, **18**, 431-437.

[65] Klyusov A. A. 3CaO·SiO2 hydration under decreased temperatures. *Cement and Concrete Research*. 1994, **24**, 127-132.

[66] Bentur A. and Berger R. L. Chemical Composition of C-S-H Gel Formed in the Hydration of Calcium Silicate Pastes. *Journal of the American Ceramic Society*. 1979, **62**, 117-120.

[67] Stein H. N. and Stevels J. M. Influence of silica on the hydration of 3CaO.SiO2. *Journal of Applied Chemistry*. 1964, **14**, 338-346.

[68] Jennings H. M. and Pratt P. L. An experimental argument for the existence of a protective membrane surrounding portland cement during the induction period. *Cement and Concrete Research*. 1979, **9**, 501-506.

[69] Bellmann F., Damidot D., Möser B. and Skibsted J. Improved evidence for the existence of an intermediate phase during hydration of tricalcium silicate. *Cement and Concrete Research*. 2010, **40**, 875-884.

[70] Livingston R. A., Schweitzer J. S., Rolfs C., Becker H.-W. and Kubsky S. Characterization of the induction period in tricalcium silicate hydration by nuclear resonance reaction analysis. *Journal of Materials Research*. 2001, **16**, 687-693.

[71] Barret P. and Ménétrier D. Filter dissolution of C3S as a function of the lime concentration in a limited amount of lime water. *Cement and Concrete Research*. 1980, **10**, 521-534.

[72] Barret P., Ménétrier D. and Bertrandie D. Mechanism of C3S dissolution and problem of the congruency in the very initial period and later on. *Cement and Concrete Research*. 1983, **13**, 728-738.

[73] Thomas J. J., Jennings H. M. and Allen A. J. The surface area of cement paste as measured by neutron scattering: evidence for two C-S-H morphologies. *Cement and Concrete Research*. 1998, **28**, 897-905.

[74] Garrault-Gauffinet S. and Nonat A. Experimental investigation of calcium silicate hydrate (C-S-H) nucleation. *Journal of Crystal Growth*. 1999, **200**, 565-574.

[75] Garrault S., Finot E., Lesniewska E. and Nonat A. Study of C-S-H growth on C3S surface during its early hydration. *Materials and Structures*. 2005, **38**, 435-442.

[76] Damidot D., Nonat A. and Barret P. Kinetics of Tricalcium Silicate Hydration in Diluted Suspensions by Microcalorimetric Measurements. *Journal of the American Ceramic Society*. 1990, **73**, 3319-3322.

[77] Brown P. W., Franz E., Frohnsdorff G. and Taylor H. F. W. Analyses of the aqueous phase during early C3S hydration. *Cement and Concrete Research*. 1984, **14**, 257-262.

[78] Young J. F., Tong H. S. and Berger R. L. Compositions of Solutions in Contact with Hydrating Tricalcium Silicate Pastes. *Journal of the American Ceramic Society*. 1977, **60**, 193-198.

[79] Sowoidnich T. *A study of retarding effects on cement and tricalcium silicate hydration induced by superplasticisers.* University of Weimar, 2015.

[80] Damidot D. and Nonat A. C3S hydration in diluted and stirred suspensions: (I) study of the two kinetic steps. *Advances in Cement Research*. 1994, **6**, 27-35.

[81] Bishnoi S. and Scrivener K. L. Studying nucleation and growth kinetics of alite hydration using μic. *Cement and Concrete Research*. 2009, **39**, 849-860.

[82] Costoya M. M. *Effect of particle size on the hydration kinetics and microstructural development of tricalcium silicate.* Lausanne, Switzerland, Ecole Polytechnique Federale De Lausanne, 2008.

[83] Taylor H. F. W. *Cement chemistry*. 2nd ed. London: Thomas Telford Publishing, 1997.

[84] Rinaldi D. and Valenti G. Influence of some mineralizers on synthesis and hydration ofβ-dicalcium silicate. *Journal of Materials Science Letters*. 1986, **5**, 620-622.

[85] Fierens P. and Tirlocq J. Nature and concentration effect of stabilizing elements of beta-dicalcium silicate on its hydration rate. *Cement and Concrete Research*. 1983, **13**, 267-276.

[86] Lai G.-C., Nojiri T. and Nakano K.-i. Studies of the stability of β-Ca2SiO4 doped by minor ions. *Cement and Concrete Research*. 1992, **22**, 743-754.

[87] Fierens P. and Tirlocq J. Effect of synthesis temperature and cooling conditions of beta-dicalcium silicate on its hydration rate. *Cement and Concrete Research*. 1983, **13**, 41-48.

[88] Pritts I. M. and Daugherty K. E. The effect of stabilizing agents on the hydration rate of β-C2S. *Cement and Concrete Research*. 1976, **6**, 783-795.

[89] Kantro D. L. and Weise C. H. Hydration of Various Beta-Dicalcium Silicate Preparations. *Journal of the American Ceramic Society*. 1979, **62**, 621-626.

[90] Trettin R., Oliew G., Stadelmann C. and Wieker W. Very early hydration of dicalcium silicate-polymorphs. *Cement and Concrete Research*. 1991, **21**, 757-764.

[91] Minard H., Garrault S., Regnaud L. and Nonat A. Mechanisms and parameters controlling the tricalcium aluminate reactivity in the presence of gypsum. *Cement and Concrete Research*. 2007, **37**, 1418-1426.

[92] Breval E. C3A hydration. *Cement and Concrete Research*. 1976, **6**, 129-137.

[93] Boikova A. I., Domansky A. I., Paramonova V. A., Stavitskaja G. P. and Nikushchenko V. M. The influence of Na2O on the structure and properties of 3CaO.Al2O3. *Cement and Concrete Research*. 1977, **7**, 483-492.

[94] Plowman C. and Cabrera J. G. Mechanism and kinetics of hydration of C3A and C4AF. Extracted from cement. *Cement and Concrete Research*. 1984, **14**, 238-248.

[95] Pommersheim J. and Chang J. Kinetics of hydration of tricalcium aluminate. *Cement and Concrete Research*. 1986, **16**, 440-450.

[96] Collepardi M., Baldini G., Pauri M. and Corradi M. Tricalcium aluminate hydration in the presence of lime, gypsum or sodium sulfate. *Cement and Concrete Research*. 1978, **8**, 571-580.

[97] Pommersheim J. and Chang J. Kinetics of hydration of tricalcium aluminate in the presence of gypsum. *Cement and Concrete Research*. 1988, **18**, 911-922.

[98] Collepardi M., Baldini G., Pauri M. and Corradi M. Retardation of Tricalcium Aluminate Hydration by Calcium Sulfate. *Journal of the American Ceramic Society*. 1979, **62**, 33-35.

[99] Mehta P. K. Scanning electron micrographic studies of ettringite formation. *Cement and Concrete Research*. 1976, **6**, 169-182.

[100] Birchall J. D., Howard A. J. and Double D. D. Some general considerations of a membrane/osmosis model for portland cement hydration. *Cement and Concrete Research*. 1980, **10**, 145-155.

[101] Skalny J. and Tadros M. Retardation of tricalcium aluminate hydration by sulfates. *Journal of the American Ceramic Society*. 1977, **60**, 174-175.

[102] Negro A. and Stafferi L. THE HYDRATION OF CALCIUM FERRITE AND CALCIUM ALUMINO FERRITE. *Zement-Kalk-Gips*. 1979.

[103] Fukuhara M., Goto S., Asaga K., Daimon M. and Kondo R. Mechanisms and kinetics of C4AF hydration with gypsum. *Cement and Concrete Research*. 1981, **11**, 407-414.

[104] Chatterji S. and Jeffery J. W. Studies of Early Stages of Paste Hydration of Cement Compounds, I. *Journal of the American Ceramic Society*. 1962, **45**, 536-543.

[105] Collepardi M., Monosi S., Moriconi G. and Corradi M. Tetracalcium aluminoferrite hydration in the presence of lime and gypsum. *Cement and Concrete Research*. 1979, **9**, 431-437.

[106] Brown P. W. Early Hydration of Tetracalcium Aluminoferrite in Gypsum and Lime-Gypsum Solutions. *Journal of the American Ceramic Society*. 1987, **70**, 493-496.

[107] Beaudoin J. J. and Ramachandran V. A new perspective on the hydration characteristics of cement phases. *Cement and Concrete Research*. 1992, **22**, 689-694.

[108] Liang T. and Nanru Y. Hydration products of calcium aluminoferrite in the presence of gypsum. *Cement and Concrete Research*. 1994, **24**, 150-158.

[109] Ramachandran V. S. and Beaudoin J. J. Hydration of C4AF+ gypsum: study of various factors. 1980.

[110] Escalante-García J. I. and Sharp J. H. Effect of temperature on the hydration of the main clinker phases in portland cements: part i, neat cements. *Cement and Concrete Research*. 1998, **28**, 1245-1257.

[111] Kjellsen K. O. and Detwiler R. J. Reaction kinetics of portland cement mortars hydrated at different temperatures. *Cement and Concrete Research*. 1992, **22**, 112-120.

[112] Odler I., Abdul-Maula S. and Zhongya L. Effect of hydration temperature on cement paste structure. In: *MRS Proceedings*, Cambridge Univ Press, 1986, pp. 139.

[113] Kjellsen K. O., Detwiler R. J. and Gjørv O. E. Development of microstructures in plain cement pastes hydrated at different temperatures. *Cement and Concrete Research*. 1991, **21**, 179-189.

[114] Gallucci E., Zhang X. and Scrivener K. L. Effect of temperature on the microstructure of calcium silicate hydrate (C-S-H). *Cement and Concrete Research*. 2013, **53**, 185-195.

[115] Escalante-Garcia J. I. and Sharp J. H. The chemical composition and microstructure of hydration products in blended cements. *Cement and Concrete Composites*. 2004, **26**, 967-976.

[116] Sylla H. Reactions in cement stone due to heat treatment. *Benton*. 1988, **38**, 449-454.

[117] Escalante-García J . I. and Sharp J. H. The microstructure and mechanical properties of blended cements hydrated at various temperatures. *Cement and Concrete Research*. 2001, **31**, 695-702.

[118] Kjellsen K. O., Detwiler R. J. and Gjørv O. E. Pore structure of plain cement pastes hydrated at different temperatures. *Cement and Concrete Research*. 1990, **20**, 927-933.

[119] Kjellsen K. O., Detwiler R. J. and Gjørv O. E. Backscattered electron imaging of cement pastes hydrated at different temperatures. *Cement and Concrete Research*. 1990, **20**, 308-311.

[120] Richardson I. G. and Groves G. W. The incorporation of minor and trace elements into calcium silicate hydrate (C瑁S瑁H) gel in hardened cement pastes. *Cement and Concrete Research*. 1993, **23**, 131-138.

[121] Richardson I. G., Brough A. R., Brydson R., Groves G. W. and Dobson C. M. Location of Aluminum in Substituted Calcium Silicate Hydrate (C-S-H) Gels as Determined by 29Si and 27Al NMR and EELS. *Journal of the American Ceramic Society*. 1993, **76**, 2285-2288.

[122] Bae S., Meral C., Oh J.-e., Moon J., Kunz M. and Monteiro P. J. M. Characterization of morphology and hydration products of high-volume fly ash paste by monochromatic scanning x-ray micro-diffraction (μ-SXRD). *Cement and Concrete Research*. 2014, **59**, 155-164.

[123] Dai Z., Tran T. T. and Skibsted J. Aluminum Incorporation in the C–S–H Phase of White Portland Cement–Metakaolin Blends Studied by 27Al and 29Si MAS NMR Spectroscopy. *Journal of the American Ceramic Society*. 2014, **97**, 2662-2671.

[124] Berodier E. and Scrivener K. Understanding the Filler Effect on the Nucleation and Growth of C-S-H. *Journal of the American Ceramic Society*. 2014, **97**, 3764-3773.

[125] Utton C. A., Hayes M., Hill J., Milestone N. B. and Sharp J. H. Effect of Temperatures up to 90°C on the Early Hydration of Portland–Blastfurnace Slag Cements. *Journal of the American Ceramic Society*. 2008, **91**, 948-954.

[126] Wu X., Roy D. M. and Langton C. A. Early stage hydration of slag-cement. *Cement and Concrete Research*. 1983, **13**, 277-286.

[127] Antoni M., Rossen J., Martirena F. and Scrivener K. Cement substitution by a combination of metakaolin and limestone. *Cement and Concrete Research*. 2012, **42**, 1579-1589.

[128] Dittrich S., Neubauer J. and Goetz-Neunhoeffer F. The influence of fly ash on the hydration of OPC within the first 44 h—A quantitative in situ XRD and heat flow calorimetry study. *Cement and Concrete Research*. 2014, **56**, 129-138.

[129] Snellings R., Mertens G., Adriaens R. and Elsen J. In situ synchrotron X-ray powder diffraction study of the early age hydration of cements blended with zeolitite and quartzite fines and water-reducing agent. *Applied Clay Science*. 2013, **72**, 124-131.

[130] Regourd M., Thomassin J. H., Baillif P. and Touray J. C. Blast-furnace slag hydration. Surface analysis. *Cement and Concrete Research*. 1983, **13**, 549-556.

[131] Güneyesi E. and Gesoğlu M. A study on durability properties of high-performance concretes incorporating high replacement levels of slag. *Materials and Structures*. 2008, **41**, 15.

[132] Regourd M. Structure and behaviour of slag Portland cement hydrates. In: *Proceedings of the 7th ICCC*, 1980, pp. 10-26.

[133] Matschei T., Bellmann F. and Stark J. Hydration behaviour of sulphate-activated slag cements. *Advances in Cement Research*. 2005, **17**, 167-178.

[134] Richardson I. G., Brough A. R., Groves G. W. and Dobson C. M. The characterization of hardened alkali-activated blast-furnace slag pastes and the nature of the calcium silicate hydrate (C-S-H) phase. *Cement and Concrete Research*. 1994, **24**, 813-829.

[135] Whittaker M., Zajac M., Ben Haha M., Bullerjahn F. and Black L. The role of the alumina content of slag, plus the presence of additional sulfate on the hydration and microstructure of Portland cement-slag blends. *Cement and Concrete Research*. 2014, **66**, 91-101.

[136] Ben Haha M., Le Saout G., Winnefeld F. and Lothenbach B. Influence of activator type on hydration kinetics, hydrate assemblage and microstructural development of alkali activated blast-furnace slags. *Cement and Concrete Research*. 2011, **41**, 301-310.

[137] Lumley J. S., Gollop R. S., Moir G. K. and Taylor H. F. W. Degrees of reaction of the slag in some blends with Portland cements. *Cement and Concrete Research*. 1996, **26**, 139-151.

[138] Richardson J. M., Biernacki J. J., Stutzman P. E. and Bentz D. P. Stoichiometry of Slag Hydration with Calcium Hydroxide. *Journal of the American Ceramic Society*. 2002, **85**, 947-953.

[139] Tanaka H., Totani Y. and Saito Y. Structure of Hydrated Glassy Blast Furnace Slag in Concrete. *Fly Ash, Silica Fume and Other Mineral By Products in Concrete*, 1983, pp. 963.

[140] Barker A. An electron optical examination of zoning in blastfurnace slag hydrates: Part I. Slag cement pastes at early ages. *Advances in Cement Research*. 1989, **2**, 171-179.

[141] Feng Q., Lachowski E. and Glasser F. Densification and migration of ions in blast furnace slag-portland cement pastes. In: *MRS Proceedings*, Cambridge Univ Press, 1988, pp. 419.

[142] Rajaokarivony-Andriambololona Z., Baillif P., Thomassin J. H. and Touray J. C. Mécanismes d'hydratation d'un verre de type laitier de haut fourneau dans l'eau et en milieu alcalin. *Comptes rendus de l'Académie des sciences Série 2, Mécanique, Physique, Chimie, Sciences de l'univers, Sciences de la Terre*. 1988, **307**, 347-354.

[143] Glasser F. Chemical, mineralogical, and microstructural changes occurring in hydrated slag-cement blends. *Materials Science of Concrete II*. 1991, 41-81.

[144] Luke K. and Glasser F. P. Internal chemical evolution of the constitution of blended cements. *Cement and Concrete Research*. 1988, **18**, 495-502.

[145] Gao J. M., Qian C. X., Liu H. F., Wang B. and Li L. ITZ microstructure of concrete containing GGBS. *Cement and Concrete Research*. 2005, **35**, 1299-1304.

[146] Escalante-Garcia J. I. and Sharp J. H. The effect of temperature on the early hydration of Portland cement and blended cements. *Advances in Cement Research*. 2000, **12**, 121-130.

[147] Richardson I. G., Wilding C. R. and Dickson M. J. The hydration of blastfurnace slag cements. *Advances in Cement Research*. 1989, **2**, 147-157.

[148] Ma W., Sample D., Martin R. and Brown P. W. Calorimetric study of cement blends containing fly ash, silica fume, and slag at elevated temperatures. *Cement, Concrete and Aggregates*. 1994, **16**, 93-99.

[149] Courtault B. and Briand J. Thermal activation of cements. *Cim Betons Platres Chaux*. 1979, 86-98.

[150] Regourd M., Mortureux B., Gautier E., Hornain H. and Volant J. Characterization of thermal activation of slag cements. In: *Proceedings of the 7th International Congress on the Chemistry of Cements (Paris)*, 1980, pp. 105-111.

[151] Knudsen T. On particle size distribution in cement hydration. In: *Proceedings, 7th International congress on the chemistry of cement*, *Paris*, 1980, pp. 170-175.

[152] Roy D. M. and Idorn G. M. Developments of structure and properties of blastfurnace slag cements. *Journal of the American Concrete Institute*. 1982, **97**, 444-457.

[153] Kocaba V., Gallucci E. and Scrivener K. L. Methods for determination of degree of reaction of slag in blended cement pastes. *Cement and Concrete Research*. 2012, **42**, 511-525.

[154] Pane I. and Hansen W. Investigation of blended cement hydration by isothermal calorimetry and thermal analysis. *Cement and Concrete Research*. 2005, **35**, 1155-1164.

[155] Snellings R., Salze A. and Scrivener K. L. Use of X-ray diffraction to quantify amorphous supplementary cementitious materials in anhydrous and hydrated blended cements. *Cement and Concrete Research*. 2014, **64**, 89-98.

[156] Scrivener K. L., Lothenbach B., De Belie N., Gruyaert E., Skibsted J., Snellings R. and Vollpracht A. TC 238-SCM: hydration and microstructure of concrete with SCMs. *Materials and Structures*. 2015, **48**, 835-862.

[157] Skibsted J. Unpublished results. 2014.

[158] Sivasundaram V. and Malhotra V. M. Properties of concrete incorporating low quantity of cement and high volumes of ground granulated slag. *ACI Materials Journal*. 1992, **89**, 554-563.

[159] Wainwright P. J. and Ait-Aider H. The influence of cement source and slag additions on the bleeding of concrete. *Cement and Concrete Research*. 1995, **25**, 1445-1456.

[160] Ballim Y. and Graham P. The effects of supplementary cementing materials in modifying the heat of hydration of concrete. *Materials and Structures*. 2009, **42**, 803-811.

[161] Al-Amoudi O. S. B., Rasheeduzzafar, Maslehuddin M. and Al-Mana A. I. Prediction of long-term corrosion resistance of plain and blended cement concretes. *ACI Materials Journal*. 1993, **90**, 564-570.

[162] Roy D. M. and Idorn G. M. Hydration, structure, and properties of blast furnace slag cement, mortars, and concrete. *ACI Materials Journal*. 1982, **79**, 444-457.

[163] Hogan F. J. and Meusel J. W. Evaluation for durability and strength development of a ground granulated blast furnace slag. *Cement Concrete Aggregate*. 1981, **3**, 40-52.

[164] Chen H. J., Huang S. S., Tang C. W., Malek M. A. and Ean L. W. Effect of curing environments on strength, porosity and chloride ingress resistance of blast furnace slag cement concretes: A construction site study. *Construction and Building Materials*. 2012, **35**, 1063-1070.

[165] Ogirigbo O. R. and Black L. Influence of slag composition and curing duration on the performance of slag blends in chloride environments. In: *International Conference on Sustainable Structural Concrete*, *15-18 September 2015, La Plata, Argentina*, 2015, pp. 110-119.

[166] Ogirigbo O. R. and Black L. Combined influence of slag composition and temperature on the performance of slag blends. In: *Concrete Repair, Rehabilitation and Retrofitting IV*, *Leipzig, Germany*, London: Taylor and Francis Group, 2015, pp. 501-506.

[167] Young J. F. A review of pore structure of cement paste and concrete and its influence on permeability. *Permeability Concrete ACI SP*. 1988, **108-1**, 1-18.

[168] Uchikawa H. Blended cements. Effect of blending components on hydration and structure formation. In: *Proceedings of the 8th International Congress on the Chemistry of Cement*, *Rio de Janeiro*, 1986, pp. 250-280.

[169] Yen T., Liu Y.-W., Cheng A.-S. and Sheen Y.-N. Relation between Porosity and Compressive Strength of Slag Concrete. *Structures Congress 2008*, pp. 1-8.

[170] Feldman R. F. Pore structure, permeability and diffusivity as related to durability. In: *Proceedings of the 8th International Congress on Chemistry of Cement*, *Rio de Janeiro*, 1986, pp. 336-356.

[171] Bastidas-Arteaga E., Chateauneuf A., Sánchez-Silva M., Bressolette P. and Schoefs F. A comprehensive probabilistic model of chloride ingress in unsaturated concrete. *Engineering Structures*. 2011, **33**, 720-730.

[172] Saassouh B. and Lounis Z. Probabilistic modeling of chloride-induced corrosion in concrete structures using first- and second-order reliability methods. *Cement and Concrete Composites*. 2012, **34**, 1082-1093.

[173] Shi X., Yang Z., Liu Y. and Cross D. Strength and corrosion properties of Portland cement mortar and concrete with mineral admixtures. *Construction and Building Materials*. 2011, **25**, 3245-3256.

[174] Neville A. M. *Properties of concrete*. 4th ed. New York: Wiley, 1996.

[175] Rasheeduzzafar, Hussain S. E. and Al-Saadoun S. S. Effect of tricalcium aluminate content of cement on chloride binding and corrosion of reinforcing steel in concrete. *ACI Materials Journal*. 1992, **89**, 3-12.

[176] Nireki T. and Kabeya H. Monitoring and analysis of seawater salt content. Fourth International Conference on Durability of Building Materials and Structures. Singapore, 1987, pp. 531-536.

[177] Neville A. M. Chloride attack of reinforced concrete: an overview. *Materials and Structures*. 1995, **28**, 63-70.

[178] Janotka I., Krajci L., Komlos K., Frtalova M. D. and Halas P. Investigations on the relationship between phase composition and chloride

corrosion of steel fibre reinforcement in cement mortar. *ACI Materials Journal*. 1992, **89**, 223-229.

[179] Nagesh M. and Bhattacharjee B. Modelling of chloride diffusion in concrete and determination of diffusion coefficients. *ACI Materials Journal*. 1998, **95**, 113-120.

[180] Maes M., Gruyaert E. and De Belie N. Resistance of concrete with blast-furnace slag against chlorides, investigated by comparing chloride profiles after migration and diffusion. *Materials and Structures*. 2013, **46**, 89-103.

[181] Galan I. and Glasser F. P. Chloride in cement. *Advances in Cement Research*. 2015, **27**, 63-97.

[182] Ben Fraj A., Bonnet S. and Khelidj A. New approach for coupled chloride/moisture transport in non-saturated concrete with and without slag. *Construction and Building Materials*. 2012, **35**, 761-771.

[183] Hong K. and Hooton R. D. Effects of cyclic chloride exposure on penetration of concrete cover. *Cement and Concrete Research*. 1999, **29**, 1379-1386.

[184] Nielsen E. P. and Geiker M. R. Chloride diffusion in partially saturated cementitious material. *Cement and Concrete Research*. 2003, **33**, 133-138.

[185] Martín-Pérez B., Pantazopoulou S. J. and Thomas M. D. A. Numerical solution of mass transport equations in concrete structures. *Computers & Structures*. 2001, **79**, 1251-1264.

[186] Song H. W. and Saraswathy V. Studies on the corrosion resistance of reinforced steel in concrete with ground granulated blast-furnace slag-An overview. *Journal of Hazardous Materials*. 2006, **138**, 226-233.

[187] Aldea C.-M., Young F., Wang K. and Shah S. P. Effects of curing conditions on properties of concrete using slag replacement. *Cement and Concrete Research*. 2000, **30**, 465-472.

[188] Yang C. C. On the relationship between pore structure and chloride diffusivity from accelerated chloride migration test in cement-based materials. *Cement and Concrete Research*. 2006, **36**, 1304-1311.

[189] Yang C. C., Cho S. W. and Wang L. C. The relationship between pore structure and chloride diffusivity from ponding test in cement-based materials. *Materials Chemistry and Physics*. 2006, **100**, 203-210.

[190] Ababneh A., Benboudjema F. and Xi Y. Chloride penetration in nonsaturated concrete. *Journal of Materials in Civil Engineering*. 2003, **15**, 183-191.

[191] Bermudez M. A. and Alaejos P. Models for chloride diffusion coefficients of concretes in tidal zone. *ACI Materials Journal*. 2010, **107**, 3-11.

[192] Arya C., Buenfeld N. R. and Newman J. B. Factors influencing chloride-binding in concrete. *Cement and Concrete Research*. 1990, **20**, 291-300.

[193] Angst U., Elsener B., Larsen C. K. and Vennesland Ø. Critical chloride content in reinforced concrete — A review. *Cement and Concrete Research*. 2009, **39**, 1122-1138.

[194] Jaegermann C. Effect of water-cement ratio and curing on chloride penetration into concrete exposed to Mediterraean Sea climate. *ACI Materials Journal*. 1990, **87**, 333-339.

[195] Leng F., Feng N. and Lu X. An experimental study on the properties of resistance to diffusion of chloride ions of fly ash and blast furnace slag concrete. *Cement and Concrete Research*. 2000, **30**, 989-992.

[196] Page C. L., Short N. R. and El Tarras A. Diffusion of chloride ions in hardened cement pastes. *Cement and Concrete Research*. 1981, **11**, 395-406.

[197] Olsson N., Baroghel-Bouny V., Nilsson L.-O. and Thiery M. Non-saturated ion diffusion in concrete – A new approach to evaluate conductivity measurements. *Cement and Concrete Composites*. 2013, **40**, 40-47.

[198] Thomas M. D. A. and Bamforth P. B. Modelling chloride diffusion in concrete: Effect of fly ash and slag. *Cement and Concrete Research*. 1999, **29**, 487-495.

[199] Detwiler R. J., Fapohunda C. A. and Natale J. Use of supplementary cementing materials to increase the resistance to chloride ion penetration of concretes cured at elevated temperatures. *ACI Materials Journal*. 1994, **91**, 63-66.

[200] Güneyisi E. and Mermerdaş K. Comparative study on strength, sorptivity, and chloride ingress characteristics of air-cured and water-cured concretes modified with metakaolin. *Materials and Structures*. 2007, **40**, 1161-1171.

[201] Ramezanianpour A. A. and Malhotra V. M. Effect of curing on the compressive strength, resistance to chloride-ion penetration and porosity of concretes incorporating slag, fly ash or silica fume. *Cement and Concrete Composites*. 1995, **17**, 125-133.

[202] Güneyisi E., Özturan T. and Gesog˘lu M. Effect of initial curing on chloride ingress and corrosion resistance characteristics of concretes made with plain and blended cements. *Building and Environment*. 2007, **42**, 2676-2685.

[203] Suryavanshi A. K., Scantlebury J. D. and Lyon S. B. The binding of chloride ions by sulphate resistant portland cement. *Cement and Concrete Research*. 1995, **25**, 581-592.

[204] Hussain S. E., Rasheeduzzafar, Al-Musallam A. and Al-Gahtani A. S. Factors affecting threshold chloride for reinforcement corrosion in concrete. *Cement and Concrete Research*. 1995, **25**, 1543-1555.

[205] Oh B. H. and Jang S. Y. Effects of material and environmental parameters on chloride penetration profiles in concrete structures. *Cement and Concrete Research*. 2007, **37**, 47-53.

[206] Rasheeduzzafar, Al-Saadoun S. S., Al-Gahtani A. S. and Dakhil F. H. Effect of tricalcium aluminate content of cement on corrosion of reinforcing steel in concrete. *Cement and Concrete Research*. 1990, **20**, 723-738.

[207] Al-Khaja W. A. Influence of temperature, cement type and level of concrete consolidation on chloride ingress in conventional and high-strength concretes. *Construction and Building Materials*. 1997, **11**, 9-13.

[208] Feldman R., Beaudoin J. and Philipose K. Effect of cement blends on chloride and sulfate ion diffusion in concrete. *II Cemento*. 1991, **88**, 3-18.

[209] Tumidajski P. J. and Chan G. W. Effect of sulfate and carbon dioxide on chloride diffusivity. *Cement and Concrete Research*. 1996, **26**, 551-556.

[210] Zuquan J., Wei S., Yunsheng Z., Jinyang J. and Jianzhong L. Interaction between sulfate and chloride solution attack of concretes with and without fly ash. *Cement and Concrete Research*. 2007, **37**, 1223-1232.

[211] Niu D. and Sun C. Study on interaction of concrete carbonation and chloride corrosion. *Kuei Suan Jen Hsueh Pao/Journal of the Chinese Ceramic Society*. 2013, **41**, 1094-1099.

[212] Suryavanshi A. K. and Narayan Swamy R. Stability of Friedel's salt in carbonated concrete structural elements. *Cement and Concrete Research*. 1996, **26**, 729-741.

[213] Chindaprasirt P., Rukzon S. and Sirivivatnanon V. Effect of carbon dioxide on chloride penetration and chloride ion diffusion coefficient of blended Portland cement mortar. *Construction and Building Materials*. 2008, **22**, 1701-1707.

[214] Uysal M., Yilmaz K. and Ipek M. The effect of mineral admixtures on mechanical properties, chloride ion permeability and impermeability of self-compacting concrete. *Construction and Building Materials*. 2012, **27**, 263-270.

[215] Sandberg P., Tang L. and Andersen A. Recurrent studies of chloride ingress in uncracked marine concrete at various exposure times and elevations. *Cement and Concrete Research*. 1998, **28**, 1489-1503.

[216] Bai J., Wild S. and Sabir B. B. Chloride ingress and strength loss in concrete with different PC–PFA–MK binder compositions exposed to synthetic seawater. *Cement and Concrete Research*. 2003, **33**, 353-362.

[217] Dhir R. K., El-Mohr M. A. K. and Dyer T. D. Developing chloride resisting concrete using PFA. *Cement and Concrete Research*. 1997, **27**, 1633-1639.

[218] Song H.-W., Pack S.-W., Nam S.-H., Jang J.-C. and Saraswathy V. Estimation of the permeability of silica fume cement concrete. *Construction and Building Materials*. 2010, **24**, 315-321.

[219] Badogiannis E. and Tsivilis S. Exploitation of poor Greek kaolins: Durability of metakaolin concrete. *Cement and Concrete Composites*. 2009, **31**, 128-133.

[220] Goñi S., Frias M., Vigil de la Villa R. and García R. Sodium chloride effect on durability of ternary blended cement. Microstructural characterization and strength. *Composites Part B: Engineering*. 2013, **54**, 163-168.

[221] Bouteiller V., Cremona C., Baroghel-Bouny V. and Maloula A. Corrosion initiation of reinforced concretes based on Portland or GGBS cements: Chloride contents and electrochemical characterizations versus time. *Cement and Concrete Research*. 2012, **42**, 1456-1467.

[222] Sengul O. and Tasdemir M. Compressive Strength and Rapid Chloride Permeability of Concretes with Ground Fly Ash and Slag. *Journal of Materials in Civil Engineering*. 2009, **21**, 494-501.

[223] Mackechnie J. and Alexander M. Exposure of Concrete in Different Marine Environments. *Journal of Materials in Civil Engineering*. 1997, **9**, 41-44.

[224] Gouda V. and Halaka W. Corrosion and corrosion inhibition of reinforcing steel: II. Embedded in concrete. *British Corrosion Journal*. 1970, **5**, 204-208.

[225] Schiessl P. and Breit W. Local repair measures at concrete structures damaged by reinforcement corrosion-aspects of durability. *SPECIAL PUBLICATION-ROYAL SOCIETY OF CHEMISTRY*. 1996, **183**, 525-534.

[226] Oh B. H., Jang S. Y. and Shin Y. Experimental investigation of the threshold chloride concentration for corrosion initiation in reinforced concrete structures. *Magazine of Concrete Research*. 2003, **55**, 117-124.

[227] Yeau K. Y. and Kim E. K. An experimental study on corrosion resistance of concrete with ground granulate blast-furnace slag. *Cement and Concrete Research*. 2005, **35**, 1391-1399.

[228] Andrade C. and Buják R. Effects of some mineral additions to Portland cement on reinforcement corrosion. *Cement and Concrete Research*. 2013, **53**, 59-67.

[229] Loser R., Lothenbach B., Leemann A. and Tuchschmid M. Chloride resistance of concrete and its binding capacity – Comparison between

experimental results and thermodynamic modeling. *Cement and Concrete Composites*. 2010, **32**, 34-42.

[230] Basheer P. A. M., Gilleece P. R. V., Long A. E. and Mc Carter W. J. Monitoring electrical resistance of concretes containing alternative cementitious materials to assess their resistance to chloride penetration. *Cement and Concrete Composites*. 2002, **24**, 437-449.

[231] Jau W. C. and Tsay D. S. A study of the basic engineering properties of slag cement concrete and its resistance to seawater corrosion. *Cement and Concrete Research*. 1998, **28**, 1363-1371.

[232] Otieno M., Beushausen H. and Alexander M. Effect of chemical composition of slag on chloride penetration resistance of concrete. *Cement and Concrete Composites*. 2014, **46**, 56-64.

[233] Glasser F. P., Marchand J. and Samson E. Durability of concrete — Degradation phenomena involving detrimental chemical reactions. *Cement and Concrete Research*. 2008, **38**, 226-246.

[234] Buenfeld N. R., Glass G. K., Hassanein A. M. and Zhang J.-Z. Chloride transport in concrete subjected to an electric field. *Journal of Materials in Civil Engineering*. 1998, **10**, 220-228.

[235] Tang L. *Chloride transport in concrete - measurement and prediction.* PhD Thesis. Goteborg, Chalmers University of Technology, 1996.

[236] Glass G. K. and Buenfeld N. R. The presentation of the chloride threshold level for corrosion of steel in concrete. *Corrosion Science*. 1997, **39**, 1001-1013.

[237] Glass G. K. and Buenfeld N. R. The influence of chloride binding on the chloride-induced corrosion risk in reinforced concrete. *Corrosion Science*. 2000, **42**, 329-344.

[238] Reddy B., Glass G. K., Lim P. J. and Buenfeld N. R. On the corrosion risk presented by chloride bound in concrete. *Cement and Concrete Composites*. 2002, **24**, 1-5.

[239] Suryavanshi A. K., Scantlebury J. D. and Lyon S. B. Mechanism of Friedel's salt formation in cements rich in tri-calcium aluminate. *Cement and Concrete Research*. 1996, **26**, 717-727.

[240] Wowra O. and Setzer M. J. Sorption of chlorides on hydrated cements and C_3S pastes. In: Setzer M. J., Auberg R., editors. Frost resistance of Concrete. London: E&FN Spon, 1997, pp. 146-153.

[241] Xu Y. The influence of sulphates on chloride binding and pore solution chemistry. *Cement and Concrete Research*. 1997, **27**, 1841-1850.

[242] Wowra O. and Setzer M. About the interaction of chloride and hardened cement paste. In: *2nd Int RILEM Workshop on Testing and Modelling the Chloride Ingress into Concrete*, *Paris, France*, 2000, pp. 3-12.

[243] Luping T. and Nilsson L.-O. Chloride binding capacity and binding isotherms of OPC pastes and mortars. *Cement and Concrete Research*. 1993, **23**, 247-253.

[244] Zibara H. *Binding of external chlorides by cement pastes.* PhD Thesis. Canada, University of Toronto, 2001.

[245] Delagrave A., Marchand J., Ollivier J.-P., Julien S. and Hazrati K. Chloride binding capacity of various hydrated cement paste systems. *Advanced Cement Based Materials*. 1997, **6**, 28-35.

[246] Delagrave A., Pigeon M. and Revertégat É. Influence of chloride ions and pH level on the durability of high performance cement pastes. *Cement and Concrete Research*. 1994, **24**, 1433-1443.

[247] Delagrave A., Pigeon M., Marchand J. and Revertégat É. Influence of chloride ions and pH level on the durability of high performance cement pastes (part II). *Cement and Concrete Research*. 1996, **26**, 749-760.

[248] Ipavec A., Vuk T., Gabrovšek R. and Kaučič V. Chloride binding into hydrated blended cements: The influence of limestone and alkalinity. *Cement and Concrete Research*. 2013, **48**, 74-85.

[249] Tritthart J. Chloride binding in cement II. The influence of the hydroxide concentration in the pore solution of hardened cement paste on chloride binding. *Cement and Concrete Research*. 1989, **19**, 683-691.

[250] Page C., Lambert P. and Vassie P. Investigations of reinforcement corrosion. 1. The pore electrolyte phase in chloride-contaminated concrete. *Materials and Structures*. 1991, **24**, 243-252.

[251] Holden W. R., Page C. L. and Short N. R. The influence of chlorides and sulphates on durability. In: Crane A. P., editor. *Corrosion of Reinforcement in Concrete Construction*. Chickester: Ellis Horwood Ltd, 1983, pp. 143-150.

[252] Arya C. and Xu Y. Effect of cement type on chloride binding and corrosion of steel in concrete. *Cement and Concrete Research*. 1995, **25**, 893-902.

[253] Mangat P. S. and Molloy B. T. Chloride binding in concrete containing PFA, ggbs or silica fume under sea water exposure. *Magazine of Concrete Research*. 1995, **47**, 129-141.

[254] Wiens U. and Schiessl P. Chloride binding of cement paste containing fly ash. *Proceedings of the 10th ICCC, Goteborg, Sweden*. 1997, 4-10.

[255] Balonis M., Lothenbach B., Le Saout G. and Glasser F. P. Impact of chloride on the mineralogy of hydrated Portland cement systems. *Cement and Concrete Research*. 2010, **40**, 1009-1022.

[256] Glasser F. P., Kindness A. and Stronach S. A. Stability and solubility relationships in AFm phases: Part I. Chloride, sulfate and hydroxide. *Cement and Concrete Research*. 1999, **29**, 861-866.

[257] Birnin-Yauri U. A. and Glasser F. P. Friedel's salt, Ca2Al(OH)6(Cl,OH)·2H2O: its solid solutions and their role in chloride binding. *Cement and Concrete Research*. 1998, **28**, 1713-1723.

[258] Johannesson B., Yamada K., Nilsson L.-O. and Hosokawa Y. Multi-species ionic diffusion in concrete with account to interaction between ions in the pore solution and the cement hydrates. *Materials and Structures*. 2007, **40**, 651-665.

[259] Jones M. R., Macphee D. E., Chudek J. A., Hunter G., Lannegrand R., Talero R. and Scrimgeour S. N. Studies using 27Al MAS NMR of AFm and AFt phases and the formation of Friedel's salt. *Cement and Concrete Research*. 2003, **33**, 177-182.

[260] Csizmadia J., Balázs G. and Tamás F. D. Chloride ion binding capacity of aluminoferrites. *Cement and Concrete Research*. 2001, **31**, 577-588.

[261] Elakneswaran Y., Nawa T. and Kurumisawa K. Electrokinetic potential of hydrated cement in relation to adsorption of chlorides. *Cement and Concrete Research*. 2009, **39**, 340-344.

[262] Henocq P., Marchand J., Samson E., Lavoie J.-A., Marchand J., Bissonnette B., Gagné R., Jolin M. and Paradis F. Modeling of ionic interactions at the C–S–H surface—Application to CsCl and LiCl solutions in comparison with NaCl solutions. In: *2nd Int Symp On Advances in Concrete through Science and Engineering, RILEM Proceedings*, 2006, pp.

[263] Hosokawa Y., Yamada K., Johannesson B., Nilsson L.-O., Marchand J., Bissonnette B., Gagné R., Jolin M. and Paradis F. Models for chloride ion bindings in hardened cement paste using thermodynamic equilibrium calculations. In: *2nd International RILEM symposium on advances in concrete through science and engineering*, 2006, pp.

[264] Hirao H., Yamada K., Takahashi H. and Zibara H. Chloride binding of cement estimated by binding isotherms of hydrates. *Journal of Advanced Concrete Technology*. 2005, **3**, 77-84.

[265] Elakneswaran Y., Nawa T. and Kurumisawa K. Electrokinetic potential of hydrated cement in relation to adsorption of chlorides. *Cement and Concrete Research*. 2009, **39**, 340-344.

[266] Kayali O., Khan M. S. H. and Sharfuddin Ahmed M. The role of hydrotalcite in chloride binding and corrosion protection in concretes with ground granulated blast furnace slag. *Cement and Concrete Composites*. 2012, **34**, 936-945.

[267] Douglas G. B., Wendling L. A., Pleysier R. and Trefry M. G. Hydrotalcite formation for contaminant removal from Ranger mine process water. *Mine Water and the Environment*. 2010, **29**, 108-115.

[268] Lin J. K. and Uan J. Y. Formation of Mg, Al-hydrotalcite conversion coating on Mg alloy in aqueous HCO_3^-/CO_3^{2-} and corresponding protection against corrosion by the coating. *Corrosion Science*. 2009, **51**, 1181-1188.

[269] Wang J., Li D., Yu X., Jing X., Zhang M. and Jiang Z. Hydrotalcite conversion coating on Mg alloy and its corrosion resistance. *Journal of Alloys and compounds*. 2010, **494**, 271-274.

[270] Arya C. and Newman J. B. An assessment of four methods of determining the free chloride content of concrete. *Materials and Structures*. 1990, **23**, 319-330.

[271] Browne F. P. and Bolling N. B. New technique for analysis of chlorides in mortar. *Journal of Materials*. 1971, **6**, 524-531.

[272] Ramachandran V. S. Possible states of chloride in the hydration of tricalcium silicate in the presence of calcium chloride. *Matériaux et Construction*. 1971, **4**, 3-12.

[273] Arya C., Buenfeld N. R. and Newman J. B. Assessment of simple methods of determining the free chloride ion content of cement paste. *Cement and Concrete Research*. 1987, **17**, 907-918.

[274] Meck E. and Sirivivatnanon V. Field indicator of chloride penetration depth. *Cement and Concrete Research*. 2003, **33**, 1113-1117.

[275] EN12390-11:2015. Determination of the chloride resistance of concrete, unidirectional diffusion: Testing hardened concrete. *Brussels*: BSI; 2010.

[276] BS1881-124:1988. Testing concrete: Methods for analysis of hardened concrete. *London*: BSI; 1998.

[277] RILEM. Analysis of total chloride content in concrete. *Materials and Structures*. 2002, **35**, 583-585.

[278] Dhir R. K., Jones M. R. and Ahmed H. E. H. Determination of total and soluble chlorides in concrete. *Cement and Concrete Research*. 1990, **20**, 579-590.

[279] Samson E., Marchand J. and Snyder K. A. Calculation of ionic diffusion coefficients on the basis of migration test results. *Materials and Structures*. 2003, **36**, 156-165.

[280] Friedmann H ., Amiri O ., Aït-Mokhtar A. and Dumargue P. A direct method for determining chloride diffusion coefficient by using migration test. *Cement and Concrete Research*. 2004, **34**, 1967-1973.

[281] ASTM. C1202-12: Standard test method for electrical indication of concrete's ability to resist chloride ion penetration. *West Conshohoken, PA, USA*: ASTM International; 2012.

[282] Andrade C., Alonso C., Arteaga A. and Tanner P. Methodology based on the electrical resistivity for the calculation of reinforcement service life. In: *Proceedings of the 5th CANMET/ACI International Conference on Durability of Concrete*, 2000, pp. 899-915.

[283] Streicher P. E. and Alexander M. G. A chloride conduction test for concrete. *Cement and Concrete Research*. 1995, **25**, 1284-1294.

[284] Alexander M., Ballim Y. and Mackechnie J. Concrete durability index testing manual. Research monograph. Cape Town, South Africa: Department of Civil Engineering, University of Cape town, 1999.

[285] Shi M., Chen Z. and Sun J. Determination of chloride diffusivity in concrete by AC impedance spectroscopy. *Cement and Concrete Research*. 1999, **29**, 1111-1115.

[286] Lindvall A. Chloride ingress data from field and laboratory exposure – Influence of salinity and temperature. *Cement and Concrete Composites*. 2007, **29**, 88-93.

[287] Detwiler R. J., Kjellsen K. O. and Gjørv O. E. Resistance to chloride intrusion of concrete cured at different temperatures. *ACI Materials Journal*. 1991, **88**, 19-24.

[288] Samson E. and Marchand J. Modeling the effect of temperature on ionic transport in cementitious materials. *Cement and Concrete Research*. 2007, **37**, 455-468.

[289] Chini A. R. and Acquaye L. Effect of elevated curing temperatures on the strength and durability of concrete. *Materials and Structures*. 2005, **38**, 673-679.

[290] Brooks J. J. and Al-kaisi A. F. Early strength development of Portland and slag cement concretes cured at elevated temperatures. *ACI Materials Journal*. 1990, **87**, 503-507.

[291] Lothenbach B., Winnefeld F., Alder C., Wieland E. and Lunk P. Effect of temperature on the pore solution, microstructure and hydration products of Portland cement pastes. *Cement and Concrete Research*. 2007, **37**, 483-491.

[292] Panesar D. and Chidiac S. Effect of Cold Temperature on the Chloride-Binding Capacity of Cement. *Journal of Cold Regions Engineering*. 2011, **25**, 133-144.

[293] Dousti A. and Shekarchi M. Effect of exposure temperature on chloride-binding capacity of cementing materials. *Magazine of Concrete Research*. 2015, **67**, 821-832.

[294] Hussain S. E. and Rasheeduzzafar. Effect of temperature on pore solution composition in plain cements. *Cement and Concrete Research*. 1993, **23**, 1357-1368.

[295] Maslehuddin M., Paget C. L. and Rasheeduzzafar. Temperature effect on the pore solution chemistry in contaminated cements. *Magazine of Concrete Research*. 1997, **49**, 5-14.

[296] Jensen O. M., Korzen M. S. H., Jakobsen H. J. and Skibsted J. Influence of cement constitution and temperature on chloride binding in cement paste. *Advances in Cement Research*. 2000, **12**, 57-64.

[297] Xu J., Song Y., Jiang L., Feng W., Cao Y. and Ji W. Influence of elevated temperature on release of bound chlorides from chloride-admixed plain and blended cement pastes. *Construction and Building Materials*. 2016, **104**, 9-15.

[298] Rasheeduzzafar. Influence of cement composition on concrete durability. *ACI Materials Journal*. 1992, **89**, 574-586.

[299] Blunk G., Gunkel P. and Smolczyk H. On the distribution of chloride between the hardening cement paste and its pore solution. In: *Proceedings of the 8th international congress on the chemistry of cement*, *Rio de Janeiro, Brazil*, 1986, pp. 85-90.

[300] EN12620:2002+A1. Aggregates for concrete. *Brussels*: BSI; 2008.

[301] EN196-1:2005. Methods of testing cement: Determination of strength. *Brussels*: BSI.

[302] Willson R. J. Calorimetry. *Principles of Thermal Analysis and Calorimetry*: The Royal Society of Chemistry, 2002, pp. 129-165.

[303] Wadsö L. Operational issues in isothermal calorimetry. *Cement and Concrete Research*. 2010, **40**, 1129-1137.

[304] De Schutter G. and Taerwe L. Specific Heat and Thermal Diffusivity of Hardening Concrete. *Magazine of Concrete Research*. 1995, **47**, 203-208.

[305] Whittaker M. J. *The Impact of Slag Composition on the Microstructure of Composite Slag Cements Exposed to Sulfate Attack.* PhD Thesis. Leeds, UK, University of Leeds, 2014.

[306] Collier N. C., Sharp J. H., Milestone N. B., Hill J. and Godfrey I. H. The influence of water removal techniques on the composition and microstructure of hardened cement pastes. *Cement and Concrete Research*. 2008, **38**, 737-744.

[307] Gallé C. Effect of drying on cement-based materials pore structure as identified by mercury intrusion porosimetry: A comparative study between oven-, vacuum-, and freeze-drying. *Cement and Concrete Research*. 2001, **31**, 1467-1477.

[308] Konecny L. and Naqvi S. J. The effect of different drying techniques on the pore size distribution of blended cement mortars. *Cement and Concrete Research*. 1993, **23**, 1223-1228.

[309] Zhang J. and Scherer G. W. Comparison of methods for arresting hydration of cement. *Cement and Concrete Research*. 2011, **41**, 1024-1036.

[310] Beaudoin J. J., Tamtsia B., Marchand J. and Myers H. R. Solvent exchange in partially saturated and saturated microporous systems: Length change anomalies. *Cement and Concrete Research*. 2000, **30**, 359-370.

[311] Hughes D. C. The use of solvent exchange to monitor diffusion characteristics of cement pastes containing silica fume. *Cement and Concrete Research*. 1988, **18**, 321-324.

[312] Aligizaki K. K. *Pore structure of cement-based materials: testing, interpretation and requirements*. London: Taylor & Francis, 2006.

[313] Chatterjee A. K. X-Ray Diffraction. In: Ramachandran V. S., Beaudoin J. J., editors. *Handbook of analytical techniques in concrete science and technology*. New York, U.S.A: William Andrew Publishing, 2001, pp. 275-332.

[314] Aranda M. A. G., De La Torre A. G. and Leon-Reina L. Rietveld Quantitative Phase Analysis of OPC Clinkers, Cements and Hydration Products. *Reviews in Mineralogy and Geochemistry*. 2012, **74**, 169-209.

[315] McCusker L. B., Von Dreele R. B., Cox D. E., Louer D. and Scardi P. Rietveld Refinement Guidelines. *Journal of Applied Crystallography*. 1999, **32**, 36-50.

[316] Warrington S. B. Simulataneous thermal analysis techniques. *Principles of Thermal Analysis and Calorimetry*: The Royal Society of Chemistry, 2002, pp. 166-189.

[317] Ramachandran V. S. Thermal Analysis. In: Ramachandran V. S., Beaudion J. J., editors. *Handbook of Analytical Techniques in Concrete Science Technology - Principles, Techniques and Applications*: William Andrew Publishing, 2001, pp. 127-173.

[318] Feng X., Garboczi E. J., Bentz D. P., Stutzman P. E. and Mason T. O. Estimation of the degree of hydration of blended cement pastes by a scanning electron microscope point-counting procedure. *Cement and Concrete Research*. 2004, **34**, 1787-1793.

[319] Scrivener K. L. Backscattered electron imaging of cementitious microstructures: understanding and quantification. *Cement and Concrete Composites*. 2004, **26**, 935-945.

[320] Famy C., Scrivener K. L. and Crumbie A. K. What causes differences of C-S-H gel grey levels in backscattered electron images? *Cement and Concrete Research*. 2002, **32**, 1465-1471.

[321] ammrf. *Scanning Electron Microscope Training Manual*. [Online]. 2014. [Accessed: 25/6/2015]. Available from: http://www.ammrf.org.au/myscope/sem/practice/principles/imagegeneration.php.

[322] Kjellsen K. O., Monsøy A., Isachsen K. and Detwiler R. J. Preparation of flat-polished specimens for SEM-backscattered electron imaging and X-ray microanalysis—importance of epoxy impregnation. *Cement and Concrete Research*. 2003, **33**, 611-616.

[323] Haha M. B., De Weerdt K. and Lothenbach B. Quantification of the degree of reaction of fly ash. *Cement and Concrete Research*. 2010, **40**, 1620-1629.

[324] Scrivener K. L., Patel H. H., Pratt P. L. and Parrott L. J. Analysis of Phases in Cement Paste using Backscattered Electron Images, Methanol Adsorption and Thermogravimetric Analysis. *MRS Online Proceedings Library*. 1986, **85**, null-null.

[325] Wong H. S., Zobel M., Buenfeld N. R. and Zimmerman R. W. Influence of the interfacial transition zone and microcracking on the diffusivity, permeability and sorptivity of cement-based materials after drying. Magazine of Concrete Research, 2009, pp. 571-589.

[326] Safiuddin M. and Hearn N. Comparison of ASTM saturation techniques for measuring the permeable porosity of concrete. *Cement and Concrete Research*. 2005, **35**, 1008-1013.

[327] Wu Z., Wong H. S. and Buenfeld N. R. Influence of drying-induced microcracking and related size effects on mass transport properties of concrete. *Cement and Concrete Research*. 2015, **68**, 35-48.

[328] Tasdemir C. Combined effects of mineral admixtures and curing conditions on the sorptivity coefficient of concrete. *Cement and Concrete Research*. 2003, **33**, 1637-1642.

[329] BS1881-122:2011. Testing concrete: Method for determination of water absorption. *Brussels*: BSI; 2011.

[330] Otsuki N., Nagataki S. and Nakashita K. Evaluation of AgNO3 solution spray method for measurement of chloride penetration into hardened cementitious matrix materials. *ACI Materials Journal*. 1992, **89**, 587-592.

[331] Baroghel-Bouny V., Belin P., Maultzsch M. and Henry D. AgNO3 spray tests: advantages, weaknesses, and various applications to quantify chloride ingress into concrete. Part 1: Non-steady-state diffusion tests and exposure to natural conditions. *Materials and Structures*. 2007, **40**, 759-781.

[332] RILEM. Analysis of water soluble chloride content in concrete. *Materials and Structures*. 2002, **35**, 586-588.

[333] Tang L. and Nilsson L. O. A new approach to the determination of pore distribution by penetrating chlorides into concrete. *Cement and Concrete Research*. 1995, **25**, 695-701.

[334] Stutterheim H. Properties and uses of high-magnesia portland slag cement concretes. *Journal of the American Concrete Society*. 1960, 1027-1045.

[335] Gutteridge W. A. and Dalziel J. A. Filler cement: The effect of the secondary component on the hydration of Portland cement: Part 2: Fine hydraulic binders. *Cement and Concrete Research*. 1990, **20**, 853-861.

[336] Shi C. and Day R. L. A calorimetric study of early hydration of alkali-slag cements. *Cement and Concrete Research*. 1995, **25**, 1333-1346.

[337] Angulski da Luz C. and R. D H. Influence of curing temperature on the process of hydration of supersulfated cements at early age. *Cement and Concrete Research*. 2015, **77**, 69-75.

[338] Gruskovnjak A., Lothenbach B., Winnefeld F., Figi R., Ko S. C., Adler M. and Mäder U. Hydration mechanisms of super sulphated slag cement. *Cement and Concrete Research*. 2008, **38**, 983-992.

[339] Lothenbach B., Le Saout G., Gallucci E. and Scrivener K. Influence of limestone on the hydration of Portland cements. *Cement and Concrete Research*. 2008, **38**, 848-860.

[340] Kakali G., Tsivilis S., Aggeli E. and Bati M. Hydration products of C3A, C3S and Portland cement in the presence of CaCO3. *Cement and Concrete Research*. 2000, **30**, 1073-1077.

[341] Zajac M., Rossberg A., Le Saout G. and Lothenbach B. Influence of limestone and anhydrite on the hydration of Portland cements. *Cement and Concrete Composites*. 2014, **46**, 99-108.

[342] Taylor R., Richardson I. G. and Brydson R. M. D. Composition and microstructure of 20-year-old ordinary Portland cement–ground granulated blast-furnace slag blends containing 0 to 100% slag. *Cement and Concrete Research*. 2010, **40**, 971-983.

[343] Kjellsen K. O. Heat curing and post-heat curing regimes of high-performance concrete: Influence on microstructure and C-S-H composition. *Cement and Concrete Research*. 1996, **26**, 295-307.

[344] De Weerdt K., Haha M. B., Le Saout G., Kjellsen K. O., Justnes H. and Lothenbach B. Hydration mechanisms of ternary Portland cements containing limestone powder and fly ash. *Cement and Concrete Research*. 2011, **41**, 279-291.

[345] Röβler M. and Odler I. Investigations on the relationship between porosity, structure and strength of hydrated portland cement pastes I. Effect of porosity. *Cement and Concrete Research*. 1985, **15**, 320-330.

[346] Igarashi S., Kawamura M. and Watanabe A. Analysis of cement pastes and mortars by a combination of backscatter-based SEM image analysis and calculations based on the Powers model. *Cement and Concrete Composites*. 2004, **26**, 977-985.

[347] Zajac M. and Ben Haha M. Experimental investigation and modeling of hydration and performance evolution of fly ash cement. *Materials and Structures*. 2014, **47**, 1259-1269.

[348] Khatib J. M. Effect of initial curing on absorption and pore size distribution of paste and concrete containing slag. *KSCE Journal of Civil Engineering*. 2014, **18**, 264-272.

[349] De Weerdt K., Orsáková D. and Geiker M. R. The impact of sulphate and magnesium on chloride binding in Portland cement paste. *Cement and Concrete Research*. 2014, **65**, 30-40.

[350] Paul G., Boccaleri E., Buzzi L., Canonico F. and Gastaldi D. Friedel's salt formation in sulfoaluminate cements: A combined XRD and 27Al MAS NMR study. *Cement and Concrete Research*. 2015, **67**, 93-102.

[351] Kuzel H. J. and Pöllmann H. Hydration of C3A in the presence of Ca(OH)2, CaSO4·2H2O and CaCO3. *Cement and Concrete Research*. 1991, **21**, 885-895.

[352] Brown P. W. Kinetics of Tricalcium Aluminate and Tetracalcium Aluminoferrite Hydration in the Presence of Calcium Sulfate. *Journal of the American Ceramic Society*. 1993, **76**, 2971-2976.

[353] Talero R., Trusilewicz L., Delgado A., Pedrajas C., Lannegrand R., Rahhal V., Mejía R., Delvasto S. and Ramírez F. A. Comparative and semi-quantitative XRD analysis of Friedel's salt originating from pozzolan and Portland cement. *Construction and Building Materials*. 2011, **25**, 2370-2380.

[354] Wu K., Shi H., Xu L., Ye G. and De Schutter G. Microstructural characterization of ITZ in blended cement concretes and its relation to transport properties. *Cement and Concrete Research*. 2016, **79**, 243-256.

[355] Song H.-W., Lee C.-H. and Ann K. Y. Factors influencing chloride transport in concrete structures exposed to marine environments. *Cement and Concrete Composites*. 2008, **30**, 113-121.

[356] Ma Q., Nanukuttan S., Basheer P. A. M., Bai Y. and Yang C. Chloride transport and the resulting corrosion of steel bars in alkali activated slag concretes. *Materials and Structures*. 2015, 1-15.

Appendix A
Relationship between hydration and compressive strength

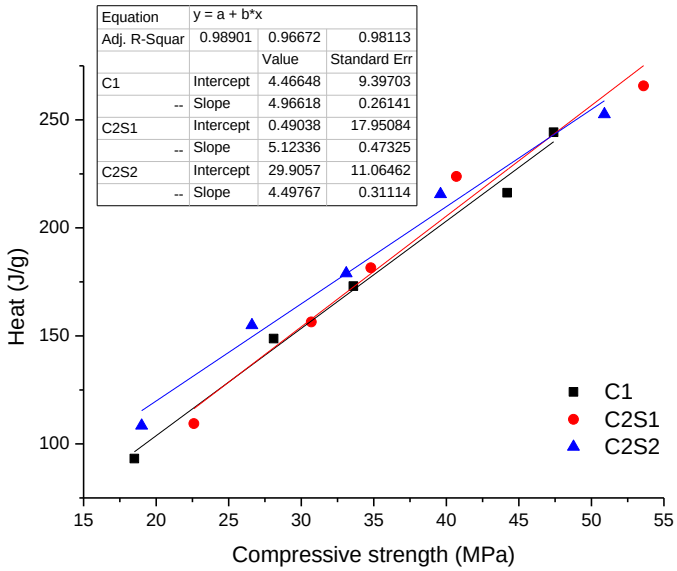

Figure A 1: Linear relationship between UCS and total heat evolved at 20°C

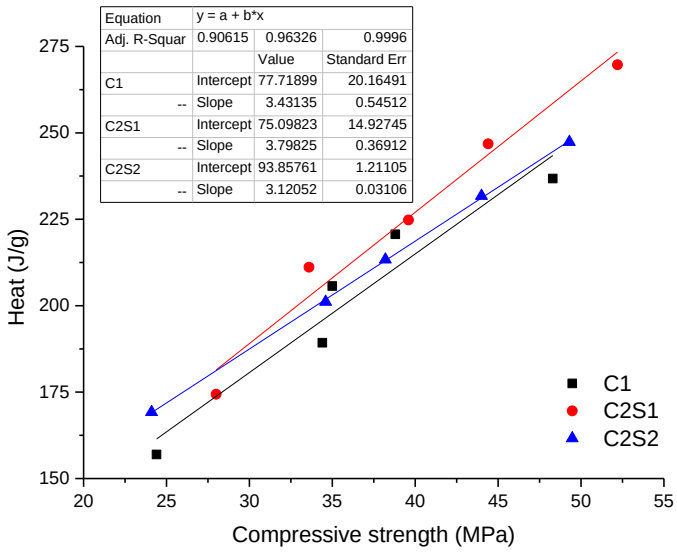

Figure A 2: Linear relationship between UCS and total heat at 38°C

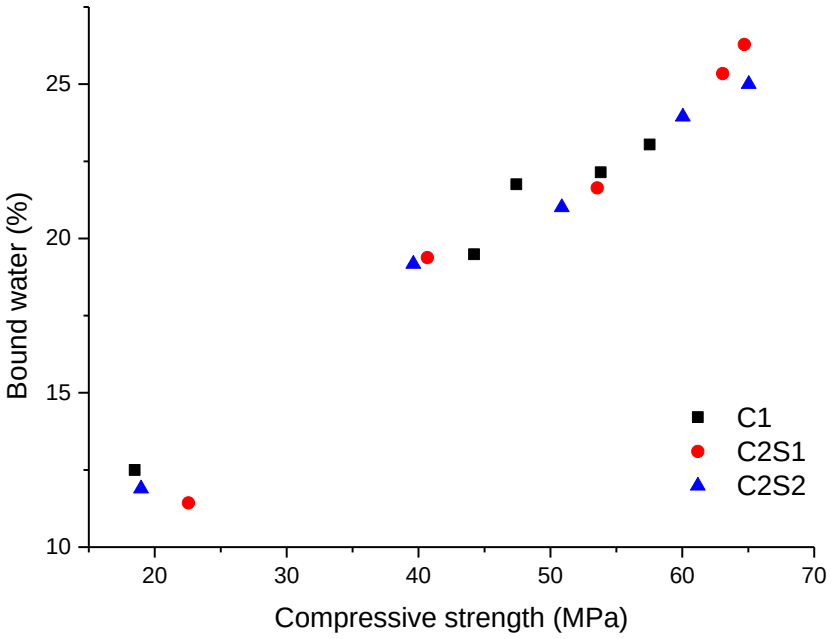

Figure A 3: Relationship between UCS and bound water content at 20°C

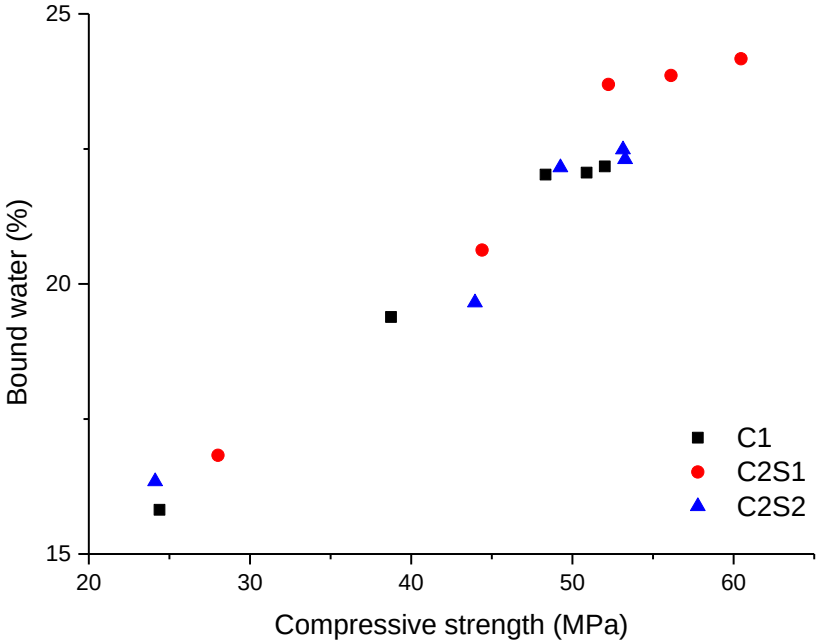

Figure A 4: Relationship between UCS and bound water content at 38°C

Appendix B

B.1 Linear regression plots showing values obtained for sorptivity coefficient (k)

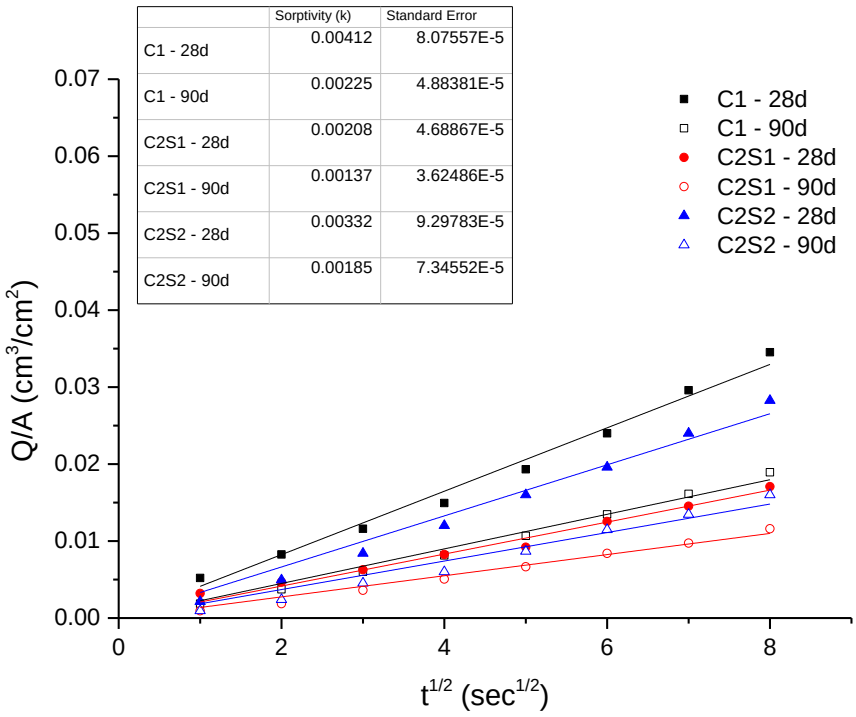

Figure A 5: Linear fit to obtain sorptivity coefficient (*k*) at 20°C

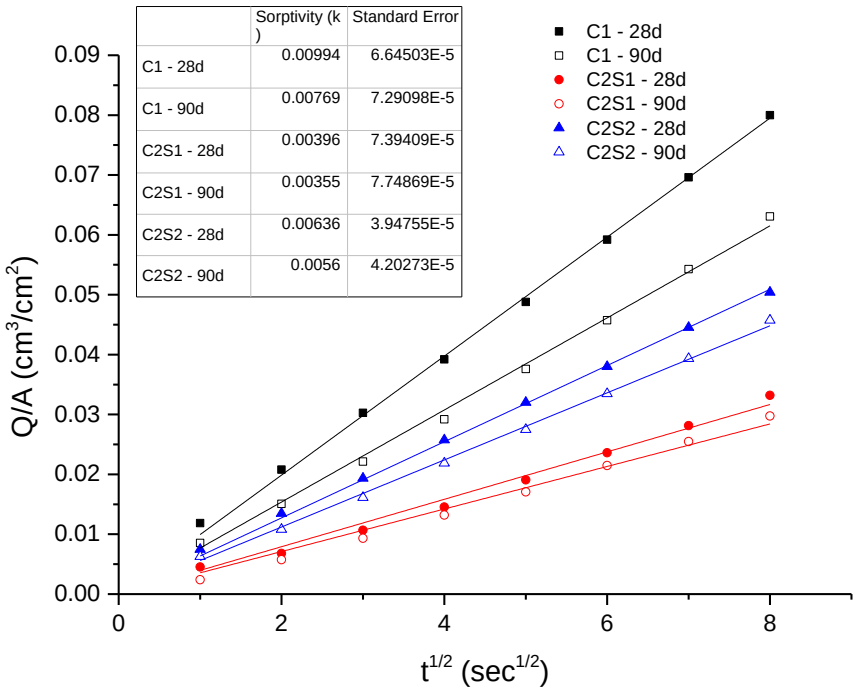

Figure A 6: Linear fit to obtain sorptivity coefficient (*k*) at 38°C

B.2 Relationship between sorptivity coefficient (k) and UCS

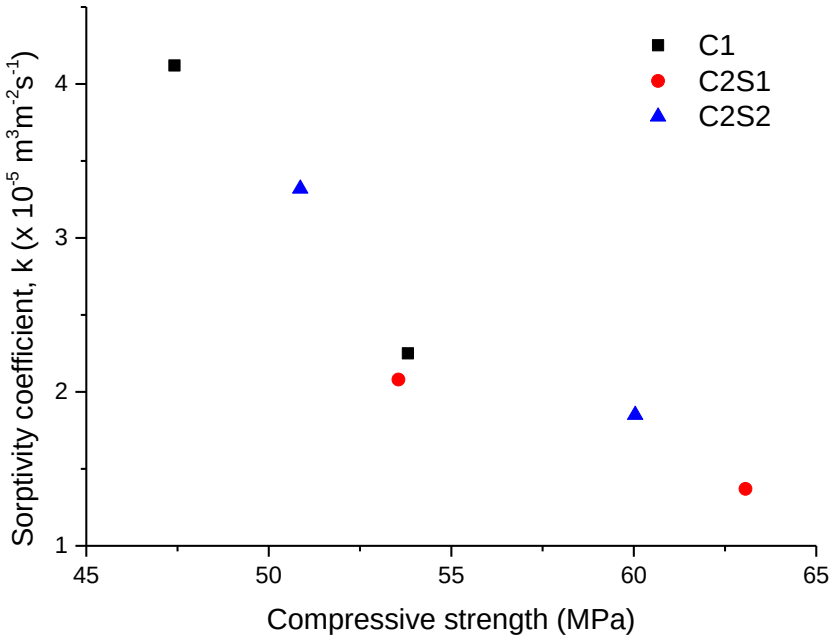

Figure A 7: Relationship between UCS and sorptivity coefficient (*k*) at 20°C

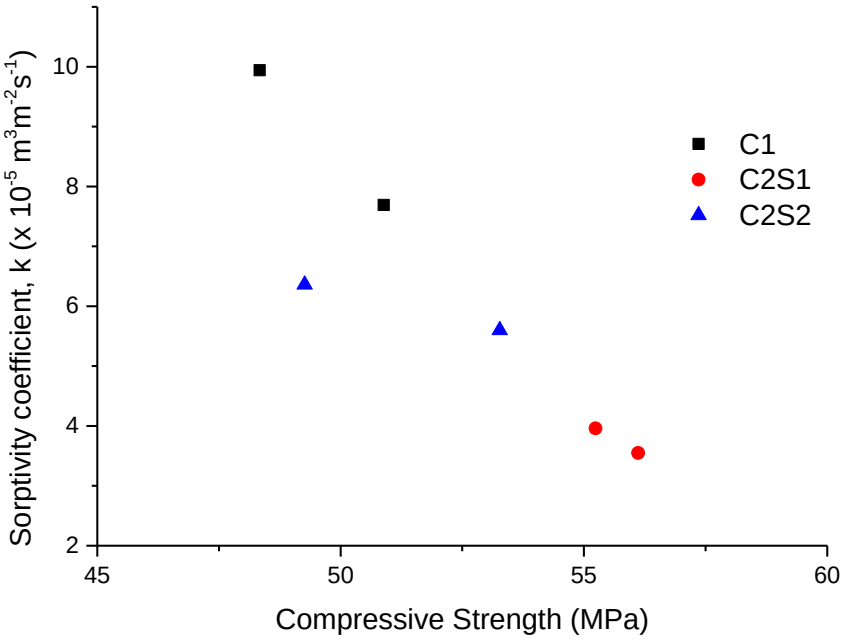

Figure A 8: Relationship between UCS and sorptivity coefficient (*k*) at 38°C

Appendix C
Calculating the activation energies of the cementitious materials

The activation energy of the slag blends was determined from the cumulative heat flow, by applying an Arrhenius-type equation as shown below:

$$\frac{t_1}{t_2} = exp\frac{E}{R}(\frac{1}{T_1} - \frac{1}{T_2})$$

Where t_1 and t_2 = time at 50% degree of hydration at temperatures T_1 and T_2 respectively, E = activation energy in kJ/mol, and R = gas constant taken as 8.314 $JK^{-1}mol^{-1}$.

Obtaining t_{50} (time at 50% degree of hydration) values:

The total heat evolved (Q) was plotted against the inverse of time (1/t). Q_∞ was extrapolated from the data at 1/t = 0. The degree of hydration was approximated as Q/Q_∞, and plotted against time (t). t_{50} is taken as the time when the degree of hydration is 50%.

(a) (b)

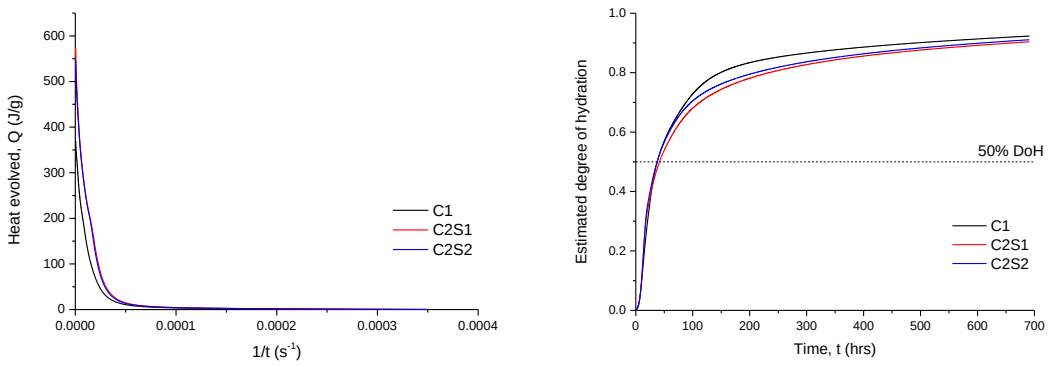

Figure A 9: Obtaining t_{50} at 20°C (a) Heat evolved vs *1/t* (b) Estimated degree of hydration vs time

(a) (b)

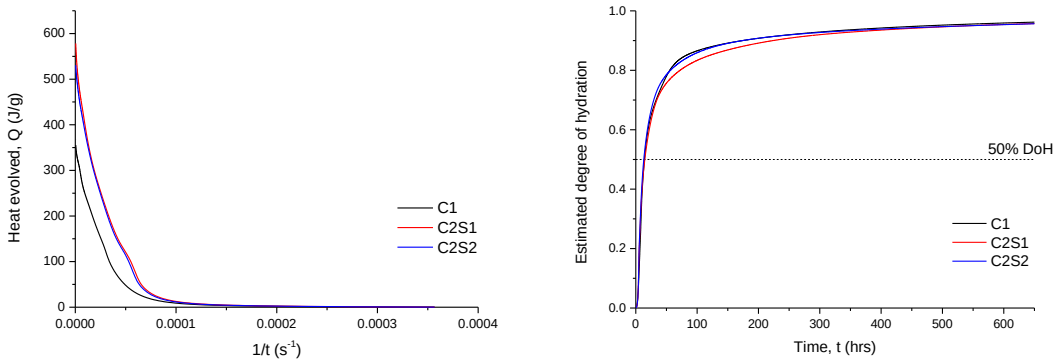

Figure A 10: Obtaining t_{50} at 38°C (a) Heat evolved vs *1/t* (b) Estimated degree of hydration vs time

Table A 1: Calculated activation energy using Q_∞ and t_{50} values obtained at 20 and 38°C

	Q_∞ at 20°C (J/kg)	Q_∞ at 38°C (J/kg)	t_{50} at 20°C (hrs)	t_{50} at 38°C (hrs)	Activation energy (kJ/mol)
C1	397.72	368.86	37.55	14.14	41.15
C2S1	631.66	603.17	41.61	14.76	43.65
C2S2	595.81	553.55	37.49	13.02	44.57

Appendix D
Tables showing chloride binding and chloride ingress results

Table A 2: Bound chloride contents at 20°C

C1		C2S1		C2S2		C2S1$		C2S2$	
C_f mol/l	C_b mg/g	C_f mol/l	C_b mg/g	C_f mol/l	C_b mg/g	C_f mol/l	C_b mg/g	C_f mol/l	C_b mg/g
0.08	1.89	0.041	5.83	0.05	4.60	0.05	5.11	0.06	3.82
0.45	8.41	0.42	12.26	0.43	10.67	0.42	11.81	0.45	8.64
0.89	11.64	0.84	17.74	0.84	16.78	0.85	16.51	0.86	14.54
1.95	16.07	1.85	27.71	1.86	25.78	1.85	26.81	1.86	24.31
2.93	17.69	2.85	34.01	2.88	30.31	2.89	29.77	2.92	25.57

Table A 3: Bound chloride contents at 38°C uncorrected for evaporation losses

C1		C2S1		C2S2		C2S1$		C2S2$	
C_f mol/l	C_b mg/g	C_f mol/l	C_b mg/g	C_f mol/l	C_b mg/g	C_f mol/l	C_b mg/g	C_f mol/l	C_b mg/g
0.06	3.91	0.05	5.59	0.06	4.29	0.05	5.25	0.06	4.01
0.48	5.34	0.45	9.80	0.46	7.89	0.44	10.04	0.47	7.92
0.93	8.27	0.88	13.99	0.89	13.12	0.90	14.22	0.91	13.68
2.02	9.37	1.97	15.17	1.97	15.48	1.93	18.95	1.97	15.17
3.05	12.16	3.00	19.32	3.00	19.70	2.93	26.22	3.00	20.17

Correcting for evaporation losses:

Evaporation occurred at rates ranging from 3 – 12% at 38°C and this was corrected for. The correction was based on two assumptions:

- The ratio of the initial and equilibrium volume of the chloride solutions is equal to the ratio of the initial and equilibrium weight of the chloride solutions

- The evaporation does not affect the equilibrium between the bound and free chlorides

$$\frac{V_i}{V_{ee}} = \frac{W_i}{W_{ee}}$$

$$C_e \times V_i = C_{ee} \times V_{ee}$$

$$C_e = C_{ee} \times \frac{V_{ee}}{V_i} = C_{ee} \times \frac{W_{ee}}{W_i}$$

where:

V_i initial volume of host solution (without evaporation) in ml

V_{ee} volume of host solution after evaporation occurred in ml

W_i initial weight of host solution in grams

W_{ee} weight of host solution after evaporation occurred in grams

C_e chloride concentration at equilibrium (without evaporation) in mol/l

C_{ee} measured chloride concentration at equilibrium after evaporation occurred in mol/l

Table A 4: Evaporation losses (%) measured at the end of the equilibrium period at 38°C

Host chloride conc.	C1	C2S1	C2S2	C2S1$	C2S2$
0.1M	8.98	9.14	10.15	5.30	3.71
0.5M	10.92	12.66	11.25	4.63	4.13
1.0M	8.64	11.48	8.69	4.74	3.75
2.0M	8.32	9.24	8.10	3.87	4.63
3.0M	6.64	9.17	7.14	3.90	2.86

Table A 5: Bound chloride contents at 38°C after correcting for evaporation effect

C1		C2S1		C2S2		C2S1$		C2S2$	
C_f mol/l	C_b mg/g	C_f mol/l	C_b mg/g	C_f mol/l	C_b mg/g	C_f mol/l	C_b mg/g	C_f mol/l	C_b mg/g
0.05	4.39	0.04	6.03	0.05	4.88	0.05	5.48	0.06	4.21
0.44	10.20	0.40	15.47	0.42	13.14	0.42	11.93	0.45	9.69
0.85	15.80	0.79	24.23	0.82	21.07	0.86	18.14	0.87	16.83
1.86	25.23	1.81	33.99	1.82	31.98	1.86	25.87	1.88	23.54
2.86	31.62	2.75	47.76	2.80	42.03	2.82	36.81	2.91	28.18

Table A 6: Average depth of chloride penetration in mm, for samples wet-cured for 7 and 28 days before immersion in a 3% NaCl solution at 20°C

Exposure	C1		C2S1		C2S2	
duration	7 days	28 days	7 days	28 days	7 days	28 days
14 days	7.9	6.1	4.7	3.8	5.3	4.9
28 days	10.2	8.3	7.5	5.5	8.3	6.7
56 days	14.8	8.6	9.4	6.3	11.1	7.0
90 days	21.5	11.3	11.4	6.4	13.1	7.3

Table A 7: Average depth of chloride penetration in mm, for samples wet-cured for 7 and 28 days before exposure to a 6-hr wet/dry cyclic condition with a 3% NaCl solution at 20°C

Exposure	C1		C2S1		C2S2	
duration	7 days	28 days	7 days	28 days	7 days	28 days
14 days	6.5	10.0	5.9	5.2	6.3	6.9
28 days	10.3	10.6	6.9	7.2	9.0	7.3
56 days	14.8	12.6	10.5	8.0	11.1	8.5
90 days	19.8	15.8	11.2	8.8	12.6	9.6

Table A 8: Average depth of chloride penetration in mm, for samples wet-cured for 7 and 28 days before immersion in a 3% NaCl solution at 38°C

Exposure	C1		C2S1		C2S2	
duration	7 days	28 days	7 days	28 days	7 days	28 days
14 days	7.2	7.3	3.5	3.2	4.6	3.8
28 days	11.6	7.9	7.4	6.4	8.6	7.2
56 days	16.2	11.1	9.9	6.6	11.7	7.4
90 days	23.8	16.2	12.0	8.3	14.0	10.8

Plate 1: Pictures showing extent of chloride penetration into mortar samples exposed to a 3% NaCl solution at 20°C for 90 days

C1-7 days wet-cured

C2S1-7 days wet-cured

C2S2-7 days wet-cured

C1-28 days wet-cured

C2S1-28 days wet-cured

C2S2-28 days wet-cured

Plate 2: Pictures showing extent of chloride penetration into mortar samples exposed to a 3% NaCl solution at 38°C for 90 days

C1-7 days wet-cured

C2S1-7 days wet-cured

C2S2-7 days wet-cured

C1-28 days wet-cured

C2S1-28 days wet-cured

C2S2-28 days wet-cured

Plate 3: Pictures showing extent of chloride penetration into mortar samples subjected to 6-hr wet/dry cyclic chloride exposure at 20°C for 90 days

C1-7 days wet-cured

C2S1-7 days wet-cured

C2S2-7 days wet-cured

C1-28 days wet-cured

C2S1-28 days wet-cured

C2S2-28 days wet-cured

Table A 9: Total chloride contents in %, obtained for mortar samples wet-cured for 7 and 28 days before subjected to salt ponding test at 20°C

Distance from exposed face	C1		C2S1		C2S2	
(mm)	7 days	28 days	7 days	28 days	7 days	28 days
2.5	0.41	0.44	0.35	0.41	0.40	0.44
10.5	0.23	0.27	0.08	0.08	0.12	0.09
18.5	0.13	0.12	0.07	0.05	0.08	0.06
27.0	0.13	0.05	0.05	0.04	0.06	0.05
36.0	0.11	0.03	0.04	0.03	0.04	0.03
44.5	0.10	0.02	0.03	0.03	0.03	0.03

Table A 10: Total chloride contents in %, obtained for mortar samples wet-cured for 7 and 28 days before subjected to salt ponding test at 38°C

Distance from exposed face	C1		C2S1		C2S2	
(mm)	7 days	28 days	7 days	28 days	7 days	28 days
2.5	0.52	0.95	0.67	0.86	0.63	0.82
10.5	0.30	0.38	0.13	0.09	0.13	0.12
18.5	0.16	0.11	0.08	0.07	0.10	0.09
27.0	0.14	0.07	0.06	0.05	0.09	0.07
36.0	0.14	0.06	0.05	0.04	0.07	0.06
44.5	0.13	0.06	0.04	0.04	0.05	0.05

Table A 11: Water soluble chloride contents in ppm, obtained for mortar samples wet-cured for 7 and 28 days before subjected to salt ponding test at 20°C

Distance from exposed face	C1		C2S1		C2S2	
(mm)	7 days	28 days	7 days	28 days	7 days	28 days
2.5	3253	2616	2241	1328	2643	1801
10.5	1215	1085	451	107	751	251
18.5	590	373	155	60	196	73
27.0	468	137	131	49	144	68
36.0	355	87	122	34	121	65
44.5	352	65	35	0	105	55

Table A 12: Water soluble chloride contents in ppm, obtained for mortar samples wet-cured for 7 and 28 days before subjected to salt ponding test at 38°C

Distance from exposed face	C1		C2S1		C2S2	
(mm)	7 days	28 days	7 days	28 days	7 days	28 days
2.5	6668	5775	5371	2661	5793	4679
10.5	1763	1443	624	337	943	440
18.5	650	432	352	75	466	98
27.0	468	217	153	49	315	69
36.0	355	147	128	46	218	67
44.5	352	142	117	0	168	58